

NHM-WS 2023

# The 6th International Workshop on Nonhydrostatic Models (NHM-WS 2023)

(The 25th Workshop on Nonhydrostatic Models)

31 August - 2 September 2023

Sapporo, Japan

## Extended Abstracts



JSPS



Local Organize Committee of NHM-WS 2023

Research Group on Nonhydrostatic Numerical Models

Meteorological Society of Japan

© Author(s) of each abstract. The articles in this extended abstract are distributed under the Creative Commons Attribution 4.0 License 

#### Organizers

- Research committee of Nonhydrostatic Model, The Meteorological Society of Japan
- The Meteorological Society of Japan
- The Meteorological Society of Japan, HOKKAIDO
- International Core-to-Core Project on Global Storm Resolving Analysis, supported by JSPS Core-to-Core Program
- RIKEN
  - SATREPS Project "The project for numerical weather prediction and warning communication system for densely populated and vulnerable cities (PREVENIR)" supported by JICA/JST
  - RIKEN Pioneering Project "Prediction for Science"
  - Moonshot Goal 8 R&D Project "Development of an Atmospheric Simulation Model for Estimating the Probability of Local Atmospheric Phenomena"
- Collaborative Research Program 2023, supported by Hokkaido University Information Initiative Center
- Japan Agency for Marine-Earth Science and Technology (JAMSTEC)
  - Weather/Climate Sci. App. Area sub-G, Application Research Group, System Research Team by RIKEN, Feasibility Studies on Next-Generation Supercomputing Infrastructures

#### Sponsors

- The Kajima Foundation's Support Program for International Research Meetings
- Inoue Foundation for Science

#### Supporters

- Japan Meteorological Agency
- Research group on Computational Science and Technology, The Meteorological Society of Japan

#### LOC

Yousuke Sato (Hokkaido University)

Masaru Inatsu (Hokkaido University)

Junshi Ito (Tohoku University)

## Index [Page]

Session A (Computation)	[1]
Session B (Machine learning, Numerical prediction, Ocean Modeling)	[14]
Session C (Cloud Physics, Radiation, Lightning 1)	[31]
Session D (Data assimilation 1)	[42]
Session E (Cloud Physics, Radiation, Lightning 2)	[53]
Session F (Data assimilation 2)	[64]
Session G (Cloud Physics, Radiation, Lightning 2)	[73]
Session H (Event analyses)	[86]
Session I (Global storm-resolving simulations)	[99]
Session J (Tropical Cyclone)	[112]
Session K (Framework)	[127]
Session L (Urban Modeling, Local scale phenomena)	[138]
Session M (Dynamical core, LES)	[149]
Session N (Radiative convective equilibrium, Convection)	[160]

## Session A: Computation

# **Innovative Supercomputing by Integration of Simulation/Data/Learning at the Information Technology Center, The University of Tokyo**

Kengo Nakajima<sup>12</sup>

<sup>1</sup>Information Technology Center, The University of Tokyo, Kashiwa, Japan

<sup>2</sup>RIKEN Center for Computational Science (R-CCS), Kobe, Japan

(Corresponding author: Kengo Nakajima, e-mail: nakajima@cc.u-tokyo.ac.jp)

This work is distributed under the Creative Commons Attribution 4.0 License (CC BY 4.0)

Supercomputing is shifting from the traditional simulation for computational science to the integration with data science and machine learning/AI. Since 2015, the Information Technology Center, the University of Tokyo (ITC/U.Tokyo) has been working on the “Big Data & Extreme Computing (BDEC)” project aimed at new supercomputing through the integration of “Simulation/Data/Learning (S+D+L)”. In May 2021, Wisteria/BDEC-01, the first system of the BDEC project, began its operation. Wisteria/BDEC-01 has a total peak performance of 33+PF, and consists of a simulation node group (Odyssey) consisting of 7,680x A64FX nodes and a data/learning node group (Aquarius) equipped with 360x NVIDIA A100 GPUs. Aquarius can be directly connected to the outside and real-time acquisition of observation data is also possible. Some nodes of Aquarius are directly connected to the outside, and real-time acquisition of observation data etc. is also possible via SINET. Since 2019, we have been developing an innovative software platform "h3-Open-BDEC" that realizes the integration of (S+D+L), with the support of Grant-in-Aid for Scientific Research (S). Integration of (S+D+L) is now being realized on Wisteria/BDEC-01. Those activities are described in the talk with future perspectives.

## **References**

1. Supercomputing Research Division, Information Technology Center, The University of Tokyo, <https://www.cc.u-tokyo.ac.jp/>
2. Sumimoto, S., Arakawa, T., Sakaguchi, Y., Matsuba, H., Yashiro, H., Hanawa, T., Nakajima, K., A System-Wide Communication to Couple Multiple MPI Programs for Heterogeneous Computing, Proceedings of the 23rd International Conference on Parallel and Distributed Computing, Applications and Technologies (PDCAT'22), 2022

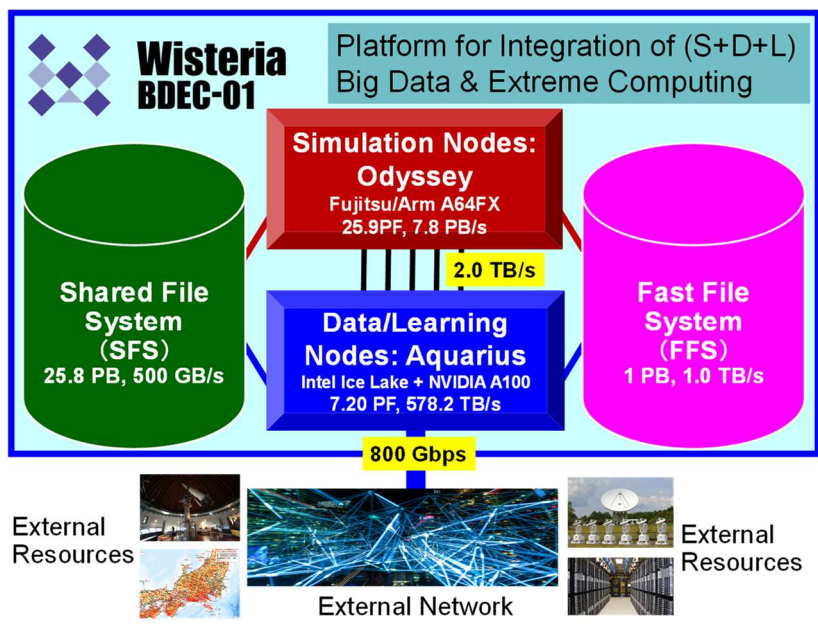


Fig.1 Overview of Wisteria/BDEC-01 [1]

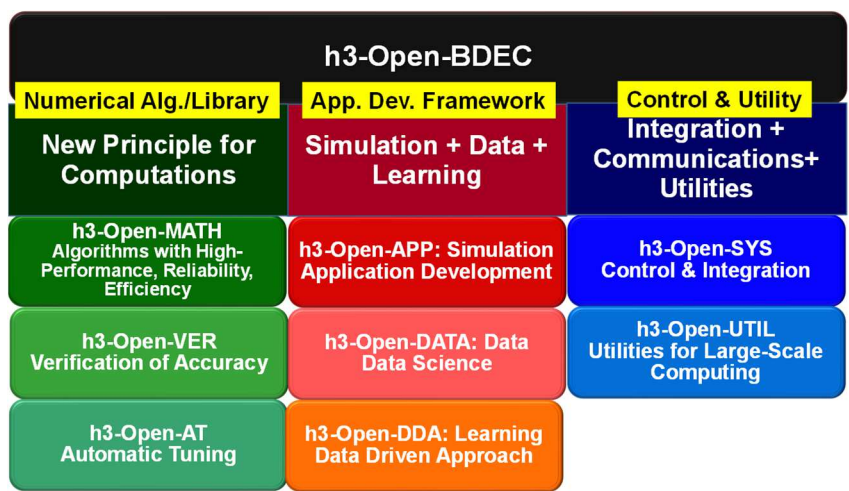


Fig.2 Overview of h3-Open-BDEC [2]

# Performance, scalability, and portability of Nonhydrostatic ICosahedral Atmospheric Model on GPUs

Hisashi Yashiro<sup>1</sup>

<sup>1</sup>National Institute for Environmental Studies, Tsukuba, Japan

(Corresponding author: Hisashi YASHIRO, e-mail: yashiro.hisashi@nies.go.jp)

This work is distributed under the Creative Commons Attribution 4.0 License (CC BY 4.0)

## 1. Backgrounds and motivation

Among the machines currently listed in the TOP500, one of the worldwide performance rankings for computers, 30% are equipped with accelerators such as GPUs. These accelerators maintain higher energy efficiency compared to traditional CPUs and, driven by the recent explosive growth in AI research, offer a cost-effective means of providing big computational resources. Climate and weather models continue to require more computational resources in the future, highlighting the importance of utilizing state-of-the-art supercomputers equipped with a significant number of accelerators. Our simulation model is noteworthy for lacking distinct hotspots (=source code sections that constitute the majority of floating-point operation amount and calculation time). We refer to this as a "flat profile," and in accordance with Amdahl's Law, optimizing nearly all source code sections is crucial for speeding up the entire simulation. This principle applies to accelerator optimization as well. Specifically, executing the entire time marching of the simulation on an accelerator is essential for achieving sufficient performance. Even though no new meteorological findings will arise, this labor-intensive work remains important for users of simulation results both now and in the future. In this presentation, we introduce the GPU optimization efforts applied to Nonhydrostatic ICosahedral Atmospheric Model (NICAM, Satoh et al., 2014).

## 2. Porting of NICAM Dynamical Core using OpenACC

The first GPU optimization for NICAM was carried out in late 2013. Leveraging the directive-based accelerator standard, OpenACC version 2.0, released in 2013, the dycore optimization was carried out without resorting to the CUDA coding. The incorporation of directives was completed within two months, and in March 2014, a large-scale benchmark using the TSUBAME2.5 was performed (Yashiro et al., 2016). Two key factors contributed to the swift completion of this optimization. First, NICAM's dycore featured well-structured code. Utility routines were appropriately extracted and modularized, and enough size of the innermost loops provided sufficient

parallelism for offloading computations to the accelerator. Moreover, due to encapsulated functions and clear variable scope, there was minimal confusion during the "\$acc data" clause application. It is worth emphasizing that program cleanliness, unified coding rules, and proper structuring are essential before optimizing the code for the accelerators. The second reason for rapid optimization progress stemmed from OpenACC being a directive-based language extension, enabling a step-by-step approach. Developers iterate through cycles of applying optimization and confirming results. In development with OpenACC, we can carry out such processes with an appropriate codebase size.

### 3. Porting of full-app and multidirectional consideration of future development

Currently, we are advancing the optimization of the entire model using OpenACC. Optimization of three highly utilized schemes—the single-moment cloud microphysics scheme, the broadband atmospheric radiation scheme, and the MYNN-type PBL closure scheme—has been completed. However, due to the challenges in optimizing the less-structured upper-layer driver, the overall speedup has not yet reached a satisfactory level. On the other hand, to accommodate the diversifying accelerators, we are also exploring optimization approaches that do not only rely on the OpenACC. In the SPPEXA/AIMES project(2016-2019, Kunkel et al., 2020), we have conducted the re-implementation and performance evaluation of the dynamical core kernel using GridTools (Afanasyev et al., 2021), yielding the anticipated acceleration. Furthermore, we started considerations regarding implementations using GT4Py, Julia, and JAX from the perspectives of sustainable software development, learning cost, and a step-by-step transition from huge legacy Fortran code.

### References

1. Afanasyev, A. *et al.*, (2021). GridTools: A framework for portable weather and climate applications, *SoftwareX*, 15, 100707, <https://doi.org/10.1016/j.softx.2021.100707>
2. Kunkel, J. *et al.* (2020). AIMES: Advanced Computation and I/O Methods for Earth-System Simulations. In: Software for Exascale Computing - SPPEXA 2016-2019. *Lecture Notes in Computational Science and Engineering*, vol 136. Springer, Cham. [https://doi.org/10.1007/978-3-030-47956-5\\_5](https://doi.org/10.1007/978-3-030-47956-5_5)
3. Satoh, M. *et al.*, (2014), The Non-hydrostatic Icosahedral Atmospheric Model: description and development. *Prog. in Earth and Planet. Sci.* 1, 18. <https://doi.org/10.1186/s40645-014-0018-1>
4. Yashiro, H. *et al.*, (2016), Performance analysis and optimization of nonhydrostatic icosahedral atmospheric model (NICAM) on the K computer and TSUBAME2.5. *in Proceedings of the Platform for Advanced Scientific Computing Conference*, doi: 10.1145/2929908.2929911

# Porting MIROC-SCALE Super-parameterization to GPU using OpenACC

Kazuya Yamazaki<sup>1</sup>

<sup>1</sup>The University of Tokyo, Kashiwa, Japan

(Corresponding author: Kazuya Yamazaki, e-mail: kyamazaki@cc.u-tokyo.ac.jp)

This work is distributed under the Creative Commons Attribution 4.0 License (CC BY 4.0)

## 1. Introduction

Global climate models (GCMs) depend on cumulus parameterization to represent cumulus activities. However, the reproducibility of such parameterization schemes is limited. This has caused GCMs to suffer difficulties in accurately depicting tropical synoptic phenomena including equatorial waves and MJOs. Super-parameterization is a technique to cope with this challenge by coupling small domains of a cloud-resolving model (CRM) to each column of a GCM and allowing the CRM component to handle cumulus convection explicitly. The author has implemented SP-MIROC, a superparameterized version of the MIROC6 GCM coupled to the SCALE-RM CRM.

While CPUs have been widely used for numerical atmospheric simulations, GPUs are becoming dominant in supercomputers thanks to its high energy efficiency. Thus, it is desirable for existing codes to be ported to GPUs if one wants to run them on near-future supercomputers in large scales. OpenACC helps CPU-targeted codes to adapt to GPUs with relatively low implementation costs using directives similar to OpenMP. The author adopted OpenACC to port a modified version of SCALE-RM v5.3.6 used as the CRM component of SP-MIROC, and evaluated the performance on NVIDIA A100 GPUs on the Wisteria/BDEC01 supercomputer at the University of Tokyo.

## 2. Procedures of the GPU porting and performance evaluation

OpenACC directives allow large loops called kernels to be offloaded to GPUs, while the CPU acts as a host that launches kernels and controls CPU-GPU data communications. Generally, array data transfer between CPUs and GPUs is slow. This imposes performance penalties at boundaries between CPU-only loops and GPU-aware loops because array data need to be transferred at such boundaries. Thus, in this study, essentially all loops manipulating gridded variables in the main loop of SCALE-RM were offloaded to GPUs. Loops were divided to collapsible simple ones because some complex loops could not be parallelized well on GPUs due to register shortages and conflicts in temporary memory allocation. While Norman et al. (2022) ported their super-parameterized GCM called E3SM-MMF using the Unified Memory technology, the author opted to explicitly handle CPU-GPU memory transfer in order to visualize data transfer on source codes. The GCM component of SP-MIROC remained on CPUs because it is computationally lightweight and the data size of the GCM-CRM communication is small.

The performance of the GPU-aware SP-MIROC was tested on three types of processors on Wisteria/BDEC01. One is the A100 GPU of the Aquarius subcluster. The Fujitsu A64FX CPU aboard the FX1000 nodes of the Odyssey subcluster and the Intel Xeon 8360Y CPU, the host processor of the Aquarius PRIMERGY GX2570 M6 nodes, were also used for comparison against the A100 GPU.

SP-MIROC contains numerous independent 2D CRM domains for small-scale processes. Each domain has 39 vertical layers and 32 horizontal grids spaced every 2 km. At a timestep of 12 seconds, the model was integrated for two simulation days in the double precision. The computational throughput and power usage were compared among the three processors. In the CPU runs, the OpenACC directives were deactivated and SP-MIROC CRM simulations were performed on one node in the flat MPI configuration. Two CRM domains were assigned to each process. Power consumption was measured as that of the entire node, except for unused GPUs if present, and were divided by the number of CPUs per node. In the GPU run, all eight A100 GPUs aboard one PRIMERGY GX2570 M6 node were activated. Each GPU, controlled by one host process, handled 256 CRM domains. Power consumption per GPU was measured as that of the entire node, including the host CPUs, divided by the number of GPUs per node.

### 3. Result and conclusion

Table 1 shows the throughput and power consumption of the SP-MIROC CRM component on the three processors. The FLOPS throughput is far smaller than the processors’ theoretical peak values likely because the model is memory-bound. Although Xeon 8360Y achieved a high FLOPS throughput relative to its memory bandwidth, the power consumption is also high, resulting in low performance per power. A64FX, in contrast, is somewhat slow compared to its memory bandwidth but is more than twice as energy-efficient as Xeon 8360Y. The A100 GPU is further twice as efficient as A64FX in terms of performance-per-watt. This indicates that the A100 GPU is a promising platform for atmospheric supercomputing, even though its bytes per FLOP is small than some CPUs such as F64FX.

### References

1. Norman, M. R., Bader D. C., Eldred C., et al., (2022), Unprecedented cloud resolution in a GPU-enabled full-physics atmospheric climate simulation on OLCF’s summit supercomputer, *I. J. High Perf. Comp. App.*, **36(1)**, 93-105

Table 1. Specifications of processors used in this study and measured performance of the SP-MIROC CRM.

Processor	Cores / CPU	Theoretical FLOPS (FP64)	Theoretical Memory bandwidth	Measured simulation year per day	Estimated throughput	Measured power	Estimated GFLOPS/W
A100 GPU	—	9.7 TFLOPS (CUDA core)	1555 GB/s	1.78	531 GFLOPS	206 W	2.6
A64FX CPU	48	3.4 TFLOPS	1024 GB/s	1.73	182 GFLOPS	155 W	1.2
Xeon 8360Y CPU	36	2.3 TFLOPS	205 GB/s	1.67	131 GFLOPS	274 W	0.5

# GPU porting of ASUCA using OpenACC directives

Ryoga ISHIDA<sup>1</sup>

<sup>1</sup>Japan Meteorological Agency

(e-mail: r-ishida@met.kishou.go.jp)

## 1. Introduction

The Japan Meteorological Agency (JMA) has operated the Local Forecast Model (LFM) for aviation weather information and disaster prevention. The JMA plans extension of forecast period and increase of horizontal resolution of the LFM to improve accuracy of torrential rain prediction. Since these plans increase computation time, it is required to improve computational efficiency of the model ASUCA used in the LFM. On the other hand, growth on the performance of CPU-based HPCs in the market is slowing down, and a number of studies are shown the successful GPU porting of weather and climate models. Therefore, using heterogeneous architectures with CPU and GPU accelerator should be considered in the future. Here, as a feasibility study, GPU porting of ASUCA using OpenACC directives has been conducted. We will show workload of GPU porting, acceleration rate, and issues on the porting.

## 2. GPU porting approach and experimental setting

ASUCA employs hybrid parallelization using the OpenMP and MPI. The three-dimensional arrays are allocated so that the vertical loop is taken as innermost dimension, thereby enabling ASUCA to effectively use the CPU cache. The OpenMP parallelization is applied for outer horizontal loop<sup>1</sup>. When ASUCA is ported to GPU, OpenACC directives are used instead of OpenMP to minimize the code changes. The performance is measured with a small domain configuration of the LFM and 216 time steps using a node which consists of two Intel Xeon CPUs and one Tesla V100 GPU.

## 3. Result

Fig. 1 shows the acceleration rate of GPU over CPU of dynamical and physical processes in ASUCA. In the advection computation, the GPU performance is faster than the CPU by just inserting OpenACC directives, because the most vertical loops can be vectorized and the computational complexity in a loop is low. The performance of dynamical core is faster by changing tridiagonal matrix solver used in the vertical implicit solver for HE-VI to suitable algorithm for GPU (CR algorithm<sup>2</sup>) and overlapping computations and MPI communications.

In physical processes, the GPU performance is slower than the CPU by just inserting OpenACC directives due to non-vectorizable vertical main loops and computational complexity. Work arrays are allocated locally in the individual subroutines called in horizontal loops, which leads to the slower GPU performance by the allocation / deallocation and to the insufficient GPU memory in some cases. The local work arrays have been changed to arguments, but the GPU performance is still slower than the CPU. In addition, to prevent insufficient GPU memory, parallelization granularity of horizontal loop in physical processes needs to be finer.

#### 4. Conclusion and Lesson

When code structure of ASUCA is not changed, dynamical core on GPU is faster, but physical processes on GPU are slower due to the non-vectorizable innermost loops, and locally allocated work arrays slow the GPU performance and consume memory. Therefore, speedup of physical processes is limited. Investigate is currently underway to explore a more suitable code structure of ASUCA for CPU and GPU and maintainability of CPU and GPU codes.

#### References

1. Ishida, J., K. Aranami, K. Kawano, K. Matsubayashi, Y. Kitamura, and C. Muroi, (2022), ASUCA: The JMA operational non-hydrostatic model, *J. Meteor. Soc. Japan*, **100**, 825–846
2. Zhang, Y., J. Cohen, and J. D. Owens, (2010), Fast Tridiagonal Solvers on the GPU, *Proceedings of the 15th ACM SIGPLAN Symposium on PPOPP'10.*, 127-136

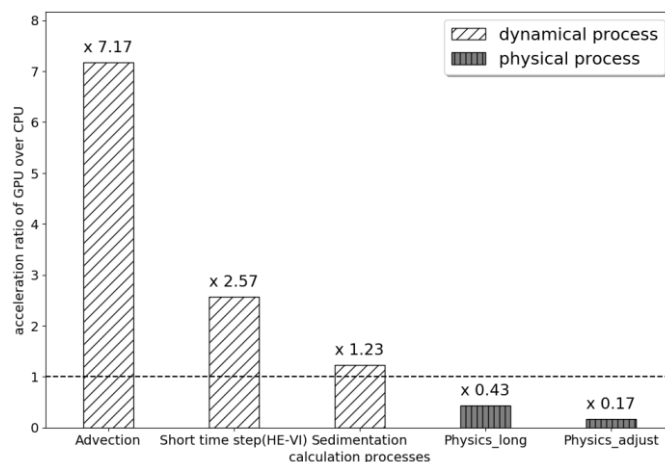


Fig.1. acceleration rate of GPU over CPU of dynamical and physical processes in ASUCA. “Physics\_long” includes several physical processes such as boundary layer, radiation, convection, etc. “Physics\_adjust” includes cloud microphysics.

# Potential for Improving Ensemble Forecast Accuracy Using Mixed Floating-Point Numbers

Tsuyoshi Yamaura<sup>1</sup>

<sup>1</sup>RIKEN Center for Computational Science, Kobe, Japan

(Corresponding author: Tsuyoshi Yamaura, e-mail: tyamaura@riken.jp)

## 1. Introduction

Numerical weather forecast models are implemented on the basis of partial differential equations, which deterministically fix a single value, but often have slight deviations from observations due to lack of spatio-temporal resolution or other reasons. Stochastic parameterization (Palmer 2001) works to compensate for such misalignments by introducing stochastic behavior inside numerical model operations. In addition to ensemble forecasting of initial conditions, it is also known that the accuracy of ensemble forecasting can be increased by simultaneously using stochastic parameterizations such as Stochastic Perturbed Physics Tendency and Stochastic Kinetic Energy Backscatter (Palmer et al. 2009). Generating stochastic behavior in a numerical model usually requires the use of random numbers, but the generation of random numbers incurs extra computational costs. This study suggests to apply rounding errors in floating-point arithmetic to stochastic parameterization. Yamaura et al. (2019) stated that rounding errors exhibit a probabilistic distribution. At present, a software emulator is used to represent fine bit differences in floating-point arithmetic, but in the future, it can be implemented as hardware using Field Programmable Gate Array (FPGA) to reduce the arithmetic cost of random number generation to zero.

## 2. Model description and experimental setup

In this research, an emulator that software-emulates the IEEE754 arithmetic method can perform variable-precision floating-point number (FPN) operations. Therefore, the size of machine epsilon can be adjusted arbitrarily, and it can be operated beyond the IEEE754 specifications such as single or double precision in the creation of the next ensemble member. Numerical experiments will be conducted by implementing the the FPN emulator in the Scalable Computing for Advanced Library and Environment-Regional Model (SCALE-RM), which is based on the weather infrastructure library SCALE Ver 5.4.5 developed at RIKEN. The calculation is set for the Japan area, with a spatial resolution of 18 km and 40 vertical layers, and Japan Meteorological Agency (JMA) Grid Point Value (GPV) EPSW ensemble forecast data for October 15, 22, and 29, 2019 00 UTC are used for initial values and boundary values. The time interval for one step is 40 seconds, and the time integration is performed over a 5-day period. The precision of floating-point operations by the FPN emulator is based on double-precision operations, and the bit length of the mantissa part is varied from original precision to 10 (= half precision).

## 3. Result and conclusion

Figure 1 shows the ensemble mean geopotential height on the 500-hPa after 120 hours from the start of integration and its error. Comparing the case with and without the rounding error due to the mixed floating-point calculation, it is confirmed that the case

with the error is smaller and the ensemble spread is larger.

Ensemble forecasting with numerical weather models often suffers from a decrease in the magnitude of the ensemble spread. The R index, an index for assessing the adequacy of the magnitude of the ensemble spread, is defined as follows (Takano 2002):

$$R = \frac{M+1}{M-1} \frac{\langle S^2 \rangle}{\langle E_M^2 \rangle},$$

where  $M$  is the number of ensemble members,  $S$  is the size of the spread,  $E_M$  is the ensemble average RMSE, and the mountain brackets indicate the multiple-case average; the closer R is to 1, the better.

Figure 2 shows the time variation of R obtained from the ensemble forecast-only experiment with EPSW, the ensemble forecast-only experiment with FPN emulator for rounding errors, and the experiment with both effects added. The resulting R from the experiment with both effects added is closest to 1, suggesting that the effect of rounding errors may be working to improve the reduction in spread size.

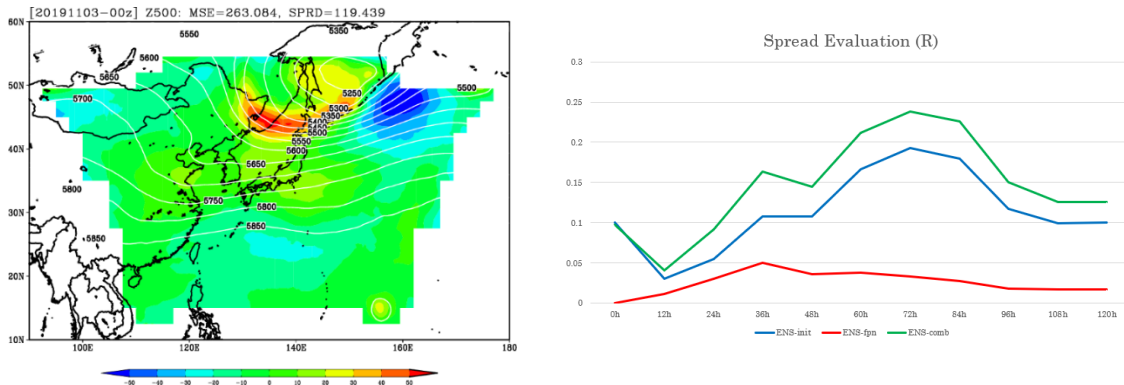


Fig. 1 (left). Ensemble averaged geopotential height on the 500-hPa after 120 hours from the start of integration and its error.

Fig. 2 (right). The blue line shows the time series of the R index for the ensemble members of the EPSW only, the red line shows the rounding error due to the FPN emulator only, and the green line shows the R index with both effects added.

## Acknowledgment

This work was supported by JSPS KAKENHI Grant Number JP21K03663.

## References (in alphabetical order according to author)

1. Palmer, T. N., (2001), A nonlinear dynamical perspective on model error: A proposal for non-local stochasticdynamic parametrization in weather and climate prediction models, *Q. J. R. Meteorol. Soc.*, **127**, 279–304.
2. Palmer, T.N., R. Buizza, F. Doblas-Reyes, T. Jung, M. Leutbecher, G.J. Shutts, M. Steinheimer, and A. Weisheimer, (2009), Stochastic Parametrization and Model Uncertainty, *ECMWF Technical Memoranda*, **598**, 1-42.
3. Takano K., (2002), The application technique of ensemble forecasts, *Meteorological Research Note*, **201**, 73-103 (in Japanese).
4. Yamaura, T., S. Nishizawa, and H. Tomita, (2019), Theoretical time evolution of numerical errors when using floating point numbers in shallow-water models. *J. Adv. Model. Earth. Sy.*, doi:10.1029/2019MS001615.

# EXCLAIM: a python-based test driven development for km-scale global modelling

Anurag DIPANKAR<sup>1</sup> and Mauro BIANCO<sup>2</sup>

<sup>1</sup>Institute for Atmospheric and Climate Science, ETH Zürich, Zürich, Switzerland

<sup>2</sup>Swiss National Supercomputing Centre, ETH Zürich, Lugano, Switzerland

(Corresponding author: Anurag DIPANKAR, e-mail: anurag.dipankar@c2sm.ethz.ch)

This work is distributed under the Creative Commons Attribution 4.0 License (CC BY 4.0)

## 1. Introduction

The *Extreme scale computing and data platform for cloud-resolving weather and climate modeling* (EXCLAIM) aims to develop a simulation platform that is capable of making a step change in our ability to simulate the global ocean-sea-ice-atmosphere-land system at km-scale. Special attention is given to the usability and transferability of the model while maintaining a high computational throughput. This requires significant attention to establishing efficient workstreams and data-flows that deal with the data avalanche generated due to higher resolution (Schulthess et al., 2019; Schär et al., 2020). The simulation platform is based on the ICOSahedral Nonhydrostatic Model (ICON; Zängl et al., 2015) developed jointly by the Deutscher Wetterdienst and Max Planck Institute for Meteorology.

## 2. The simulation platform

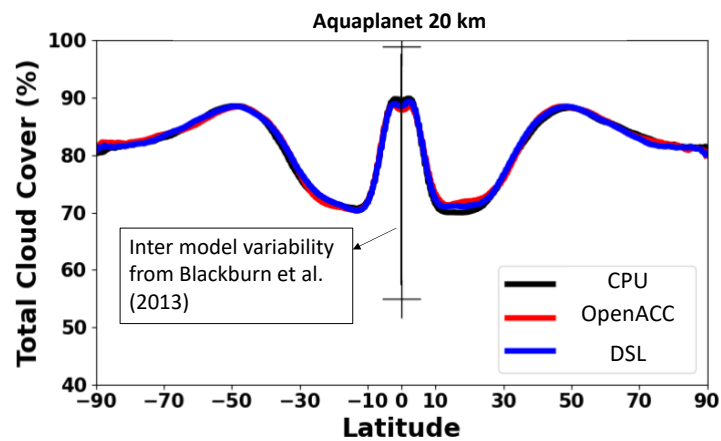
The simulation platform will orchestrate the entire workflow of a typical climate simulation and is envisioned to be python based because of its wide adoption and the large ecosystem of tools and packages it provides for enhanced usage. The core of the platform, i.e. the model, is currently being developed. The existing Fortran modules are refactored and rewritten using a domain specific language called GridTools for Python (GT4Py), developed at ETH. GT4Py has a set of steps that allows the code written in GT4Py to be compiled into a C++ or CUDA executable that is then called in a python framework as a “callable” function. A similar effort to re-write a conventional Fortran based model using GT4Py was undertaken by Dahm et al. (2023).

## 3. Development status

Our development strategy has three steps: (a) identify a physically meaningful granule and re-write it in GT4Py, (b) test the granule through scientific use cases, and (c) once tested tune it further to be called from a Python driver. The last step requires a python

based driver which would allow a typical user to stay within python ecosystem. This is one of the crucial part of the development and requires the model infrastructure (e.g., variable declaration, input-output, etc) also to be called from Python.

The large part of the atmospheric code has already been translated into GT4Py. Current effort focuses on porting the model infrastructure into Python and testing the developed graunles. Preliminary results from global aquaplanet experiment show that the results compare well against benchmark (see figure below). The default performance of GT4Py is comparable to that of OpenACC directives. More performance tunings are underway.



## References

Dahm, J., et al. (2023), Pace v0.2: a Python-based performance-portable atmospheric model, *GMD*, 16, 2719–2736, <https://doi.org/10.5194/gmd-16-2719-2023>

Zängl, G., et al. (2015). The ICON (ICOsahedral Non-hydrostatic) modelling framework of DWD and MPI-M: Description of the non-hydrostatic dynamical core. *QJRM*S, 563–579, 10.1002/qj.2378.

Schär, C., et al. (2020). Kilometer-scale climate models: Prospects and challenges. *BAMS*, 101, 10.1175/BAMS-D-18-0167.1.

Schulthess, T. C., et al. (2019). Reflecting on the Goal and Baseline for Exascale Computing: A Roadmap Based on Weather and Climate Simulations. *CSE*, 30–41, 10.1109/MCSE.2018.2888788.

Session B: Machine learning, Numerical  
prediction, Ocean Modeling

# Exploring Potential Typhoon Control with Deep Reinforcement Learning

Lin LI<sup>1,2</sup>, Takemasa MIYOSHI<sup>1,2</sup>

<sup>1</sup>Prediction Science Laboratory, RIKEN Cluster for Pioneering Research (CPR), Kobe, Japan

<sup>2</sup>Data Assimilation Research Team, RIKEN Center for Computational Science (R-CCS), Kobe, Japan

This work is distributed under the Creative Commons Attribution 4.0 License (CC BY 4.0)

## 1. Introduction

We envision a typhoon-threat-free society in 2050 by controlling typhoons, a vision depicted in Japan’s *Moonshot* Goal #8. A core challenge in controlling typhoons is to design a smart control strategy that links weather perturbation techniques (e.g., cloud seeding) to the goal of typhoon control (e.g., weakening the intensity). This requires a highly efficient, real-time, closed-loop control strategy, which is not trivial to achieve with traditional control theory. Here we propose to use Deep Reinforcement Learning (DRL) in typhoon simulations to autonomously learn the control strategy. DRL is a recent emerging control tool that has been proven successful in strategic games such as Atari, chess, and *Go*, and complex engineering targets such as controlling robots and *Tokamak* fusion plant. Our long-term goal is to find a control strategy that tells when, where, and how much to add perturbations into typhoons.

## 2. Model description and experimental setup

Our system consists of two parts: a typhoon simulator and a DRL algorithm. The typhoon simulator is Cloud Model 1 (CM1), a non-hydrostatic, open-sourced atmospheric model that has been widely used to study typhoons<sup>1</sup>. The DRL algorithm will be the Proximal Policy Optimization (PPO), the performance of which is state-of-the-art in terms of sample efficiency and robustness<sup>2</sup>.

## 3. Result and conclusion

In this study, we aim to suppress the genesis of typhoons (i.e., birth of typhoons) with DRL. We first show that, in the natural, unperturbed state, the typhoon develops from a weak vortex into a strong, mature typhoon (blue curve). We then specify the action space as reducing sea-surface temperature (SST) by 1 K with an axisymmetric, annulus-shaped Gaussian kernel of 20 km width. We then let the

DRL algorithm explore and iteratively find the optimal strategy (as a self-training process). In the initial stage of training, the DRL algorithm succeeds in slightly suppressing the intensification but fails to suppress the genesis (red curve). In the final stage of training, the DRL algorithm succeeds in completely suppressing the genesis of typhoon (purple curve).

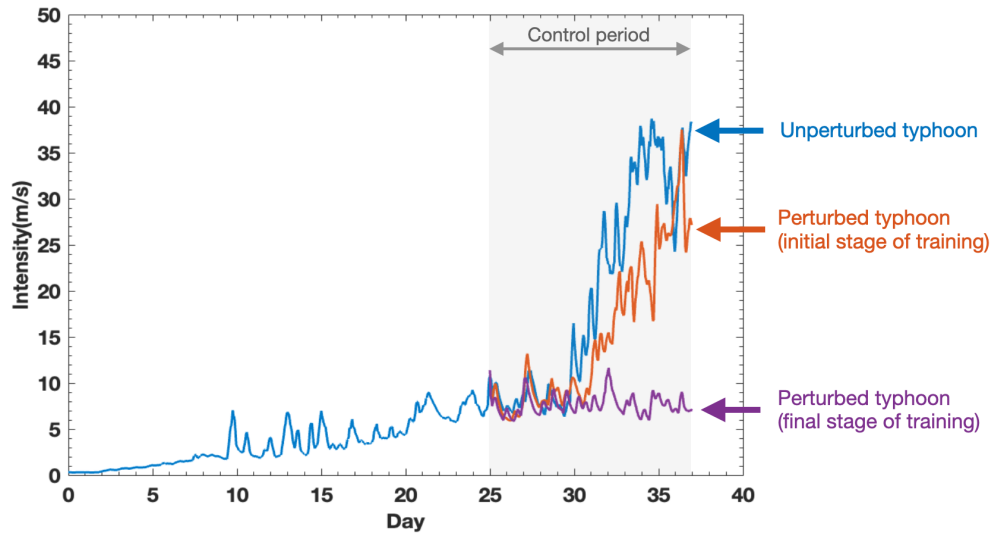


Figure 1. Preliminary results of controlling typhoons by DRL.

## References

1. Bryan, G. H., and R. Rotunno, 2009: The maximum intensity of tropical cyclones in axisymmetric numerical model simulations. *Mon. Wea. Rev.*, **137**, 1770-1789
2. Schulman, J., Wolski, F., Dhariwal, P., Radford, A., & Klimov, O., 2017: Proximal Policy Optimization Algorithms. *arXiv*, 1707.06347.

# Temporally extending the prediction of surface winds from Regional Climate Models by Machine Learning

Yiwen Mao<sup>2</sup>, and Tomohito Yamada<sup>1</sup>

<sup>1,2</sup>Hokkaido University, Sapporo, Japan

(Corresponding author: Yiwen Mao, e-mail: ymaopanda@gmail.com)

This work is distributed under the Creative Commons Attribution 4.0 License (CC BY 4.0)

## 1. Introduction

Regional climate models (RCMs) are obtained by dynamical downscaling. The d4PDF database consists of data from ensemble climate experiments of a 60-km resolution dataset at the global scale, a 20-km and 5-km resolution dataset at the regional scale. In particular, the 5-km dataset covering the Hokkaido region and its surrounding oceans is obtained by dynamical downscaling the 20-km dataset using the non-hydrostatic RCMs (NHRCMs). Although d4PDF-5km data are characterized by finer spatial resolution than d4PDF-20km, the temporal coverage of d4PDF-5km is generally less than that of d4PDF-20km because dynamical downscaling requires heavy computational resources. For example, missing values can be found for a one-year simulation of surface winds by d4PDF-5km. This study provides an alternative method to extend the temporal coverage of surface winds simulated by d4PDF-5km through machine learning.

## 2. Model description and experimental setup

In this study, the model was built and tested on surface wind data from 1980 to 2009 of one ensemble member of the historical simulation from d4PDF. The data are separated into winter (DJF) and summer (JJA), and one model is built for each season. At each grid point of d4PDF-5km dataset, the statistical relationship between the surface zonal and meridional winds (U,V) of d4PDF-5km and d4PDF-20km is obtained by machine learning based training, and the trained relationship is then applied in another time period. In other words, the predictand is the time series of U,V of d4PDF-5km at each grid point. The predictors of the model are the leading two principal components (PCs) of surface wind vectors (U,V) from d4PDF-20km of three sub-regions (R1, R2 and R3) of the Hokkaido island. Among the three regions, R1 (139E-142E) is characterized by most variable curvature of coastlines; R2 (142E-143.5E) contains the two major mountain ranges in Hokkaido (i.e. the Kitami range and the Hidaka range). R3 (143.5E-145.5E) is relatively flat in topography. Mathematically, the model can be described as  $Y_{ij} = f(X)$ , where

$X = [PC1_{R1}, PC2_{R1}, PC1_{R2}, PC2_{R2}, PC1_{R3}, PC2_{R3}]$ , and  $f$  is the link function. In this study, we explored the possibility of building the link function using the linear regression as well as more complex regression models, such as random forest.

### 3. Result and conclusions

In most land regions over the Hokkaido island, R-square resulting from building the link function with linear regression are above 0.5. In general, regions that are adjacent to the east/south side of the Hidaka/Kitami mountain are generally characterized by lower predictability of U/V (Fig.1). Overall the predictability of the U is better than that of V, especially between 141E and 142.5E, and the predictability in winter is generally better than that in summer. A subregion east of the Hidaka mountain is selected for prediction by random forest. The results shows that U and V at all grid points in this region can be better modeled by using random forest than linear regression in DJF, but not in JJA. In other words, random forest has no significant advantage over linear regression in JJA. Finally, the statistical relationship between kurtosis of U/V and the predictability by the machine learning model suggests that grid points with heavier tails are more likely to be poorly predicted.

### References

1. Sugimoto, S., & Ishihara, K. (2019). database for Policy Decision making for Future climate change (P-level data for dynamical downscaling over Japan). (*No Title*).

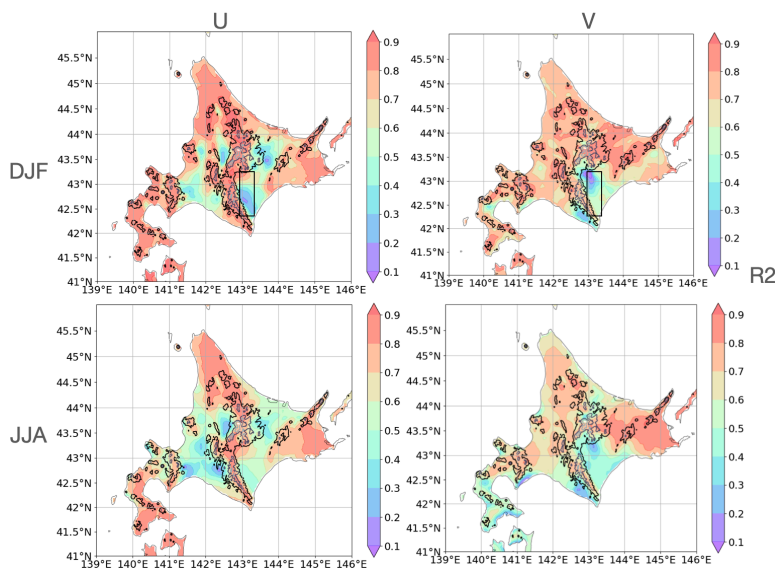


Fig.1.R-square between surface U,V from the machine learning model (with linear regression) and the original d4PDF-5km in DJF and JJA

# Toward 3D precipitation nowcasting by fusing NWP-DA-AI: application of adversarial training

Shigenori OTSUKA and Takemasa MIYOSHI  
RIKEN, Kobe, Japan

(Corresponding author: Shigenori OTSUKA, e-mail: shigenori.otsuka@riken.jp)

This work is distributed under the Creative Commons Attribution 4.0 License (CC BY 4.0)

## 1. Introduction

Recent advances of deep learning allowed us to seek for new data-driven algorithms to predict precipitation based on past observations by weather radars. In parallel, high-end supercomputers enabled us to perform “big data assimilation,” rapidly-updated numerical weather prediction at high spatiotemporal resolution by assimilating dense and frequent observations such as the Phased Array Weather Radar (PAWR) (e.g., Miyoshi et al. 2016a,b, Honda et al. 2022a,b). In conventional precipitation nowcasting, blending of numerical weather prediction and extrapolation-based nowcasting is known to outperform either of these (e.g., Sun et al. 2014).

## 2. Experimental setup

We have been testing a convolutional long short-term memory (ConvLSTM, Shi et al. 2015)-based neural network. Recently, an adversarial training is considered a promising technique for deep learning-based precipitation nowcasting to avoid blurring effect (Ravuri et al. 2021). Therefore, we applied an adversarial training to a three-dimensional extension of ConvLSTM with PAWR.

## 3. Result and conclusion

Preliminary results indicate that the use of adversarial loss increases small-scale features compared to the training without the adversarial loss. In future, a numerical weather prediction output will be fed to the network to combine it with a deep learning-based prediction in a nonlinear manner.

## References

1. Honda, T., A. Amemiya, S. Otsuka, G.-Y. Lien, J. Taylor, Y. Maejima, S. Nishizawa, T. Yamaura, K. Sueki, H. Tomita, S. Satoh, Y. Ishikawa, and T. Miyoshi, 2022: Development of the real-time 30-s-update big data assimilation system for convective rainfall prediction with a phased array weather radar: description and preliminary

- evaluation. *J. Adv. Modeling Earth Systems*, 14, e2021MS002823. doi: 10.1029/2021MS002823.
2. Honda, T., A. Amemiya, S. Otsuka, J. Taylor, Y. Maejima, S. Nishizawa, T. Yamaura, K. Sueki, H. Tomita, and T. Miyoshi, 2022: Advantage of 30-s-updating numerical weather prediction with a phased-array weather radar over operational nowcast for a convective precipitation system. *Geophys. Res. Lett.*, 49, e2021GL096927. doi: 10.1029/2021GL096927.
  3. Miyoshi, T., M. Kunii, J. J. Ruiz, G.-Y. Lien, S. Satoh, T. Ushio, K. Bessho, H. Seko, H. Tomita, and Y. Ishikawa, 2016a: "Big Data Assimilation" Revolutionizing Severe Weather Prediction. *Bull. Amer. Meteor. Soc.*, 97, 1347-1354. doi: 10.1175/BAMS-D-15-00144.1.
  4. Miyoshi, T., G.-Y. Lien, S. Satoh, T. Ushio, K. Bessho, H. Tomita, S. Nishizawa, R. Yoshida, S.A. Adachi, J. Liao, B. Gerofi, Y. Ishikawa, M. Kunii, J. J. Ruiz, Y. Maejima, S. Otsuka, M. Otsuka, K. Okamoto, and H. Seko, 2016b: "Big Data Assimilation" Toward Post-Petascale Severe Weather Prediction: An Overview and Progress. *Proc. IEEE*, 104, 2155-2179, doi: 10.1109/JPROC.2016.2602560.
  5. Ravuri, S., K. Lenc, M. Willson, et al., 2021: Skilful precipitation nowcasting using deep generative models of radar. *Nature* 597, 672-677, doi: 10.1038/s41586-021-03854-z.
  6. Shi, X., Z. Chen, H. Wang, D.-Y. Yeung, W.-K. Wong, and W.-C. Woo, 2015: Convolutional LSTM network: A machine learning approach for precipitation nowcasting. *Advances in Neural Information Processing Systems* 28, 802-810.
  7. Sun, J., M. Xue, J. W. Wilson, I. Zawadzki, S. P. Ballard, J. Onvlee-Hooimeyer, P. Joe, D. M. Barker, P.-W. Li, B. Golding, M. Xu, and J. Pinto, 2014: Use of NWP for nowcasting convective precipitation: Recent progress and challenges. *Bull. Amer. Meteor. Soc.*, 95, 409-426.

# **Narrowing Uncertainties of Climate Projections using Data-driven Methods**

Pierre TANDEO<sup>1,2,3</sup>, Pierre LE BRAS<sup>4</sup>, Florian SEVELLEC<sup>2,4</sup>,

Pierre AILLIOT<sup>5</sup>, and Juan RUIZ<sup>3,6</sup>

<sup>1</sup>IMT Atlantique, Lab-STICC, UMR CNRS 6285, 29238, Brest, France

<sup>2</sup>Odyssey, Inria/IMT/CNRS, Rennes, France

<sup>3</sup>RIKEN Center for Computational Science, Kobe, 650-0047, Japan

<sup>4</sup>Laboratoire d'Océanographie Physique et Spatiale, Univ Brest CNRS IRD Ifremer, Brest, France

<sup>5</sup>Laboratoire de Mathématiques de Bretagne Atlantique, Univ Brest, UMR CNRS 6205, Brest, France

<sup>6</sup>Centro de Investigaciones del Mar y la Atmósfera, Facultad de Ciencias Exactas y Naturales, Universidad de Buenos Aires, CONICET-UBA, Buenos Aires, Argentina, UMI-IFAECI (CNRS-CONICET-UBA), Buenos Aires, Argentina

(Corresponding author: Pierre TANDEO, e-mail: pierre.tandeo@imt-atlantique.fr)

This work is distributed under the Creative Commons Attribution 4.0 License (CC BY 4.0)

## **1. Introduction**

Climate simulations are available from different numerical models and gathered within the Coupled Model Intercomparison Project (CMIP, see Eyring et al. 2016). Each of these models has its own strengths and weaknesses, which impact its ability to predict future climate.

In this presentation, we focus on a specific climate index, which has a major influence on the climate of Europe and North America, the Atlantic Meridional Overturning Circulation (AMOC). All CMIP6 future projections show a slowdown of this circulation in the coming decades (see Lyu et al. 2020). This decrease is not homogeneous: several models predict a dramatic reduction of the AMOC while others predict small changes in the future.

The goal of this presentation is to improve the projections of the AMOC in the next decades by reducing their spread. To do this, we investigate new data-driven methods to weight climate simulations, assuming that some climate models are better than others at describing this climate index.

## 2. Model description and experimental setup

In this work, numerical simulations are weighted by comparing their short-term dynamics to noisy observations. This is done using a combination of data assimilation and analog forecasting, to compute a likelihood function for each simulation (see Ruiz et al. 2022 for more details). Moreover, the methodology takes into account the dependency between the different models, as highlighted in Sanderson et al. 2015.

Here, the methodology is applied to synthetic simulations of an idealized AMOC system, based on three ordinary differential equations (see Sévellec and Fedorov 2014). Different AMOC simulations and observations are artificially created, modifying the parameters of the idealized model. Weights are then calculated by evaluating the dependency between the observations and the different numerical simulations.

## 3. Result and conclusion

The results show that the method can recognize numerical simulations that share similarities with observed short-term variations. The method is also used to construct a weighted AMOC index which is compared to the classic model democracy and the dictatorial approach. Results show improvements when numerical simulations are weighted using the proposed strategy.

As the methodology is purely data-driven, it is finally applied to CMIP6 simulations of the AMOC for the next decade. The results show that the projected mean and associated spread are different between the model democracy and the proposed approach.

## References

1. Eyring, Veronika, Sandrine Bony, et al. (2016). “Overview of the Coupled Model Intercomparison Project Phase 6 (CMIP6) experimental design and organization”. In: *Geoscientific Model Development* 9.5, pp. 1937–1958.
2. Lyu, K., Zhang, X., & Church, J. A. (2020). Regional dynamic sea level simulated in the CMIP5 and CMIP6 models: Mean biases, future projections, and their linkages. *Journal of Climate*, 33(15), 6377-6398.
3. Ruiz, J., Ailliot, P., Chau, T. T. T., Le Bras, P., Monbet, V., Sévellec, F., & Tandeo, P. (2022). Analog data assimilation for the selection of suitable general circulation models. *Geoscientific Model Development*, 15(18), 7203-7220.
4. Sanderson, B. M., Knutti, R., & Caldwell, P. (2015). A representative democracy to reduce interdependency in a multimodel ensemble. *Journal of Climate*, 28(13), 5171-5194.
5. Sévellec, F., & Fedorov, A. V. (2014). Millennial variability in an idealized ocean model: predicting the AMOC regime shifts. *Journal of Climate*, 27(10), 3551-3564.

## **PREVENIR: Japan-Argentina Cooperation Project for Heavy Rain and Urban Flood Disaster Prevention**

Takemasa MIYOSHI<sup>1</sup>, Celeste SAULO<sup>2</sup>, Shigenori OTSUKA<sup>1</sup>, Juan RUIZ<sup>3</sup>,  
Yanina G. SKABAR<sup>2</sup>, Arata AMEMIYA<sup>1</sup>, Tomoo USHIO<sup>4</sup>, Hirofumi TOMITA<sup>1</sup>,  
Tomoki USHIYAMA<sup>5</sup>, and Masaya KONISHI<sup>6</sup>

<sup>1</sup>RIKEN, Kobe, Japan

<sup>2</sup>National Meteorological Service, Buenos Aires, Argentina

<sup>3</sup>University of Buenos Aires, Buenos Aires, Argentina

<sup>4</sup>Osaka University, Suita, Japan

<sup>5</sup>ICHARM, Tsukuba, Japan

<sup>6</sup>Japan Meteorological Agency, Tokyo, Japan

(Corresponding author: Takemasa MIYOSHI, e-mail: takemasa.miyoshi@riken.jp)

This work is distributed under the Creative Commons Attribution 4.0 License (CC BY 4.0)

This presentation provides an overall summary of the project PREVENIR and recent activities about data assimilation and numerical weather prediction (NWP) research. PREVENIR is an international cooperation project between Argentina and Japan since 2022 for five years under the Science and Technology Research Partnership for Sustainable Development (SATREPS) program jointly funded by the Japan International Cooperation Agency (JICA) and the Japan Science and Technology Agency (JST).

Figure 1 shows the overall structure and work packages (WPs) of PREVENIR. The main goal is to develop an impact-based early warning system for heavy rains and urban floods in Argentina. PREVENIR takes advantage of leading research on Big Data Assimilation (BDA) with the Japan's flagship supercomputer "Fugaku" and its predecessor "K" (Miyoshi et al. 2016a; 2016b) and develops a total package for disaster prevention, namely, monitoring, quantitative precipitation estimates (QPE), nowcasting, BDA and NWP, hydrological model prediction, warning communications, public education, and capacity building. The total package for disaster prevention will be the first of its kind in Argentina and will provide useful tools and recommendations for the implementation of similar systems in other parts of the world.

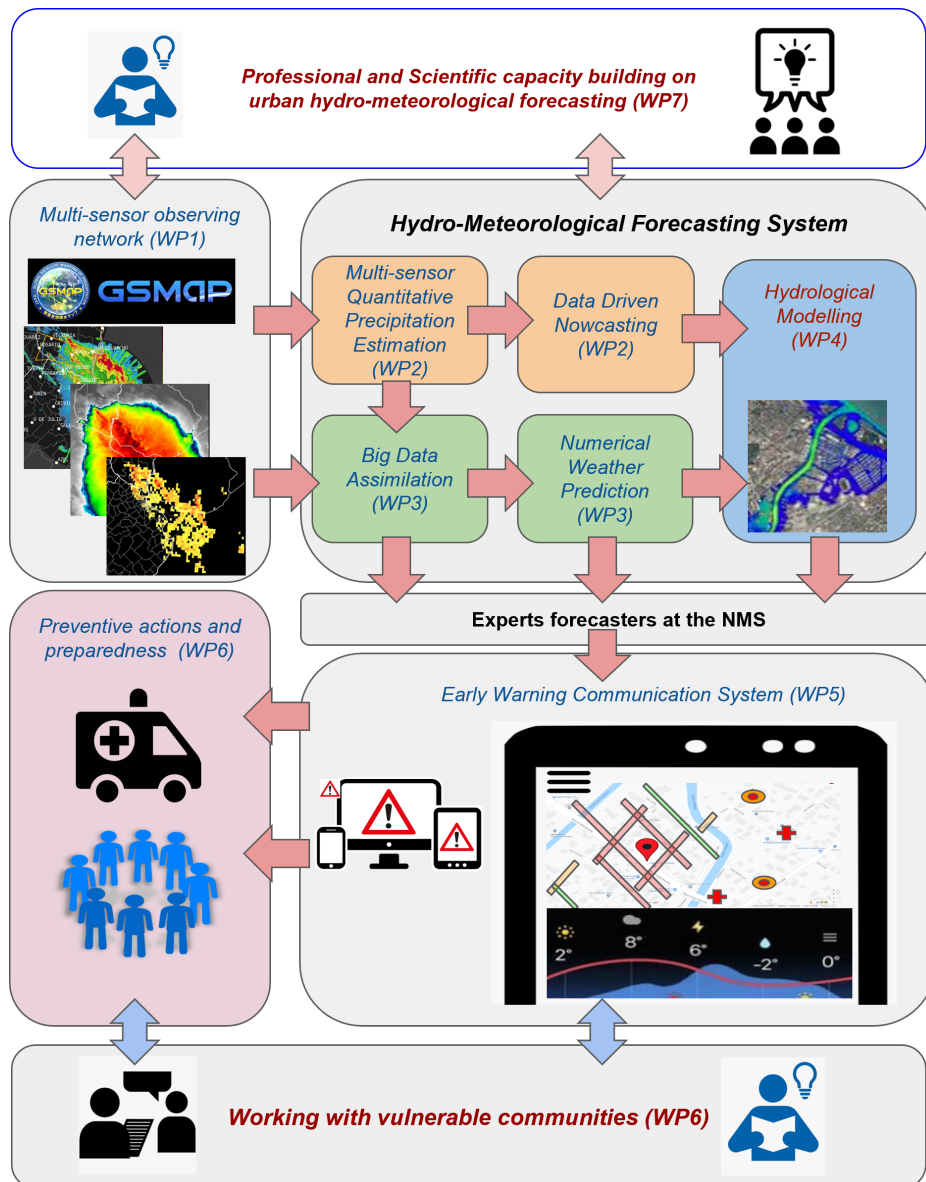


Fig. 1. Overall structure and work packages (WPs) of PREVENIR

**References** (in alphabetical order according to author)

1. Miyoshi, T., M. Kunii, J. Ruiz, G.-Y. Lien, S. Satoh, T. Ushio, K. Bessho, H. Seko, H. Tomita and Y. Ishikawa, (2016a), "Big Data Assimilation" Revolutionizing Severe Weather Prediction, *Bull. Amer. Meteor. Soc.*, **97**, 1347-1354
2. Miyoshi, T., G.-Y. Lien, S. Satoh, T. Ushio, K. Bessho, H. Tomita, S. Nishizawa, R. Yoshida, S. A. Adachi, J. Liao, B. Gerofi, Y. Ishikawa, M. Kunii, J. Ruiz, Y. Maejima, S. Otsuka, M. Otsuka, K. Okamoto and H. Seko, (2016b), "Big Data Assimilation" toward Post-peta-scale Severe Weather Prediction: An Overview and Progress, *Proc. of the IEEE*, **104**, 2155-2179

# **A short-range data assimilation and numerical weather prediction system using the LETKF for urban areas in Argentina**

Arata AMEMIYA<sup>1</sup>, Maria Eugenia DILLON<sup>2,3</sup>, Paula Soledad MALDONADO<sup>2</sup>, Gimena CASARETTO<sup>2,3,5</sup>, Federico CUTRARO<sup>2</sup>, Yanina GARCÍA SKABAR<sup>2,3,6</sup>, Juan Jose RUIZ<sup>4,5,6</sup>, Manuel PULIDO<sup>6,7</sup>, Jorge Gacitua GUTIERREZ<sup>4</sup>, Maite CANCELADA<sup>4,5,6</sup>, Daichi KITAHARA<sup>8</sup>, Martin RUGNA<sup>2</sup>, Takemasa MIYOSHI<sup>1</sup>

<sup>1</sup>RIKEN Cluster for Pioneering Research, Kobe, Japan

<sup>2</sup>Servicio Meteorológico Nacional, Argentina

<sup>3</sup>Consejo Nacional de Investigaciones Científicas y Técnicas.(CONICET), Argentina

<sup>4</sup>Centro de Investigaciones del Mar y la Atmósfera (CIMA), Argentina

<sup>5</sup>Universidad de Buenos Aires, Facultad de Ciencias Exactas y Naturales, Argentina

<sup>6</sup>CNRS – IRD – CONICET – UBA Instituto Franco-Argentino para el Estudio del Clima y sus Impactos (IRL 3351 IFAECI), Argentina

<sup>7</sup>Departamento de Física - Facultad Ciencias Exactas y Naturales y Agrimensura, Universidad Nacional del Nordeste, Argentina

<sup>8</sup>Osaka University, Osaka, Japan

(Corresponding author: Arata Amemiya, e-mail: arata.amemiya@riken.jp)

This work is distributed under the Creative Commons Attribution 4.0 License (CC BY 4.0)

## **1. Introduction**

The use of non-hydrostatic numerical weather prediction (NWP) models with a convection-permitting grid spacing became a common approach to regional short-range precipitation forecasts (Gustaffson et al., 2018). The assimilation of frequent and high-resolution remote-sensing observation data such as satellite and weather radar data plays an essential role in providing accurate initial conditions for NWP model forecasts.

The Argentinian National Weather Service (ANWS) has recently conducted studies utilizing high-resolution NWP models. The operational deterministic and 20-member downscaled ensemble forecasts are produced using the Weather Research and Forecasting (WRF) model with a 4-km horizontal grid spacing (García Skabar et al., 2018). The experimental data assimilation system using the local ensemble transform Kalman filter (LETKF) with the WRF model over Argentinian domain has been developed (Dillon et al., 2016; 2021). In this study, we developed a rapid-refresh ensemble data assimilation and numerical weather prediction system for short-range precipitation forecast for urban areas in Argentina, assimilating observation data from radar and surface weather stations. This study is conducted under PREVENIR, a 5-year cooperative project between Argentina and Japan for the development of a total package of heavy rain and urban flood disaster prevention.

## **2. Model description and experimental setup**

The data assimilation and NWP system being developed under PREVENIR project couples the LETKF assimilation method with either one of the following models: WRF and Scalable Computing for Advanced Library and Environment-Regional Model (SCALE-RM) (Nishizawa et al., 2015). Both have common 2 km horizontal grid spacing and 60 terrain-following vertical levels approximately up to 25 km. The ensemble initial and boundary conditions are provided by the ANWS operational 20-member ensemble forecast. Radar reflectivity and Doppler velocity observations are obtained and directly assimilated every 5 minutes after being re-gridded to a regular grid with 4 km horizontal and 1 km vertical resolution. Surface pressure, horizontal wind, temperature, and relative humidity are observed by automated surface weather stations and assimilated every 10 minutes for most locations. The LETKF uses 40 ensemble members, whereas the extended forecasts are initialized with the first 20 members of the analysis ensemble. We have performed case studies on

past events in two major cities in Argentina: Buenos Aires and Córdoba. A case in October 2019 in Buenos Aires is shown in this abstract. Figure 1 shows the computational domain and the location of the assimilated weather radars and automated surface weather stations. The data assimilation cycle begins at 03:00 UTC 11 October after a 6-hour spin-up period. The 20-member 6-hour extended forecasts are initialized every 30 minutes after 04:00 UTC and evaluated.

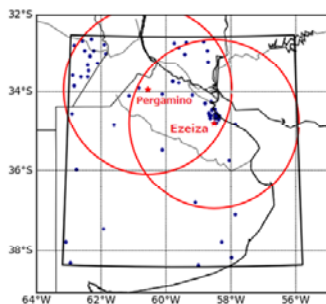


Fig. 1. Model domain (thick black rectangle) and location of two radars (red marks and circles of 240 km radius) and surface stations (blue dots).

### 3. Result

Figure 2 compares surface precipitation rate at 06:00 UTC 11 October, for (a) the estimation from reflectivity and dual polarization parameters observed by Ezeiza radar, (b) WRF forecast initialized by the analysis at 04:00 UTC, (c) SCALE forecast initialized by the analysis at the same time, and (d) SCALE forecast without data assimilation. For the forecasts, precipitation rates averaged over 05:50-06:00 UTC are shown. We found clear improvements of precipitation forecast for a few hours from the initial time by assimilating radar and surface observation data in most cases. However, we also found that the ensemble forecasts had large differences among ensemble members and between the two models. In this case of Buenos Aires, the majority of the ensemble members of SCALE 2-hour forecast shows a northward shift of the heavy rain area compared to the observed location, whereas WRF ensemble forecast predicts the location better.

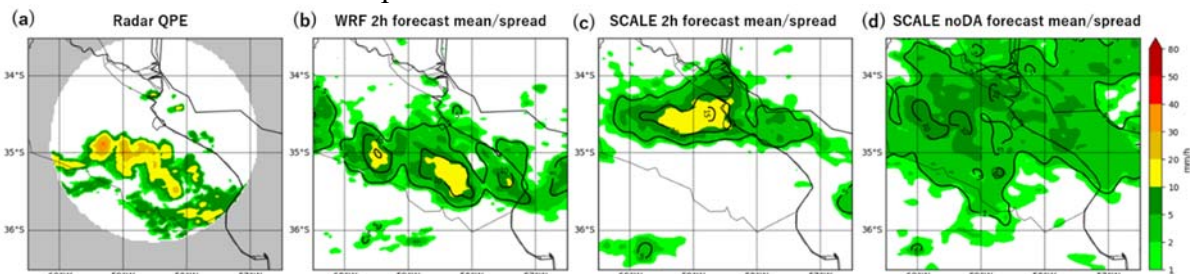


Fig.2. Comparison of surface precipitation rate at 06:00 UTC 11 October, 2019, between (a) estimation based on the Ezeiza radar observation, (b) mean (shades) and spread (contours) of the ensemble forecast from the analysis ensemble at 04:00 UTC using WRF-LETKF, (c) similar to (b) but with SCALE-LETKF, and (d) downscaled SCALE forecast without data assimilation. QPE data is available only within 150km from the radar.

### References

1. Dillon, M. E. et al., (2016). Application of the WRF-LETKF data assimilation system over southern South America: Sensitivity to model physics. *Weather and Forecasting*, 31(1), 217–236. <https://doi.org/10.1175/WAF-D-14-00157.1>
2. Dillon, M. E. et al., (2021). A rapid refresh ensemble based data assimilation and forecast system for the RELAMPAGO field campaign. *Atmospheric Research*, 264(September), 105858.
3. García Skabar, Y. et al., (2018). Implementación del modelo WRF en alta resolución en el Servicio Meteorológico Nacional. *CONGREMET XIII*.
4. Gustafsson, N. et al., (2018). Survey of data assimilation methods for convective-scale numerical weather prediction at operational centres. *Q. J. R. Meteorol. Soc.* 144, 1218–1256.
5. Nishizawa, S. et al., (2015). Influence of grid aspect ratio on planetary boundary layer turbulence in large-eddy simulations. *Geoscientific Model Development*, 8(10), 3393-3419.

# Numerical Weather Prediction performance assessment using a distributed hydrological model

Sebastián LOPEZ<sup>1,2</sup>, Maria Eugenia DILLON<sup>3</sup>, Paula MALDONADO<sup>3</sup>, Arata AMEMIYA<sup>4</sup>, Juan RUIZ<sup>5</sup>, Yanina GARCIA SKABAR<sup>3</sup>, Shigenori OTSUKA<sup>4</sup>, Daiki KAKINUMA<sup>6</sup>, Kentaro AIDA<sup>6</sup>, Tomoki USHIYAMA<sup>6</sup>, Maite CANCELADA<sup>5</sup>, Daichi KITAHARA<sup>7</sup>, Martin RUGNA<sup>3</sup>, Mariano RE<sup>8</sup>, Carlos Marcelo GARCIA<sup>1,2</sup>, Celeste SAULO<sup>3</sup>, Takemasa MIYOSHI<sup>4</sup>

<sup>1</sup>Institute for Advanced Studies in Engineering and Technology (IDIT) – National Research Council (CONICET), Córdoba, Argentina

<sup>2</sup>National University Córdoba, Córdoba, Argentina

<sup>3</sup>National Meteorological Service, Buenos Aires, Argentina

<sup>4</sup>RIKEN Cluster for Pioneering Research (CPR), Kobe, Japan

<sup>5</sup>Center for Atmospheric and Oceanographic Research (CONICET-University of Buenos Aires), Buenos Aires, Argentina

<sup>6</sup>International Center for Water Hazard and Risk Management (ICHARM), Tsukuba, Japan

<sup>7</sup>Osaka University, Osaka, Japan

<sup>8</sup>National Institute of Water, Ezeiza, Argentina

(Corresponding author: Sebastián LOPEZ, e-mail: slopez@mi.unc.edu.ar)

This work is distributed under the Creative Commons Attribution 4.0 License (CC BY 4.0)

## 1. Introduction

Urban floods and intense precipitation are highly destructive natural disasters. In the context of climate change, it is imperative to undertake novel measures for mitigating their impact on vulnerable communities. The PREVENIR initiative started in 2022, with the objective of developing an early warning system centered on the impacts caused by heavy rainfall and urban floods, focusing on two vulnerable urban basins in Argentina. In this study, the performance of two numerical weather prediction (NWP) models using different initial and boundary conditions strategies was assessed by employing forecasted precipitation as input for a distributed hydrological model in a heavy rainfall event occurred on the Suquía River (SR) basin in a mountainous region of the Córdoba Province.

## 2. Models description and experimental setup

Convection allowing (2-km horizontal resolution) NWP deterministic forecasts were performed using the nonhydrostatic regional models Weather Research and Forecasting (WRF) and Scalable Computing for Advanced Library and Environment (SCALE). Three different initial and boundary conditions (IC-BC) datasets were used to produce precipitation forecasts (seven hours): the global NCEP GFS (~25 km), the regional operational WRF from the National Meteorological Service from Argentina (4 km) and a regional SCALE (4 km). Additionally, we used the distributed hydrological modeling tool RRI based on a 2D grid cell to simultaneously simulate rainfall-runoff and flood inundation (Sayama et al, 2012). RRI hydrological parameters were calibrated using discharge and water level observed data, showing a good performance of the RRI modeling tool in the SR basin as it correctly reproduced the hydrological behavior of the basin when using observed rainfall as input (Lopez et al, 2023). The 10-minute forecasted precipitation fields from the NWP models were used to force the hydrological model, and the forecasted hydrographs were compared with the observed ones. Figure 1 shows the experimental setup workflow: the hydrological simulation started one month before the selected event forced with observed precipitation until the NWP forecast initialization time on Dec 13th 23 UTC (blue arrow in Fig. 1); then forecasted precipitation is used until Dec 14th 06 UTC (gray arrow) and finally the RRI runs until Dec 15th 23 UTC with zero precipitation (cyan arrow).

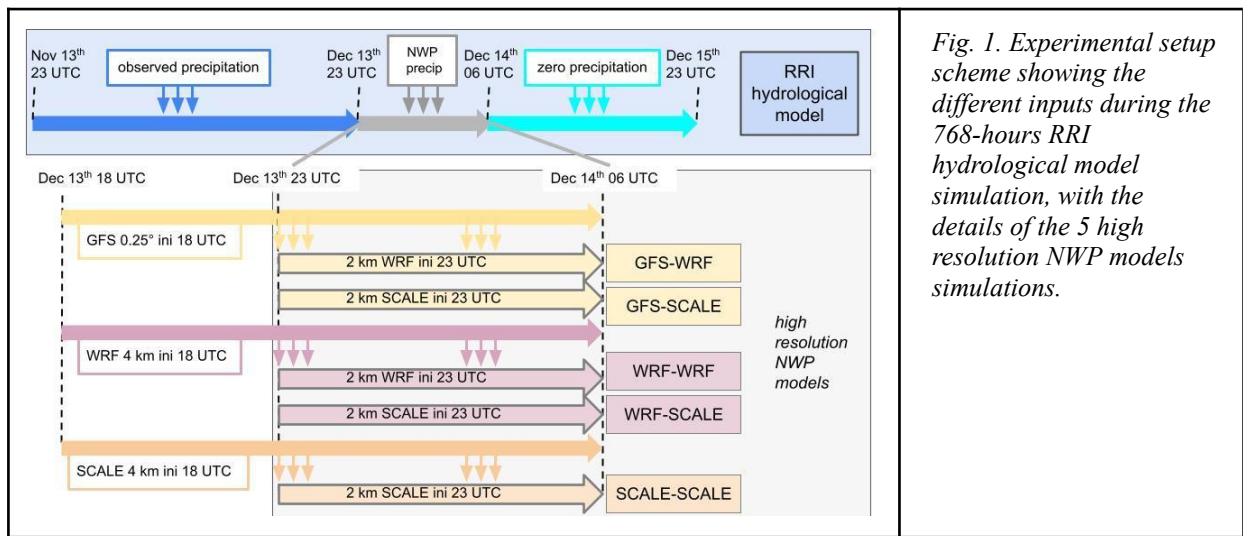


Fig. 1. Experimental setup showing the different inputs during the 768-hours RRI hydrological model simulation, with the details of the 5 high resolution NWP models simulations.

### 3. Results and conclusions

NWP forecasts using GFS and 4km-SCALE as IC-BC produced no precipitation over the SR basin, while the ones using 4km-WRF, forecasted precipitation over the basin approximately 1 hour earlier compared to the radar estimated precipitation (not shown). Figure 2 presents the hydrographs obtained by forcing the RRI model with WRF-WRF (blue line) and WRF-SCALE (green line) forecasted precipitation compared to the observed one at two water level sensors sites. Results show a close agreement between observed and predicted river discharge, especially when using WRF-SCALE forecasted precipitation as input for the hydrological model. Preliminary results coupling NWP and hydrological models are very promising and motivate to further improve both models in the near future.

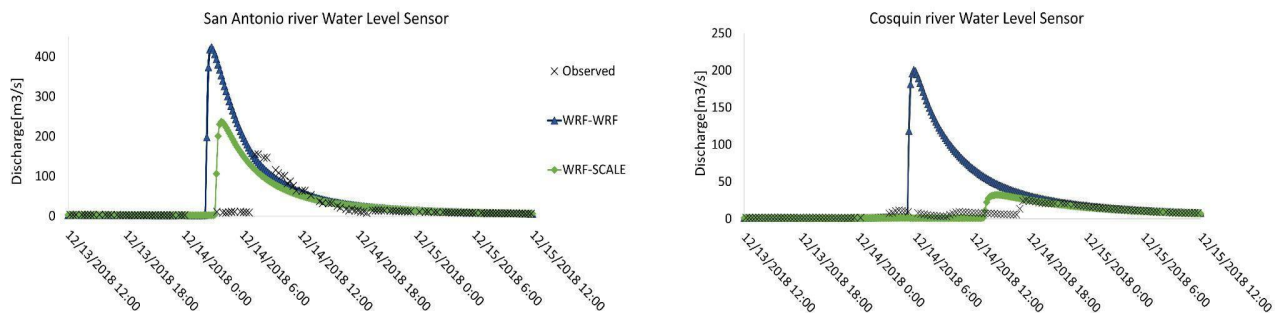


Fig. 2. Observed (black line) and WRF-WRF (blue line) and WRF-SCALE (green line) simulated hydrographs (Left: San Antonio river; Right: Cosquin river).

### References

1. López, S., Kakinuma, D., Aida, K., Ushiyama, T., Kazimierski, L., Re, M., Catalini, C., García, C. M., Saulo, C. & Miyoshi, T. (2023). Distributed Hydrological Modeling of Suquia's Basin, for Flood Warning System. *Proceedings of the 40th IAHR World Congress*.
2. Sayama, T., Ozawa, G., Kawakami, T., Nabesaka, S. & Fukami, K. (2012). Rainfall-runoff-inundation analysis of the 2010 Pakistan flood in the Kabul River basin. *Hydrological Science Journal*, 298-311.

# **A non-hydrostatic ocean model for multi-scale/multi-process simulations**

Yoshimasa MATSUMURA<sup>1</sup>, Yasuhiro HOSHIBA<sup>1</sup>, Yasushi FUJIWARA<sup>2</sup>,  
Shinichiro KIDA<sup>3</sup> and Takateru YAMAGISHI<sup>4</sup>

<sup>1</sup>The University of Tokyo, Kashiwa, Japan

<sup>2</sup>Kobe University, Kobe, Japan

<sup>3</sup>Kyushu University, Kasuga, Japan

<sup>4</sup>Research Organization for Information Science and Technology, Kobe, Japan  
(Corresponding author: Y. Matsumura, e-mail: ymatsu@aori.u-tokyo.ac.jp)

This work is distributed under the Creative Commons Attribution 4.0 License (CC BY 4.0)

## **1. Introduction**

Previously, non-hydrostatic ocean modeling had been limited to idealized simulations within narrow rectangular domains or two-dimensional planes. Successive progress of computers has made it possible to perform high-resolution ocean simulations with realistic setups dealing with small-scale phenomena where the hydrostatic assumption does not hold. To meet the present and future needs of advanced ocean modeling, we have developed a general-purpose non-hydrostatic ocean model named *kinaco*, which employs the multigrid-preconditioned conjugate-gradient (MGCG) method as a pressure solver [4]. The applications of the model include wave-resolving simulation [1], lower-trophic ecosystem modeling [3], and dispersed multiphase flow simulations by utilizing built-in Lagrangian particle tracking [2,5].

## **2. Model description**

Kinaco is a three-dimensional finite-volume CFD code of incompressible Boussinesq fluid written in Fortran. The coordinate system is horizontally orthogonal-curvilinear and vertically z-level. The non-linear term for momentum advection is represented by an energy-conserving vector-invariant form. The implicit free-surface scheme integrated within the non-hydrostatic pressure solver correctly represents the dispersion relation of deep-water waves. Potential temperature, salinity, and other tracers are predicted by integrating advection-diffusion equations, and the ocean density is diagnosed by the approximated equation of state for seawater from the distribution of tracers. Kinaco also has a built-in particle tracking module that enables Lagrangian modeling of suspended and dissolved materials, where particles can dynamically and thermodynamically interact with the velocity field of the continuous fluid phase.

### 3. Multigrid pressure solver

The MGCG solver is used to obtain a pressure field that ensures the incompressibility of the fluid in each time-step interval. The grid thickness of the uppermost layer allows variability to represent free-surface elevation, and the dynamic boundary condition for surface pressure yields the Helmholtz equation to be solved. We adopt SAI smoother in the multigrid preconditioner as it exhibits a better convergence rate even with complex domain geometry such as narrow straits or steep seamounts. The solver converges in  $\sim 10$  iterations with the relative criterion  $10^{-8}$  and shows good scalability for problem size and magnitude of parallelization. The cost of the non-hydrostatic pressure solver is typically no greater than 50% of the total time. The GPU-ported version of the solver also shows good performance even with multi-GPU configurations [6].

#### References (in alphabetical order according to author)

1. Fujiwara, Y., Y. Yoshiakawa and Y. Matsumura (2018): A Wave-Resolving Simulation of Langmuir Circulations with a Nonhydrostatic Free-Surface Model: Comparison with Craik–Leibovich Theory and an Alternative Eulerian View of the Driving Mechanism, *J. Phys. Oceanogr.*, **48**, 1691-1708.
2. Hoshiba, Y. et al. (2019): A simulation study on effects of suspended sediment through high riverine discharge on surface river plume and vertical water exchange, *Estuar. Coast. Shelf Sci.*, **228**, 106352.
3. Hoshiba, Y. et al. (2021): Biogeochemical impacts of flooding discharge with high suspended sediment on coastal seas: a modeling study for a microtidal open bay, *Sci. Rep.*, **11**, 21322.
4. Matsumura, Y. and H. Hasumi (2008): A non-hydrostatic ocean model with a scalable multigrid Poisson solver, *Ocean Model.*, **24**, 15-28.
5. Matsumura, Y. and K.I. Ohshima (2015): Lagrangian modeling of frazil ice in the ocean, *Ann. Glaciol.*, **56**, 373-382.
6. Yamagishi, T. and Y. Matsumura (2016): GPU Acceleration of a non-hydrostatic ocean model with a multigrid Poisson/Helmholtz solver, *Proc. Comp. Sci.*, **80**, 1658-1669.

Session C:  
Cloud Physics, Radiation, Lightning 1

## **Lagrangian modeling of cloud microphysics: progress and prospects**

Wojciech W. GRABOWSKI<sup>1</sup>, Kamal Kant CHANDRAKAR<sup>1</sup>, Hugh MORRISON<sup>1</sup>,  
Shin-Ichiro SHIMA<sup>2</sup>, and Piotr DZIEKAN<sup>3</sup>

<sup>1</sup>NCAR, Boulder, USA

<sup>2</sup>University of Hyogo, Kobe, Japan

<sup>3</sup>Institute of Geophysics, Faculty of Physics, University of Warsaw, Warsaw, Poland  
(Corresponding author: Wojciech W. GRABOWSKI, e-mail: grabow@ucar.edu)

This work is distributed under the Creative Commons Attribution 4.0 License (CC BY 4.0)

Lagrangian particle-based microphysics is a novel approach to represent processes leading to cloud and precipitation formation in cloud-scale numerical models. This approach replaces traditional methodologies based on Eulerian microphysical schemes that use density-like variables to represent liquid and solid cloud and precipitation particles. Lagrangian microphysics applies computational point particles, super-droplets (or super-particles), to represent the enormous number of aerosol, cloud, and precipitation particles typically present inside the grid cell of a cloud model. Each super-particle represents a multitude of natural cloud particles and an additional parameter, the multiplicity, is used to describe the total number of real particles each super-particle represents. The super-particles are traced in the physical space using the model-predicted flow field, and they grow as they move with the flow. Lagrangian approach promises to eliminate key problems of Eulerian schemes, see Grabowski et al. (2019).

When compared to traditional Eulerian bin microphysics in simulations of warm (ice-free) nonprecipitating clouds, Lagrangian microphysics eliminates numerical diffusion of Eulerian approaches (Grabowski 2020). It also allows physically-based representations of unresolved small-scale processes driven by vertical velocity fluctuations and entrainment/mixing (Chandrakar et al. 2021). The focus of current studies involving Lagrangian microphysics concerns representation of collisional growth of cloud droplets and warm rain development. Applying 1D kinematic tests, Hill et al. (2023) suggest that rain formation simulated by the Lagrangian microphysics is still uncertain because of a relatively large spread of model results when compared to the Eulerian bin microphysics. It is unclear where the differences between Eulerian and Lagrangian schemes in box and 1D kinematic frameworks come from. It is possible that the discrepancies between

Lagrangian models come from different numbers of super-droplets applied in the simulations or different discretizations of the initial CCN distribution. Both impact the representation of the droplet spectra and thus droplet collisions above the cloud base. It is also possible that various approaches to represent stochastic aspects of droplet collisions in Lagrangian schemes impact simulated rain formation. Some of those issues are investigated in Morrison et al. (2023) using various numerical representations of super-droplet collisions, including the stochastic all-or-nothing super-droplet method (SDM; Shima et al. 2009) and a version of SDM that applies a fractional approach similar to the average impact method. Rain initiation averaged over many realizations of the box model in Morrison et al. (2023) is delayed and rain variability increases as the number of super-drops per collision volume ( $N_{SD}$ ) is decreased using SDM. In contrast, rain initiation only weakly depends on the number of super-drops per grid cell  $N_{SD}$  in the dynamic multidimensional cloud simulations. This is explained by the interactions between microphysical and dynamical processes occurring in different grid volumes in multidimensional simulations. Details of simulation results highlighted above will be discussed at the conference. Challenges to model other microphysical processes, such as drop collisional breakup and ice initiation and growth, as well as ice melting, will also be briefly discussed.

## References:

- Chandrakar, K. K., W. W. Grabowski, H. Morrison, and G. H. Bryan (2021): Impact of entrainment-mixing and turbulent fluctuations on droplet size distributions in a cumulus cloud: An investigation using Lagrangian microphysics with a sub-grid-scale model. *J. Atmos. Sci.*, 78, 2983-3005.
- Grabowski, W. W. (2020): Comparison of Eulerian bin and Lagrangian particle-based microphysics in simulations of nonprecipitating cumulus. *J. Atmos. Sci.*, 77, 3951-3970.
- Grabowski, W. W., H. Morrison, S. Shima, G. C. Abade, P. Dziekan, and H. Pawlowska (2019): Modeling of cloud microphysics: Can we do better? *Bull. Amer. Meteor. Soc.*, 100, 655-672.
- Hill, A. A., and Coauthors (2023): Toward a numerical benchmark for warm rain processes. *J. Atmos. Sci.*, 80, 1329–1359.
- Morrison H., K. K. Chandrakar, S. Shima, P. Dziekan, and W. W. Grabowski (2023): Impacts of stochastic coalescence variability on warm rain initiation using Lagrangian microphysics in box and large-eddy simulations. *J. Atmos. Sci.* (submitted).
- Shima, S.-I., K. Kusano, A. Kawano, T. Sugiyama, and S. Kawahara (2009): The super-droplet method for the numerical simulation of clouds and precipitation: A particle-based and probabilistic microphysics model coupled with a non-hydrostatic model, Q. J. Roy. Meteor. Soc., 135, 1307–1320.

# Unraveling the Microphysics of Isolated Cumulonimbus Clouds: Advances in Simulation with the Super-Droplet Method (SDM)

Manhal ALHILALI<sup>1</sup>, Shin-ichiro SHIMA<sup>1</sup>, Soumya SAMANTA<sup>2</sup> and Thara PRABHAKARAN<sup>2</sup>

<sup>1</sup> University of Hyogo, Kobe, Japan

<sup>2</sup> Indian Institute of Tropical Meteorology, Pune, India

(Corresponding author: Shin-ichiro SHIMA, e-mail: s\_shima@gsis.u-hyogo.ac.jp)

This work is distributed under the Creative Commons Attribution 4.0 License (CC BY 4.0)

## Abstract

The Super-Droplet Method (SDM) is a numerical technique that greatly enhances the precision of cloud microphysics simulations while reducing computational requirements compared to multi-dimensional bin schemes. It successfully addresses various limitations present in bin and bulk models (Grabowski et al., 2019). This research specifically focuses on utilizing the SDM model, which has been previously integrated into SCALE, a library of weather and climate models for Earth and other planets (Nishizawa et al., 2015; Sato et al., 2015; <https://scale.riken.jp/>). As a result, a mixed-phase cloud model called SCALE-SDM was constructed, representing a significant advancement in this field. SCALE-SDM explicitly predicts ice particle morphology, eliminating the need for assumptions about ice categories or mass-dimension relationships, as shown in (Shima et al., 2020), where a 2D LES of a cumulonimbus was conducted for performance evaluation.

Our main objective is to conduct comprehensive atmospheric simulations using both the SCALE-SDM model and conventional schemes. We primarily focus on studying the spatio-temporal evolution of cloud clusters, particularly those experiencing heavy precipitation events. To achieve this, we conduct a detailed comparison of the simulated data from the simulation with both SCALE-SDM and conventional schemes, in addition to observations gathered from in-situ aircraft measurements and polarimetric Doppler radar data. We also evaluate grid convergence and the influence of aerosols on the simulations.

Preliminary results from our ongoing investigation demonstrate the promising consistency of the SCALE-SDM model with observational data. Additionally, we have observed significant improvements in the numerical convergence characteristics of the SCALE-SDM model, further reinforcing its accuracy and reliability. Under the parameter range we tested, the internal structure of the cumulonimbus was sensitive to the number concentrations of mineral dust and hygroscopic aerosols, but the precipitation amount was less sensitive to aerosol particles.

During this presentation, we will highlight the crucial findings from our work on simulating isolated convective clouds. We will provide insights into the ongoing efforts for the development and refinement of the SCALE-SDM model. Furthermore, we will outline the prospective trajectory of our research, emphasizing how we plan to enhance and expand the capabilities of the SCALE-SDM model.

## Acknowledgments

This research is supported by JST [Moonshot R&D][Grant Number JPMJMS2286]. SS was supported by JSPS KAKENHI, Grant Number 20H00225 and 23H00149. This research partly used the computational resources of Hokkaido University through the HPCI System Research Project (project IDs: hp200078, hp210059, hp220062, and hp230166), and the computer facilities of the Center for Cooperative Work on Data science and Computational science, University of Hyogo. The SCALE library was developed by Team-SCALE of RIKEN Center for Computational Sciences (<https://scale.riken.jp/>, last access: 31 July 2023).

## References

- Grabowski, W. W., Morrison, H., Shima, S.-I., Abade, G. C., Dziekan, P., & Pawlowska, H. (2019). Modeling of Cloud Microphysics: Can We Do Better? *Bulletin of the American Meteorological Society*, *100*(4), 655–672. <https://doi.org/10.1175/BAMS-D-18-0005.1>
- Nishizawa, S., Yashiro, H., Sato, Y., Miyamoto, Y., & Tomita, H. (2015). Influence of grid aspect ratio on planetary boundary layer turbulence in large-eddy simulations. *Geoscientific Model Development*, *8*(10), 3393–3419. <https://doi.org/10.5194/gmd-8-3393-2015>
- Sato, Y., Nishizawa, S., Yashiro, H., Miyamoto, Y., Kajikawa, Y., & Tomita, H. (2015). Impacts of cloud microphysics on trade wind cumulus: Which cloud microphysics processes contribute to the diversity in a large eddy simulation? *Progress in Earth and Planetary Science*, *2*(1), 23. <https://doi.org/10.1186/s40645-015-0053-6>
- Shima, S., Sato, Y., Hashimoto, A., & Misumi, R. (2020). Predicting the morphology of ice particles in deep convection using the super-droplet method: Development and evaluation of SCALE-SDM 0.2.5-2.2.0, -2.2.1, and -2.2.2. *Geoscientific Model Development*, *13*(9), 4107–4157. <https://doi.org/10.5194/gmd-13-4107-2020>

# Process-oriented simulations of winter snowfall in Japan

Akihiro Hashimoto<sup>1</sup>, Masaaki Ishizaka<sup>2</sup>, Hiroki Motoyoshi<sup>2</sup>, Katsuya Yamashita<sup>2</sup>,  
Sento Nakai<sup>2</sup>, and Satoru Yamaguchi<sup>2</sup>

<sup>1</sup>Meteorological Research Institute, Japan Meteorological Agency, Tsukuba, Japan

<sup>2</sup>Snow and Ice Research Center, National Research Institute for Earth Science and  
Disaster Resilience, Nagaoka, Japan

(Corresponding author: Akihiro Hashimoto, e-mail: ahashimo@mri-jma.go.jp)

This work is distributed under the Creative Commons Attribution 4.0 License (CC BY 4.0)

## 1. Introduction

Ice particles in the atmosphere have a wide range of microphysical properties, which basically depend on local thermodynamic conditions. Local thermodynamic conditions change in various scales of time and space. Nakamura (2019) shows that characteristics of snow crystal in surface snowfall are different depending on the position in a thousand-kilometer wide cyclone. We performed numerical simulations using a weather prediction model incorporating the process tracking scheme (Hashimoto et al., 2020) to address the spatial distribution of the characteristics of snow crystals over the entire Sea of Japan in a winter cold outbreak event.

## 2. Model description and experimental setup

Numerical simulations were carried out using the Japan Meteorological Agency's non-hydrostatic model incorporating the process tracking scheme (Hashimoto et al., 2020), and the contributions of depositional growth and riming growth processes to hourly surface precipitation were investigated. Regarding the depositional growth of snow crystals, its contribution was evaluated separately according to local temperature and humidity. Changes in the contribution due to different temperature and humidity represent changes in the habit of snow crystals (Nakaya, 1954).

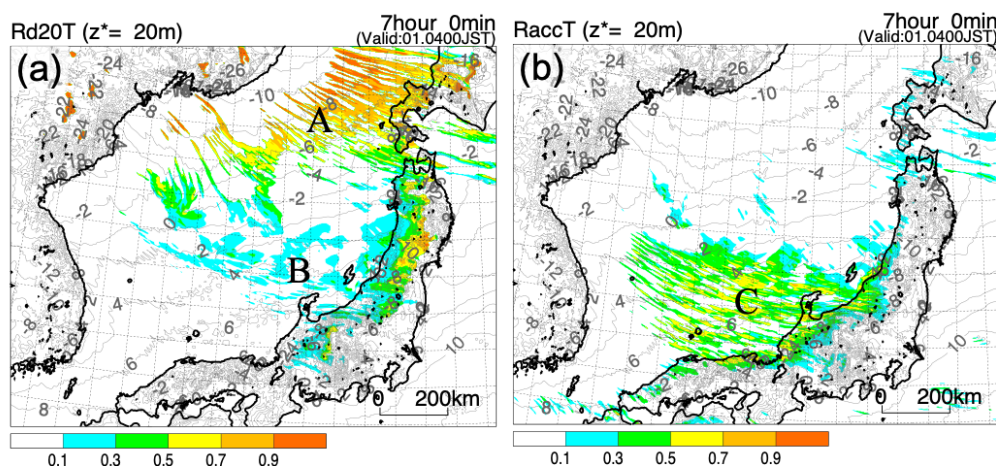


Fig. 1. Contribution ratio of (a) depositional growth of ice particles (cloud ice, snowflakes, graupel) in the temperature range  $-36$  to  $-20$  °C to the hourly rainfall above ground [0-1]. (b) Same as (a) but for contribution ratio of riming growth [0-1]. The solid gray lines indicate surface air temperature.

### 3. Results and conclusions

Figure 1a shows the result of the numerical simulations for the contribution ratio of depositional growth of ice particles under low-temperature conditions from  $-36$  to  $-20$  °C to surface precipitation at 04:00 on January 1, 2021 (JST: UTC+9). Depositional growth in this temperature range considerably contributes to the surface precipitation, in the precipitation area associated with streak clouds over the northeast of the Sea of Japan (A in Fig. 1a), where the surface air temperature is low (around  $-8$ °C). Some precipitation bands with relatively high cloud top altitudes extending northeastward from the Japan sea Polar airmass Convergence Zone (JPCZ) (B in Fig. 1a) showed contributions of 10 to 30%, and some reached the coasts of the Hokuriku and Tohoku regions. At Nagaoka city in winter, snow crystals with cold-type habits have been observed sometimes during snowfall associated with low-pressure systems passing south coast of Japan and JPCZ (Ishizaka et al., 2017; Motoyoshi et al., 2019). The simulation results may represent a facet of the generation and transportation processes of such snow crystals with cold-type habits. On the other hand, depositional growth in the temperature range from  $-20$  to  $-10$  °C mainly contributed to the precipitation around the middle of the Sea of Japan, where the surface air temperature is higher (around  $0$ °C) (not shown).

Figure 1b shows the contribution ratio of riming growth. In the 200 km wide area of southwest from the JPCZ with high surface temperature (C in Fig. 1b, around  $5$  °C), the riming growth contributed around 70% to the surface precipitation. In the same region, the contribution of graupel particles was also high (not shown). The numerical simulations using the process tracking scheme enabled us to quantify the contribution of the microphysical processes to surface precipitation over the Sea of Japan, which showed that the snow crystal habit systematically changes in a thousand-kilometer scale covering the entire Sea of Japan depending on the environmental conditions such as surface air temperature.

### Acknowledgements

This work was supported in part by the Japan Society for the Promotion of Science, KAKENHI Grant Numbers 19K04978, 20H04196, and 22K03724.

### References

1. Hashimoto, A., H. Motoyoshi, N. Orikasa, and R. Misumi, 2020: Process-tracking scheme based on bulk microphysics to diagnose the features of snow particles. *SOLA*, **16**, 51-56, <https://doi.org/10.2151/sola.2020-009>.
2. Ishizaka, M., H. Motoyoshi, and S. Yamaguchi, 2017: Low temperature habits snow crystals brought by a low pressure system and relevance to an avalanche, *Summaries of JSSI & JSSE Joint Conference on Snow and Ice Research – 2017 in Tokamachi*, 106, [https://doi.org/10.14851/jcsir.2017.0\\_106](https://doi.org/10.14851/jcsir.2017.0_106).
3. Motoyoshi, H., T. Fujino, K. Kanda, and M. Ishizaka, 2019: On snow crystals like column with multiple planes observed at Hokuriku area, *Summaries of JSSI & JSSE Joint Conference on Snow and Ice Research – 2019 in Yamagata*, 38, [https://doi.org/10.14851/jcsir.2019.0\\_38](https://doi.org/10.14851/jcsir.2019.0_38).
4. Nakamura, K., 2019: Implementation and demonstration of a system for the forecasting of surface avalanche potential caused by snowfall from a cyclone, *J. Disaster Res.*, **14**, 1201-1226, <https://doi.org/10.20965/jdr.2019.p1201>.
5. Nakaya, U., 1954: *Snow Crystals: Natural and Artificial*. Harvard University Press, 510 pp.

# Future change of the solid precipitation in Hokkaido, Japan ~ an insight from process tracking cloud microphysical model

Moeka Kamada<sup>1</sup>, Yousuke Sato<sup>2</sup>, and Akihiro Hashimoto<sup>3</sup>

<sup>1</sup> Graduate School of Science, Hokkaido University, Sapporo, Japan

<sup>2</sup> Faculty of Science, Hokkaido University, Sapporo, Japan

<sup>3</sup> Meteorological Research Institute, Tsukuba, Japan

(Corresponding author: Yousuke Sato, e-mail: [yousuke.sato@sci.hokudai.ac.jp](mailto:yousuke.sato@sci.hokudai.ac.jp))

This work is distributed under the Creative Commons Attribution 4.0 License (CC BY 4.0)

## 1. Introduction

The microphysical properties of the solid precipitation particles such as the shape, the density, and the extent of riming, which is often called “habit” are closely relating to the snow quality. It is known that they also affect the occurrence of the snow avalanche, and therefore, it is important to understand the microphysical properties of the solid precipitation to predict snow quality and to prevent the disaster in cold region such as Hokkaido, northern part of Japan. Recent studies reported that the precipitation amount and the ratio of the solid precipitation will be changed over Hokkaido in the future climate due to the increase of the temperature (e.g., Kawazoe et al. 2020). The temperature increase will affect the microphysical properties of the solid precipitation because they are largely dependent upon the temperature and relative humidity (supersaturation) in the clouds (Nakaya 1954, Pflaum and Pruppacher 1979). However, the previous studies did not focus on the microphysical properties of the solid precipitation in future climate. In this study, a Process Tracking Model (PTM, Hashimoto et al. 2020), which *tracks the mass compositions of different classes of ice particles, using their microphysical process of origin, such as water vapor deposition and riming*, was implemented into a meteorological model, Scalable Computing for Advanced Library and Environment (SCALE: Nishizawa et al. 2015, Sato et al. 2015) to predicts the habit of the solid precipitation. Using the model, we aimed to understand the future change of the microphysical properties of the solid precipitation in future climate in Hokkaido.

## 2. Model description and experimental setup

The model used in this study is SCALE, coupled with the PTM. The components used in this study were the same as Inatsu et al. (2020) except for the cloud microphysical model. The double-moment bulk microphysical scheme (Seiki and Nakajima 2014) was used, and the breakdown of the deposition growth and the riming in each category of the solid precipitation (ice, snow, and graupel) was predicted by the PTM. Using the model, we conducted the dynamical down scaling (DDS) simulation from the Mesoscale ANALyses (MANL) data for a winter over the Hokkaido (Fig. 1a). For the DDS simulations, the geopotential height, horizontal wind, air temperature, surface pressure, relative humidity, skin temperature and soil moisture of MANL were used for the initial and boundary condition. The DDS calculations were conducted from 18 UTC to 00 UTC the next days (30 hours) for each day from December, 2020 to February 2021. In addition, we conducted the pseudo-global warming simulation for each day. For the pseudo-global warming simulation, the mean variance of the temperature profile between the present days and the future climate of 4K scenario by the database for policy decision making for

future climate change (d4PDF: Mizuta et al. 2017) was added to the temperature of MANL data to represent the impacts of the global warming. The relative humidity was fixed for representing the increase of the vapor in the future climate. The horizontal resolution was 1 km. The vertical layer was divided into 57 from the surface to the model top (20 km). The layer thickness was increased from 40 m to 650 m.

### 3. Result and conclusion

Figure 1b shows the difference of the surface flux of each category of solid precipitation average over the Hokkaido during the target period. The results indicate that the contribution of the depositional growth between  $-20^{\circ}\text{C}$  and  $-36^{\circ}\text{C}$  to surface precipitation will be decreased in the future climate, in contrast, that of the depositional growth with higher temperature will be increased. As well as the depositional growth, the contribution of the riming will also be increased in the future climate, because the temperature in most of the cloud in future climate simulation was between  $-5^{\circ}\text{C}$  and  $-15^{\circ}\text{C}$ , which is suitable for the riming (Pflaum and Pruppacher 1979). These results suggest that the solid precipitation in Hokkaido will become similar to that over the Hokuriku area which is well known as heavy snow area in Japan.

### References

1. Hashimoto, A., H. Motoyoshi, N. Orikasa, and R. Misumi, (2020), Process-Tracking Scheme Based on Bulk Microphysics to Diagnose the Features of Snow Particles, *SOLA*, **16**, 51-56.
2. Inatsu, M., S. Tanji, and Y. Sato, (2020), Toward predicting expressway closures due to blowing snow events, *Cold Reg. Sci. Tech.*, **177**, 103123, doi: 10.1016/j.coldregions.2020.103123
3. Kawazoe, S., M. Inatsu, T. J. Yamada, and T. Hoshion, (2020), Climate Change Impacts on Heavy Snowfall in Sapporo Using 5-km Mesh Large Ensemble Simulations, *SOLA*, **16**, 223-239.
4. Nakaya, (1954), Snow crystals, natural and artificial. *Harvard Univ. Press*, 510 pp.
5. Nishizaea, S., H. Yashito, Y. Sato, Y. Miyamoto, and H. Tomita, (2015), Influence of grid aspect ratio on planetary boundary layer turbulence in large-eddy simulations, *Geosci. Model. Dev.*, **8**, 3393-3419.
6. Pflaum, J., and H. R. Pruppacher, (1979), A wind tunnel investigation of the growth of graupel initiated from frozen drops. *J. Atmos. Sci.*, **36**, 680-689.
7. Sato, Y., S. Nishizawa, H. Yashiro, Y. Miyamoto, Y. Kajikawa, and H. Tomita, (2015), Impacts of cloud microphysics on trade wind cumulus: which cloud microphysics processes contribute to the diversity in a large eddy simulation?, *Prog. Earth Planet. Sci.*, **2**, doi: 10.1186/s40645-015-0053-6
8. Seiki, T., and T. Nakajima, (2014), Aerosol effects of the condensation process on a convective cloud simulation, *J. Atmos. Sci.*, **71**, 833-853

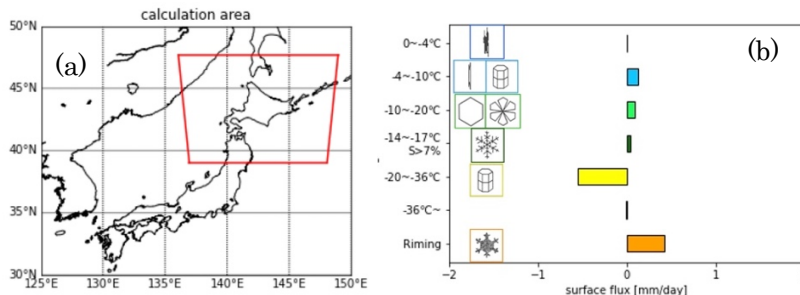


Fig.1 (a) Calculation domain shown as red rectangle. (b) Difference in the contribution of the depositional growth with temperature range of (blue)  $0 \sim -4^{\circ}\text{C}$ , (sky blue)  $-4 \sim -10^{\circ}\text{C}$ , (light green)  $-10 \sim -20^{\circ}\text{C}$ , (green)  $-14 \sim -17^{\circ}\text{C}$  with super saturation over 7 %, (yellow)  $-20 \sim -36^{\circ}\text{C}$ , (grey) lower than  $-36^{\circ}\text{C}$ , and riming to the surface flux of solid precipitation between the present day and future climate averaged over Hokkaido during whole target days.

# Effects of introducing three types of snow particle shapes and bimodal raindrops size distribution into cloud microphysics scheme

Yasutaka IKUTA<sup>1,2</sup>, Masaki SATOH<sup>2</sup>, Woosub ROH<sup>2</sup>, Shuhei MATSUGISHI<sup>2</sup>,  
Naomi KUBA<sup>2</sup>, Tatsuya SEIKI<sup>3</sup>, Akihito UMEHARA<sup>1</sup>, Hisaki EITO<sup>1</sup>

<sup>1</sup>Meteorological Research Institute, Japan Meteorological Agency, Tsukuba, Japan

<sup>2</sup>Atmosphere and Ocean Research Institute, The University of Tokyo, Kashiwa, Japan

<sup>3</sup>Japan Agency for Marine-Earth Science and Technology, Yokohama, Japan

(Corresponding author: Yasutaka IKUTA, e-mail: yasutaka.ikuta@mri-jma.go.jp)

This work is distributed under the Creative Commons Attribution 4.0 License (CC BY 4.0)

## 1. Introduction

There are many unresolved elementary processes of cloud precipitation processes, and the diversity of solid precipitation particles makes the modeling of cloud precipitation processes uncertain. In recent years, as observational technology has improved, studies have been conducted to use wide-area and continuous remote sensing observations by radar and satellites to improve cloud physics schemes in numerical models. In the research project ULTIMATE (ULtra sIte for Measuring the Atmosphere of Tokyo metropolitan Environment: Satoh et al. 2022), which is a collaborative research project between numerical models and observation data in the metropolitan area, the numerical model was validated using ground-based polarimetric radar and optical disdrometer as reference values, and the cloud microphysics scheme was improved.

## 2. Methods

The JMA non-hydrostatic model ASUCA was used, and the 3-ice 6-class 1-moment bulk scheme (Ikuta et al. 2021) was used as the cloud microphysics scheme. To compare the model with polarimetric radar observation, the polarimetric radar observation was simulated from the model predictions using a simulator. The particle size distribution (PSD) of raindrops in the new scheme was enhanced to the new bimodal PSD based on observed PSD by an optical disdrometer. Three types of shape characteristics were introduced to the snow particles in the new scheme. The implemented shapes were assumed plate, dendrite, and aggregation. The same assumptions for precipitation particles in the cloud microphysics scheme were used in the polarimetric radar simulator.

### 3. Results and conclusion

The sensitivity experiment was conducted in the case of Typhoon Faxai (2019). Figure 1 shows the observed and simulated RHI scans at 1800 UTC on September 8, 2019. In the current scheme, the specific differential phase (KDP) was over-predicted below 5 km altitude and under-represented at 6–10 km altitude compared to the observed values. KDP in the new scheme was closer to the observed values. The improvement in the lower layers was due to the improved PSD of rain, while the improvement in the upper layers was due to the change in the shapes of snow particles. In this study, the numerical weather prediction model was validated using ground-based polarimetric radar and optical disdrometer to improve the cloud microphysics scheme. The knowledge gained from the prediction of the vertical structure of the precipitation system using the new cloud microphysics scheme supported by observations will contribute significantly to the advancement of the cloud microphysics scheme and the reduction of uncertainty in cloud precipitation processes. It is also expected to contribute to the advancement of the understanding of cloud precipitation processes and the accuracy of their prediction.

#### References (in alphabetical order according to author)

1. Ikuta, Y., M. Satoh, M. Sawada, H. Kusabiraki, and T. Kubota, (2021), Improvement of the cloud microphysics scheme of the mesoscale model at the Japan Meteorological Agency using space-borne radar and microwave imager of the Global Precipitation Measurement as reference, *Mon. Wea. Rev.*, **149**, 3803–3819
2. Satoh, M., and Coauthors, (2022), Evaluation of cloud and precipitation processes in regional and global models with ULTIMATE (ULTra-sIte for Measuring Atmosphere of Tokyo metropolitan Environment): A case study using the dual-polarization Doppler weather radars, *Prog. Earth and Planet. Sci.*, **9**, 51

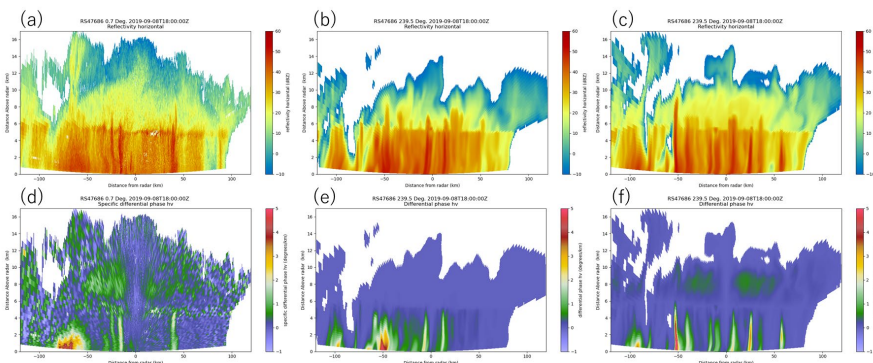


Fig. 1. (a)–(c) Reflectivities and (d)–(f) KDPs from RHI scan. Observations (left), simulations with the current scheme (middle), and simulations with the new scheme (right).

## Session D: Data assimilation 1

# **Direct Assimilation of GOES-R Geostationary Lightning Mapper (GLM) Data within JEDI LETKF and Hybrid System for Operational UFS Convection-Allowing Predictions**

Rong Kong<sup>1</sup>, Ming Xue<sup>1</sup>, Chengsi Liu<sup>1</sup>, Jun Park<sup>1</sup>, Tao Sun<sup>1</sup>

<sup>1</sup>Center for Analysis and Prediction of Storms, University of Oklahoma, USA

(Corresponding author: Ming Xue, e-mail: mxue@ou.edu)

This work is distributed under the Creative Commons Attribution 4.0 License (CC BY 4.0)

## **1. Introduction**

The Geostationary Lightning Mapper (GLM) carried by the Geostationary Operational Environmental Satellite “R-series” (GOES-R) satellites measures from space the total lightning rate in convective storms at high spatial and temporal frequencies. The products contain valuable information on convective storm activity and complement weather radar networks over mountainous regions and oceans. Recently, a research team led by CAPS/OU in USA developed direct Flash Extent Density (FED) assimilation capabilities within the Gridpoint Statistical Interpolation (GSI) data assimilation (DA) framework, which, in case studies, noticeably improved the initial representation and prediction of convective storms in numerical weather prediction models for up to several hours (Kong et al., 2020; 2022; 2023). It was found that even for continental storms, the FED DA produces positive impacts comparable to those of radar DA.

For next-generation weather forecasting, the National Weather Service is adopting the FV3 dynamical core for both global and regional (FV3-LAM, or limited area model) systems in the Unified Forecasting System (UFS). The Rapid Refresh Forecast System (RRFS) will be the next-generation convection-allowing operational weather forecasting system, employing a ~3 km grid covering North America including parts of the Atlantic and Pacific Oceans where ground-based radar data are absent. Thus effective assimilation of GLM data into operational RRFS is expected to be highly beneficial. Whereas the current generation convection-allowing High Resolution Rapid Refresh (HRRR) performs DA using Gridpoint Statistical Interpolation (GSI), the RRFS system is expected to employ the Joint Effort for DA Integration (JEDI) framework.

In this study, the existing FED DA capability in GSI is migrated into JEDIlocal ensemble transform Kalman filter (LETKF) and Pure ensemble variational (PEnVar)

frameworks coupled with FV3-LAM. Performance of FED DA using JEDI LETKF and PEnVar are compared and influence of FED DA in addition to conventional DA are examined using five convective cases in 2019.

## **2. Model description and experimental setup**

The data assimilation and forecast experiments use a single domain with horizontal grid spacing of 3 km and 310×310 horizontal grid points. The stretched vertical grid consists of 64 vertical levels. The ‘RRFS\_v1\_alpha’ physics suite with the Thompson microphysics scheme from the Common Community Physics Packages is used. The initial ensembles are from the NCEP operational Global Data Assimilation System (GDAS) EnKF forecasts valid at 1800 Z and the GDAS 3-hourly ensemble forecasts up to 9 hours provide lateral boundary conditions. FED(conventional) observations are assimilated every five(sixty) minutes within one(four)-hour DA window. Based on the final analysis, the ensuing 6-h ensemble forecasts with 40 members are made. Two sets of experiments are conducted: 1) Assimilate FED observations only using LETKF and pure EnVar for an MCS case; 2) Assimilate conventional observations with (ConvFED) and without (OnlyConv) FED observations for five convective cases. A experiment without DA (NoDA) is also compared with the above DA experiments.

## **3. Result and conclusion**

In the first set of experiment, performance of FED DA are compared among LETKF, EnVar, and NoDA for an MCS case. Both JEDI EnVar and JEDI LETKF greatly improve the Fractional Skill Scores (FSS) of the FED field relative to NoDA. JEDI PEnVar outperforms JEDI LETKF in terms of FSSs in either FED or composite reflectivity analyses and forecasts during 1-h DA cycle period and 6 h ensuing forecasts for this case. PEnVar also better captures the convective precipitation in Texas relative to LETKF for 0-3 h hourly precipitation forecasts. In the second set of experiments, both OnlyConv and ConvFED outperform NoDA in terms of ETS and RMSIs in 6-h reflectivity forecasts. ConvFED produces higher ETS and smaller RMSIs in reflectivity forecasts relative to OnlyConv, suggesting positive impacts of FED DA on storm forecasts.

# Exploring the Advantages of Assimilating High Temporal Frequency Satellite Microwave Radiances

Jianyu Liang, Rakesh Teja Konduru, and Takemasa Miyoshi

RIKEN Center for Computational Science, Kobe, Japan

(Corresponding author: Jianyu Liang, e-mail: Jianyu.liang@riken.jp)

This work is distributed under the Creative Commons Attribution 4.0 License (CC BY 4.0)

## 1. Introduction

Data assimilation (DA) combines observations and model simulation to improve the weather forecast. Satellite observations play an important role in providing crucial observational data for global numerical weather prediction. Before launching new meteorological satellites, it would be beneficial to investigate their potential benefit to weather forecasts. This study uses the observation system simulation experiments (OSSE) framework to study the benefits of assimilating more frequent satellite microwave observations.

## 2. Model description and experimental setup

We used the non-hydrostatic icosahedral atmospheric model (NICAM) (Satoh et al., 2014) with a horizontal resolution of approximately 56 km and a model top situated at around 50 km. The OSSE comprises three main components: the nature run, synthetic observations, and data assimilation (DA) experiments. (1) For the nature run, we initialized it using the NCEP FNL (Final) Operational Global Analysis data. (2) Synthetic Prepbufr (conventional) observations were generated by interpolating the nature run to realistic Prepbufr observation locations, with realistic observation errors for different observation types. We added synthetic AMSU-A microwave radiance observations, utilizing a radiative transfer model called RTTOV. These synthetic microwave radiance observations were assumed to have global coverage at approximately 100 km resolution, with observation errors having a standard deviation of 0.3 K. (3) Data assimilation was performed using the LETKF (Local Ensemble Transform Kalman Filter) method with 32 ensemble members. The initial conditions of the ensemble members were obtained from the FNL at 0000 UTC on different days in the same month in different years. We then conducted a 1-month DA experiment

to spin up those ensemble members. We utilized the relaxation to prior spread method (RTPS) for covariance inflation during the assimilation process.

We performed four groups of experiments: one group with only conventional observations (NOSAT) and the others with additional satellite observations every hour (1H), every 3 hours (3H), and every 6 hours (6H). For each group, when assimilating synthetic AMSU-A observations, we tested different combinations of vertical localization parameters ( $\sigma$  in the vertical natural-log-pressure coordinate) and RTPS parameters to optimize the DA performance. The global-mean vertically averaged RMSE for temperature was used for evaluating the performance of the experiments. We picked the best experiment from each group and compared them.

### 3. Result and conclusion

Global-mean RMSE for temperature suggested poor performance of 1H compared to 3H and 6H. By calculating the second-order time derivative of the surface pressure and vertical velocity, we found that 1H has a higher model imbalance (Figure 1). We increased the observation error of the satellite observations and reran the 1H experiment (1H\_new). The imbalance measure was reduced in 1H\_new to a similar level as the other experiments, and the RMSE became the lowest. In conclusion, provided that the model has less imbalance issue, assimilating more frequent satellite microwave observations has benefits.

### References

Satoh, M., et al, 2014: The Nonhydrostatic Icosahedral Atmospheric Model: Description and development. Prog. Earth Planet. Sci., 1, 18, doi:10.1186/s40645-014-0018-1.

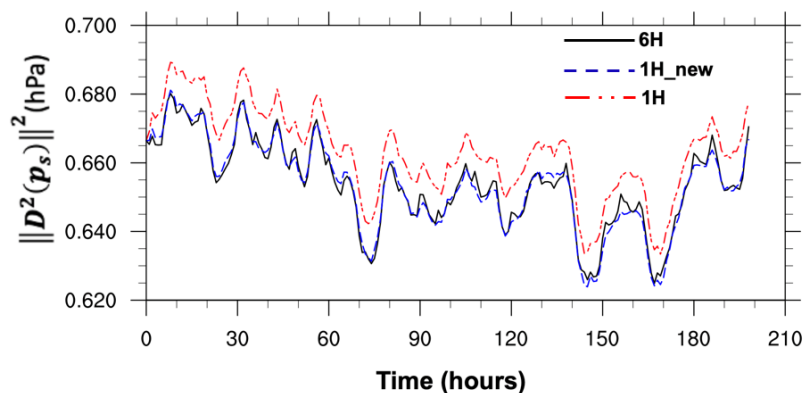


Fig. 1. RMS of the second derivative of the surface pressure from 1H (dotted dash red line), 6H (solid black line), and 1H\_new (after increasing observation error) (dashed blue line) at 500 hPa.

# Diagnostic Scale Decomposition of RMSE in Data Assimilation: Insights from OSSEs with NICAM-LETKF

Konduru Rakesh Teja<sup>1</sup>, Shigenori Otsuka<sup>1</sup>, Jianyu Liang<sup>1</sup> and Takemasa Miyoshi<sup>1</sup>

<sup>1</sup> Data Assimilation Research Team, RIKEN Center for Computational Science, Kobe, Japan.

(Corresponding author: Rakesh Teja Konduru, e-mail: rakeshteja.konduru@riken.jp)

This work is distributed under the Creative Commons Attribution 4.0 License (CC BY 4.0)

## 1. Introduction

The Root Mean Square Error (RMSE) is a standard metric in data assimilation to assess a model's accuracy, but it lacks the ability to evaluate scale-dependent errors. To address this issue, we introduced the Diagnostic Scale Decomposition of RMSE (DSDR), a method that decomposes RMSE across temporal and spatial scales, offering a more nuanced understanding of a model's accuracy. DSDR exposes a model's effectiveness in capturing phenomena of various scales, enabling targeted identification and rectification of a model's weaknesses at different scales. For instance, a model might have a low overall RMSE, suggesting good performance, but DSDR could reveal that it is only accurately capturing large-scale phenomena while struggling with small-scale details. Conversely, a model might have a high RMSE due to issues at larger scales, even if it handles small-scale details well. In this study, we apply DSDR to examine scale-dependent errors in a data assimilation experiment (DA) using the NICAM-LETKF (Terasaki and Miyoshi 2017).

## 2. Model description and experimental setup

We performed Observing System Simulation Experiments (OSSEs) using the NICAM-LETKF to assess the impact of varying AMSU-A microwave observation temporal coverages. We employed the NICAM (Sato et al. 2008) model with a horizontal resolution of 56 km and 78 vertical levels, and the model's top is located at 50 km. The single-moment bulk microphysics scheme was employed without cumulus parameterization. The NCEP FNL analysis was used to initialize the nature run at 0000 UTC on May 25, 2019. Synthetic satellite brightness temperature data were generated by using the radiative transfer for TOVS (RTTOV) version 13.0 for the channels of the Advanced Microwave Sounding Unit-A (AMSU-A) radiometer. Synthetic Prepbufr (conventional) observations were generated by considering the observation locations and error standard deviations.

We conducted a DA experiment for a month from August 1, 2019, utilizing 32 ensemble members. The ensemble initial conditions were obtained from the FNL at 0000 UTC on different days of July in different years. The relaxation to the prior spread method was employed for covariance inflation. Synthetic conventional observations were assimilated hourly, and synthetic AMSU-A observations for every six hours during a one-month spinup. Four experiments, NODA (no assimilation), NOSAT (no AMSU-A coverage), 6H and 3H (6- and 3-hourly AMSU-A coverages, respectively), were conducted post-spinup to assess the AMSU-A's impact. The RMSE was calculated between these three tests and nature for temperature, winds, and humidity.

## 3. DSDR method

This method involves the decomposition of the RMSE time series using a data-driven

adaptive technique Complete Ensemble Empirical Mode Decomposition (CEEMD; Torres et al. 2011) into different oscillatory and non-oscillatory intrinsic mode functions (IMFs). Each IMF represents a specific scale dependency embedded in the RMSE. When it comes to spatial data or a spatial series, CEEMD can be applied to each point in space, assuming that there is some form of temporal or sequential ordering in the spatial series.

#### 4. Result and conclusion

The RMSE time series of each experiment was decomposed using DSDR method into 7 Intrinsic Mode Functions (IMFs), both horizontally and vertically, at each grid point. The first 6 IMFs represented different scales: hourly, 3-hourly, daily, diurnal, mesoscale, and synoptic, while the 7th IMF symbolized a non-oscillatory component, reflecting the background mean or trend. Each scale was then assessed for its absolute errors. This scale-dependent analysis revealed notable differences between the experiments. NODA has a larger error at all scales compared to NOSAT. In contrast to NOSAT, 6H, and 3H substantially decreased the synoptic scale and high-frequency scale errors. This suggests that microwave observation assimilation has a larger impact on synoptic scales compared to NOSAT. 3H demonstrated the ability to mitigate the errors in high-frequency scales and mesoscales as compared to 6H, underlining the importance of high-frequency satellite observations.

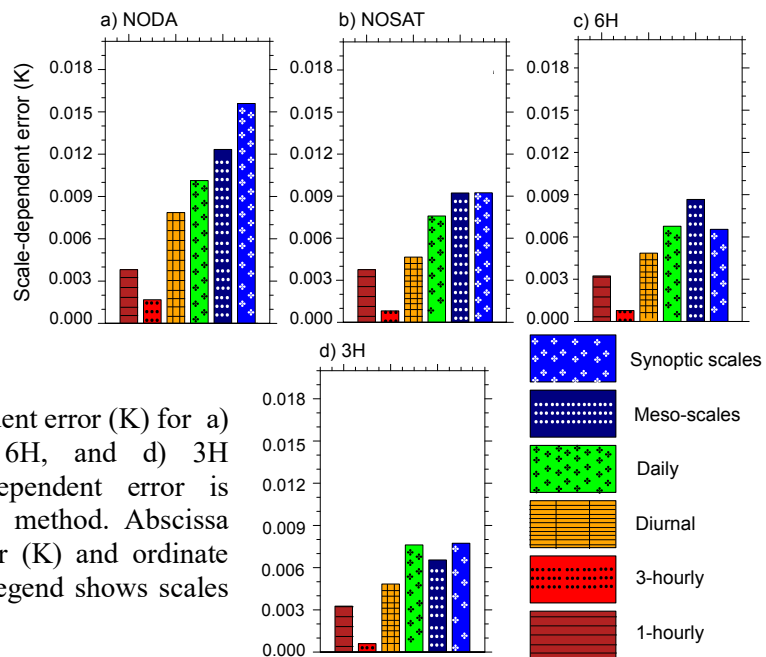


**Fig. 1** Absolute scale dependent error (K) for a) NODA, b) NOSAT, c) 6H, and d) 3H experiments. This scale-dependent error is calculated by using DSDR method. Abscissa shows scale-dependent error (K) and ordinate points to different scales. Legend shows scales used in these figures.

DSDR-based analysis demonstrated that AMSU-A assimilation reduced the RMSE at daily-to-synoptic scales (1-3 days) in both 6H and 3H compared to NOSAT. Therefore, DSDR can be used for a better understanding of the errors and for targeted model based comparisons, and it provides a better narrative about the DA's strengths and weaknesses. This method can also contribute to the design of observing systems that target specific scales, leading to more effective data assimilation.

#### References

Satoh, M., et al., (2008). Nonhydrostatic icosahedral atmospheric model (NICAM) for global cloud resolving simulations. *Journal of Computational Physics*, 227, 3486-3514.  
Terasaki, K. and Miyoshi, T., (2017). Assimilating AMSU-A Radiances with the NICAM-LETKF. *Journal of the Meteorological Society of Japan. Ser. II*, 95, 433-446.

## **Toward efficient control of extreme weather events**

Takemasa MIYOSHI<sup>1</sup>, Qiwen SUN<sup>1\*</sup>, Serge RICHARD<sup>2</sup>, Lin LI<sup>1</sup>,

Yasumitsu MAEJIMA<sup>1</sup>, Koji TERASAKI<sup>1\*</sup>

<sup>1</sup>RIKEN, Kobe, Japan

<sup>2</sup>Nagoya University, Nagoya, Japan

\*at the time of research

(Corresponding author: Takemasa MIYOSHI, e-mail: [takemasa.miyoshi@riken.jp](mailto:takemasa.miyoshi@riken.jp))

This work is distributed under the Creative Commons Attribution 4.0 License (CC BY 4.0)

Since the weather system is chaotic, small differences generally lead to big differences, particularly for storms associated with dynamical instability. We have been exploring controllability through the Control Simulation Experiment (CSE), the same procedure as the well-known Observing Systems Simulation Experiment (OSSE) but with control inputs to the nature run. Our first paper (Miyoshi and Sun, 2022) proposed the CSE for the first time with proof-of-concept experiments addressing controllability to stay on a chosen regime of the two-regime Lorenz-63 3-variable model (Fig. 1). Our second paper (Miyoshi, Sun, and Richard, 2023) investigated controllability to avoid extreme events with the Lorenz-96 40-variable model (Fig. 2). Moreover, we performed CSEs with our global and regional NWP systems for realistic typhoon and heavy rain cases, respectively. In parallel, we applied reinforcement learning to find effective control inputs to a parameter of the Lorenz-63 model. Here, we explored single-sided control inputs to increase the model's instability, considering realistic situations such that e.g., adding cloud condensation nuclei is more feasible than removing them. In this presentation, we will summarize RIKEN's activities toward efficient control of extreme weather events.

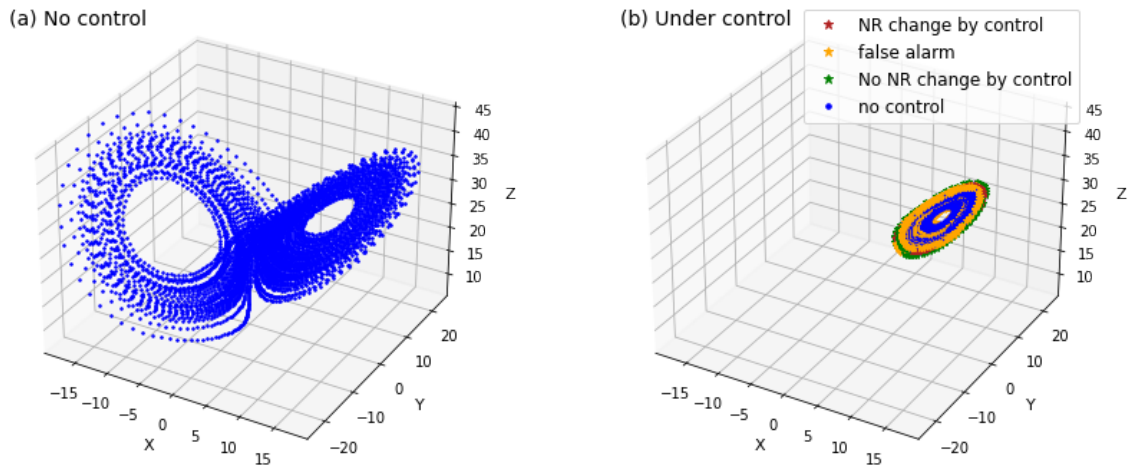


Fig. 1. (a) Lorenz's butterfly attractor and (b) that with control. Adopted from Fig. 1 of Miyoshi and Sun (2022).

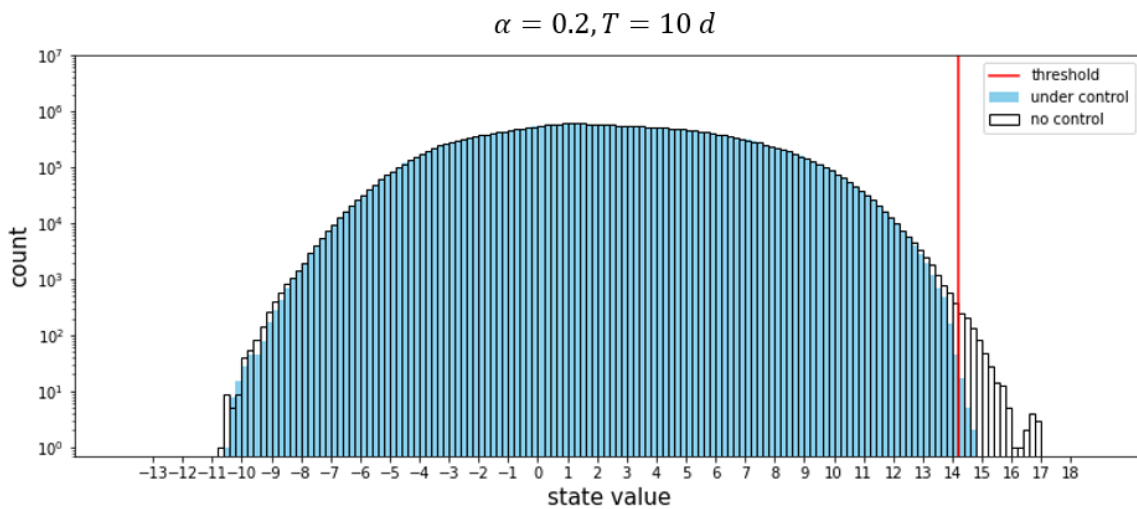


Fig. 2. Histograms of state values for 100-year Lorenz-96 model runs. White bars: no control, red line: threshold for the twice-a-year extreme value, blue bars: under control.

Adopted from Fig. 5 of Sun et al. (2023).

### References (in alphabetical order according to author)

1. Miyoshi, T. and Q. Sun, (2022), Control Simulation Experiment with the Lorenz's Butterfly Attractor, *Nonlin. Processes Geophys.*, **29**, 133-139
2. Sun, Q., T. Miyoshi, and S. Richard, (2023), Control Simulation Experiments of Extreme Events with the Lorenz-96 Model, *Nonlin. Processes Geophys.*, **30**, 117-128

# Control Simulation Experiment for August 2014 Severe Rainfall Event Using a Regional Model

Yasumitsu Maejima<sup>1</sup> and Takemasa, Miyoshi<sup>1,2,3</sup>

1. *RIKEN Center for Computational Science (R-CCS), Kobe, Japan*
2. *Department of Atmospheric and Oceanic Science, University of Maryland, College Park, MD, U.S.A.*
3. *Application Laboratory, Japan Agency for Marine-Earth Science and Technology, Yokohama, Japan*

Torrential rainfall is a threat in the modern society. To predict severe weather, convection resolving numerical weather prediction (NWP) is effective. This study explores a Control Simulation Experiment (CSE; Miyoshi et al. 2022, Sun et al. 2023) aimed at controlling precipitation amount and locations to potentially prevent catastrophic disasters by simulating different scenarios of interventions of small perturbations taking advantage of the chaotic nature of dynamics. In this study, we perform a CSE using a regional model SCALE-RM (Nishizawa et al. 2015) for a severe rainfall event which caused catastrophic landslides and 77 fatalities in Hiroshima, Japan on August 19 and 20, 2014. In this preliminary CSE, we try to control the heavy rainfall by giving the perturbations to the nature run in the OSSE at each time step from 1500 UTC to 1600 UTC on August 19, although the perturbations for all variables at all grid points are something beyond human's engineering capability.

In the series of CSEs, we consider three scenarios for giving the perturbations to the nature run : (a) perturbed all model variables in the whole domain (TEST), (b) perturbed horizontal wind in the whole domain (UV), and (c) perturbed horizontal wind below 1000-m vertical layer (UV-1000).

Figure 1 shows 6-hour-accumulated rainfall amount [mm] from 1500 UTC to 2100 UTC on August 19, 2014. In the nature run, it reaches 210 mm at the peak grid point (Fig. 1d). By contrast, the rainfall amounts decrease to 113 mm in TEST, 151 mm in UV, and 178 mm in UV-1000. By giving effective perturbations to the Nature run at each time step, we succeeded in controlling the rainfall amounts.

## References

1. Miyoshi, T. and Q. Sun, 2022: Control simulation experiment with the Lorenz's butterfly attractor, *Nonlin. Processes Geophys.*, **29**, 133-139. doi: 10.5194/npg-29-133-2022.
2. Nishizawa, S., H. Yashiro, Y. Sato, Y. Miyamoto, and H. Tomita, 2015: Influence of grid aspect ratio on planetary boundary layer turbulence in large-eddy simulations.

*Geosci. Model Dev.*, **8**, 3393–3419.

3. Sun, Q., T. Miyoshi, and S. Richard, 2023: Control Simulation Experiments of Extreme Events with the Lorenz-96 Model. *Nonlin. Processes Geophys.*, **30**, 117-128. doi:10.5194/npg-30-117-2023.

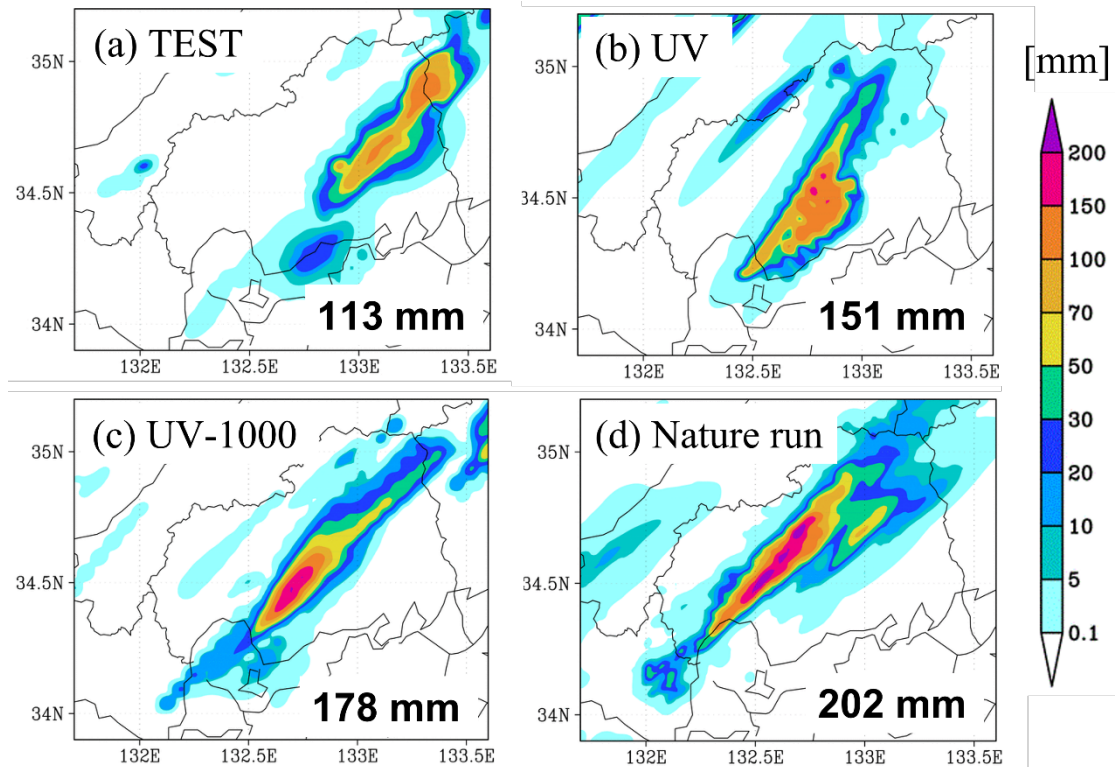


Fig. 1. 6-hour-accumulated rainfall amount [mm] from 1500 UTC to 2100 UTC on August 19, 2014 in (a) TEST, (b) UV, (c) UV-1000 and (d) the Nature run,

Session E:  
Cloud Physics, Radiation, Lightning 2

# Evaluation of cloud microphysics schemes in WRF for Hokuriku winter clouds using videosonde observations

Yuki Kanno<sup>1</sup> and Soichiro Sugimoto<sup>1</sup>

<sup>1</sup>Central Research Institute of Electric Power Industry, Abiko, Japan  
(Corresponding author: Yuki Kanno, e-mail: kanno3830@criepi.denken.or.jp)  
This work is distributed under the Creative Commons Attribution 4.0 License (CC BY 4.0)

## 1. Introduction

Hokuriku winter clouds are maritime convective clouds that are formed over Hokuriku area, coastal area in D2 of Figure 1, during cold air outbreaks from Eurasia continent. They often bring heavy snowfall in the area and frequent winter lightning with large peak positive current (Murakami et al., 2019; Takahashi et al., 2019). To predict the hazardous heavy snowfall and lightning, it is important to understand how Hokuriku winter clouds are expressed in the numerical weather prediction models and how sensitive they are to cloud microphysics schemes. In this study, we evaluated simulated hydrometers in six bulk cloud microphysics schemes in the Weather Research and Forecasting Model (WRF) from a comparison with in-situ cloud observations.

## 2. Model description and observation data

We used the latest version of the WRF (version 4.4.2). Real case simulations were conducted with initial and boundary conditions produced from 3-hourly ERA-5 reanalysis dataset and sea surface temperature produced from the ensemble median of the daily GHRSSST. The model grids consist of two nested domains with a horizontal grid spacing of 4.5 and 1.5 km, respectively (Figure 1). We evaluated six bulk cloud microphysics schemes, including WSM6, WDM6, Morrison, Thompson, Milbrandt-Yau (MY), and NSSL.

Simulated hydrometer characteristics were compared with observations by Videosonde system. The videosonde records the images of precipitation particles larger than 0.5 mm in clouds, which enables us to evaluate the simulated characteristics of snow, graupel, and hail. Special sondes were launched about 60 times at Kashiwazaki city during cold air outbreak events in three winters of 2010-2012 (see details in Takahashi et al., 2019).

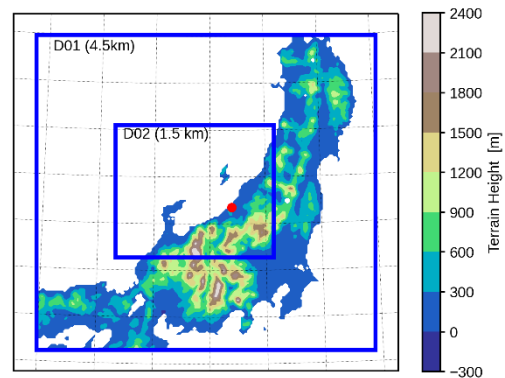


Figure 1. Calculation domain and elevation. Red circle indicates Kashiwazaki city.

## 3. Comparison of ice hydrometer characteristics

We compared the ratio of snow and graupel particles. Figure 2 shows the ratio of snow to solid hydrometer (snow and graupel) mass density at altitudes where observed solid hydrometer number density is greatest for the cold air outbreak event on Dec. 24, 2012. Simulated hydrometers for the lead times longer than 5 hours were compared. Observations showed that snow was dominant for four cases and graupel for two cases. The dominant solid hydrometers were not correctly reproduced by the six schemes across cases. However, there was a systematic difference between the schemes. For

example, snow mass density always dominates graupel mass density in Thompson, Morrison, and NSSL schemes. MY is the only scheme that varies the dominant ice hydrometer from case to case. In contrast, the number density was better reproduced in the six schemes than the mass density (figure not shown). These results suggest that MY scheme outperforms to simulate the kind of solid state of precipitation particles.

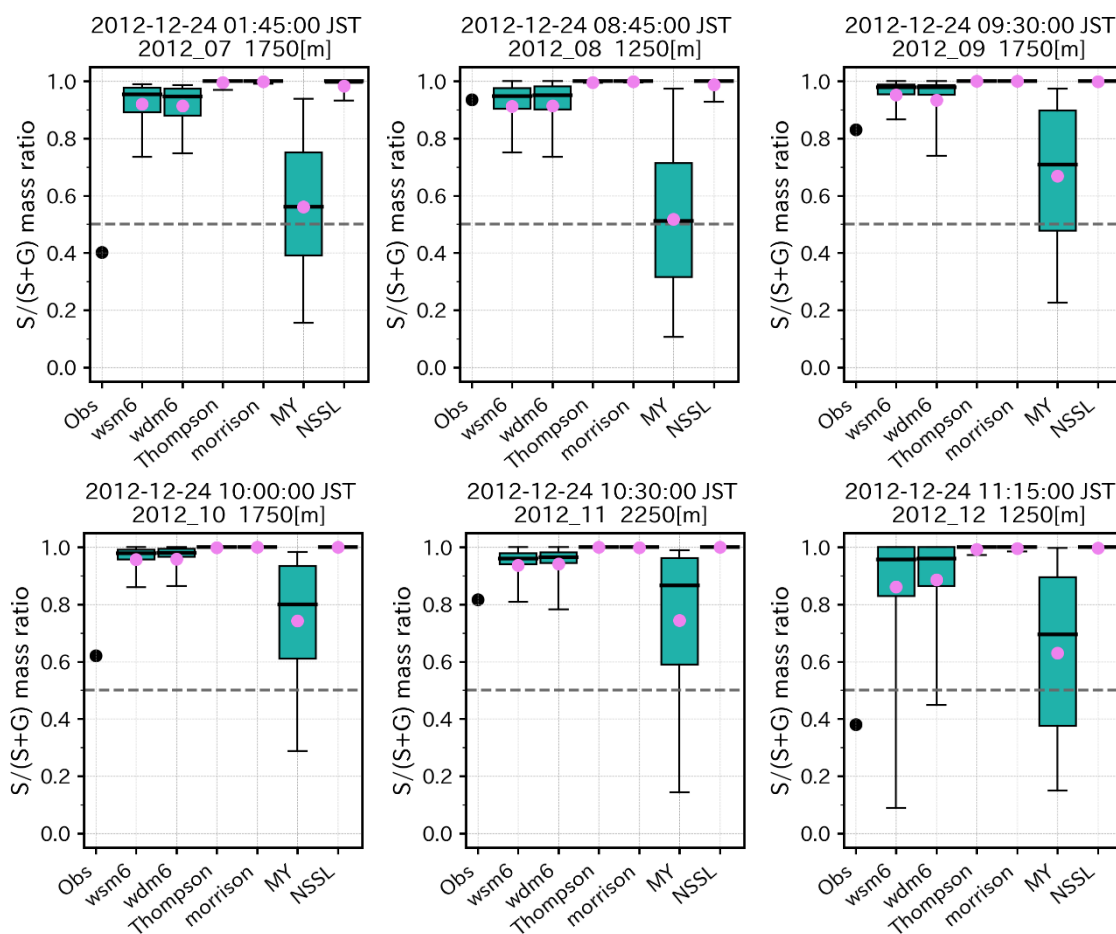


Figure 2. Ratio of snow to solid hydrometer mass density at altitudes where observed solid hydrometer number density is greatest. Whisker plots show 5, 25, 50, 75, and 95 percentile values of the ratio of simulated solid hydrometer mass density of clouds with cloud top height within 250 m to observation cloud around the observed points. Pink circles denote mean values of the ratio.

## References

1. Murakami, M. (2019), Inner Structures of Snow Clouds over the Sea of Japan Observed by Instrumented Aircraft: A Review., *J. Meteor. Soc. Japan*, **97**(1), 5-38.
2. Takahashi, T., S. Sugimoto, T. Kawano, and K. Suzuki (2019), Microphysical Structure and Lightning Initiation in Hokuriku Winter Clouds, *J. Geophys. Res. Atmos.*, **124**(23), 13156-13181.

# Effects of Number Concentration of Cloud Condensation Nuclei on Moist Convection Formation

Yoshiaki Miyamoto<sup>1</sup>

<sup>1</sup>Keio University, Fujisawa, Japan

(Corresponding author: Yoshiaki Miyamoto, e-mail: ymiya@sfc.keio.ac.jp)

## 1. Introduction

Moist convection forms as a result of conditional instability as interpreted by parcel theory. One key process in parcel theory is the condensation of water vapor. For condensation or the formation of cloud droplets to occur, cloud condensation nuclei (CCN) are necessary (Pruppacher and Klett 1997). The number and size of droplets depend largely on the number of CCNs,  $N_{CCN}$ . When  $N_{CCN}$  is small, a smaller number of large droplets will form given a degree of supersaturation. The intensity and structure of convection are affected by  $N_{CCN}$ .

Previous studies performed numerical simulations for real cases of convective phenomena, including isolated convection (e.g., Wang 2005, Li et al. 2008), supercells (e.g., Grabowski and Morrison 2017), and squall lines (e.g., Khain et al. 2004), using cloud microphysics models. Wang (2005) and Li et al. (2008) showed that the convection intensifies with  $N_{CCN}$  when  $N_{CCN}$  is less than several thousands per cubic centimeter. Because moist convection forms under various conditions and the effects of  $N_{CCN}$  on convection are complicated, further studies to elucidate these impacts are desired for deeper understanding.

This study examines the impacts of  $N_{CCN}$  on the formation of moist convection by conducting a set of numerical experiments using a three dimensional full-physics model for a wide parameter range of  $N_{CCN}$ . Furthermore, we developed a parcel model that includes the effects of  $N_{CCN}$  and performed a linear stability analysis to demonstrate stable and unstable regimes depending on  $N_{CCN}$ .

## 2. Model description and experimental setup

We used a fully compressible atmospheric model, SCALE (Nishizawa et al. 2015, Sato et al. 2015). The horizontal and vertical grid spacings were 500 m and 200 m, respectively, with the numerical domain covering  $30 \times 30 \times 20 \text{ km}^3$ . The boundary condition for lateral boundaries was periodic and no fluxes were allowed at the vertical boundaries. The integration period was 1.5 h with a time interval of 6 s. The cloud model used in this study has a bin microphysics model (Suzuki et al. 2010). The number of bins for aerosol and each of water species were 33 and 20. The minimum and maximum resolved radii of aerosol were  $10^{-2}$  and  $10^0 \text{ }\mu\text{m}$ .

The details for experimental setting such as the initial condition for environmental thermodynamic quantities are described in Miyamoto (2021). A warm bubble defined as potential-temperature perturbation was inserted at  $(x,y,z)=(15,15,0.5) \text{ km}$  of the numerical domain. We conducted two sets of sensitivity experiments to parameters: the environmental mixing ratio of aerosols and diffusivity.

### 3. Result and conclusion

Figure 1 shows the lifetime maximum of the domain maximum vertical velocity  $w_{l_{tm}}$  as a function of  $N_{CCN}$  in the sensitivity experiments.  $w_{l_{tm}}$  is approximately  $40 \text{ m s}^{-1}$  when  $N_{CCN} > 10^1 \text{ cm}^{-3}$ , while  $w_{l_{tm}} \sim 10 \text{ m s}^{-1}$  when  $N_{CCN} < 10^{-1} \text{ cm}^{-3}$ .  $w_{l_{tm}}$  increases with  $N_{CCN}$  from  $N_{CCN} = 10^{-1}$  to  $10^1 \text{ cm}^{-3}$ , and the dependence of  $w_{l_{tm}}$  on  $N_{CCN}$  is consistent with the previous studies (Wang 2005, Li et al. 2008).

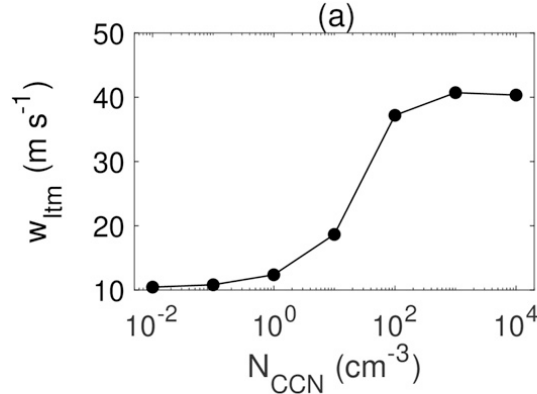


Fig. 1. Lifetime maximum of domain-maximum vertical velocity as a function of  $N_{CCN}$ .

### References

1. Grabowski, W. W., and H. Morrison, (2017), Modeling condensation in deep convection. *J. Atmos. Sci.*, **74**, 2247–2267.
2. Khain, A. P., A. Pokrovsky, M. Pinsky, A. Seifert, and V. Phillips, (2004), Simulation of effects of atmospheric aerosols on deep turbulent convective clouds using a spectral microphysics mixed-phase cumulus cloud model. Part I: Model description and possible applications. *J. Atmos. Sci.*, **61**, 2963–2982.
3. Li, G., Y. Wang, and R. Zhang, (2008), Implementation of a two-moment bulk microphysics scheme to the WRF model to investigate aerosol-cloud interaction. *J. Geophys. Res.*, **113**, D15 211.
4. Miyamoto, Y., (2021), Effects of Number Concentration of Cloud Condensation Nuclei on Moist Convection Formation, *J. Atmos. Sci.*, **78**, 3401- 3413.
5. Nishizawa, S., H. Yashiro, Y. Sato, Y. Miyamoto, and H. Tomita, (2015), Influence of grid aspect ratio on planetary boundary layer turbulence in large-eddy simulations. *Geosci. Model Dev.*, **8**, 3393–3419.
6. Pruppacher, H. R., and J. D. Klett, (1997), *Microphysics of Clouds and Precipitation*. Kluwer Academic, 976 pp.
7. Sato, Y., S. Nishizawa, H. Yashiro, Y. Miyamoto, Y. Kajikawa, and H. Tomita, (2015), Impacts of cloud microphysics on trade wind cumulus: Which cloud microphysics processes contribute to the diversity in a large eddy simulation? *Prog. Earth Planet. Sci.*, **2**, 23.
8. Suzuki, K., T. Nakajima, T. Y. Nakajima, and A. P. Khain, (2010), A study of microphysical mechanisms for correlation patterns between droplet radius and optical thickness of warm clouds with a spectral bin microphysics cloud model. *J. Atmos. Sci.*, **67**, 1126–1141.
9. Wang, C., (2005), A modeling study of the response of tropical deep convection to the increase of cloud condensation nuclei concentration: 1. Dynamics and microphysics. *J. Geophys. Res.*, **110**, D21211.

# **Aerosol induced rare winter-hailstorm in dry region of North India**

Anu Gupta<sup>1,2</sup>, Rakesh Teja Konduru<sup>3</sup>, Vivek Singh<sup>4</sup>, Atul Kumar Srivastava<sup>4</sup>, Vijay P. Kanawade<sup>5</sup>, Chandan Sarangi<sup>6</sup>

<sup>1</sup>Department of Geography, Tokyo Metropolitan University, Hachioji, Tokyo, Japan.

<sup>2</sup>Department of Information Science, University of Hyogo, Kobe, Japan.

<sup>3</sup>Data Assimilation Research Team, RIKEN Center for Computational Sciences, Kobe, Japan.

<sup>4</sup>Indian Institute of Tropical Meteorology, Ministry of Earth Sciences, New Delhi, India.

<sup>4</sup>Centre for Earth, Ocean and Atmospheric Sciences, University of Hyderabad, Hyderabad, India.

<sup>5</sup>Department of Civil Engineering, Indian Institute of Technology Madras, Chennai, India.

(Corresponding author: Anu GUPTA, e-mail: gupta.anu1819@gmail.com)

## **1. Introduction**

India's northwestern and northern semi-arid regions have been witnessing intensified hailstorms during the winter season. These hailstorms have far-reaching impacts on the agricultural sector, leading to extensive damage to crops and infrastructure, and causing significant economic losses to farmers and the economy as a whole. Despite their destructive consequences, winter hailstorms in the region have remained poorly understood and not extensively studied.

In an effort to shed light on this phenomenon, a comprehensive study was conducted, focusing on a specific hailstorm event that occurred on December 12, 2019, in the northern dry region of India. The researchers sought to unravel the factors contributing to the intensified hailstorms.

## **2. Model description and experimental setup**

In this study, we performed non-hydrostatic Weather Research and Forecasting (WRF) simulations with two nested domains of 10 km and 3.33 km. Using WRF in the convection-permitting mode, we could simulate the precipitation and hail event triggered by the western disturbance. A CTRL simulation was conducted with Milbrandt-Yau 2-moment microphysical scheme for the period of the western disturbance 8-15 December 2019. First, three days of the simulation were considered for spin-up. The analysis is performed for the duration of 11-13 December 2019.

## **3. Result and conclusion**

### **3.1 AOD simulated rainfall and hails formation**

A deep western disturbance (WD) played a vital role as a trigger in the atmospheric dynamics that caused the hailstorm event. This WD led to the formation of a cyclonic circulation in the lower atmosphere, enabling the transportation and redistribution of numerous aerosols across the northwest regions of India.

The study investigated the time series of model-simulated rainfall and hail formation in northwest India, comparing it with CTRL and different AOD experiments (Fig. 1a,b). Results revealed a linear increase in both rainfall and hail formation with higher AOD values, peaking at an AOD of 1.0, which led to a 50% increase in hail rate compared to CTRL. The order of hail and precipitation rate increase was AOD1.0 > AOD0.75 > AOD0.50 > AOD0.25 > CTRL, indicating that winter aerosols intensify precipitation and hail. Moreover, the presence of winter

aerosols induced a notable delay of 3-6 hours in precipitation onset, while the hail process commenced much earlier. Comparable delays in rainfall initiation have also been observed in various other types of rain. Such a delay in the rainfall process due to aerosols is also noted in the cold-rain process [Rosenfeld and Woodley 2000] and the warm-rain process.

### 3.2 Cloud microphysics

The investigation also explored the impact of Aerosol Optical Depth (AOD) on cloud condensates (Fig. 1). The analysis revealed a consistent rise in cloud hydrometeors from the lower to the middle atmosphere (700–500 hPa) with increasing AOD. Essentially, the hail mixing ratio exhibited an increase of 30–40% at AOD1.0 in the 800–700 hPa range (Fig. 1 c,d), while the rain mixing ratio showed a 10–20% increase at AOD1.0 below 800 hPa (Fig. 1e). Furthermore, the peak height of hail and cloud condensate mixing ratio increased with higher AOD. This suggests that an increase in winter AOD leads to a clear intensification of hail and rainfall, as evident in their respective mixing ratios.

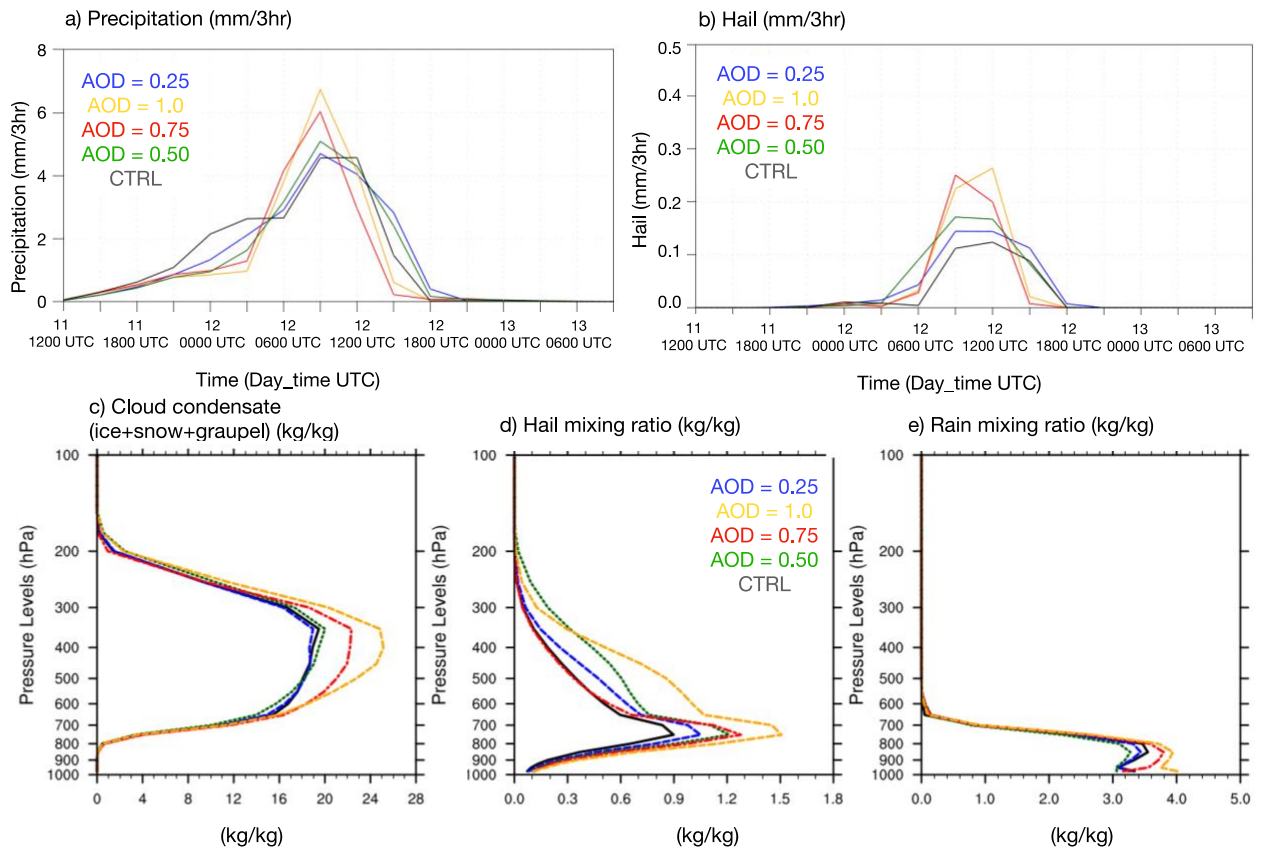


**Fig. 1.** Time series of the area average a) precipitation (mm/3hr), b) hails (mm/3hr), area average vertical profiles of c) cloud condensate (snow, ice, and graupel; kg/kg), d) hail mixing ratio (kg/kg), and e) rain mixing ratio (kg/kg) using the convection-permitting experiments over the northwest India region (27°–30° N & 73°–78° E).

### References

1. Rosenfeld, D. and W.L. Woodley, (2000), Deep convective clouds with sustained supercooled liquid water down to -37.5 C, *Nature*, **405**, 440-442

# Applications of a global nonhydrostatic model to test retrieval algorithms for the EarthCARE satellite

Woosub Roh<sup>1\*</sup>, Masaki Satoh<sup>1</sup>  
(<sup>1</sup>AORI, the University of Tokyo)

## 1. Introduction

The Earth Clouds, Aerosol and Radiation Explorer (EarthCARE, Illingworth, et al. 2015) satellite is scheduled for launch in 2024, which is a joint mission by the European Space Agency (ESA) and Japanese Aerospace Exploration Agency (JAXA). The EarthCARE has multiple passive and active sensors in the same body to investigate clouds, aerosols, precipitation, and associated radiation budgets. It has a Cloud Profiling Radar (CPR), ATmospheric LIDar (ATLID), Multi-Spectral Imager (MSI), and Broad Band Radiometer (BBR). EarthCARE's CPR has the Doppler capability to provide information on the terminal velocity of rain and ice and convective motion. Pre-launch simulated satellite data are useful for developing retrieval algorithms and facilitating rapid post-launch release of retrieval products.

In this study, we introduce the JAXA EarthCARE-like synthetic data (Roh et al. 2023) based on simulations using a Nonhydrostatic ICosahedral Atmospheric Model (NICAM, Satoh et al. 2014) and the Joint simulator (Hashino et al. 2013). We also discuss about applications of the EarthCARE to evaluate and improve a nonhydrostatic model.

## 2. Data and model descriptions

The JAXA EarthCARE-like synthetic data (JAXA L1) simulation data are based on input data for meteorological conditions, distributions and properties of clouds, precipitation and aerosols associated with signals from satellite sensors. We used NICAM data to drive the instrument simulations. NICAM was configured with a horizontal resolution of about 3.5 km, and the vertical grid had 40 levels. Aerosol data were simulated using the NICAM Spectral Radiation–Transport Model for Aerosol Species (NICAM–SPRINTARS), which was implemented using a global 3D aerosol transport–radiation model. The horizontal resolution was ~240 km, and the vertical resolution was the same as that used in the 3.5 km mesh simulation.

## 3. Examples of the EarthCARE signals

The relationship between orbits and cloud distribution in the NICAM simulation is shown in Fig. 1, where simulated 11  $\mu\text{m}$  brightness temperatures (representing cloud top temperatures) indicate high clouds. The lines indicate the expected EarthCARE orbits corresponding to the simulations.

The CPR is a 94 GHz cloud profiling radar capable of measuring radar reflectivity and Doppler velocities. The minimum radar reflectivity is -36 dBZ, which is a higher sensitivity than CloudSat due to the larger antenna and lower orbit than CloudSat.

Radar reflectivity and Doppler velocity were simulated using the EarthCARE Active Sensor Simulator (EASE; Okamoto et al., 2007; Nishizawa et al., 2008).

ATLID is the 355 nm high spectral resolution lidar capable of observing 355 nm Mie and Rayleigh backscatter. The co-polarised Mie scattering channel is related to cloud and aerosol particles, and the co-polarised Rayleigh scattering channel is related to atmospheric molecules. The total attenuated cross-polarised backscatter channel is related to the shapes of hydrometeors and aerosols.

EASE simulates the lidar signals from ATLID by taking into account the scattering and attenuation of molecules, hydrometeors and aerosols. The outputs from ATLID are 355 nm total attenuated backscatter from Mie or Rayleigh scattering. The effect of multiple scattering by liquid hydrometeors on the lidar signals was considered using a correction factor parameterised by Monte Carlo simulation.

We will also introduce the MSI and BBR simulations shortly.

#### 4. Discussions

After the launch of EarthCARE, its data will provide new insights for the evaluation and improvement of a global nonhydrostatic model. We will discuss the future perspective of the EarthCARE satellite for evaluations and improvements of a global non-hydrostatic model.

#### References:

Hashino, T., and Coauthors, 2013: Evaluating Arctic cloud radiative effects simulated by NICAM with A-train., *J. Geophys. Res. Atmos.*, **121(12)**, 7041–7063.

Nishizawa, T., and Coauthors, 2008: Aerosol retrieval from two-wavelength backscatter and on e-wavelength polarization lidar measurement taken during the MR01K02 cruise of the R/V Mirai and evaluation of a global aerosol transport model, *J. Geophys. Res.*, **113**, D21201.

Okamoto, H., and Coauthors, 2007: Vertical cloud structure observed from shipborne radar and lidar; mid-latitude case study during the MR01/K02 cruise of the R/V Mirai, *J. Geophys. Res.*, **112**, D08216.

Illingworth, A. J., and Coauthors, 2015.: The EarthCARE satellite: The next step forward in global measurements of clouds, aerosols, precipitation, and radiation, *Bull. Am. Meteorol. Soc.*, **96**, 1311–1332.

Roh, W., and Coauthors 2023: Introduction to EarthCARE synthetic data using a global storm-resolving simulation. *Atmos. Meas. Tech.*, **16**, 3331–3344.

Satoh, M., and Coauthors 2014: The Non-hydrostatic Icosahedral Atmospheric Model: Description and development. *Progress in Earth and Planetary Science*. **1**, 18.

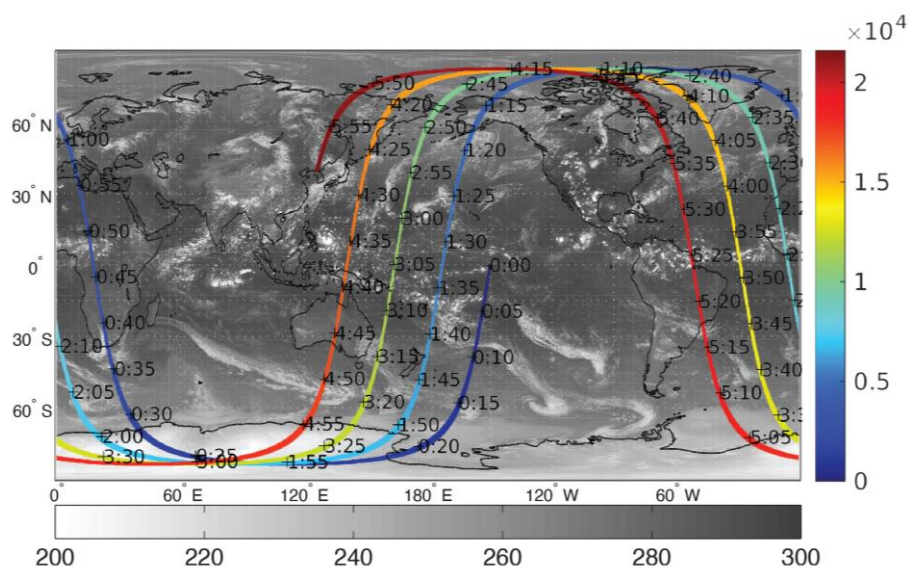


Figure 1. Simulated tracks and a swath of the EarthCARE satellite. The black/white contour is the 11  $\mu\text{m}$  brightness temperature (K). Colors indicate the time from the starting point (00:00Z) in seconds.

# Improving Representation of Scattered Radiation in Three-Dimensional Radiative Transfer Calculations for High-Resolution Numerical Models

Ken Hirata<sup>1,2</sup>, Miho Sekiguchi<sup>3</sup>, and Yosuke Sato<sup>4,5</sup>

<sup>1</sup>Department of Atmospheric and Oceanic Sciences, University of Colorado Boulder, Boulder, CO, USA

<sup>2</sup>Laboratory for Atmospheric and Space Physics, University of Colorado Boulder, Boulder, CO, USA

<sup>3</sup>Tokyo University of Marine Science and Technology, Tokyo, Japan

<sup>4</sup>Faculty of Science, Hokkaido University, Sapporo, Japan

<sup>5</sup>RIKEN Center for Computational Science, Kobe, Japan

(Corresponding author: Ken Hirata, e-mail: [ken.hirata@colorado.edu](mailto:ken.hirata@colorado.edu))

This work is distributed under the Creative Commons Attribution 4.0 License (CC BY 4.0)

## 1. Introduction

Radiative transfer calculation in most numerical atmospheric models has assumed that horizontal transport of radiation is negligible. For recent numerical models with increasingly high resolutions, this approximation causes a significant bias in both local and domain-averaged irradiance at the surface and within clouds (e.g., O’Hirok and Gautier, 2005), affecting the radiative heating and resulting circulation. The *TenStream* solver (Jakub and Mayer, 2015) was developed to efficiently and approximately solve full three-dimensional radiative transfer (3D RT). The novelty of this solver was that it extended the idea of two-stream approximation in an one-dimensional RT problem to 10 streams in a 3D setting.

Although the *TenStream* solver is a powerful approach to help represent 3D RT, it produces a biased transfer of shortwave radiation due to its simple angular discretization (Hirata et al, 2023). The bias can be attributed to the configuration of ten streams which only partially represent the horizontal radiative transfer through the streams on lateral surfaces of the grids. The purpose of this study is to investigate methods to mitigate the unphysical bias by testing these possible approaches.

## 2. Model description and experimental setup

The 3D radiative transfer model (Hirata et al., 2023) that was previously developed following the *TenStream* approach was used for testing the performance of the following two implementations. The first method was to increase the number of scattered radiation streams to 24. The second method was to implement a grid-level truncation on the 10-stream scheme; a subset of scattered radiation that exits a grid with an angle that is less than 30 degrees away from the solar angle was assumed to maintain the solar angle. Monte Carlo Atmospheric Radiative Transfer Simulator (MCARaTS; Iwabuchi, 2006) was used to calculate benchmark irradiance which was regarded as the true solution of 3D RT.

To test these implementations, an atmospheric field of shallow convection was provided by a Large Eddy Simulation (Sato et al. 2017, 2018) performed by atmospheric model SCALE (Nishizawa et al. 2015; Sato et al. 2015). The domain size was 6.4 km × 7.2 km × 3.0 km and the grid spacing was 100 m horizontally and 80 m vertically. The cloud optical properties were derived from the liquid water

mixing ratio and number density using the Mie theory and assuming the log-normal droplet size distribution. Molecular scattering was incorporated but the molecular absorption was not included. 15 bands spanning from 0.2  $\mu\text{m}$  to 4  $\mu\text{m}$  were used to represent the shortwave broadband. The surface albedo was assumed to be a constant value of 0.06 across all the wavelength range.

### 3. Result and conclusion

Both the 24-stream approach and grid-level truncation were able to mitigate the vertically localized bias of downward irradiance but did not reproduce the signature of the cloud-side leakage. On the other hand, the 24-stream approximation did not largely overestimate the upward irradiance whereas the truncated 10-stream method computed a similar magnitude of localized bias compared to the original 10-stream approach. Overall, the 24-stream approximation successfully improved the representation of the horizontal radiative transfer, while the grid-level truncation resulted in less diffusive downward irradiance.

### References

1. Hirata, K., M. Sekiguchi, Y. Sato, and M. Inatsu, (2023). Biases in Shortwave Three-Dimensional Radiative Transfer Calculations for High-Resolution Numerical Models. *SOLA*, **19**, 50-56.
2. Iwabuchi, H., (2006). Efficient Monte Carlo methods for radiative transfer modeling. *J. Atmos. Sci.*, **63**(9), 2324-2339.
3. Jakub, F., and B. Mayer, (2015). A three-dimensional parallel radiative transfer model for atmospheric heating rates for use in cloud resolving models—The TenStream solver. *J. Quant. Spectrosc. Ra.*, **163**, 63-71.
4. Nishizawa, S., H. Yashiro, Y. Sato, Y. Miyamoto, and H. Tomita, (2015). Influence of grid aspect ratio on planetary boundary layer turbulence in large-eddy simulations. *Geosci. Model Dev.*, **8**(10), 3393-3419.
5. O'Hirok, W., and C. Gautier, (2005). The impact of model resolution on differences between independent column approximation and Monte Carlo estimates of shortwave surface irradiance and atmospheric heating rate. *J. Atmos. Sci.*, **62**(8), 2939-2951.
6. Sato, Y., S. Nishizawa, H. Yashiro, Y. Miyamoto, Y. Kajikawa, and H. Tomita, (2015). Impacts of cloud microphysics on trade wind cumulus: which cloud microphysics processes contribute to the diversity in a large eddy simulation?. *Progr. Earth Planet. Sci.*, **2**, 1-16.
7. Sato, Y., S. I. Shima, and H. Tomita, (2017). A grid refinement study of trade wind cumuli simulated by a Lagrangian cloud microphysical model: the super-droplet method. *Atmos. Sci. Lett.*, **18**(9), 359-365.
8. Sato, Y., S. I. Shima, and H. Tomita, (2018). Numerical convergence of shallow convection cloud field simulations: Comparison between double-moment Eulerian and particle-based Lagrangian microphysics coupled to the same dynamical core. *J. Adv. Model. Earth Syst.* **10**(7), 1495-1512.

## Session F: Data assimilation 2

# Consideration of distortion from Gaussian error distribution in relative humidity assimilation

Ken Sawada

Meteorological Research Institute, Tsukuba, Japan

(Corresponding author: Ken Sawada, e-mail: ksawada@mri-jma.go.jp)

This work is distributed under the Creative Commons Attribution 4.0 License (CC BY 4.0)

## 1. Introduction

To improve the prediction of localized heavy precipitation events, it is important to obtain precise spatial distributions of water substances such as water vapor and cloud water in the atmosphere at initial data. The states of these meteorological variables are estimated by data assimilation systems, but accurate estimation is difficult because some simplifying assumptions are employed due to computational resource constraints. For example, in large variational data assimilation systems, Gaussian error distributions are often assumed. Although this assumption is valid in many cases, for variables with bounded value ranges, such as water substances, deviations from the Gaussian distribution are expected to become apparent when values are taken near the boundaries of the range. Therefore, it is required to consider error distributions that are based on Gaussian error distributions but whose kurtosis and skewness vary with the value of the variables. Here we report a simple method for introducing such non-Gaussian error distributions.

## 2. Method

As an example of a meteorological variable that takes values within a bounded range, we focus on relative humidity. First, based on the theory of constrained optimization problems, we implemented an exterior penalty function method within a variational data assimilation system to suppress unrealistic supersaturated or negative relative humidity states caused by inappropriate error distributions. In particular, we added a penalty term defined by

$$J_{qv}(x) = \lambda \sum_i (g_i(x))^\alpha$$
$$g_i(x) = \max \{0, -qv_i(x), qv_i(x) - qvs_i(x)\}$$

to the cost function of a variational assimilation system. Here,  $x$  denotes the control variables,  $qv_i$ , and  $qvs_i$  denote the mixing ratio and saturation mixing ratio at the  $i$ -th grid, respectively.  $\lambda > 0$  and  $\alpha \geq 1$  are penalty parameters. In our experiments, we set  $\alpha = 1$ , and examined various values of  $\lambda$  to investigate the effects of this penalty term. Second, we considered the effect of distortion from Gaussian error distribution. As such a non-Gaussian error distribution  $f^{NG}$  on the bounded domain, we used a distribution of the form represented by

$$f^{NG}(x) = l(x)f^G(m(x)) + n(x),$$

where  $f^G$  is a conventional Gaussian distribution  $N(\mu, \sigma^2)$ , and  $l, m, n$  are suitable

transform functions such that  $f^{NG}$  is a probability density function. In the case distortion from  $f^G$  is not so large,  $f^{NG}$  is written by

$$f^{NG}(x) = \frac{1}{\sqrt{2\pi\sigma^2}} \exp [q(x) + h(x)]$$

$$q(x) = -\frac{1}{2} \left( \frac{x - \mu}{\sigma} \right)^2.$$

Then, we have

$$h(x) = \log \left( l(x) e^{q(m(x)-q(x))} + \frac{n(x)}{f^G(x)} \right).$$

Determining  $f^{NG}$  is a difficult problem in itself, but based on the error statistics from the mesoscale analysis data for 2021, we roughly expressed  $f^{NG}$  by a truncated Gaussian, a folded Gaussian, or a coordinate-transformed distribution. In addition, we approximated  $h(x)$  with a piecewise quadratic function to avoid using a too complicated function which would be detrimental to the minimization process.

### 3. Result and discussion

Effects of the penalty term for water vapor mixing ratio were examined in JNoVA system which was a previous operational meso-scale analysis-forecast system in JMA. The following effects were revealed: 1) Added penalty term did not do harm to minimization as long as the penalty parameter  $\lambda$  is too large. 2) In high humidity regions, new method, while analyzing higher temperature and lower mixing ratio field on average, could analyze localized higher equivalent potential temperature regions. 3) Initial shock was reduced and smooth generation of convections that form precipitation was promoted. 4) These effects contributed to improving the reproducibility of precipitation in the early stages of the forecast, see Fig. 1. We will also discuss the effects of distortion from Gaussian error distribution in the assimilation system.

### References

1. Sawada, K., and Y. Honda, (2021), A constraint method for supersaturation in a variational data assimilation system, *Mon. Wea. Rev.*, **149**, 3707-3724.

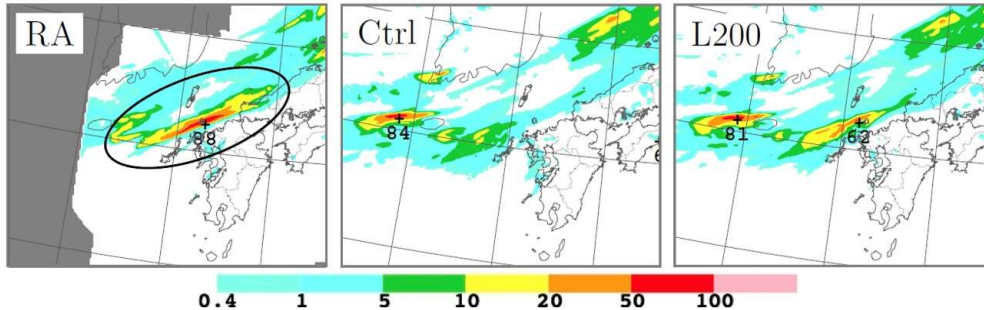


Fig. 1. The 3-h accumulated precipitation [ $\text{mm } 3\text{h}^{-1}$ ]. The left panel labeled RA shows the radar/rain-gauge analyzed precipitation, the middle and right panels show the forecasted precipitation distributions given by a conventional JNoVA system and a new JNoVA system with the penalty term  $J_{qv}(x)$ .

# The impact-based forecasting with a large-ensemble DA

Takuya KAWABATA<sup>1</sup>, Tsutao OIZUMI<sup>1</sup>, Ping-Yin Wu<sup>1,2</sup>, Le Duc<sup>1,3</sup>, Kazuo SAITO<sup>1,3</sup>

<sup>1</sup> Meteorological Research Institute, Tsukuba, Japan, <sup>2</sup> Meteorological Business Support Center, Chiyoda, Japan, <sup>3</sup> University of Tokyo, Kashiwa, Japan

(Corresponding author: Takuya KAWABATA, e-mail: tkawabat@mri-jma.go.jp)

This work is distributed under the Creative Commons Attribution 4.0 License (CC BY 4.0)

## 1. Introduction

Impact-based forecasting (IBF) aims to encourage people's behavioral changes for reducing the damage when meteorological disasters occur. For realizing the IBF, probabilistic prediction is an important component, because the behavior of MCSs and typhoons is essentially chaotic due to their high nonlinearity. Therefore, accurately estimating the probability of its occurrence is rather important than to accurately predicting meteorological phenomena, especially for predictions beyond half a day.

To realize this concept, we developed a probabilistic forecast system coupled with a hydrological model based on a 1000-member ensemble. The objective is to show the probability of disaster itself such as floodings, landslides and strong winds. This large ensemble simulation is conducted on the supercomputer Fugaku, which is the Japanese flagship supercomputer.

## 2. Experimental Settings and cases

We ran NHM-LETKF (EnVar) with 1000 members at a 5-km resolution and downscaled-into a 2- (1-) km resolution for two cases. The first one is a quasi-stationary line-shaped rainband case in July 2020, whose scales of the rainband in space and time were about 200 km in east-west and 12 hours, respectively (Duc et al. 2021). In this event, over 80 lives were claimed by a flood of the Kuma river in Kyushu. The second is Typhoon Hagibis, which caused recordbreaking damages by floodings, landslides and strong winds over eastern Japan.

## 3. Results

For the first case, the deterministic and ensemble forecasts of NHM-LETKF outperformed the JMA operational mesoscale forecasts 12-h before the flooding. By applying the ensemble forecast results to a hydrological model, we obtained amazing 60% of probability of the occurrence of flooding hazard (Oizumi et al. 2023).

For the second case, the 1-km ensemble well predicted the probability of the strong winds. It is shown that the large-size ensemble simulations at a high-resolution deliver accurate and detailed forecasts for high-impact strong wind events (Wu et al. 2023). In this presentation, we will show these case studies for the impact-based forecast.

4.

**Acknowledgement**

This study is supported by Fugaku General Access “Study on mechanisms of quasi-stationary linear convective systems with meteorological and mathematical approaches” (hp230067) and KAKENHI (23K03498).

**References**

1. Le Duc, T. Kawabata, K. Saito, T. Oizumi (2021), Forecasts of the July 2020 Kyushu Heavy Rain Using a 1000-Member Ensemble Kalman Filter, *SOLA*, **17**, 41-47.
2. Oizumi T., T. Kawabata, L. Duc, K. Kobayashi, K. Saito, T. Ota (2023), Impact of a Number of Ensemble Members in Numerical Weather Prediction Models on Flood Prediction, AOGS 20th Annual Meeting.
3. Wu, P.-Y., T. Kawabata, and L. Duc, (2023), High-resolution 1000-member Ensemble Simulations of Typhoon Hagibis (2019). Japan Geoscience Union Meeting 2023, Chiba, Japan, 21-26 May 2023.

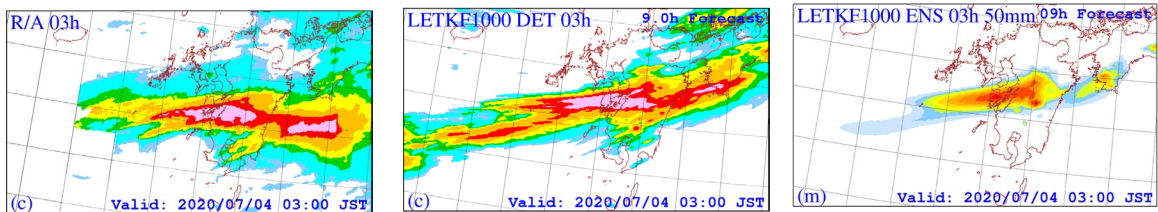


Fig. 1. 3-h accumulated rainfall distribution of observation (left) and prediction (middle). Probability of rainfall over 50 mm/(3-h) (right). After Duc et al. (2021).

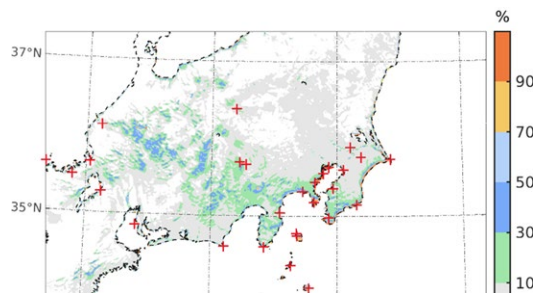


Fig. 2. The probability of the wind speed over 15 m/s, (color shaded) and the surface observations over 15 m/s (red cross). After Wu et al. (2023).

# Predictability of moist convection through ensemble convective-scale data assimilation

Masashi MINAMIDE<sup>1,2</sup>, and Derek J. POSSELT<sup>2</sup>

<sup>1</sup> The Department of Civil Engineering, The University of Tokyo, Tokyo, Japan

<sup>2</sup> Jet Propulsion Laboratory, California Institute of Technology, Pasadena, CA, USA

(Corresponding author: Masashi MINAMIDE,

e-mail: [minamide@hydra.t.u-tokyo.ac.jp](mailto:minamide@hydra.t.u-tokyo.ac.jp))

This work is distributed under the Creative Commons Attribution 4.0 License (CC BY 4.0)

## 1. Introduction

Atmospheric deep moist convection has emerged as one of the most challenging topics for numerical weather prediction, due to its chaotic nature of the development with multi-scale physical interactions. Not only do individual convective storms cause tremendous damage to society, such as through severe thunderstorms, but convective systems also play a critical role in developing organized severe weather events. Our recent investigation found that meso- $\alpha$  (2000-200 km) and meso- $\beta$  (200-20 km) scale initial features helped to constrain the general location of convective system with a few hours of lead time, contributing to enhancing convective activity, but meso- $\gamma$  (20-2 km) or even smaller scale features with less than 30-minute lead time were identified to be essential for capturing individual convective storms (Minamide and Posselt, 2022). In this talk, to further explore the potentials of data assimilation in capturing the convective signals in meso- $\beta$  and - $\gamma$  scales that determines the spatiotemporal characteristics of individual convective development, we have conducted large ensemble convection-permitting data assimilation experiments with more than thousand members using the highly-spatiotemporally-resolving all-sky satellite radiances from GOES-16. We chose to model a mesoscale convective system (MCS) over Gulf of Mexico in 2017 that was observed through NASA's Convective Processes Experiment (CPEX) field campaign, and the early stage of hurricane Harvey (2017).

## 2. Model description and experimental setup

We used the ensemble-Kalman Filter (EnKF) data assimilation system build around the Weather Research and Forecasting Model (WRF) and Community Radiative Transfer Model (CRTM) originally developed at Pennsylvania State University. We assimilated all-sky infrared brightness temperatures from GOES-16 together with a

conventional set of observations. The EnKF analysis and subsequent ensemble forecasts were utilized to explore the relationships between the convective occurrence and its environmental control.

### 3. Result and conclusion

We found that the greater number of ensembles more effectively suppressed the spurious correlation for convective-scale data assimilation. Particularly, the ensemble correlations showed similar structures with more than or equal to 500 members, indicating the importance of increasing the ensemble size. Meanwhile, the large ensemble also resulted in the loss of small-scale correlation structures. The convective-scale signals that determines the exact location and timing of convective development were not clear in covariances even with thousands of ensemble members. This is potentially because the scales of individual convection are so short and small that vast amount of ensemble members do not resolve the convective activity at the corresponding time and location, suggesting the potential importance of situation-dependence in addition to the flow-dependence in background covariances to capture and constrain the signals of individual convective activity in numerical weather prediction.

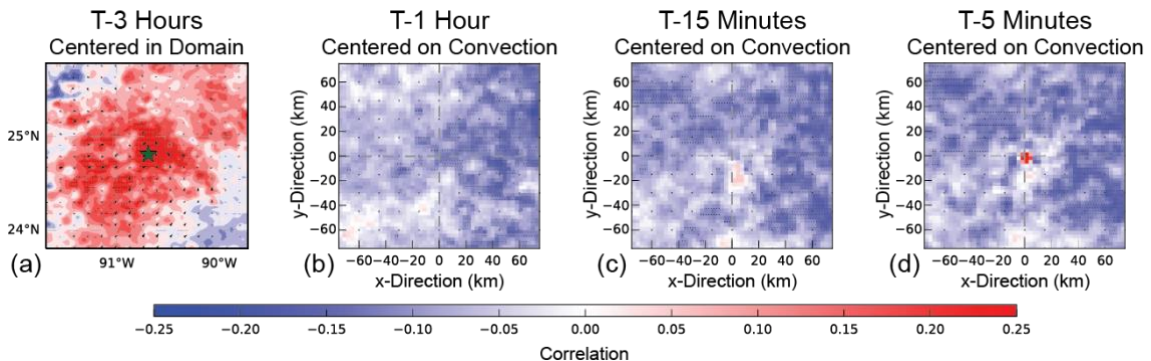


Fig. 1. An example of the lag-time correlation patterns between the vertically-averaged vertical wind at the convective peak vs. moisture at 500 hPa (modified from Minamide and Posselt, 2022).

#### References (in alphabetical order according to author)

1. Minamide, M., and D. J. Posselt, (2022): Using Ensemble Data Assimilation to Explore the Environmental Controls on the Initiation and Predictability of Moist Convection. *J. Atmos. Sci.*, **79**, 1151–1169

# ASSIMILATION OF C-BAND RADAR DATA USING THE SCALE-LETKF SYSTEM: A SUPERCELL CASE STUDY DURING THE RELAMPAGO FIELD CAMPAIGN

Paula Maldonado<sup>1</sup>, Juan Ruiz<sup>2,3</sup>, Celeste Saulo<sup>1,2</sup>, Takumi Honda<sup>4</sup>, Takemasa Miyoshi<sup>5</sup>

<sup>1</sup> Servicio Meteorológico Nacional, Argentina (SMN)

<sup>2</sup> Centro de Investigaciones del Mar y la Atmósfera (CIMA/CONICET-UBA)

<sup>3</sup> Departamento de Ciencias de la Atmósfera y los Océanos (DCAO-FCEN-UBA)

<sup>4</sup> Faculty of Science, Hokkaido University, Sapporo, Japan

<sup>5</sup> RIKEN Center for Computational Science (R-CCS)

(Corresponding author: Paula MALDONADO, e-mail: pmaldonado@smn.gob.ar)

This work is distributed under the Creative Commons Attribution 4.0 License (CC BY 4.0)

## 1. Introduction

Southern South America is frequently affected by strong convection that produces negative impacts on the population and their activities. Forecasting high-impact weather events associated with deep, moist convection is an open challenge due to the limited predictability and observability of mesoscale circulations. In recent years, significant advances have been made in using convective-scale numerical weather prediction and data assimilation systems to produce very short-range forecasts (on the scale of minutes) of high-impact weather events (see, for example, Yano et al. 2018). However, only few studies have focused on the application of high-resolution data assimilation systems in South America (e.g., Vendrasco et al. 2020). Recently, the radar network in Argentina has been significantly expanded, creating new opportunities for the improvement of very short-range forecasts of high-impact weather events. In this work, we investigate the implementation of an ensemble-based data assimilation system based on the Local Ensemble Transform Kalman filter (LETKF) coupled with the Scalable Computing for Advanced Library and Environment (SCALE) regional model (Lien et al. 2017) and its performance in a case of a supercell thunderstorm that occurred in central Argentina during the RELAMPAGO field campaign (Nesbitt et al. 2021).

## 2. Methodology

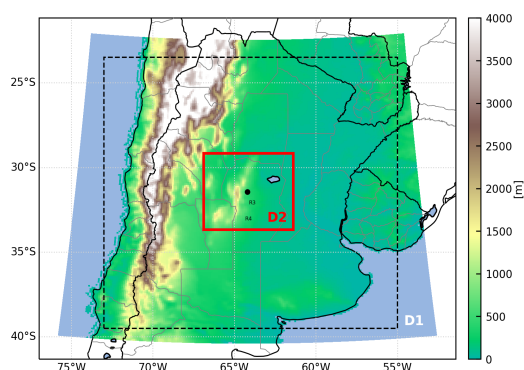


**Figure 1: Model domains and terrain height (m)**

The selected case study took place on November 10<sup>th</sup>, 2018 and consisted of strong isolated convective cells that developed along a cold front, acquiring supercell characteristics. Radar data (reflectivity and Doppler velocity) from the RMA-1 radar site was assimilated every 5 minutes. Radar observations were quality controlled and superobed to a resolution of 2 km in the horizontal and 500 m in the vertical. Observations were assimilated between 18 and 21 UTC using the LETKF with 60 ensemble members.

The model's horizontal resolution was 2 km, covering the domain shown in Figure 1

(red square D2), approximately centered at the location of the RMA-1 radar. Boundary conditions were generated by a 10-km-resolution analysis ensemble nested in the Global Ensemble Forecasting System (D1 in Figure 1). Between 19.30 and 20.30 UTC, five 1-hour ensemble forecasts were initialized from the analysis every 15 minutes.

### 3. Results and conclusion

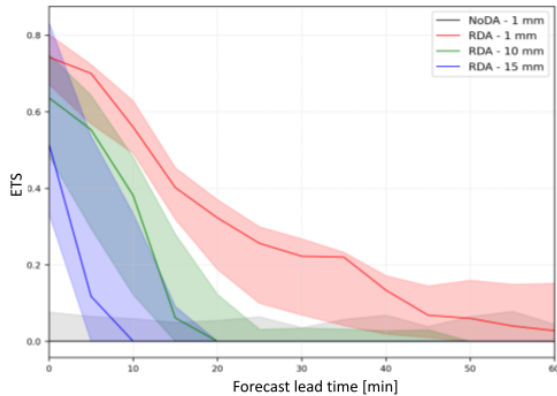


**Figure 2: Short-range equitable threat score as a function of the forecast lead time (min)**

The assimilation of radar observations using the SCALE-LETKF system was successful in the sense that the analysis could reproduce the location and timing of the observed convection. Also, the dynamic and main features of the supercellular storm were successfully retrieved. Short-range ensemble forecasts of precipitation were significantly improved with respect to forecasts that do not assimilate radar observations (RDA and NoDA in Figure 2, respectively).

The results obtained are encouraging and suggest that the system is suitable for monitoring and producing short-range forecasts of high-impact weather events using conventional weather radar data. Additional experiments are being conducted in the context of the PREVENIR project to fine-tune the SCALE-LETKF system and conduct a more robust evaluation. Also, numerical weather prediction forecasts are being coupled with hydrological simulations to produce a flash-flood forecast.

### References

- Nesbitt, S. W., and Coauthors, 2021: A Storm Safari in Subtropical South America: Proyecto RELAMPAGO. *Bull. Amer. Meteor. Soc.*, **102**, E1621–E1644, <https://doi.org/10.1175/BAMS-D-20-0029.1>.
- Lien, G.-Y., Miyoshi, T., Nishizawa, S., Yoshida, R., Yashiro, H., Adachi, S. A., Yamaura, T., and Tomita, H., 2017: The Near-Real-Time SCALE-LETKF System: A Case of the September 2015 Kanto-Tohoku Heavy Rainfall. *SOLA*, 13, 1–6, doi:10.2151/sola.2017-001.
- Yano, J., and Coauthors, 2018: Scientific Challenges of Convective-Scale Numerical Weather Prediction. *Bull. Amer. Meteor. Soc.*, **99**, 699–710, <https://doi.org/10.1175/BAMS-D-17-0125.1>.
- Vendrasco, E., Machado, L., Ribeiro, B., Freitas, E., Ferreira, R., y Negri, R., 2020b: Cloud resolving model applied to nowcasting: An evaluation of radar data assimilation and microphysics parameterization. *Wea. Forecasting*, 35 (6), 2345–2365, doi:10.1175/WAF-D-20-0017.1.

Session G:  
Cloud Physics, Radiation, Lightning 3

# Overview of bulk lightning model coupled with a Japanese community model SCALE

Yousuke Sato<sup>1</sup>

<sup>1</sup> Faculty of Science, Hokkaido University, Sapporo, Japan

(Corresponding author: Yousuke Sato, e-mail: [yousuke.sato@sci.hokudai.ac.jp](mailto:yousuke.sato@sci.hokudai.ac.jp))

This work is distributed under the Creative Commons Attribution 4.0 License (CC BY 4.0)

## 1. Introduction

The lightning is the large threat to the human life and the highly computerized current society. More than one thousand people are killed every year in the world, and the damage cost by lightning estimated based on the insurance claim costs has been increasing during this decade. The numerical weather prediction (NWP) has contributed to reduce the damage caused by the disaster. However, the lightning has not been explicitly calculated in the numerical model for NWP, alternatively, the lightning activity and lightning frequency have been diagnosed based on the empirical parameterizations (e.g., McCaul et al. 2009). The parameterizations, which diagnose the lightning frequency according to the empirical relationship between the lightning and other variables such as mixing ratio cloud hydrometeor, vertical velocity, CAPE and so on, are powerful tool to forecast the lightning. However, it is not clear that the empirical relationship is applicable for the sever events that we have never experienced. The bulk lightning models (BLM) have been developed to overcome the problem. Using BLMs, the lightning can be explicitly calculated based on the physical model. We have developed a BLM (Sato et al. 2019) and implemented it into a Japanese community model Scalable Computing for Advanced Library and Environment (SCALE: Nishizawa et al. 2015, Sato et al. 2015). In this presentation, we aim to introduce the basic characteristic of the BLM, to show the advantage of the BLM to the empirical parameterization (Tomioka et al. 2023) and to show an application of BLM (Sato et al. 2023).

## 2. Bulk Lightning Model (Sato et al., 2019)

The BLM of Sato et al. (2019) predicts the charge density of each hydrometeor considered in the cloud microphysical models in SCALE. The non-inductive charge separation (Takahashi 1984) is considered as the charge separation of ice, snow, and graupel, and the two neutralization parameterizations (Fierro et al., 2013 and MaGormann et al., 2001) are implemented. The electric field is calculated from the charge density by solving Poisson equation, and the Bi-Conjugate Gradient STABILized method (Bi-CGSTAB: van der Vorst, 1992) with symmetric Gauss-Seidel preconditioning is applied for solving the Poisson equation.

## 3. Results

Figure 1 shows the geographical distribution of the lightning frequency simulated by BLM, diagnosed by the empirical parameterization (MaCaul et al. 2009), and measured by the lightning detection system (Ishii et al. 2014). The BLM well reproduced the geographical distribution of measured lightning. In contrast, the empirical parameterization overestimated the lightning. According to statistical scores such as the root means square error (RMSE), the correlation coefficient for temporal correlation, and the equitable thread score (ETS), it is clarified that the

BLM shows the similar performance to the empirical parameterization for the temporal variation and the location of the lightning. It is also elucidated that BLM has the advantage to the empirical parameterization for simulating the lightning frequency.

An application of the BLM is the study of the lightning-induced nitrogen oxides (LNO<sub>x</sub>), which is one of the most uncertain sources of NO<sub>x</sub>, the precursor a greenhouse gas, Ozone. To investigate the impacts of the LNO<sub>x</sub>, we coupled SCALE-BLM with a photochemical model (Kajino et al. 2021), and we examined the impacts of the LNO<sub>x</sub> on nitrogen monoxide (NO), nitrogen dioxide (NO<sub>2</sub>), and total reactive nitrogen oxide (NO<sub>y</sub>) observed in Summer of 2017 at the summit of Mt. Fuji, Japan.

## References

1. Fierro, A. O., E. R. Mansell, D. R. MacGorman, and C. L. Ziegler, (2013), The implementation of an explicit charging and discharge lightning scheme within the WRF-ARW model: benchmark simulations of a continental squall line, a tropical cyclone, and a winter storm., *Mon. Wea. Rev.*, **141**, 2390-2415.
2. Ishii, K., S. Hayashi, and F. Fujibe, (2014), Statistical analysis of temporal and spatial distributions of cloud-to-ground lightning in Japan from 2002 to 2008., *J. Atmos. Elect.*, **34**, 79-86.
3. Kajino, M., M. Deushi, T. Sekiyama, N. Oshima, K. Yumimoto, T. Tanaka, J. Ching, A. Hashimoto, T. Yamamoto, M. Ikegami, A. Kamada, M. Miyashita, Y. Inomata, S. Shima, A. Takami, A. Shimizu, and S. Hatakeyama, (2019), NHM- Chem, the Japan meteorological agency's regional meteorology – chemistry model: model evaluations toward the consistent predictions of the chemical, physical, and optical properties of aerosols. *J. Meteorol. Soc. Japan*, **97**, 337–374
4. MacGorman, D., J. Straka, and C. Ziegler, (2001), A lightning parameterization for numerical cloud models. *Journal of Applied Meteorology*, **40**, 459-478
5. MaCaul, E., S. Goodman, and K. LaCasse, and D. Cecil, (2009), Forecasting lightning threat using cloud-resolving model simulations. *Wea. Forecast.*, **24**, 709-729
6. Nishizawa, S., H. Yashito, Y. Sato, Y. Miyamoto, and H. Tomita, (2015), Influence of grid aspect ratio on planetary boundary layer turbulence in large-eddy simulations, *Geosci. Model. Dev.*, **8**, 3393-3419.
7. Sato, Y., S. Nishizawa, H. Yashiro, Y. Miyamoto, Y. Kajikawa, and H. Tomita, (2015), Impacts of cloud microphysics on trade wind cumulus: which cloud microphysics processes contribute to the diversity in a large eddy simulation?, *Prog. Earth Planet. Sci.*, **2**, doi: 10.1186/s40645-015-0053-6
8. Sato, Y., M. Kajino, S. Hayashi, and R. Wada, (2023), A numerical study of lightning-induced NO<sub>x</sub> and formation of NO<sub>y</sub> observed at the summit of Mt. Fuji using an explicit bulk lightning and photochemistry model, *Atmos. Environ. X*, **18**, doi: 10.1016/j.aeoa.2023.100218
9. Takahashi, T., (1978) Riming electrification as a charge generation mechanism in thunderstorms. *J. Atmos. Sci.*, **35**, 1536-1548
10. Tomioka, T., Y. Sato, S. Hayashi, S. Yoshida, and T. Iwashita, (2023), Advantage of bulk lightning models for predicting lightning frequency over Japan, *Prog. Earth Planet. Sci.*, in revision.
11. van der Vorst H. A., (1992), Bi-CGSTAB: a fast and smoothly converging variant of BiCG for the solution of nonsymmetric linear systems. *SIAM J. Sci. Stat. Comput.*, **13**, 631–644.

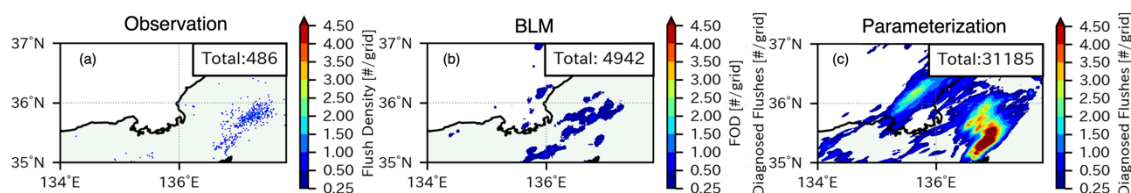


Fig.1 The cumulative lightning frequency from 03 UTC of July 7 to 00 UTC of July 8 of 2018 by (a) the observation (Ishii et al. 2014), (b) the simulation of BLM, and (c) the empirical parameterization (MaCaul et al. 2009). The figures are from Tomioka et al. (2023)

# Effect of graupel growth on the increase in lightning activity preceding severe wind

Makoto Kondo<sup>1</sup> and Yousuke Sato<sup>1,2</sup>

<sup>1</sup>Graduate School of Science, Hokkaido University, Sapporo, Japan

<sup>2</sup>RIKEN Center for Computational Science, Kobe, Japan

(Corresponding author: Makoto Kondo, e-mail: konchasu56@eis.hokudai.ac.jp)

This work is distributed under the Creative Commons Attribution 4.0 License (CC BY 4.0)

## 1. Introduction

Lightning occurs within well-developed convective clouds, and the relationship between lightning activity and convective cloud development and/or updraft volume has been investigated (e.g., Goodman et al. 2005). Lightning Jump (LJ; Williams et al. 1999) was suggested as an indicator focusing on lightning activity that precedes the initiation of severe weather events (e.g., tornadoes and downbursts; DBs). Among severe weather events, we focused on DBs developed due to gravitational loading and latent heat cooling caused by large graupel (hail) (Fujita 1985). The main charge separation mechanism for lightning is non-inductive charge separation via the collision of graupel and ice/snow (Takahashi 1978). Existence of graupel is necessary for the occurrence of both phenomena. Thus, to understand LJs preceding DBs, an understanding of the physical processes of the graupel is necessary.

A meteorological model coupled with a bulk lightning model (Fierro et al. 2013; Sato et al. 2019) is a powerful tool for this analysis focusing on LJ and DB because it explicitly calculates both the charge separation via the collision of graupel and ice/snow and the DB generation originated from the gravitational loading and latent heat cooling by the graupel.

This study aims to examine the physical processes between LJ and DB focused on graupel by using a meteorological model coupled with a bulk lightning model.

## 2. Model description and experimental setup

The model used in this study is the meteorological model, Scalable Computing for Advanced Library and Environment (SCALE Nishizawa et al. 2015; Sato et al. 2019), coupled with a bulk lightning model (Sato et al. 2019). In the bulk lightning model, the charges of cloud hydrometeors (e.g., cloud, rain, ice, snow, graupel, and so on) are calculated as prognosis variables. The non-inductive charge separation was calculated based on a look-up table based on Takahashi (1978) and the neutralized scheme by Fierro et al. (2013) was used.

The idealized experiment was conducted using a horizontally homogeneous initial meteorological field according to the soundings at Maebashi and Tateno when the DBs occurred at Misato-machi, Saitama Prefecture on September 8th, 1994 (Takayama et al. 1997). The warm bubble with a maximum temperature 4 K was placed on the southwest side of the model domain to trigger the convection (Guo et al. 1999). The calculation time was 90 min. The calculation domain covered 18 km and 12 km for the  $x$  and  $y$  directions with the grid interval of 100 m. The vertical layer was divided into 100 layers, and the layer thickness was stretched from the surface to the model top 20.2 km ( $dz = 20 \text{ m} \sim 1578 \text{ m}$ ). The 2-moment bulk microphysical scheme (Seiki and Nakajima 2014) and Smagorinsky-type sub-grid scale model (Brown et al. 1994) were used for including effects of clouds and turbulence, and the radiation was ignored.

For the evaluation, the balance between the cold pool strength ( $C$ ) and vertical shear ( $\Delta U$ ) which is ( $C/\Delta U$ ), and the maximum vertical wind velocity ( $W$ ) at the lower level were derived based on the RKW theory (Rotunno et al. 1988; Takemi 2006).

## 3. Result and Discussion

Figure 1 shows the temporal evolution of the maximum wind speed, Flash Origin Density (FOD), and the number concentration of large graupel particles (LGN) over the whole grids

with column mass of hydrometeor exceeding 50 mg. Throughout the calculation period, the convective clouds triggered by the initial warm bubble developed as long-lasting multi-cell cumulonimbus (Cb) clouds. In this multi-cell Cb, DBs exceeding 40 m/s occurred four times, and LGNs increased preceding the DBs. Before about 15 minutes of the second DB, which occurred around 45 minutes into the calculation, a rapid increase in lightning activity corresponding to LJ occurred (Fig. 1). During the LJ, charge separation of graupel increased, while LGN decreased. Focusing on the change in LGN between DB and LJ, we show the LGN distribution on  $C/\Delta U$  and  $W$  fields for each convective cell at the early developing stage of the Cb clouds.  $C/\Delta U \sim 1$  and  $W$  was small when the DB occurred. In contrast,  $C/\Delta U > 1$  and  $W$  was larger when the cell LJ was generated. These results indicate that Cb clouds tend upright at DB generating cells, while the LJ generating cell tend to tilt.

## References

1. Brown, A. R., S. H. Derbyshire, and P. J. Mason, 1994: Large-eddy simulation of stable atmospheric boundary layers with a revised stochastic subgrid model. *Q. J. R. Meteorol. Soc.*, **120**, 1485–1512
2. Fierro, A. O., E. R. Mansell, D. R. Macgorman, and C. L. Ziegler, (2013): The Implementation of an Explicit Charging and Discharge Lightning Scheme within the WRF-ARW Model: Benchmark Simulations of a Continental Squall Line, a Tropical Cyclone, and a Winter Storm. *Mon. Weather Rev.*, **141**, 2390–2415
3. Fujita 1985: The downburst: Microburst and macroburst. SMRP Research Paper 210, University of Chicago, 122 pp. [NTISPB85-148880.]
4. Guo, X., H. Niino, X. Guo, and R. Kimura, (1999): Numerical Modeling on A Hazardous Microburst-Producing Hailstorm *Science Press*,
5. Goodman, S. J., and Coauthors, 2005: The North Alabama Lightning Mapping Array: Recent severe storm observations and future prospects. *Atmos. Res.*, **76**, 423–437
6. Mansell, E. R., D. R. MacGorman, C. L. Ziegler, and J. M. Straka, (2005): Charge structure and lightning sensitivity in a simulated multicell thunderstorm. *J. Geophys. Res. Atmos.*, **110**, 1–24.
7. Nishizawa, S., H. Yashiro, Y. Sato, Y. Miyamoto, and H. Tomita, (2015): Influence of grid aspect ratio on planetary boundary layer turbulence in large-eddy simulations. *Geosci. Model Dev.*, **8**, 3393–3419
8. Rotunno, R., J. B. Klemp, and M. L. Weisman, (1988): A Theory for Strong, Long-Lived Squall Lines. *J. Atmos. Sci.*, **45**, 463–485
9. Sato, Y., S. Nishizawa, H. Yashiro, Y. Miyamoto, Y. Kajikawa, and H. Tomita, (2015): Impacts of cloud microphysics on trade wind cumulus: which cloud microphysics processes contribute to the diversity in a large eddy simulation? *Prog. Earth Planet. Sci.*, **2**
10. —, Y. Miyamoto, and H. Tomita, (2019): Large dependency of charge distribution in a tropical cyclone inner core upon aerosol number concentration. *Prog. Earth Planet. Sci.*, **6**, 1–13
11. Takahashi, T., 1978: Riming Electrification as a Charge Generation Mechanism in Thunderstorms. *J. Atmos. Sci.*, **35**, 1536–1548
12. Takayama, H., H. Niino, S. Watanabe, J. Sugaya, and M. of T. A. P. Studies, (1997): Downbursts in the Northwestern Part of Saitama Prefecture on 8 September 1994. *J. Meteorol. Soc. Japan. Ser. II*, **75**, 885–905
13. Takemi, T., 2006: Impacts of moisture profile on the evolution and organization of midlatitude squall lines under various shear conditions. *Atmos. Res.*, **82**, 37–54,
14. Tapla, A., J. A. Smith, and M. Dixon, (1998): Estimation of convective rainfall from lightning observations. *J. Appl. Meteorol.*, **37**, 1497–1509,
15. Williams, E., and Coauthors, (1999): The behavior of total lightning activity in severe Florida thunderstorms. *Atmos. Res.*, **51**, 245–265

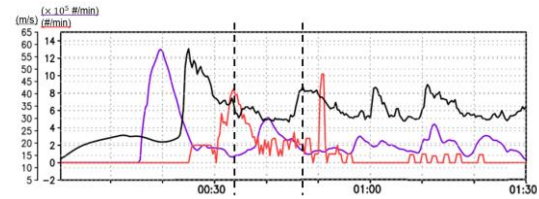


Fig. 1. Time series of model domain (black line) strongest wind speed, (red line) cumulative Flash Origin Density, and (purple line) cumulative LGN. Dashed lines show LJ and 2<sup>nd</sup> DB period.

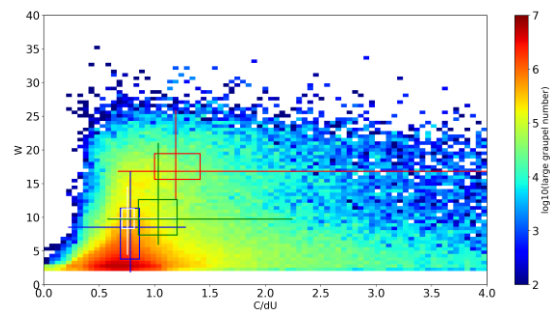


Fig. 2. Distribution of  $C/\Delta U$  and  $W$ . The red, blue, green, and white box plots are LJ, 2<sup>nd</sup> DB, 3<sup>rd</sup> DB, and 4<sup>th</sup> DB, respectively. Shade area shows the LGN amount above  $C/\Delta U$  and  $W$  area.

# Evaluation of the effect of electro-coalescence with conducting sphere approximation on the formation of warm cumulus cloud and stratocumulus cloud

Ruyi ZHANG<sup>1,2</sup>, Limin ZHOU<sup>1</sup>, Shin-ichiro SHIMA<sup>2</sup>

<sup>1</sup>Key Laboratory of Geographic Information Science, Ministry of Education, East China Normal University, Shanghai, 200241, China

<sup>2</sup>Graduate School of Simulation Studies, University of Hyogo, Kobe, 6512103, Japan  
(Correspondence to: Limin ZHOU([lmzhou@geo.ecnu.edu.cn](mailto:lmzhou@geo.ecnu.edu.cn)))

This work is distributed under the Creative Commons Attribution 4.0 License (CC BY 4.0)

## 1. Introduction

Clouds are considered to play a key role in climate systems, and the collision-coalescence of cloud droplets plays a key role in cloud formation. Droplet coalescence is one of the main processes affecting cloud microphysics. Several studies shown that the electrostatics on charged droplets could significantly influence the droplet coalescence and droplet-aerosol coagulation in weakly electrified clouds [2]. This electrostatic force induced effect is called electro-coalescence or electro-anti-coalescence [3].

In this work, the effect of the electro-coalescence from Jz on a warm cumulus with an exact electric force treatment with the CS method is estimated based on particle-based cloud modeling with the real-time collision efficiency calculation using the super-droplet method. The lower charging rate threshold for electro-coalescence is discussed. The extreme assumption of the droplet charging scenario of opposite and same sign charge is investigated.

## 2. Model description and experimental setup

We generalize the exact electric force treatment with the CS method approach for the particle-based cloud model is used with the particle size resolved treatment following the Super-Droplet Method (SDM) by Shima et al. [4]. To evaluate the effect of electro-coalescence on warm clouds, 2D simulation of an isolated cumulus is performed following the setup of Lasher-Trapp et al. [5].

## 3. Result and Conclusion

Figure 1 shows the results of the domain-averaged precipitation amount under different electrostatic force settings, and the charging rate is 0.3. The domain-averaged precipitation amount with the CS-O setting is 52.5% higher than that with the NC setting; with the CS-O-Khain04 setting, it is 5.36% larger; with the CS-q0 setting, it is 9.6% larger; and with the IM-O setting, it is 8.45% larger.

The electro-coalescence effect on a weakly electrified warm cumulus was revisited. The electro-coalescence effect on a weakly charged droplets has significantly changed the warm cumulus cloud evolution of the electrostatic force with exact treatment.

## References

1. KHAIN, A., ARKHIPOV, V., PINSKY, M., FELDMAN, Y., and RYABOV, Y.: Rain Enhancement and Fog Elimination by Seeding with Charged Droplets. Part I: Theory and Numerical Simulations, *Journal of applied meteorology*, 43, 1513-1529, 10.1175/JAM2131.1, 2004.
2. Zhou, L., Tinsley, B. A., and Plemmons, A.: Scavenging in weakly electrified saturated and subsaturated clouds, treating aerosol particles and droplets as conducting spheres, *Journal of Geophysical Research*, 114, 10.1029/2008jd011527, 2009.
3. Tinsley, B. A.: The global atmospheric electric circuit and its effects on cloud microphysics, *Reports on Progress in Physics*, 71, 066801, 10.1088/0034-4885/71/6/066801, 2008.
4. Shima, S., Kusano, K., Kawano, A., Sugiyama, T., and Kawahara, S.: The super-droplet method for the numerical simulation of clouds and precipitation: a particle-based and probabilistic microphysics model coupled with a non-hydrostatic model, *Quarterly Journal of the Royal Meteorological Society*, 135, 1307-1320, 10.1002/qj.441, 2009.
5. Lasher-trapp, S. G., Cooper, W. A., and Blyth, A. M.: Broadening of droplet size distributions from entrainment and mixing in a cumulus cloud, *Quarterly Journal of the Royal Meteorological Society*, 131, 195-220, 10.1256/qj.03.199, 2005.

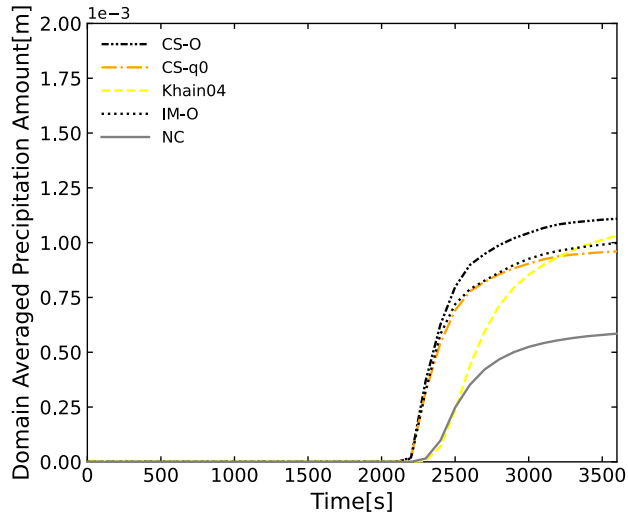


Figure 1: Comparison of the time evolution of the domain-averaged precipitation amount for variable evaluation of the electric force. The grey solid line represents the NC setting. The black dashed-dotted-dotted lines represent the results of the opposite electric force evaluated by the CS method (CS-O). The orange dashed-dotted line represents the condition where the charge is only on the large droplet (CS-q0), the yellow dashed-dotted line represents the result of droplets with opposite sign charges and the method based on Khain et al. [1] (Khain04). The black dotted line is the result of droplets with opposite sign charges, and the electric force is evaluated by the image charge method (IM-O).

# Preliminary investigation on the future changes in lightning frequency in Japan using a bulk lightning model

Sho Kawazoe<sup>1</sup> and Yousuke Sato<sup>2</sup>

<sup>1</sup>*Hokkaido University, Sapporo, Japan*

(Corresponding author: Sho Kawazoe, e-mail: kawazoe@sci.hokudai.ac.jp)

## 1. Introduction

Understanding how climate change may affect the frequency of lightning events is increasingly important, particularly as society continues to shift toward a more digital world. However, previous studies investigating future responses often rely on environmental proxies such as atmospheric instability, cloud top height, and convective precipitation from climate simulations with relatively coarse resolution. While these proxies can provide an implicit understanding of climate change responses, they cannot account for the smaller scale factors such as topography and the spatial distribution of dynamical and thermodynamical features. In the case of lightning events, the representation of hydrometeor distribution in the atmosphere is essential in understanding the electrical charge generation within convective clouds. Here, we use a high-resolution numerical simulation to investigate explicitly how a warming climate may influence lightning frequency.

## 2. Model description and experimental setup

As a case study, numerical simulations were performed for a high lightning event on July 11<sup>th</sup>, 2021, which occurred in the Kanto region in eastern Japan. We utilized the Scalable Computing for Advanced Library and Environment (SCALE; Sato et al. 2015, Nishizawa et al. 2015) coupled with an explicit lightning model (Sato et al. 2019) to examine lightning frequency and their underlying environments. Simulations were conducted at 2 km grid spacing with 60 vertical levels, initialized using hourly data from the European Centre for Medium-Range Weather Forecasts high-resolution reanalysis (ERA5; Hersbach et al. 2020).

For future changes, the pseudo-global warming approach using two timeslice experiments with three sea-surface temperature patterns from the Database for Policy Decision-Making for Future Climate Change (d4PDF; Mizuta et al. 2017; Fujita et al. 2019) was applied. Monthly climatological differences in three-dimensional temperature, geopotential height, and surface temperature between historical and +2K near-future/+4K end-of-century experiments were imposed to the ERA5 to produce pseudo-warming simulations.

## 3. Results

For the control experiment, the SCALE model reproduced precipitation intensity and lightning frequency distribution, though there was a slight tendency for convective cells to propagate more easterly compared to observations.

For pseudo-warming, preliminary analysis reveals that despite large increases in instability represented by convective available potential energy (~500 to 1000 J/kg) and increases in precipitation, decreased lightning frequencies are depicted in the +2K and +4K experiments (Fig. 1). These changes were primarily attributed to the changes in the vertical structure of the charge separation rate and the charge density. In addition, lightning initiation was delayed in the +4K experiments and dissipated

earlier than in the control experiment. These results suggest that a warming climate may contribute to an environment that is less favorable for lightning activity, despite greater convective potential.

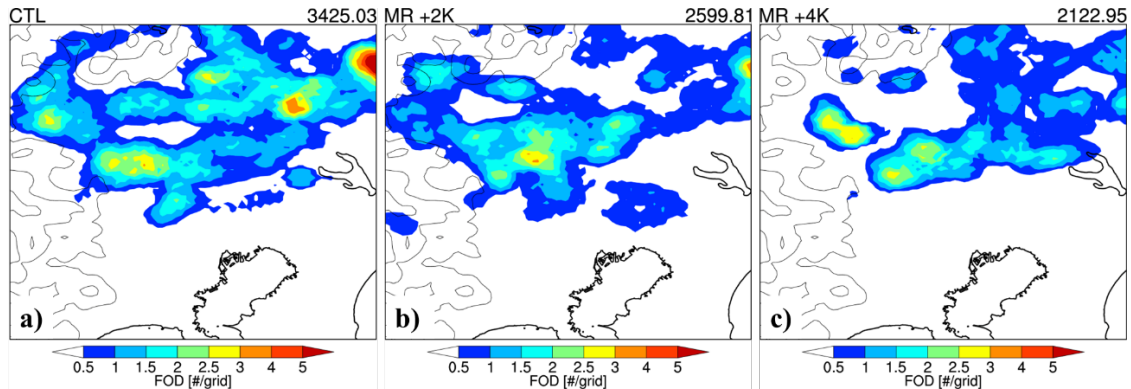


**Figure 1:** Flash origin density (#/grid) during peak lightning occurrence on July 11<sup>th</sup>, 2021, from a) the control, b) +2K warming, and c) +4K warming experiments. Top right number indicates total FOD over the analysis domain.

## References

1. Fujita, M., and coauthors, 2019: Changes in a climate with 2-K surface warming from large ensemble simulations using 60-km global and 20-km regional atmospheric models. *Geophys. Res. Lett.*, **46**, 435-442.
2. Mizuta, R., and coauthors, 2017: Over 5000 years of ensemble future climate simulations by 60 km global and 20 km regional atmospheric models. *Bull. Amer. Meteor. Soc.*, **98**, 1383-1398.
3. Nishizawa, S., H. Yashiro, Y. Sato, Y. Miyamoto, and H. Tomita, 2015: Influence of grid aspect ratio on planetary boundary layer turbulence in large-eddy simulations. *Geosci. Model Dev.*, **8**, 3393-3419.
4. Sato, Y., S. Nishizawa, H. Yashiro, Y. Miyamoto, Y. Kajikawa, and H. Tomita, 2015: Impacts of cloud microphysics on trade wind cumulus: which cloud microphysics processes contribute to the diversity in a large eddy simulation? *Prog. Earth Planet. Sci.*, **2**, 23.
5. Sato, Y., Y. Miyamoto, and H. Tomita, 2019: Large dependency of charge distribution in a tropical cyclone inner core upon aerosol number concentration. *Prog. in Earth and Planet. Sci.*, **6**, 62.
6. Hersbach, H., and coauthors, 2020: The ERA5 global reanalysis. *Q.J.R. Meteorol. Soc.*, **146**, 1999– 2049.

# Relationship between tropical high clouds and atmospheric circulations, and its future changes

Akira T. Noda<sup>1</sup>, Nagio Hirota<sup>2</sup>, Tsuyoshi Koshiro<sup>3</sup>, and Hideaki Kawai<sup>3</sup>

Corresponding author: Akira T. Noda (a\_noda@jamstec.go.jp)

1 Japan Agency for Marine-Earth Science and Technology, Yokohama, Japan

2 National Center for Environmental Studies, Tsukuba, Japan

3 Meteorological Research Institute, Japan Meteorological Agency, Tsukuba, Japan

(Corresponding author: Akira T. Noda, e-mail: a\_noda@jamstec.go.jp)

## 1. Introduction

Future changes in high-cloud cover are important for better projecting the degree of warming on our planet. However, there is large uncertainty in our evaluation of these changes. A global nonhydrostatic model is a useful tool because it computes clouds explicitly based on a cloud microphysics scheme to avoid uncertainty arisen from a cumulus parameterization, which is generally used in conventional GCMs. This study uses NICAM to examine the relationship between high clouds and atmospheric circulations, which has been pointed out as a key factor deeply relating to changes of high cloud behavior. Furthermore, we also compared data of NICAM and those of CMIP GCMs to investigate differences of modeled relationships of high clouds.

## 2. Data and definitions

We use data of 20-year long climate simulation using 14-km mesh NICAM (Kodama et al. 2015, JMSJ), and that of corresponding global warming simulation, which also considers a doubled CO<sub>2</sub> concentration homogeneously over the globe, and an increase of sea surface temperature pattern based on results of CMIP3 future climate simulations. We refer to a high cloud cover, HCC, as that evaluated by an ISCCP simulator interactively during simulations; thus, that develops between 440hPa and 50 hPa altitude, and is optically thicker than 0.3 (Rossow and Scheffer 1999, BAMS). A mass flux,  $M$ , is defined as

$$M = -\frac{1}{g} \int_{10^5}^{10^3} \omega \frac{\partial z}{\partial p} dp,$$

where  $g$  is a gravitational constant,  $\omega$  is vertical velocity (Pa/s).  $z$  and  $p$  denote height (m) and pressure (Pa), respectively.

## 3. Result and conclusion

Figure 1 shows the spatial patterns of HCC and  $M$ . The present climate simulation shows that HCC develops especially over the western Pacific, Indian Ocean, South American

and African continents, and it increases over the central Pacific and decreases over the Indian Ocean. The spatial distribution of M and its change in the present climate simulation is similar that of HCC; a notable difference in their changes is that M changes especially near equatorial regions while HCC does also in higher latitudes. Furthermore, we compare the relationship between HCC and M in the present and future climate in scatter plots (Figure 2). A strong tie is confirmed between these quantities, and the correlation coefficients exceed 0.8 in each climate state, and is 0.7 in their changes. Past numerical studies using idealized earth experiments, such as aqua planets, show a reduced HCC in response to surface warming. Bony et al. (2016, PNAS) proposed a stability IRIS hypothesis that attributes the reduced HCC to a weakened tropical upward mass flux in a warmer atmosphere. In fact, the NICAM result also shows a strong relationship between M and HCC at a almost same magnitude in present and future climate conditions, and major regions of reduced HCC coincidentally occur with those of weakened M. However, this study also shows that the stabilized atmosphere due to warming does not guarantee a reduced HCC in a tropical mean field, showing that a spatial pattern of M and its magnitudes are also important elements to project a future HCC change. In the presentation, we will also argue possible elements to cause the contrasting responses of HCC, positive and negative changes of tropical HCC, to global warming appeared in the present GCM simulations

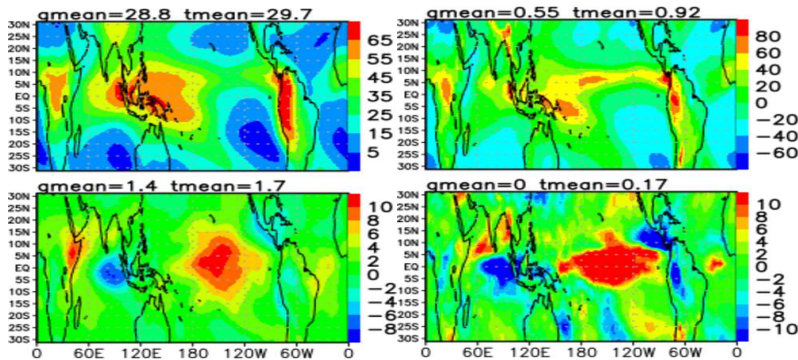


Figure 1. 20-year-means of horizontal distribution of HCC (%) in the present climate simulation (left upper), and difference of the result in the global warming simulation from that in the present climate simulation (left bottom). Right panels are same as left panels, but for M (kg/m/s).

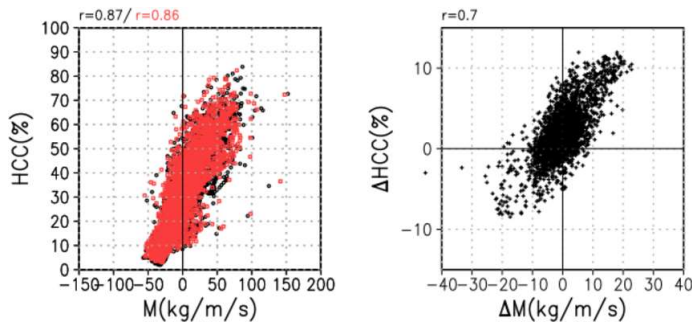


Figure 2. Scatter plots of M (kg/m/s) and HCC (%) in the present climate simulation (black dots) and in the global warming simulation (red dots) (left), and the difference of the result in the global warming simulation from that in the present climate simulation (right). Each dot shows the result of grid point values in Figure 1. Correlation coefficients are also drawn in the upper sides.

## **Evaluation of vertical transport of cumulus convection parametrization using LES**

Junichi TANOSHITA<sup>1</sup>, Kengo MATSUBAYASHI<sup>1</sup>

<sup>1</sup> Japan Meteorological Agency, Tsukuba, Japan

(Corresponding author: Junichi TANOSHITA,

e-mail: junichi.tanoshita@met.kishou.go.jp)

This work is distributed under the Creative Commons Attribution 4.0 License (CC BY 4.0)

### **Abstract**

Accurate prediction of heat and water vapour transport by cumulus convection is a very important factor in determining forecast performance. The Japan Meteorological Agency (JMA) has been operating the Local Forecast Model (LFM) with a horizontal resolution of 2 km and a forecast period of 10 hours to provide information for disaster prevention, very short-range precipitation forecasts and aviation forecasts (JMA 2023).

As previous studies have found that vertical transport is not well resolved even using kilometer-scale resolution model (Bryan et al. 2003, Whitall 2015), the model's 2 km grid spacing is insufficient to resolve cumulus convection. To represent the unresolved vertical transport of heat and moisture, the LFM employs a convective parametrization based on Kain-Fritsch scheme (Kain and Fritsch 1990; Kain 2004). However, it is not clear how much the magnitude of the parametrized vertical transport should be for the resolution. In this study, ideal experiments using 50 m resolution Large Eddy Simulation (LES) were conducted to evaluate vertical transport in the LFM configuration with/without convection scheme (2kmConv/2kmNoConv). Initial condition and surface fluxes and diabatic cooling rates were used for the TRMM-LBA case (Grabowski et al. 2006). Fig 1 shows contoured frequency by altitude diagrams (CFAD) of vertical velocity for LES results filtered to 2 km resolution (a), 2kmConv (b), 2kmNoConv (c). In comparison with LES simulation, excessive vertical velocity is predicted in 2kmNoConv, whereas it is suppressed in 2kmConv. As the target of LFM is precipitation forecast due to individual convection events, it is considered necessary to use convection scheme to predict the intensity and location of convection. However, experiments show that parametrized convection in 2kmConv tends to develop too quickly and cloud top is too high. The results suggest that improvements are needed through the evaluation of the convection scheme.

## References

1. Bryan, G. H., J. C. Wyngaard, J. M. Fritsch, (2003), Resolution requirements for the simulation of deep moist convection., *Mon. Wea Rev.* 131, 2394–2416.
2. Grabowski, W. W., and Coauthors, (2006), Daytime convective development over land: A model intercomparison based on LBA observations., *Quart. J. Roy. Meteor. Soc.*, 132, 317–344, <https://doi.org/10.1256/qj.04.147>.
3. JMA, (2023), Outline of the operational numerical weather prediction at the Japan Meteorological Agency. Appendix to WMO Technical Progress Report on the Global Data-processing and Forecasting System and Numerical Weather Prediction.
4. Kain J. S., (2004), The Kain–Fritsch convective parameterization: An update., *J. Appl. Meteorol.* 43, 170–181.
5. Kain, J. S., and J. M. Fritsch, (1990), A one-dimensional entraining/detraining plume model and its application in convective parameterization., *J. Atmos. Sci.*, 47, 2784–2802.
6. Whittall, M., (2015), Parameterization of Moist Processes for Next-Generation Weather Prediction. [https://dtcenter.org/sites/default/files/events/2015/moistphys/03\\_Whittall\\_noaa\\_dtc\\_27\\_01\\_2015.pdf](https://dtcenter.org/sites/default/files/events/2015/moistphys/03_Whittall_noaa_dtc_27_01_2015.pdf), accessed on 19 July.

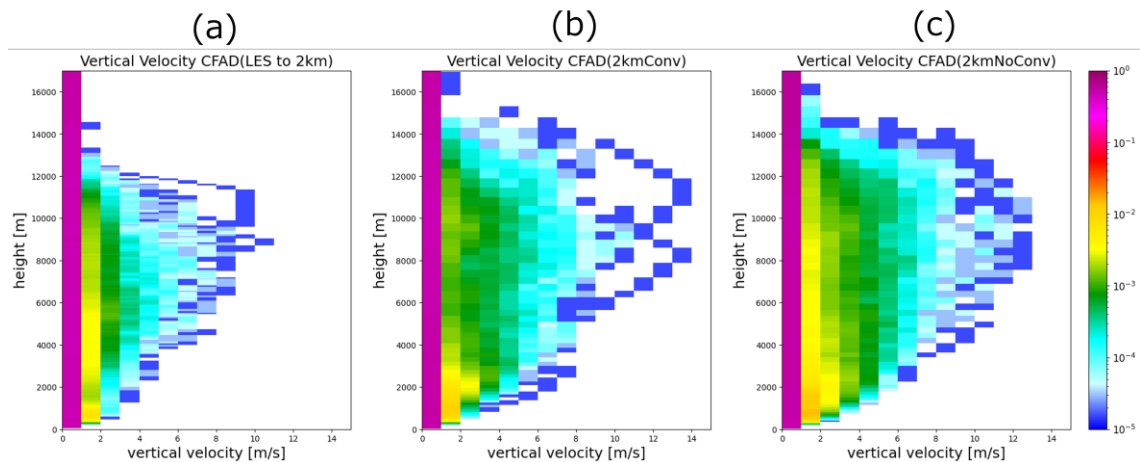


Fig 1. CFAD of 12-hour accumulated vertical velocity. (a) LES results filtered to 2km, (b) 2kmConv, and (c) 2kmNoConv, respectively.

## Session H: Event analyses

# Numerical Experiment on a Line-shaped Precipitation System Occurred in Kochi, Japan in Early July 2022

Kenta Sueki<sup>1</sup>

<sup>1</sup>Meteorological Research Institute, Tsukuba, Japan

(Corresponding author: Kenta Sueki, e-mail: ksueki@mri-jma.go.jp)

This work is distributed under the Creative Commons Attribution 4.0 License (CC BY 4.0)

## 1. Introduction

From late evening of July 4 to early morning of July 5, 2022, a line-shaped precipitation system (senjo-kousuitai in Japanese) occurred in Kochi Prefecture, Japan. There were no casualties, but some flooded houses and crop loss were reported in this event. The half-a-day warning for a line-shaped precipitation system which began to be operated by Japan Meteorological Agency (JMA) in June 2022 was not issued, because the predicted rainfall amount did not reach the criteria. In this study, we try to simulate this rainfall event, which was difficult to predict in advance, using a non-hydrostatic model and investigate dependence of the simulation on initial time and model resolution.

## 2. Model settings

We used a non-hydrostatic model ASUCA<sup>1</sup> which has been developed and used operationally by the JMA. The initial and boundary conditions for the simulation was the JMA's meso-scale analysis. The size of calculation domain was 1440 km × 1440 km in the horizontal directions and 21.8 km in the vertical direction for the control experiment. The center of the domain was located at 32°N, 132°E. The horizontal grid spacing was 2 km and the vertical grid spacing varied from 20 m at the bottom to 650 m at the top. The number of vertical layers was 76. In addition to the control experiment, we also performed the simulations with the horizontal grid spacings of 1 km, 500 m, and 250 m to investigate the resolution dependence of the precipitation system simulation. We used the Mellor–Yamada–Nakanishi–Niino<sup>3</sup> (MYNN) Lev. 3 for 2-km and 1-km simulations and the anisotropic Deardorff model<sup>2</sup> (ADM) for 500-m and 250-m simulations as subgrid scale turbulence parameterizations. Microphysical processes were parameterized using a six-class single-moment scheme.

## 3. Results

Figure 1 compares the distribution of accumulated rainfall amount in the 6-hour from 1200 UTC to 1800 UTC 4 July based on the radar/rain-gauge-analyzed precipitation data (Fig. 1a) and that calculated from the control experiment ( $\Delta x = 2$  km) with the initial time of 0900 UTC 4 July (Fig. 1b). Both location and rainfall amount of the precipitation band were well simulated. Figure 2 shows the vertical cross section of simulated convective cells along the line-shaped precipitation system. Convective cells passed over the rainfall area repeatedly. We also conducted the experiment where the topography of Shikoku Island including Kochi was removed, and found that a line-shaped rainfall area occurred at almost the same position as the control experiment while the rainfall amount decreased. As for the dependence on the initial time, the orientation of the rainfall band was different from the actual one for simulations using relatively early initial times since the Typhoon AERE passed through a wrong track for these simulations. In the case of this experiment, the rainfall amount decreased as the model resolution increased.

#### 4. Summary

We conducted a numerical experiment for the line-shaped precipitation system occurred in Kochi, Japan in early July 2022. Location and rainfall amount of the precipitation band were well simulated for the control experiment with the horizontal grid spacing of 2 km. For the simulation with relatively early initial times, poor simulations for the track of the Typhoon AERA resulted in the different orientation of the rainfall band. In this experiment, the rainfall amount decreased as the model resolution increased.

#### References

1. Ishida, J., K. Aranami, K. Kawano, K. Matsubayashi, Y. Kitamura, and C. Muroi (2022) ASUCA: The JMA operational non-hydrostatic model. *J. Meteor. Soc. Japan*, **100**, 825–846.
2. Kitamura, Y. (2016) Improving a turbulence scheme for the Terra Incognita in a dry convective boundary layer. *J. Meteor. Soc. Japan*, **94**, 491–506.
3. Nakanishi, M., and H. Niino (2006) An improved Mellor–Yamada level-3 model with condensation physics: Its design and verification. *Bound-Lay. Meteor.*, **112**, 1–31.

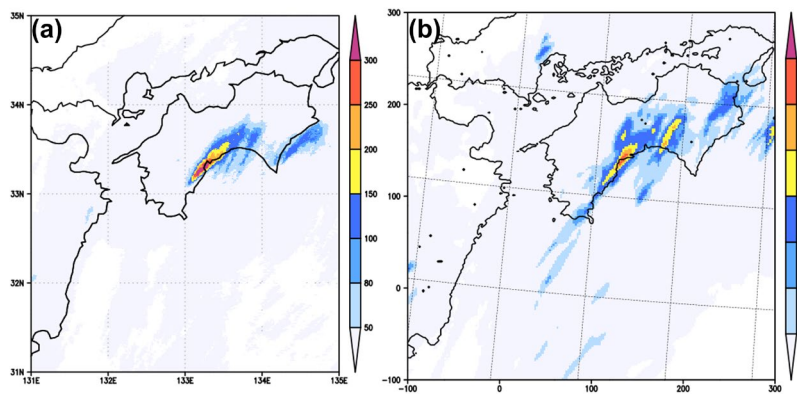


**Figure 1.** Distribution of accumulated rainfall amount (mm) in the 6-hour from 1200 UTC to 1800 UTC 4 July: (a) is based on the radar/rain-gauge-analyzed precipitation data; (b) is a simulation result in the present study.

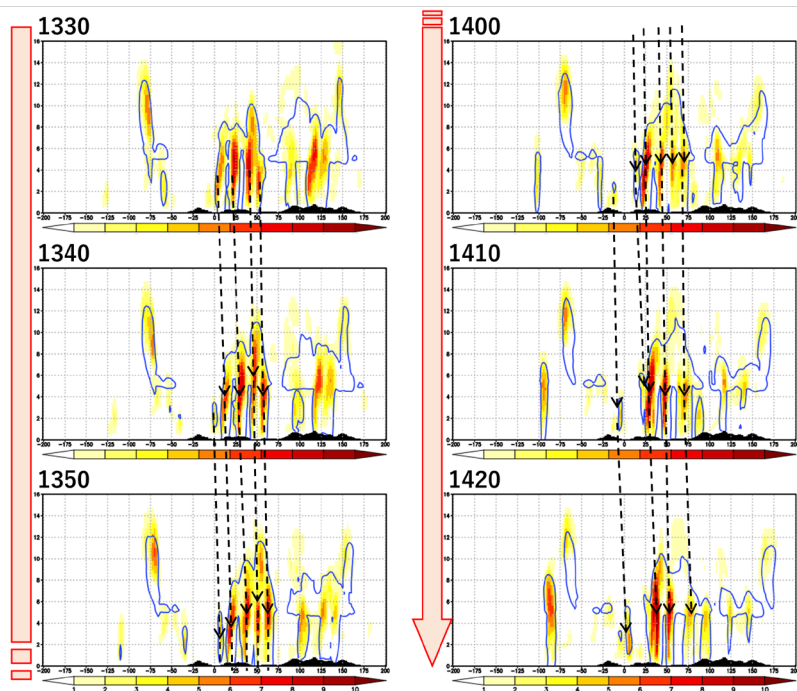


**Figure 2.** Vertical cross section of simulated convective cells along the line-shaped precipitation system. Each panel shows a snapshot every 10 minutes from 1330 UTC to 1420 UTC 4 July. Color shade indicates vertical velocity ( $\text{m s}^{-1}$ ). Blue solid lines indicate contour lines for the condensate of  $2 \text{ g kg}^{-1}$ .

# What controlled the low-level moisture transport during the extreme precipitation in Henan Province of China in July 2021?

Hao-Yan LIU<sup>1</sup>, Jian-Feng GU<sup>2</sup>, Yuqing WANG<sup>3</sup>, and Jing XU<sup>4</sup>

<sup>1</sup>Hohai University, Nanjing, China

<sup>2</sup>Nanjing University, Nanjing, China

<sup>3</sup> University of Hawaii at Manoa, Honolulu, USA

<sup>4</sup> China Meteorological Administration, Beijing, China

(Corresponding author: Haoyan LIU, e-mail: liuhaoyan@hhu.edu.cn)

This work is distributed under the Creative Commons Attribution 4.0 License (CC BY 4.0)

## 1. Introduction

A record-breaking precipitation event occurred in the Henan province of China in July 2021 (217HP). The precipitable water during this extreme event was primarily contributed by the low-level southeasterly (LLSE) water vapor transport. The LLSE was largely enhanced by the pressure gradient force maintained by the western Pacific subtropical high and further amplified by the latent heat release in the rainfall system over Henan. The positive moisture advection by the LLSE and evaporative water occurred below 950 hPa and was redistributed into higher levels by the LLSE jet-enhanced subgrid vertical turbulent transport. The combination of the enhanced LLSE centered around 950 hPa and the increase of moisture below 850 hPa were the main drivers for the continuous strengthening of LLSE moisture transport, with the former playing the dominant role. Not only the presence but also the intensity of the LLSE jet were important for reproducing the extreme rainfall. Typhoon In-Fa (2021) presented an uncertain impact on 217HP, while Typhoon Cempaka (2021) was found to be unfavorable for 217HP. Cempaka mainly acted to weaken the southwesterly wind to the southwest of Henan by reducing the pressure gradient and impeded the water vapor transport toward Henan.

## 2. Model description and experimental setup

We used the WRF model (version 3.8.1) with the horizontal grid spacing of 9 and 3 km, respectively. The model had 50 vertical levels topped at 30 hPa with 11 levels below the 3-km height. The model physics included the Thompson graupel

microphysics scheme, RRTMG shortwave and longwave radiation schemes, ACM2 planetary boundary layer scheme, Pleim-Xiu surface layer and land surface model schemes, and the Kain–Fritsch cumulus parameterization scheme. The model used the ERA5 data as the initial and lateral boundary conditions.

Six ensemble simulations were conducted at each initial time to test the robustness of the results, where the initial conditions were directly interpolated from the ERA5 data (CTL group). One member (M1) was without any initial perturbations and the other five members (M2-M6) started with different initial specific humidity perturbations. To investigate the influence of Typhoons In-Fa and Cempaka on 217HP, another three groups of sensitivity experiments were conducted, with the model settings being the same as the CTL group, but with the vortex components within 900-km radius from the TC (tropical cyclone) center associated with In-Fa (RM\_IN), Cempaka (RM\_CEM), and both In-Fa and Cempaka (RM\_BTC) artificially removed from the initial conditions, respectively.

### **3. Result and conclusion**

The source of precipitable water over Henan was mainly from the advection and evaporation below 950 hPa and PBL process above 950 hPa to the southeast of Henan, which were primarily driven by the strong LLSE. The LLSE was triggered and maintained by the western North Pacific to Henan's east and accelerated by the local rainfall system over Henan. Driven by the LLSE moisture transport, the local rainfall system over Henan lowered the local pressure and enhanced the LLSE moisture transport, further strengthening the heavy rainfall through positive feedback. Typhoon In-Fa showed large uncertainty on the heavy rainfall during 0000 UTC 18 July to 0000 UTC 21 July, while Cempaka impeded the heavy rainfall through weakening the southwesterly moisture transport into Henan.

### **References**

1. Liu, H.-Y., J.-F. Gu, Y. Wang, and J. Xu, 2023: What controlled the low-level moisture transport during the extreme precipitation in Henan Province of China in July 2021? *Mon. Wea. Rev.*, **151**, 1347–1365, <https://doi.org/10.1175/MWR-D-22-0200.1>.

# Ensemble simulations of a mesoscale convective system over East China Sea on 19 June 2022

Saori NAKASHITA<sup>1</sup>, Takeshi ENOMOTO<sup>2,3</sup>, and Satoshi ISHII<sup>4</sup>

<sup>1</sup>Graduate School of Science, Kyoto University, Kyoto, Japan

<sup>2</sup>Disaster Prevention Research Institute, Kyoto University, Uji, Kyoto, Japan

<sup>3</sup>Application Laboratory, Japan Agency for Marine-Earth Science and Technology, Yokohama, Japan

<sup>4</sup>Japan Meteorological Agency

(Corresponding author: Saori NAKASHITA, nakashita@dpac.dpri.kyoto-u.ac.jp)

This work is distributed under the Creative Commons Attribution 4.0 License (CC BY 4.0)

## 1. Introduction

During the Baiu/Mei-yu season, a large amount of water vapor is supplied from the south into a synoptic-scale Baiu front over the East China Sea. Mesoscale convective systems (MCSs) occasionally develop along the frontal zone due to the local moisture convergence, which cause devastating heavy rainfall over Japan. Since the Baiu frontal zone is characterized by a hierarchy of disturbances from synoptic- to meso- $\gamma$ -scales (Ninomiya and Akiyama 1992), better understanding of the multiscale uncertainty is necessary to clarify the predictability of MCSs. In this study, we conduct nesting ensemble simulations of the MCS developed on 19 June 2022 to reveal features of various scales affecting the uncertainty of the MCS. This case was captured by hourly dense upper observations from three research vessels during a field campaign in June 2022. We also investigate the impact of these intense observations on the MCS by ensemble assimilation experiments.

## 2. Model description and experimental setup

Ensemble simulations of 40 members are conducted by three-step nesting with the NCEP regional spectral model (Juang 2000), which allows to switch between hydrostatic and nonhydrostatic formulations. The outermost hydrostatic domain D1 (344 x 288 grids) is centered at (120E, 23.5N) with 27-km resolution in the horizontal. The initial and base fields of D1 are obtained from NCEP GFS analysis or forecast. The inner domains are nonhydrostatic: D2 (384 x 324 grids) is centered at (130E, 35N) with 9-km and D3 (384 x 324 grids) at (125E, 29N) with 3-km, respectively. The vertical discretization of 42 levels in sigma coordinates is common in all domains. The breeding method (Toth and Kalnay 1997) is used for generating initial ensemble perturbations in D1. Six-hourly breeding cycles are initiated at 0000 UTC 17th. Simulations in D2 and D3 start from 1200 UTC 18th and are run for 24 hours.

Ensemble assimilation experiments are conducted in D2 and D3 with the maximum likelihood ensemble filter (Zupanski 2005). Since the intense observations from 0000 UTC 19th are contained in PREPBUFR, we compare control experiments assimilating all conventional observations with experiments removing the upper observations by the vessels.

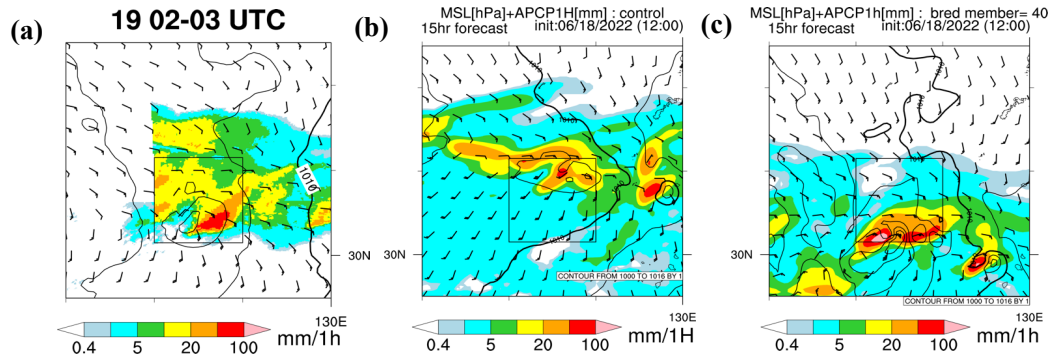


Fig. 1. Sea-level pressure and 1 hour accumulated precipitation at 0300 UTC 19th from (a) JMA meso-analysis and analyzed radar, (b) unperturbed simulation and (c) member

### 3. Results and discussions

The unperturbed control simulation has a northward bias of the MCS (Fig. 1a, b). The perturbed member (Fig. 1c) that reduces the northward bias better represents lower convergence. The ensemble spread of water vapor becomes large along the large equivalent potential temperature gradient in lower troposphere and that of kinetic energy is large to the east of lower synoptic trough extending from the continent. The ensemble sensitivity analysis (Enomoto et al. 2015) applied to D2 ensemble also confirms the relationship between the development of MCS and the upstream synoptic uncertainty.

Ensemble assimilation experiments in D3 show that the assimilation of the intense observations increase the probability of predicting strong convective cells elongated in the northeast-southwest direction as observed. The observations have the largest impact just after the MCS passed near the vessels and contribute to convective initiation by enhancing moisture gradients and convergences in the boundary layer. These results suggest that the development of MCS is sensitive to both synoptic- and convective-scales.

#### Acknowledgments

This work is supported by JSPS KAKENHI Grant Number 22KJ1966, 19H05698, 19H05605, 21K03662.

#### References

1. Enomoto, T., S. Yamane, and W. Ohfuchi, (2015), Simple sensitivity analysis using ensemble forecasts, *J. Meteor. Soc. Japan*, **93**, 199–213.
2. Juang, H-M., (2000), The NCEP mesoscale spectral model: A revised version of the nonhydrostatic regional spectral model, *Mon. Wea. Rev.*, **128**, 2329–2362.
3. Ninomiya, K., and T. Akiyama, (1992), Multi-scale features of Baiu, the summer Monsoon over Japan and the east Asia, *J. Meteor. Soc. Japan*, **70**, 467–495.
4. Toth, Z., and E. Kalnay, (1997), Ensemble forecasting at NCEP and the breeding method, *Mon. Wea. Rev.*, **125**, 3297–3319.
5. Zupanski, M., (2005), Maximum likelihood ensemble filter: Theoretical aspects, *Mon. Wea. Rev.*, **133**, 1710–1726.

# Mesoscale Convective Systems Under Weak Large-Scale Conditions over Mindanao, Philippines

Cathrene LAGARE<sup>1</sup>, Takeshi YAMAZAKI<sup>1</sup>, and Junshi ITO<sup>1</sup>

<sup>1</sup>Tohoku University, Sendai, Japan

(Corresponding author: Cathrene LAGARE, e-mail: clagare@dc.tohoku.ac.jp)

This work is distributed under the Creative Commons Attribution 4.0 License (CC BY 4.0)

## 1. Introduction

Mesoscale convective systems (MCSs) are organized clusters of convective cells, often bringing heavy to extreme precipitation. Studies on severe weather in the Philippines, a part of the Maritime Continent where frequent and intense convective activities occur, predominantly focus on synoptic-scale systems (e.g., tropical cyclones, monsoonal flows). The structure and evolution of MCSs in the Philippines remain understudied. This study examines the local-scale processes involved in the organization of MCSs through numerical simulations. The 03 May 2017 heavy rainfall event over Davao City in Mindanao Island, Philippines, was used as the case event for this study. The case event happened during the summer (April-May) when large-scale forcings (e.g., monsoonal flow) have a weak influence over the region, and local diurnal forcing is mainly in effect.

## 2. Model description and experimental setup

This study used the Advanced Research Weather Research and Forecasting Model (WRF-ARW; Skamarock et al. 2019) version 4.2.2 in the simulations. The simulations were carried out from 19:00 UTC 02 to 0:00 UTC 04 May 2017. Five nested domains were used, and two-way nesting was applied for 27, 9, 3, and 1 km grid spacing domains, while one-way nesting for the 200 m grid spacing domain to save computational time. The simulations used 60 vertical levels and utilized ERA5 reanalysis as the initial and boundary condition. The physics parameterization schemes and calibrated parameter values for the Kain-Fritsch cumulus scheme were based on Tolentino and Bagtasa (2021). The cumulus scheme was turned off from 3 km to 200 m grid spacing domains, assuming the grid spacings were fine enough to resolve convection. Meanwhile, the innermost domain (200 m grid size) was run on a large-eddy simulation (LES) mode wherein the planetary boundary layer (PBL) was turned off, and full diffusion was turned on.

## 3. Result and conclusion

On 03 May 2017, the satellite observations showed the development of MCSs in the area

during that day that could have brought in a large amount of rainfall. The numerical simulations showed that the development and merging of two meso- $\beta$  scale convective systems over the Mindanao region resulted in flood-producing rainfall. It was found that sea breeze circulation, cold pools, and complex topographical features of Mindanao Island mainly influenced the development and maintenance of these MCSs (Figure 1). The full results of this study are found in Lagare et al. (2023).

## References

1. Lagare, C., Yamazaki, T., & Ito, J. (2023). Numerical simulation of a heavy rainfall event over Mindanao, Philippines, on 03 May 2017: mesoscale convective systems under weak large-scale forcing. *Geoscience Letters*, 10(1), 23.
2. Skamarock, W. C., Klemp, J. B., Dudhia, J., Gill, D. O., Liu, Z., Berner, J., ... & Huang, X. Y. (2019). A description of the advanced research WRF version 4. *NCAR tech. note ncar/tn-556+ str*, 145.
3. Tolentino, J. T., & Bagtasa, G. (2021). Calibration of Kain–Fritsch cumulus scheme in weather research and forecasting (WRF) model over western Luzon, Philippines. *Meteorology and Atmospheric Physics*, 133(3), 771-780.

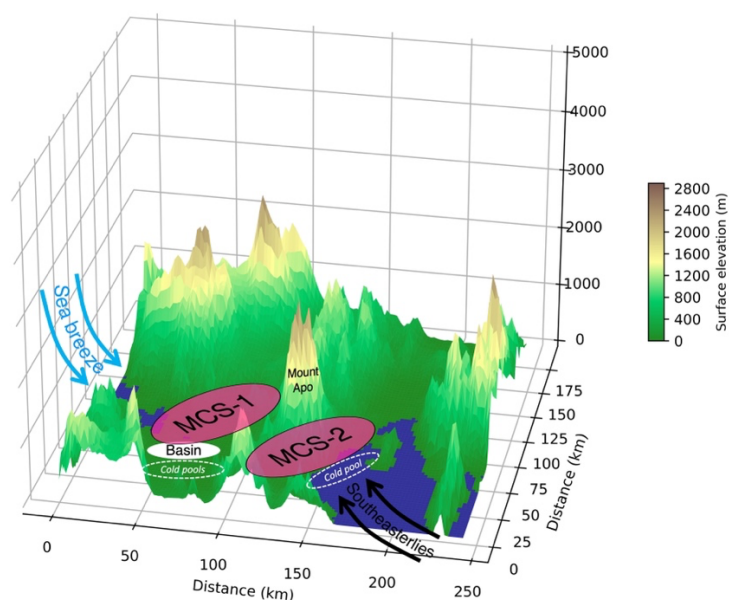


Figure 1. Schematic diagram of convective processes involved in the formation of 03 May 2017 MCSs (Fig. 9 from Lagare et al., 2023)

# Comparing Large-Scale Atmospheric Circulation Patterns Associated with 2022 and 2010 Extreme Rainfall Events in Pakistan

Abhinav Dengri<sup>1</sup>, Tomohito Yamada<sup>2</sup>

<sup>1</sup>Graduate School of Engineering, Hokkaido University, Sapporo, Japan

<sup>2</sup>Faculty of Engineering, Hokkaido University, Sapporo, Japan

(Corresponding author: Abhinav Dengri, e-mail: dengri@elms.hokudai.ac.jp)

This work is distributed under the Creative Commons Attribution 4.0 License (CC BY 4.0)

## 1. Introduction

Monsoon rainfall in Pakistan, crucial for agriculture, industry, and domestic use, has seen significant changes in intensity, volume, and distribution over the past decade. The 2010 and 2022 monsoon seasons were particularly catastrophic, causing widespread flooding and thousands of fatalities. The 2010 flood has been linked to anomalous atmospheric blocking over Western Europe (Yamada et al., 2016), leading to instabilities over northern Pakistan (Lau and Kim, 2012). This study aims to analyze the spatial distribution of precipitation and moisture transport mechanisms during these extreme rainfall periods in 2010 and 2022 and explore the potential connection between the Western European atmospheric blocking and these rainfall events.

## 2. Model description and experimental setup

We employed two datasets to study precipitation and large-scale atmospheric flows. For precipitation analysis, we utilized the NOAA Climate Prediction Center (CPC) Unified Gauge-Based Analysis of Global Daily Precipitation dataset (Xie et al., 2007, Chen et al., 2008). For the analysis of large-scale atmospheric flows, we relied on the NCEP Reanalysis-II dataset (Kanamitsu et al., 2002).

## 3. Result and conclusion

Our study illuminates the severity of the 2010 and 2022 flooding events in Pakistan, through the spatial distribution of total seasonal rainfall during June, July, and August (JJA), as shown in Figure 1. In 2022, the entire country experienced a higher volume of rainfall than in 2010, with southern Pakistan receiving over 600mm of rainfall. Figure 2 depicts the vertically integrated moisture flux transport for July and August in both years. The 2022 data reveals a significant increase in moisture transported from the Bay of Bengal to central Pakistan, facilitated by stronger southeasterlies. Additionally, a higher southerly moisture influx from the Arabian Sea was observed in 2022, contributing to the increased rainfall and subsequent flooding. Figure 3(a) and Figure 3(b) contrast the mid-tropospheric flows in 2010 and 2022. In 2022, a blocking high over western Russia was linked to a deep trough and eastern low-pressure centers. The tropical component was marked by a distinct subtropical low with a closed cyclonic circulation over southern Pakistan and the northern Arabian Sea. An anomalous anticyclonic circulation was noted northeast of the Tibetan Plateau, extending into northern Pakistan. The significant pressure gradient between the Tibetan high and the cyclonic low system triggered strong southeasterlies and southerlies over central Pakistan, enhancing moisture influx from the Bay of Bengal and the northern Arabian Sea. Figure 4 contrasts the 500hPa vertical velocity for July and August in 2022 and 2010. Negative values indicate the speed at which air is rising, a key factor in precipitation likelihood. The 2022 data reveals a more pronounced adiabatic ascent in central Pakistan, leading to enhanced cloud formation and precipitation, underscoring the meteorological conditions that contributed to the higher rainfall in 2022.

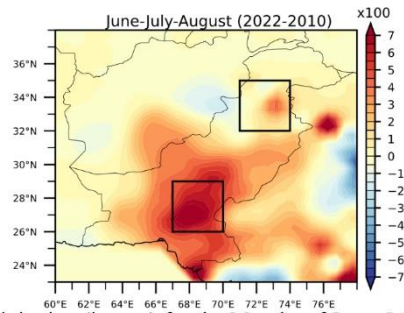


Fig.1: Difference of cumulative Precipitation (in mm) for the Months of June, July, and August in 2010 and 2022.

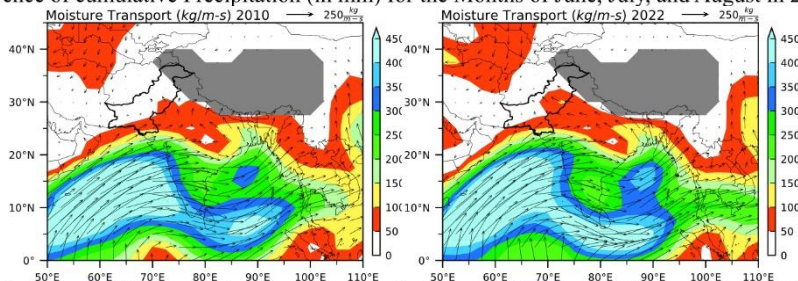


Fig.2: Vertically Integrated Moisture Transport from the Surface to 700hPa in July-August: Magnitude and Vectors for 2010 and 2022.

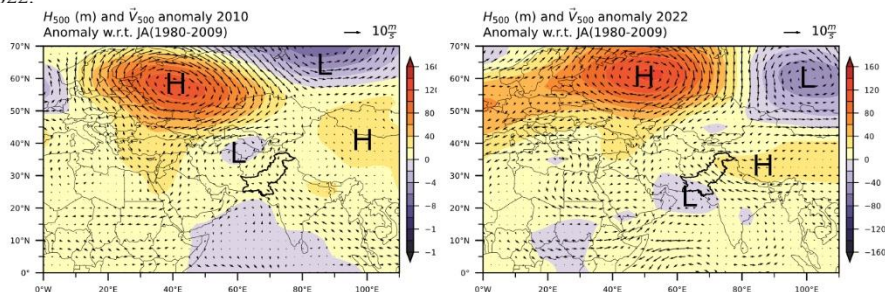


Fig.3: 500hPa Geopotential Height Anomalies and associated wind vectors in July-August for 2010 and 2022.

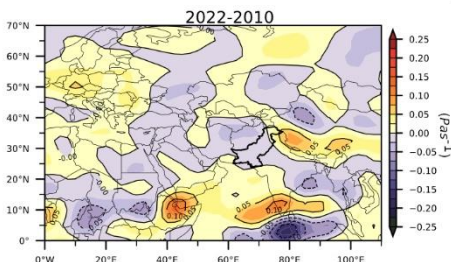


Fig.4: Difference in 500hPa Vertical wind patterns during the Months of July and August between 2022 and 2010.

### References (in alphabetical order according to author)

1. Chen, M. et al. (2008) ‘Assessing objective techniques for gauge-based analyses of global daily precipitation’, *Journal of Geophysical Research: Atmospheres*, 113(D4). Available at: <https://doi.org/10.1029/2007JD009132>.
2. Kanamitsu, M. et al. (2002) ‘NCEP–DOE AMIP-II Reanalysis (R-2)’, *Bulletin of the American Meteorological Society*, 83(11), pp. 1631–1644. Available at: <https://doi.org/10.1175/BAMS-83-11-1631>.
3. Lau, W.K.M. and Kim, K.-M. (2012) ‘The 2010 Pakistan Flood and Russian Heat Wave: Teleconnection of Hydrometeorological Extremes’, *Journal of Hydrometeorology*, 13(1), pp. 392–403. Available at: <https://doi.org/10.1175/JHM-D-11-016.1>.
4. Yamada, T.J. et al. (2016) ‘Climatological Characteristics of Heavy Rainfall in Northern Pakistan and Atmospheric Blocking over Western Russia’, *Journal of Climate*, 29(21), pp. 7743–7754. Available at: <https://doi.org/10.1175/JCLI-D-15-0445.1>.
5. Xie, P. (2010) CPC unified gauge-based analysis of global daily precipitation. Available at: [https://ams.confex.com/ams/90annual/techprogram/paper\\_163676.htm](https://ams.confex.com/ams/90annual/techprogram/paper_163676.htm) (Accessed: 27 February 2023).

# **Sensitivity to surface fluxes in the simulations of medicane Apollo (2021)**

Takeshi ENOMOTO<sup>1,2</sup>, Shunsuke MURATA<sup>3</sup>, and Saori NAKASHITA<sup>3</sup>

<sup>1</sup>Disaster Prevention Research Institute, Kyoto University, Uji, Kyoto, Japan

<sup>2</sup>Application Laboratory, Japan Agency for Marine-Earth Science and Technology, Yokohama, Japan

<sup>3</sup>Graduate School of Science, Kyoto University, Kyoto, Japan

(Corresponding author: Takeshi ENOMOTO, enomoto.takeshi.3n@kyoto-u.ac.jp)

This work is distributed under the Creative Commons Attribution 4.0 License (CC BY 4.0)

## **1. Introduction**

Medicanes are intense cyclones in the Mediterranean Sea with a thermal structure similar to that of tropical cyclones. Hurricane-like cyclones often cause devastating damages due to heavy precipitation and strong winds in the Mediterranean islands and coasts. Mediterranean cyclones are active in autumn to winter with low sea-surface temperature of approximately 20°C, much lower than the threshold for tropical cyclogenesis of 26.5°C (Cavicchia et al. 2014). Miglietta and Rotunno (2019) conducted case studies for two medicanes in October 1996 and December 2005 and show that the wind-induced surface heat exchange (WISHE) is essential for the generation of a warm core. The previous studies suggest that some cold vortices undergo baroclinic instability and develop into a hurricane-like structure through atmosphere-ocean interaction. The conditions for such development, however, are still unclear.

Medicane Apollo (2021) was generated on 23 October 2021 and caused heavy precipitation over Algeria, Tunisia, and southern Italy. Apollo developed into a thermal structure similar to tropical cyclones in the mature stage. In this study, the thermal structure and intensification mechanisms are investigated.

## **2. Data analysis and model description**

ERA5 (Hersbach et al. 2020) is used for tracking and identification of the thermal structure. The off-grid location of the cyclone centre is determined by quadratic interpolation of the sea-level pressure. The thermal structure is estimated by the cyclone phase space (CPS, Hart 2003).

Simulations were conducted with the NCEP RSM (regional spectral model) using the internally evolving pressure co-ordinate (Juang 2000). NCEP GFS global analysis and forecast provides the the initial and the base states. Note that RSM updates the difference from the base state, i.e. outer domain not only specify the boundary conditions, but also the scales that outer domain can resolve within the subdomain. GFS is interpolated to 27 km and RSM is discretized with 9 km in the horizontal and 42 levels in the vertical. The model was integrated in an approximately 2000 × 1000 km domain centred at (35°E, 18°N) for 72 h from 0000 UTC, 23 and 0000 UTC, 27 October to investigate the development and mature stages, respectively. In addition, the surface fluxes were reduced by 90% to examine the sensitivity to surface fluxes.

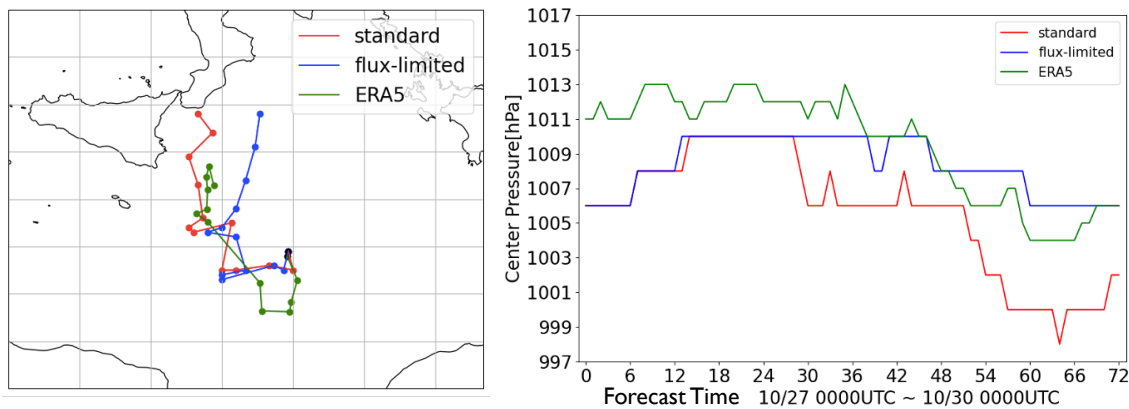


Figure 1 The six-hourly (a) position and (b) minimum sea-level pressure of Apollo in ERA5 (green), standard (red) and flux-limited (blue) experiments between the initial time of 0000 UTC. 27 October to 30 October.

### 3. Results and conclusions

Apollo had its maximum intensity at 1800 UTC 29 October. Then, the CPS estimates a warm core in the lower troposphere.

The simulated cyclone in the experiment from 23 October shows insensitivity to the latent heat flux in the early stage of development. It is suspected that the dry and warm air supply from the Sahara plays an important role for the cyclogenesis.

Towards maturity, however, the heat and moisture from the Mediterranean become crucial for the formation of the warm core by warming and moistening the cold and dry air from the Balkan Peninsula as the integration from 27 October shows. Although both standard and flux-limited experiments fail to initial southward migration, but the cyclones in the standard and flux-limited experiments take different tracks later (Fig. 1a). The former moves towards Sicily as the one in ERA5 and the latter moves northeastwards. Moreover, the full flux intensity is required to reproduce Apollo's intensity and track (Fig. 1b). The central pressure in the standard experiment is very close to the value estimated by EUMETSAT (998.6 hPa), but two hours earlier.

It is concluded that the surface flux played an important role in the formation of the hurricane-like structure at its mature stage with a warm core in the lower troposphere. The cyclone was generated by warm advection from Sahara and developed with cold advection from the Balkan Peninsula, which were moistened and warmed over the Mediterranean Sea.

### Acknowledgments

This work was supported by JSPS KAKENHI Grant Number 21H04992.

### References

1. Cavicchia, L., H. von Storch, and S. Gualdi, 2014: A long-term climatology of medicanes. *Clim Dyn*, **43**, 1183–1195.
2. Hart, R. E., (2003), A cyclone phase space derived from thermal wind and thermal asymmetry. *Mon. Wea. Rev.*, **131**, 585–616.
3. Hersbach, H., and Coauthors, (2020), The ERA5 global reanalysis. *Quart. J. Roy. Meteor. Soc.*, **146**, 1999–2049.
4. Juang, H.-M. H., (2000), The NCEP Mesoscale Spectral Model: A revised version of the nonhydrostatic regional spectral model. *Mon. Wea. Rev.*, **128**, 2329–2362.
5. Miglietta, M. M., and R. Rotunno, (2019), Development mechanisms for Mediterranean tropical-like cyclones (medicanes). *Quart. J. Roy. Meteor. Soc.*, **145**, 1444–1460.

# Session I: Global storm-resolving simulations

[Special Session of the Japan Society for the Promotion of Science (JSPS) Core-to-Core Program  
“International Core-to-Core Project on Global Storm Resolving Analysis” (ICCP-GSRA; grant  
number: JPJSCCA20220001).]

# Clouds, convection, and precipitation in the global few hundred-meter simulations

Shuhe Matsugishi<sup>1</sup>, Tomoki Ohno<sup>1</sup>, Junshi Ito<sup>2</sup>, Masaki Satoh<sup>1</sup>, Yoshiyuki Kajikawa<sup>3</sup>, Yuta Kawai<sup>3</sup>, Masuo Nakano<sup>4</sup>, Hiroshi G. Takahashi<sup>5</sup>, Daisuke Takasuka<sup>1</sup>, Hirofumi Tomita<sup>3</sup>, Hisashi Yashiro<sup>6</sup>

<sup>1</sup> The University of Tokyo, Chiba, Japan, <sup>2</sup>Tohoku University, Sendai, Japan, <sup>3</sup>RIKEN, Kobe, Japan, <sup>4</sup>JAMSTEC, Yokohama, Japan, <sup>5</sup>Tokyo Metropolitan University, Hachioji, Japan, <sup>6</sup>National Institute for Environmental Studies, Tsukuba, Japan

(Corresponding author: Shuhe Matsugishi, e-mail: matsugishi@aori.u-tokyo.ac.jp)

This work is distributed under the Creative Commons Attribution 4.0 License (CC BY 4.0)

## 1. Introduction

Global nonhydrostatic models that cover the globe with a kilometer (km)-scale mesh have been developed by various organizations worldwide and are expected as next-generation global climate/weather models that can explicitly calculate deep convective clouds. However, it is known that convective upward motions are not sufficiently represented at the km-scale resolution, and the mesh size of  $O(100\text{m})$  is required to obtain convergence of upward motions. To understand the limitation of global km-scale models, we investigate how clouds, precipitation, and convection change with the resolution in the global simulations with the sub-km-scales.

## 2. Model description and experimental setup

We conducted the global atmospheric simulations by the Nonhydrostatic Icosahedral Atmospheric Model, NICAM (Satoh et al., 2008), with a mesh size of 3.5 km, 1.7 km, 870 m, 440 m, and 220 m. The 3.5 km experiment started on August 1, 2016, the same day as DYAMOND-summer, and the higher resolution was run using the lower resolution simulation results as initial conditions. We compare the differences in mean states of simulations and representation of convection across these resolutions. The global simulation with a mesh size of 220 m was possible by taking about half node of Supercomputer Fugaku.

The simulations with a resolution between km-scale and sub-km-scale are called a gray zone that is intermediate between Reynolds Averaged Navier-Stokes (RANS) models and Large Eddy Simulation (LES) models. We compare experiments using MYNN as a RANS scheme and the Smagorinsky scheme as an LES scheme.

## 3. Result and conclusion

Figure 1 shows the results of the 220 m resolution experiment. The 3.5-km resolution results show blob like clusters of clouds and precipitation, but the higher resolution more clearly shows sharp cloud structures as seen in the satellite observations and rain bands structure near the tropical cyclone. The 220m resolution experiment provides such a clear cloud convection structure no matter where in the entire globe is cut off.

The resolution-dependent changes are described. A decrease in the lower cloud is noticeable for increasing resolution. The precipitation distribution and the zonal mean humidity do not change significantly, but the zonal mean precipitation decrease (Fig. 2). In the sub-km range, relatively stranger rainfall decreases (Fig2). Therefore, the relative weak precipitation appears to be increasing. The rainy area expands as resolution becomes

finer. Coarse-grained rainfall distribution becomes smoother in the sub-km-scale model than in the km-scale model.

Comparing the results of the RANS and LES schemes, we find a significant difference in the lower cloud cover and distribution: the LES scheme showed more low cloud cover than the RANS scheme in 3.5 km simulation but both schemes become the same trend as the resolution increases.

We will further analyze what differences in the representation of convection occur between these simulations and how this affects the large-scale environment.

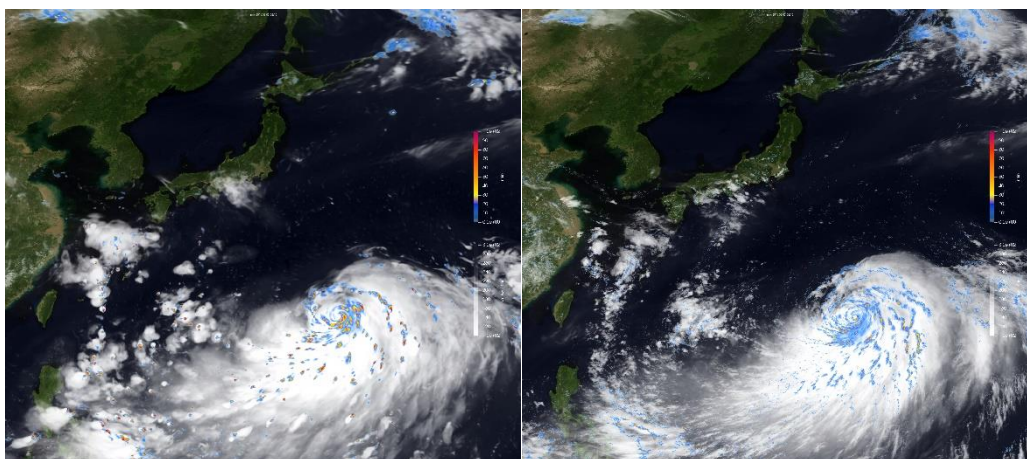


Fig. 1. Horizontal view of OLR and precipitation in (left)  $dx=3.5$  km and (right)  $dx=220$  m in simulation with smagorinsky scheme. Topography are Blue Marble NASA.

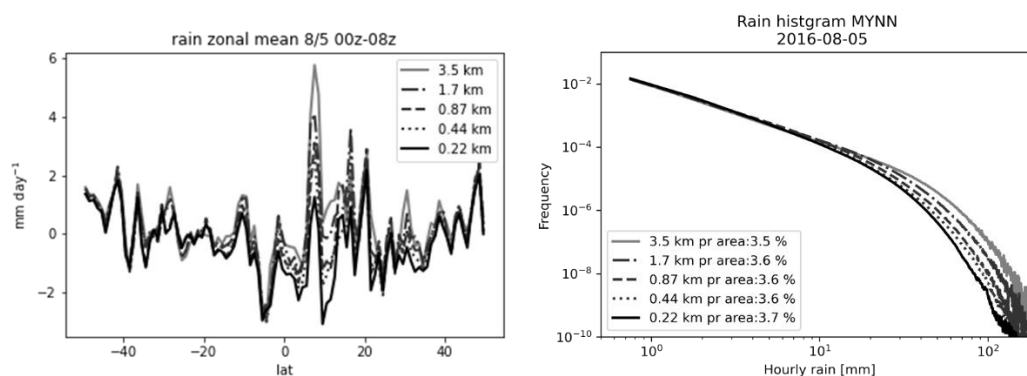


Fig. 2. (left) The difference between zonal mean precipitation (mm/day) and TRMM 3B42. (right) The histogram of hourly rain (mm) in simulation.

## References

1. Satoh, M., Matsuno, T., Tomita, H., Miura, H., Nasuno, T., & Iga, S. (2008). Nonhydrostatic icosahedral atmospheric model (NICAM) for global cloud resolving simulations. *Journal of Computational Physics*, 227(7), 3486–3514. <https://doi.org/10.1016/j.jcp.2007.02.006>

# Global convection permitting climate simulations with the Simple Cloud-Resolving E3SM Atmosphere Model (SCREAM)

Christopher Eldred<sup>1</sup>, Peter Caldwell<sup>2</sup>, et. al.

<sup>1</sup>Sandia National Laboratories, Albuquerque, NM, USA

<sup>2</sup>Lawrence Livermore National Laboratory

(Corresponding author: Christopher Eldred, e-mail: celdred@sandia.gov)

This work is distributed under the Creative Commons Attribution 4.0 License (CC BY 4.0)

## 1. Introduction

The Simple Cloud Resolving E3SM Atmosphere Model (SCREAM) is a new global atmosphere model under development by the US Department of Energy. It is designed for convection-permitting resolutions (~1-3 km horizontal grid spacing) and intended to run well on exascale-class supercomputers. Unlike many models, SCREAM is written in C++ using the Kokkos performance portability library. It also features a sophisticated cloud/turbulence scheme (SHOC) meant to handle the partially-resolved cloud dynamics expected at convection-permitting resolutions.

## 2. Model description and experimental setup

In contrast to many atmospheric models, SCREAM consists of only four components: the HOMME-NH dynamical core, P3 microphysics. SHOC macrophysics (cloud/turbulence scheme) and RRTGMP radiation. SCREAM is designed to simulate cloud permitting scales with 1-5km horizontal resolution, a model top of 40km and 128 vertical levels.

The HOMME-NH dynamical core solves the multicomponent compressible Euler equations in a rotating reference frame with the traditional, spherical geopotential and shallow atmosphere approximations, using a Lagrangian vertical coordinate and the constant kappa approximation for thermodynamics. The spatial numerics are a spectral element discretization in the horizontal along with mimetic finite differences in the vertical, plus a vertical remap. The time stepping is a horizontally-explicit vertically-implicit (HEVI) scheme optimized for maximum stable time step. The spatial numerics are stabilized with hyperviscosity, which also serves as a simple turbulence closure. Advection of trace species (such as various forms of water and aerosols) is done using an interpolation semi-Lagrangian method with a Quasi-Local Tree-based (QLT) constrained density reconstructor (CDR) for conservation, consistency and positive-definiteness. The use of the constant kappa approximation allows a decoupling between the dynamics and the moisture, permitting the use of separate spatial and temporal numerics.

Since boundary layer clouds and other small-scale features are still unresolved at 1-3km resolution, they must be parameterized. SCREAM uses the Simplified Higher Order Closure (SHOC), which is an assumed PDF-based scheme. Subgrid-scale turbulence

and cloud liquid are computed with an assumed double-Gaussian probability density function, where the higher-order moments are diagnosed for efficiency. For microphysics, SCREAM uses a double moment scheme based on the Predicted Particle Properties (P3) scheme. Significant modifications were made to the original P3 scheme to make it more consistent with the assumptions in SHOC. This included taking into account the subgrid-scale variations in liquid water potential temperature, total water mixing ratio, and vertical velocity predicted by SHOC, the fractional cloudiness and precipitation from SHOC and modifications to the computation of water vapor saturation. Finally, gas optical properties and radiative fluxes are computed using the RTE + RRTMGP radiative transfer package.

SCREAM support separate computational grids for the dynamics, physics and tracer transport (known internally as physgrid), with conservative remapping between them. Typically a coarser grid is used for the physics than the dynamics and tracer transport. Physics and dynamics are coupled using a time-split algorithm. At 3km the physics time step is 40s, while the dynamics time step is 10s. Recent computational results on Frontier have achieved ~1 SYPD (simulated year per day of compute time) for 3km global atmospheric simulation.

Recent work has introduced several new capabilities in SCREAM:

1. DP-SCREAM: A version of SCREAM that runs in a doubly periodic box domain. This has been very useful for parameterization testing since it is much cheaper than running the global model. It has also been useful for a range of scientific studies, such as horizontal resolution sensitivity.
2. RRM meshes: A version of SCREAM using a regionally refined mesh on the globe. This has been useful for regional climate simulation, running much faster than a globally refined mesh. It enables selective downscaling on regions of interest while avoiding issues of grid nesting and boundary conditions for regional models

This talk will discuss the use of C++/Kokkos and computational performance; new SCREAM capabilities such as doubly-periodic (DP-SCREAM) and regionally refined (RRM) modes; and results from recent simulations.

## References

1. Caldwell, P. M., Terai, C. R., Hillman, B., Keen, N. D., Bogenschutz, P., Lin, W., et al. (2021). Convection-permitting simulations with the E3SM global atmosphere model. *Journal of Advances in Modeling Earth Systems*, 13, e2021MS002544. <https://doi.org/10.1029/2021MS002544>
2. Bogenschutz, P. A., Eldred, C., & Caldwell, P. M. (2023). Horizontal resolution sensitivity of the Simple Convection-Permitting E3SM Atmosphere Model in a doubly-periodic configuration. *Journal of Advances in Modeling Earth Systems*, 15, e2022MS003466. <https://doi.org/10.1029/2022MS003466>

# Tracking the Rainfall Structure in DYAMOND Convection Permitting Models over the Northwest Pacific

Shao-Yu Tseng, Wei-Ting Chen

National Taiwan University, Taipei, Taiwan

(Corresponding author: Shao-Yu Tseng, e-mail: r09229003@ntu.edu.tw)

## 1. Introduction

Moist convection systems play a vital role in the Earth's climate system, including the transport of moisture, heat, and momentum. The diverse structures and lifecycles of these convection systems have varying impacts, with persisting organized convection systems exhibiting more significant transport compared to isolated and short-lived counterparts. The DYAMOND project (Stevens et al., 2019) has assembled several cutting-edge global convection-permitting models (GCPMs), enabling direct resolution of convection systems. However, Su et al. (2022) pointed that, except for models with convection parameterization, most GCPMs tend to overestimate both the frequency and intensity of small object-based precipitation systems.

During the summer season in the northwest Pacific, a range of convective systems exists at different time scales, spanning from diurnal precipitation systems to long-lasting tropical cyclones. In this study, we conducted a comprehensive evaluation of GCPMs in this region by comparing their simulations with satellite-derived precipitation data from GPM-IMERG (Huffman et al. 2020), CMORPH (Joyce et al. 2004), and the ERA5 reanalysis dataset. The analysis focused on discerning the evolution of rainfall structure throughout the lifecycle of object-based precipitation systems.

## 2. Model description and experimental setup

In this study, we conducted a comparison of eight models from the DYAMOND Phase-1 repository (Stevens et al. 2019) and a hindcast simulation of CWBGFS (Su et al. 2022) following the DYAMOND protocol. All models were initialized on August 1st, 2016, and the analysis focused on the last 38-day period of the 40-day simulation. To evaluate the models' performance, we incorporated two satellite-derived precipitation datasets, GPM-IMERG and CMORPH, as observational reference and variation. Ensuring a fair comparison, all models and observational datasets are regridded to a uniform resolution consistent with CWBGFS grids and analyzed with the one-hour temporal resolution.

Among the DYAMOND models, ARPEGE-NH, ICON, and NICAM explicitly resolved moist convection while UM, FV3, and IFS-4km employed parameterization schemes to represent shallow convection processes. In contrast, IFS-9km parameterized both shallow and deep convection effects. MAPS, operating at a horizontal resolution of 3.8km, directly resolved moist convection without relying on parameterizations. In the case of CWBGFS, an atmospheric GCM, it operated at a spatial resolution of 15 km, utilizing the spectral method for horizontal directions and

assuming hydrostatic balance in the vertical. The model employed parameterizations for both shallow and deep convection effects, while offering the flexibility to resolve deep convection when the convective updraft fraction approached unity (Su et al. 2021). The contiguous precipitation pixels which exceeded 1 mm/hr are identified as object-based precipitation systems by the iterative rain cell tracking algorithm (Moseley et al. 2013, 2019).

### 3. Result and conclusion

When examining rainfall intensity, models utilizing convection parameterization (CP) systematically underestimate it. On the other hand, models directly resolving convection (DR) display significant variations among each other, not only in terms of intensity but also in horizontal scale. Evaluating the models based on core fraction, which represents the ratio of the area with intense rainfall (>10mm/hr) to the total area, reveals that CP models underestimate this measure, while DR models tend to overestimate it. This bias is observed across systems with varying lifetimes. However, some DR models exhibit a substantial increase in core fraction in the early stage of rainfall systems. In our ongoing research, we will further investigate the relationship between core fraction bias, precipitation efficiency, and the interaction between convection and circulation within the models.

### References

1. Joyce, R. J., J. E. Janowiak, P. A. Arkin, and P. Xie, 2004: CMORPH: A method that produces global precipitation estimates from passive microwave and infrared data at high spatial and temporal resolution. *J. Hydrometeor.*, 5, 487-503.
2. Moseley, C., Berg, P., & Haerter, J. O. (2013). Probing the precipitation life cycle by iterative rain cell tracking. *Journal of Geophysical Research: Atmospheres*, 118(24), 13,361-313,370.
3. Moseley, C., Henneberg, O., & Haerter, J. O. (2019). A Statistical Model for Isolated Convective Precipitation Events. *Journal of Advances in Modeling Earth Systems*, 11(1), 360-375.
4. Stevens, B., Satoh, M., Auger, L. et al. DYAMOND: the DYnamics of the Atmospheric general circulation Modeled On Non-hydrostatic Domains. *Prog Earth Planet Sci* 6, 61 (2019).
5. Su, C. Y., Chen, W. T., & Wu, C. M. (2022). Object-based evaluation of tropical precipitation systems in DYAMOND simulations over the Maritime Continent. *Journal of the Meteorological Society of Japan. Ser. II*, 100(4), 647-659.
6. Su, C. Y., Wu, C. M., Chen, W. T., & Chen, J. H. (2021). Implementation of the unified representation of deep moist convection in the CWBGFS. *Monthly Weather Review*, 149(10), 3525-3539.

# Benefits and Issues in the Kilometer-scale Atmospheric Climate Simulation with NICAM

Daisuke TAKASUKA<sup>1,2</sup>, Chihiro KODAMA<sup>2</sup>, Tamaki SUEMATSU<sup>3</sup>, Tomoki OHNO<sup>1</sup>, Yohei YAMADA<sup>2</sup>, Tatsuya SEIKI<sup>2</sup>, Hisashi YASHIRO<sup>4</sup>, Masuo NAKANO<sup>2</sup>, Hiroaki MIURA<sup>5</sup>, Akira T. NODA<sup>2</sup>, Tomoe NASUNO<sup>2</sup>, Tomoki MIYAKAWA<sup>1</sup>, Ryusuke MASUNAGA<sup>2</sup>

<sup>1</sup>Atmosphere and Ocean Research Institute, The University of Tokyo, Kashiwa, Japan

<sup>2</sup>Japan Agency for Marine-Earth Science and Technology, Yokohama, Japan

<sup>3</sup>RIKEN Center for Computational Science, Kobe, Japan

<sup>4</sup>National Institute for Environmental Studies, Tsukuba, Japan

<sup>5</sup>Department of Earth and Planetary Science, The University of Tokyo, Tokyo, Japan  
(Corresponding author: Daisuke TAKASUKA, e-mail: takasuka@aori.u-tokyo.ac.jp)

This work is distributed under the Creative Commons Attribution 4.0 License (CC BY 4.0)

## 1. Introduction

Deep convection is a fundamental element in the Earth's atmosphere. In fact, the hierarchical structure is emergent within a scale gap between cumulus clouds and large-scale circulations (e.g., mesoscale convective systems, tropical cyclones, and the Madden–Julian oscillation [MJO]). While conventional global climate models have struggled with simulating the above phenomena seamlessly because of using cumulus parameterizations. The recent increase in computing power enables us to overcome this difficulty via the explicit convection framework. Considering this stream, we aim at clarifying merits and issues of a climate study using a global cloud-resolving model.

## 2. Model description and experimental setup

We used the Nonhydrostatic Icosahedral Atmospheric Model (NICAM; Tomita & Satoh, 2004) for a kilometer-scale multi-year simulation. We adopted a globally quasi-uniform 3.5-km horizontal mesh and 78 vertical layers. A model physics configuration is based on Takasuka et al. (2023), which is an updated version that was previously used in a HighResMIP climate simulation (Kodama et al., 2021). Toward the seamless and realistic representation of climatological statistics and weather, we updated parameters in a single-moment cloud microphysics scheme and newly implemented turbulent mixing effects represented by the Leonard term. The simulation was initialized by the ERA-Interim data on January 1st, 2011, and used a mixed-layer slab ocean model with its depth of 15 m. At present, we succeeded in about 5-year integration (still ongoing).

### 3. Result and conclusion

Both kilometer-scale horizontal resolution and model improvement in NICAM can realistically reproduce both climatological and weather fields. The simulated annual mean precipitation has the realistic ITCZ structure, zonal contrast in the tropics, and storm track positions (Figures 1a, b). MJO convection is also spontaneously realized and successfully propagates into the tropical western Pacific (Figure 1c). Furthermore, compared to the HighResMIP simulation, we confirmed much better representation of tropical cyclone intensity and structure, precipitation diurnal cycle, and monsoon-related fields (e.g., baiu-meiyu front). However, we also face challenges of the poor representation of low clouds and associated overestimation of shortwave radiation incoming, indicating that more sophisticated treatment in PBL processes is required.

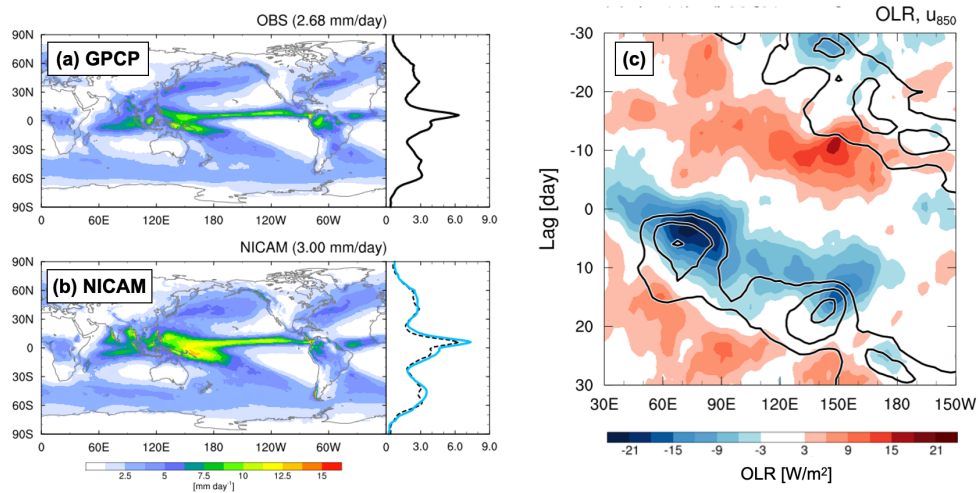


Fig. 1. (a and b) Five-year mean precipitation distributions for (a) GPCP and (b) NICAM. (c) Time-longitude diagram of  $10^{\circ}\text{N}$ – $10^{\circ}\text{S}$  averaged OLR (shading) and 850-hPa westerly wind (contours) anomalies composited for 21 MJO events in the 5-year simulation.

### References

1. Kodama, C., Ohno, T., Seiki, T., Yashiro, H., Noda, A. T., Nakano, M., ... Sugi, M. (2021). The Nonhydrostatic Icosahedral Atmospheric Model for Cmp6 HighResMIP Simulations (NICAM16-S): Experimental Design, Model Description, and Impacts of Model Updates. *Geoscientific Model Development*, **14**(2), 795–820.
2. Takasuka, D., C. Kodama, T. Suematsu, T. Ohno, Y. Yamada, T. Seiki, H. Yashiro, M. Nakano, H. Miura, A. T. Noda, T. Nasuno, T. Miyakawa, and R. Masunaga (2023), How Can We Improve the Seamless Representation of Climatological Statistics and Weather Toward Reliable Global K-scale Climate Simulations?, *ESS Open Archive*.
3. Tomita, H., and M. Satoh (2004), A new dynamical framework of nonhydrostatic global model using the icosahedral grid, *Fluid Dyn. Res.*, **34**(6), 357-400.

# Understanding tropical precipitation by using a global-coupled storm-resolving model

Hans Segura<sup>1</sup>, Cathy Hohenegger<sup>1</sup>

<sup>1</sup>Max Planck Institute for Meteorology, Hamburg, Germany

(Corresponding author: Hans Segura, e-mail: hans.segura@mpimet.mpg.de)

This work is distributed under the Creative Commons Attribution 4.0 License (CC BY 4.0)

## 1. Introduction

Models relying on statistical approaches to represent convection overestimate the frequency of precipitation intensities less than 20 mm d<sup>-1</sup> or light precipitation and underestimate the frequency of precipitation intensities higher than 20 mm d<sup>-1</sup> or heavy precipitation (Dai et al., 2006; Na et al., 2020). This bias in the spectrum of precipitation intensities is also observed even using grid spacing finer than 10 km (Judt and Rios-Berrios 2021). Contrary, atmospheric-only simulations using storm-resolving models, which can resolve processes in the meso-beta scale, show a similar frequency of light and heavy precipitation as in observations (Na et al., 2020; Stevens et al., 2020; Judt and Rios-Berrios 2021), i.e., a correct representation of the precipitation spectrum is achieved.

However, it is still unclear the role of light and heavy precipitation in the mean and variability of tropical precipitation and whether the most important component for the mean and the variability is related to a specific mode of tropical convection (shallow, congestus, and deep convection).

In this study, we use the ICOSahedral Non-hydrostatic (ICON) model in a global-coupled configuration to give insights into the role of the frequency of light and heavy precipitation in shaping the seasonal and daily variability of tropical precipitation. Moreover, we address the question of whether congestus or deep convective clouds accompany the regime governing the tropical precipitation variability. By revealing this intrinsic relationship of tropical precipitation, we also address the value added by global-coupled storm-resolving models in reproducing the different characteristics of tropical convection.

## 2. Model description and experimental setup

The global-coupled storm-resolving model ICON is used with the recently developed Sapphire configuration, which targets to explicitly resolve processes of the Earth's Climate System at kilometer scale or finer. The advantages of representing features of the Earth system in a short-term period as well as technical details related to the model development are described in Hohenegger et al. (2022). Among the set of simulations implemented by the authors, we use the G\_AO\_5km, named ICON-Sapphire in this study, which has a horizontal grid-mesh of 5 km with 91 vertical levels in the atmosphere, 128 vertical levels in the ocean and five soil layers in the continent. The simulation ran from January 21, 2020, to February 28, 2021. For this analysis, we only use data from February 2020 to January 2021, as the first ten days of simulation are considered to be a part of the spin-up period. The data is interpolated to a grid spacing of 0.1 degrees to be able to compare with observations

### 3. Result and conclusion

The probability density function of daily precipitation in ICON-Sapphire presents a similar distribution as observations in light precipitation ( $< 20 \text{ mm d}^{-1}$ ), but an overestimation in the frequency of heavy precipitation ( $> 20 \text{ mm d}^{-1}$ ) and an underestimation of extremely heavy precipitation ( $> 100 \text{ mm d}^{-1}$ ). However, those distortions do not impact the contribution to the total mean precipitation. In both observational and simulation data sets, 60% of tropical precipitation comes from heavy precipitation and 40% comes from light precipitation. On the other side, extremely heavy precipitation only contributes up to 10%.

The impact of heavy precipitation goes beyond the mean. The daily number of grid points precipitating more than  $20 \text{ mm day}^{-1}$ , and not the daily mean intensity, explains roughly 90% of the total precipitation variability in the tropics, with 56% of the variability explained by precipitation rates between 20 and  $70 \text{ mm d}^{-1}$  on seasonal and daily time scales. The precipitating region between 20 and  $70 \text{ mm d}^{-1}$  is indeed controlled by congestus and cumulonimbus clouds in terms of covered area (97%) and precipitation contribution (97%). However, the daily variations in the number of congestus clouds follow the seasonal ( $r = 0.68$ ) and daily ( $r = 0.76$ ) variations of the number of grid points precipitating between 20 and  $70 \text{ mm d}^{-1}$ . Our analysis point out that by explicitly resolving convection with a grid spacing of 5 km, basic relationships of tropical precipitation can be represented, as the role of heavy precipitation regime and congestus clouds in the tropical precipitation variability.

### References

- Dai, A., 2006: Precipitation Characteristics in Eighteen Coupled Climate Models. *J. Climate*, 19, 4605–4630, <https://doi.org/10.1175/JCLI3884.1>.
- Hohenegger, C., Korn, P., Linardakis, L., Redler, R., Schnur, R., Adamidis, P., et al. (2022). ICON-sapphire: Simulating the components of the Earth system and their interactions at kilometer and subkilometer scales. *Geoscientific Model Development Discussions*, 2022, 1–42. <https://doi.org/10.5194/gmd-2022-171>
- Judt, F., & Rios-Berrios, R. (2021). Resolved convection improves the representation of equatorial waves and tropical rainfall variability in a global nonhydrostatic model. *Geophysical Research Letters*, 48, e2021GL093265. <https://doi.org/10.1029/2021GL093265>
- Na, Y., Fu, Q., & Kodama, C. (2020). Precipitation probability and its future changes from a global cloud-resolving model and CMIP6 simulations. *Journal of Geophysical Research: Atmospheres*, 125, e2019JD031926. <https://doi.org/10.1029/2019JD031926>
- Stevens, B., Acquistapace, C., Hansen, A., Heinze, R., Klinger, C., Klocke, D., et al. (2020). The added value of large-eddy and storm-resolving models for simulating clouds and precipitation. *Journal of the Meteorological Society of Japan*, 98(2), 395–435. <https://doi.org/10.2151/jmsj.2020-021>

# Western US wintertime precipitation and response to warming in GFDL X-SHiELD

Tsung-Lin HSIEH<sup>1</sup>, Lucas HARRIS<sup>2</sup>, Kai-Yuan CHENG<sup>1</sup>

<sup>1</sup>Program in Atmospheric and Oceanic Sciences, Princeton University, United States

<sup>2</sup>NOAA/Geophysical Fluid Dynamics Laboratory, United States

(Corresponding author: Tsung-Lin HSIEH, e-mail: hsiehtl@princeton.edu)

This work is distributed under the Creative Commons Attribution 4.0 License (CC BY 4.0)

## 1 Introduction

The eXperimental System for High-resolution prediction on Earth-to-Local Domains (X-SHiELD) developed at the Geophysical Fluid Dynamics Laboratory (GFDL) is a global storm resolving model with approximately 3.25 km horizontal grid spacing. With an unprecedented simulation length of 2.5 years, we analyze wintertime precipitation in the Western United States (US) in the present and warmed climates driven by prescribed sea surface temperatures.

The Western US is both scientifically interesting and socioeconomically important due to its complex topography and population density. It is home to several large metropolitan areas, yet the complex mountain ranges result in uneven spatial distribution of precipitation. The Western US receives most of its precipitation in winter, with roughly 40% of annual total precipitation occurring between November and January. The wintertime precipitation is mainly caused by large-scale moisture influx from the Pacific Ocean often associated with atmospheric rivers. In fact, the spring and summer water supply relies on melting of snow accumulated in winter.

High-resolution modeling provides a unique opportunity to study orographic precipitation. Wintertime precipitation in the Western US is often driven by orographic uplift on the windward side of the mountain ranges. The direction of mountain slopes relative to the large-scale moisture fluxes, mesoscale turbulence, and advection of cloud hydrometeors can all affect where and how much precipitation occurs. Therefore, simulation of precipitation is expected to improve when the complex topography is better resolved.

## 2 Model description and experimental setup

X-SHiELD utilizes the Finite-Volume Cubed-sphere (FV3) dynamical core with a C3072 horizontal resolution (approximately 3.25 km) and 79 vertical levels, and deep convection is not parameterized (see Cheng et al. (2022) and Harris et al. (2023) for more detail). X-SHiELD is a configuration of SHiELD (Harris et al., 2020), which has been extensively tested and applied in weather prediction across time and space scales.

The present-day simulation is conducted by nudging the slab ocean to the real-time SST analysis of European Centre for Medium-Range Weather Forecasts on a 15-day time scale. In the uniform warming experiment, SST is nudged to the present-day SST time series plus 4 K uniformly, but the CO<sub>2</sub> concentration remains at the present-day level. In the high-CO<sub>2</sub> experiment, the CO<sub>2</sub> concentration is scaled up to 1270 ppm, roughly 3.12 times the present-day level and 4 times the mid-20th century level. The fourth experiment combines both perturbations, with +4K SST and 1270 ppm of CO<sub>2</sub>.

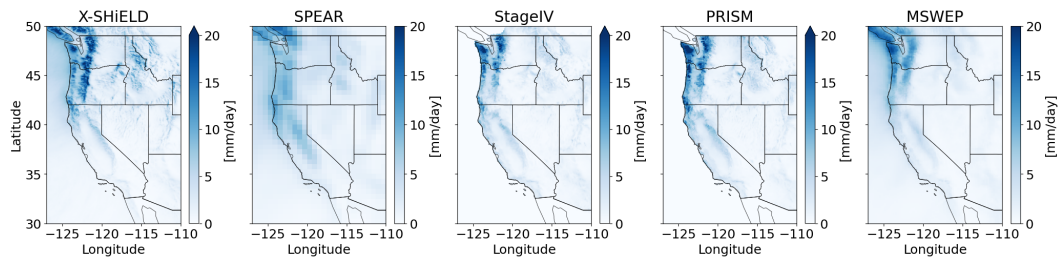


**Figure 1.** Mean wintertime precipitation in two models and three observational datasets. X-SHiELD captures detailed precipitation patterns resembling ground-based observations.

### 3 Result and conclusion

In the present-day simulation, X-SHiELD recovers the observed precipitation magnitude and spatial pattern despite not being explicitly tuned for the Western US region (Fig. 1). The agreement with observations suggest that X-SHiELD is a general-purpose model, in contrast to dynamical downscaling models that are targeted for a specific region. Compared with a conventional global climate model with a lower resolution, X-SHiELD improves the simulation of precipitation extremes and spatial distributions.

In response to global warming and increased CO<sub>2</sub> concentration, the change in precipitation pattern is mostly driven by the change in the large-scale circulation, similar to results from global climate models. The extreme precipitation is more sensitive surface warming, whose increase is slightly less than the Clausius-Clapeyron scaling and is more complicated over land than over ocean due to the more inhomogeneous land surface properties.

The response of Western US snowpack provides an interesting example of the resolution effect. Even though most studies have projected a decrease in Western US snowpack with warming, we found that it is possible to have local snowpack growth due to the occurrence of increased extreme precipitation over cold mountain tops. The snowpack on the Sierra Nevada persists throughout the winter in the warmed climate in X-SHiELD but not in the 50km climate model.

We suggest that global storm-resolving models provide tremendous value on precipitation over land, where complex topography is not resolved in coarser resolution climate models and where the human population resides. Beyond statistics of precipitation distribution, we showed that model resolution has significant influence on the snowpack, which affects the prediction of water supply, rain-on-snow floods etc. in the region.

### References

- Cheng, K.-Y., Harris, L., Bretherton, C., Merlis, T. M., Bolot, M., Zhou, L., ... Fueglistaler, S. (2022). Impact of Warmer Sea Surface Temperature on the Global Pattern of Intense Convection: Insights From a Global Storm Resolving Model. *Geophysical Research Letters*, 49(16), e2022GL099796.
- Harris, L., Zhou, L., Kaltenbaugh, A., Clark, S., Cheng, K.-Y., & Bretherton, C. (2023). A Global Survey of Rotating Convective Updrafts in the GFDL X-SHiELD 2021 Global Storm Resolving Model. *Journal of Geophysical Research: Atmospheres*, 128(10), e2022JD037823.
- Harris, L., Zhou, L., Lin, S.-J., Chen, J.-H., Chen, X., Gao, K., ... Stern, W. (2020). GFDL SHiELD: A Unified System for Weather-to-Seasonal Prediction. *Journal of Advances in Modeling Earth Systems*, 12(10), e2020MS002223.

## Session J: Tropical Cyclone

# Effects of sea spray on intensity of tropical cyclones

Alexander KHAIN<sup>1</sup> and Jacob SHPUND<sup>2</sup>

<sup>1</sup>The Hebrew University of Jerusalem, Jerusalem, Israel

<sup>2</sup>PNNL, Richland, USA

(Corresponding author: Alexander Khain, e-mail: alexander.khain@mail.huji.ac.il)

## 1. Introduction

Strong wind in the zone of tropical storms produces enormous amount of sea spray drops with sizes ranged from  $\sim 0.05 \mu m$  till  $300 \mu m$  and concentration of several hundred  $cm^{-3}$ . Large salinity allows spray drops to grow under subsaturated conditions. Most studies investigated spray effects on the drag coefficient at the ocean surface. In studies (2,3) it was shown that spray is transported upward by convective scale roll vortices within the hurricane boundary layer. Salinity of spray intensified the growth of the spray drops, decreased humidity in the BL and increased the latent heat surface flux (3,4). Rolls transport a lot of spray droplets to the base of deep convective clouds in the TC eyewall. It is known that aerosols playing the role of cloud condensational nuclei intensity of deep convective clouds (1). We follow (5) to show effects of sea spray on the intensity of TC.

## 2. Model description and experimental setup

Two models with precise description of microphysical processes were coupled:  
a) The Lagrangian-Eulerian model (LEM) of hurricane BL (2,3) in which  $\sim 2000$  adjacent Lagrangian parcels of a size of  $\sim 7$  m move within a turbulent like wind field with energetic and correlation properties obeying the observations in hurricanes. Droplet size distributions (DSD) as well as salinity of droplets were calculated in each parcel by solving equations for condensational growth, collisions, sedimentation and mixing. Spray surface fluxes increased with the surface wind speed. DSDs of spray at cloud base of deep convective clouds ( $\sim 300$ m) were calculated at different surface wind speeds.

b) The WRF with spectral bin microphysics (SBM) was used to simulate an idealized TC (5). The SBM calculates evolution of size distributions of aerosols, drops, graupel/hail and aggregates using logarithmic mass grids containing 43 bins (1,5). The spray DSD calculated by the LEM were used at the cloud base of TC deep clouds. Simulations of the TC evolution with and without spray effects were carried out.

## 3. Result and conclusion

The including of spray led to a dramatic increase in drop concentration in the eyewall of TC from a few drops  $cm^{-3}$  to a few hundred  $cm^{-3}$ . Effective cloud droplet radius,  $r_{eff}$ ,

decreased from 35-40  $\mu m$  in no spray case to 10-20  $\mu m$ , typical of polluted clouds. It was found that the effective radius decreases with the increase in wind speed in agreement with satellite observations (Fig. 1a). Spray increases the convection intensity in the TC eyewall, which is seen by the increase in the radar reflectivity (Fig.1b,c). As a result of the intensification maximum wind speed increases by 10 m/s and the area of strong winds also increases. Thus, we found the existence of positive feedback in a TC development: increase in wind speed  $\rightarrow$  increase in spray production  $\rightarrow$  intensification of convection  $\rightarrow$  increase in wind speed. We assume that the lack of sea spray over land leads to a fast decay of landfalling TCs.

## References

1. Khain A. P. and M. Pinsky (2018), *Physical Processes in Clouds and Cloud modeling*. Cambridge University Press. 642 pp
2. Shpund, J., M. Pinsky, and A.P. Khain, (2011), Microphysical structure of the marine boundary layer under strong wind and spray formation as seen from simulations using a 2D explicit microphysical model. Part I: The impact of large eddies. *J. Atmos.Sci.*, **68**, 2366–2384.
3. Shpund J., J. A. Zhang, M. Pinsky, A.P. Khain, (2012), Microphysical structure of the marine atmospheric mixed layer under strong wind and sea spray formation as seen from a 2-D explicit microphysical model. Part II: The role of sea spray. *J. Atmos. Sci.*, **69**, 3501-3514.
4. Shpund J., J. A. Zhang, M. Pinsky, and A. Khain, (2014), Microphysical Structure of the Marine Boundary Layer under Strong Wind and Sea Spray Formation as Seen from a 2D Explicit Microphysical Model. Part III: Parameterization of Height-Dependent Droplet Size Distribution. *J. Atmos. Sci.*, **71**, 1914–1934
5. Shpund J., A.P. Khain and D. Rosenfeld, 2019: "Effects of Sea Spray on the Dynamics and Microphysics of an Idealized Tropical Cyclone", *J. Atmos. Sci.*, 76, 2213-2234.

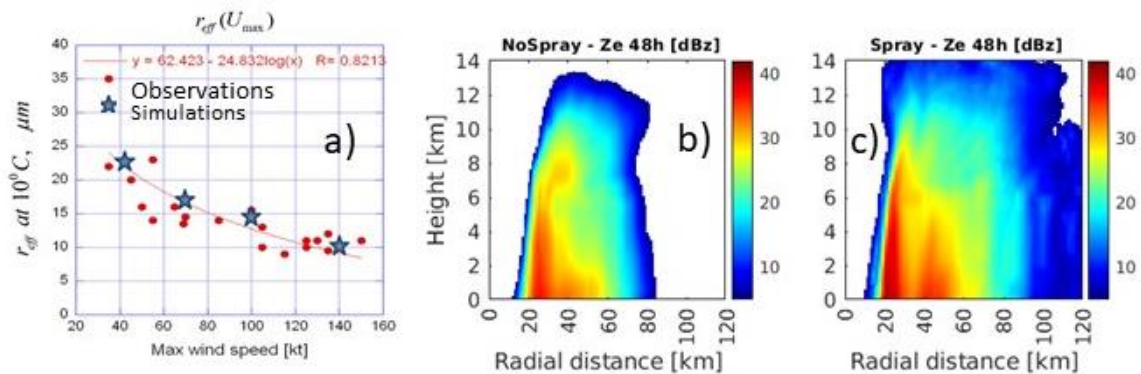


Fig. 1. a) Dependence of  $r_{eff}$  in the eyewall clouds on the wind speed maximum; b) radar reflectivity of the eyewall with no spray simulation ; c) the same, but with spray effects.

# **Ideal numerical simulations for modification of tropical cyclone from the microphysical approach in the Typhoonshot-MS program**

Ryuji YOSHIDA<sup>1</sup>, Hironori FUDEYASU<sup>1</sup>, and Masataka MURAKAMI<sup>1</sup>

<sup>1</sup>Typhoon Science and Technology Research Center, Yokohama National University,  
Yokohama, Japan

(Corresponding author: Ryuji YOSHIDA, e-mail: yoshida-ryuji-km@ynu.ac.jp)

This work is distributed under the Creative Commons Attribution 4.0 License (CC BY 4.0)

## **1. Introduction**

The JST Moonshot Goal 8 was launched in 2022. The Typhoon Science and Technology Research Center (TRC), Yokohama National University is leading "A core research program for Typhoon controlling aiming for a safe and happy society". This is named as the Typhoonshot-MS program. Various ideas are proposed in the Typhoonshot-MS program for the typhoon modification, we are currently studying to the typhoon weakening from intervening in the cloud microphysical process. Our plan is based on the explanation by Rosenfeld et al. (2012); seeding with hygroscopic aerosols at the outer region of the typhoon will increase the number of cloud droplets in the local cumulus clouds, shift the size distribution of cloud droplets toward smaller size, and facilitate adiabatic heating in the upper layers. This intervention may promote invigoration of cumulonimbus clouds instead of cumulus at the outer region of the typhoon, reduce an amount of water vapor transport toward the typhoon center, and weaken the deep convection at the center of the typhoon. Our goal is realization of the typhoon modification method, but we necessary test the idea before starting the development of the technique. To properly understand how cloud droplets formation and ice crystal formation processes can be modified by seeding in a typhoon environment, we are studying a feasibility to weaken the typhoon by using numerical simulations.

## **2. Model description and experimental setup**

To investigate the feasibility of seeding methods, we have conducted ideal typhoon experiments using a numerical model. For the ideal experiments, the regional atmospheric model SCALE-RM that is developing by RIKEN was used. To investigate the maximum efficacy, experiments were conducted assuming infinite seeding conditions by varying the cloud particle number concentration ( $N_c$ ) from 30 cm<sup>-3</sup>, 300 cm<sup>-3</sup>, and 3000 cm<sup>-3</sup>. We tested at 10 km and 5 km horizontal grid spacing so far and are testing at 3 km horizontal grid spacing. The single-moment Tomita08 scheme was used for microphysics

process and the Smagorinsky scheme, the MYNN scheme, and a bulk scheme were used for turbulence, planetary boundary layer, and surface flux, respectively. No radiation process was included for simplicity. Time integration period was 10 days from steady state and an initial profile was given by the mean sounding from Jordan (1958).

### **3. Result and conclusion**

In the experiment at a horizontal grid spacing of 10 km, the minimum sea level pressure of typhoon tends to be weaker for the larger Nc number setting than for the smaller Nc number setting. However, in the experiment at a horizontal grid spacing of 5 km, the minimum sea level pressure was weakest when the Nc number was 300 cm<sup>-3</sup> (middle setting in the three cases). This implies that numerical simulations to investigate the seeding sensitivity through cloud microphysical processes have a large sensitivity to horizontal grid spacing, and that the tendency of seeding effects differs depending on the setting. So, we need to conduct the experiment with sufficiently small horizontal grid spacing. Although further investigation at a finer grid spacing is needed, it was found in this ideal experiment that if a very large amount of material (infinite) could be seeded, there would be a possibility of weakening of typhoon. But this is not realistic for operation. So, we are currently conducting an experiment in which seeding is assumed to be done over a limited area, for a limited time, and in a limited amount.

### **References**

1. Rosenfeld, D., W. L. Woodley, A. Khain, W. R. Cotton, G. Carrió, I. Ginis, and J. H. Golden, 2012: Aerosol Effects on Microstructure and Intensity of Tropical Cyclones. *Bull. Amer. Meteor. Soc.*, 93, 987–1001, <https://doi.org/10.1175/BAMS-D-11-00147.1>.
2. Jordan, C.L., 1958: Mean soundings for the West Indies area. *J. Meteor.* , 15, 91-97.

# Parameter estimation of an atmospheric model using geostationary satellite data to improve prediction of tropical cyclones

Yuki Hirose<sup>1</sup>, Futo Tomizawa<sup>1</sup>, Le Duc<sup>2,3</sup>, and Yohei Sawada<sup>2,3</sup>

<sup>1</sup> Department of civil engineering, The University of Tokyo, Japan

<sup>2</sup> Institute of Engineering Innovation, The University of Tokyo, Japan

<sup>3</sup> Meteorological Research Institute, Japan Meteorological Agency, Japan

(Corresponding author: Yuki Hirose, e-mail: yuuhiro0414@g.ecc.u-tokyo.ac.jp)

This work is distributed under the Creative Commons Attribution 4.0 License (CC BY 4.0)

## 1. Introduction

One of the major uncertainties in atmospheric models is the parametric uncertainty. Since different physical processes interact in a complex manner and influence the reproducibility of tropical cyclones, it is important to analyze the contributions of all major parameters in physical processes to the forecasting skill and prioritize their relative importance. Baki et al. (2022a) conducted a sensitivity analysis of seven key parameters of a meteorological model for eight meteorological variables concerning tropical cyclones in the Bay of Bengal. Baki et al. (2022b) calibrated the sensitive eight parameters to minimize the prediction errors of precipitation and 10m wind speed induced by tropical cyclones. They demonstrated that this calibration led to an improvement in tropical cyclone prediction accuracy.

Although these previous efforts on the calibration of parameters in atmospheric models are promising, they heavily relied on in-situ observations, which are often unavailable in the case of monitoring and predicting tropical cyclones. In this study, we estimate parameters in multiple schemes of a meso-scale atmospheric model using geostationary meteorological satellites' observations. We integrate observations from geostationary meteorological satellites with the model to construct a framework for parameter estimation and identify parameters which can be estimated. To efficiently optimize parameters by satellite images, we incorporate similarity metrics that have not been traditionally used in meteorology. Additionally, we validate the performance of the predictions by conducting forecasting using the obtained posterior distribution of parameters.

## 2. Experimental design and model description

We conducted an Observation System Simulation Experiment (OSSE) to evaluate our parameter optimization method. We performed Bayesian parameter estimation based on the differences between observed and predicted brightness temperature from a geostationary satellite. By comparing the predicted data with actual observations, we conducted inverse estimation of the parameter distribution. To reduce the computational cost of Bayesian inference by Markov Chain Monte Carlo (MCMC), we employed surrogate models which can efficiently mimic the relationship between parameters and skill scores. Furthermore, we validated the improvement in the tropical cyclone prediction accuracy by running the model using the parameters sampled from the estimated posterior distribution.

In assessing the error between observations and predictions, the skill score for image similarities was used. In addition to conventionally used Mean Squared Error (MSE), the Structural Similarity Index (SSIM; Wang & Bovik (2009)) was used as

the basis for the score. SSIM is a metric that enables the measurement of structural distortions. SSIM has been extensively applied to evaluate image quality and similarity by accurately quantifying perceptual differences between two images.

For the numerical weather model, a modified version based on WRF-ARW was used, in which the values of each parameter can be specified at runtime, and CRTM was used for the radiative transfer model. Typhoon Nanmadol (2022) was selected as the target event.

### 3. Result and conclusion

We find that utilizing the SSIM as an evaluation metric realizes an efficient estimation of parameters in cloud microphysics and boundary layer schemes. The estimated posterior distribution of parameters not only improves the accuracy of the prediction of satellite images but also reduces errors in the prediction of tropical cyclone intensity (Fig 1). We demonstrate the potential of adjusting multiple parameters based on satellite data and the implications of model development to improve the accuracy of tropical cyclone simulations.

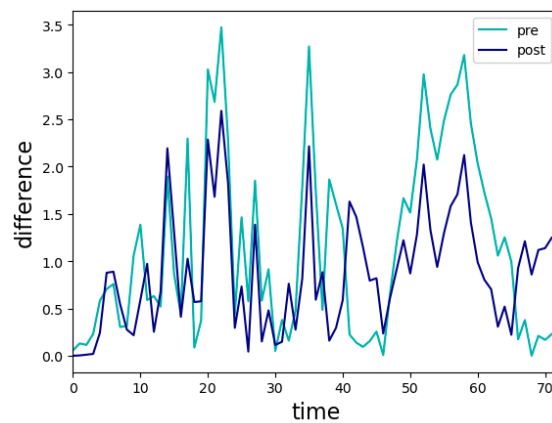


Fig1. The differences between the observed values (nature run) and the ensemble average for the minimum central pressure of the tropical cyclone. The green line represents the differences based on the prior distribution, while the blue line represents the differences based on the posterior distribution. The differences are shown at each time step, with a one-hour interval, comparing the ensemble average with the observed values.

### References

1. Baki, H., Chinta, S., C Balaji, & Srinivasan, B. (2022a). Determining the sensitive parameters of the Weather Research and Forecasting (WRF) model for the simulation of tropical cyclones in the Bay of Bengal using global sensitivity analysis and machine learning. *Geoscientific Model Development*, 15(5), 2133–2155.
2. Baki, H., Chinta, S., Balaji, C., & Srinivasan, B. (2022b). Parameter Calibration to Improve the Prediction of Tropical Cyclones over the Bay of Bengal Using Machine Learning–Based Multiobjective Optimization. *Journal of Applied Meteorology and Climatology*, 61(7), 819–837.
3. Wang, Z., & Bovik, A. C. (2009). Mean squared error: Lot it or leave it? A new look at signal fidelity measures. *IEEE Signal Processing Magazine*, 26(1), 98–117.

# **Analysis of the Factors that Led to Uncertainty of Track Forecast of Typhoon Krosa (2019) by 101-Member Ensemble Forecast Experiments Using NICAM**

Masuo NAKANO<sup>1</sup>, Ying-Wen CHEN<sup>2</sup>, and Masaki SATOH<sup>3</sup>

<sup>1</sup>Japan Agency for Marine-Earth Science and Technology (JAMSTEC), Yokohama, Japan

<sup>2</sup>APcommunications, Tokyo, Japan

<sup>3</sup>Atmosphere and Ocean Research Institute, The University of Tokyo, Kashiwa, Japan  
(Corresponding author: Masuo NAKANO, e-mail: masuo@jamstec.go.jp)

This work is distributed under the Creative Commons Attribution 4.0 License (CC BY 4.0)

## **1. Introduction**

Typhoon Krosa (2019) formed in the eastern part of the Philippine Sea and ~1400 km east of another typhoon Lekima on 6 August and made a landfall in the western part of Japan's mainland on 15 August. The operational global model forecasts, which were initialized just after Krosa's formation, showed a very large uncertainty and totally failed to predict the actual track of Krosa. In this study, we investigated the causes of this large uncertainty through 101-member ensemble forecast experiments by using a 28-km mesh global nonhydrostatic model.

## **2. Model description and experimental setup**

The model used in this study is a 28-km mesh NICAM (version NICAM.18; Kodama et al. 2021). The number of vertical layers was set to 38, and the model top was located at 37 km. The moist convection was explicitly calculated using a single-moment cloud microphysics scheme without any cumulus parameterization. The atmospheric initial condition was provided by an operational weather analysis system called NICAM-LETKF JAXA Research Analysis (NEXRA, [https://www.eorc.jaxa.jp/theme/NEXRA/index\\_e.htm](https://www.eorc.jaxa.jp/theme/NEXRA/index_e.htm)). The ensemble size and horizontal resolution of NEXRA were 100 and 112 km, respectively. We used all the ensemble analysis members (100) and their mean for the model initialization. SST was predicted by a slab ocean model with a constant depth of 15 m. Moreover, SST was nudged toward the initial values with an e-folding time of 7 days. The initial value of SST ( $1^\circ \times 1^\circ$  horizontal resolution) was obtained from the GDAS of NCEP. The model simulations were initialized at 1200 UTC from the 6th to the 9th of August and integrated for 10 days.

### 3. Result and conclusion

The large uncertainty in the model initialized at 1200 UTC 6 August and the decrease in uncertainty as the model initialization time went by, as predicted by the operational systems, were successfully reproduced by NICAM. The ensemble-based sensitivity analysis of Krosa's track forecast error suggested that the track error was sensitive to the intensity of the western North Pacific subtropical high (WNPSH) over Japan and the distance between Krosa and Lekima. The best and worst members (20 for each) in terms of Krosa's forecast track error were compared. The westward extension of WNPSH was stronger with the best members, and the northward movement of Krosa was faster with the worst members. The distance between Krosa and Lekima decreased by 250 km in 36 hours after the model initialization time with the worst members, whereas the distance was almost constant in 24 hours after the model initialization time with the best members. These results suggest that a strong interaction between Krosa and Lekima occurred with the worst members, leading to a fast northward movement and a large track forecast error.

The difference in the composite fields between the best and worst members indicates that Krosa had a larger vortex size with the worst members than with the best members at the initial conditions. However, little differences were found around Lekima. These differences led to its larger vortex size with the worst members of the NICAM forecasts. This larger storm size with the worst member should result in retreat of the WNPSH through the mechanism proposed by Sun et al. (2015) and lead to faster northward movement of Krosa. These results suggest that the analysis error of the meteorological field including the TC position around Krosa in NEXRA, which was used in the NICAM forecasts, determines whether a strong interaction between Krosa and Lekima and the retreat of WNPSH would occur or not. More details can be found in Nakano et al. (2023)

### References

1. Kodama, C., and Coauthors, (2021), The Nonhydrostatic ICosahedral Atmospheric Model for CMIP6 HighResMIP simulations (NICAM16-S): experimental design, model description, and impacts of model updates, *Geosci. Model Dev.*, **14**, 795-820
2. Nakano, M., Y.-W. Chen, M. Satoh, (2023): Analysis of the Factors that Led to Uncertainty of Track Forecast of Typhoon Krosa (2019) by 101-Member Ensemble Forecast Experiments Using NICAM, *J. Meteor. Soc. Jpn.*,101, 191-207

# A large ensemble simulation for seasonal scale tropical cyclone activity by a nonhydrostatic model

Yohei Yamada

<sup>1</sup>Japan Agency for Marine-Earth Science and Technology, Yokohama, Japan

(Corresponding author: Yohei Yamada, e-mail: yoheiy@jamstec.go.jp)

This work is distributed under the Creative Commons Attribution 4.0 License (CC BY 4.0)

## 1. Introduction

Genesis potential indexes (GPIs) have been proposed for diagnosing tropical cyclone (TC) formation by previous studies (i.e., Emanuel and Nolan, 2004), consisting of some of the above-mentioned parameters. These indexes usually consist of some parameters associated with TC formation: the Coriolis parameter, low-level relative vorticity, ocean thermal energy, manifest as ocean temperatures more than 26°C to a depth of 60 meters, relative humidity in the mid-troposphere, the difference in equivalent potential temperature between the surface and 500 mb, and inverse of the tropospheric vertical wind shear (Gray, 1998). By using a reanalysis and best-track dataset, Camargo et al (2007) showed GPI well represents seasonal cycle of TC formation although Interannual variability of TC formation is poorly represented by GPI compared with the seasonal cycle.

By using a numerical model explicitly simulating TCs, Cavicchia et al (2023) reported the poor skill of GPI for predicting performance of GPI for predicting interannual variability and multi-decadal trends of TC formation. However, the number of TC genesis frequencies varies among ensemble members, even if the same condition of sea surface temperature (e.g., Roberts et al., 2020). This variation may complicate evaluation of relationship between GPI and TC formation. In this study, We evaluate the predictive skill of GPI for interannual variability of TC formation by using a large ensemble member simulation with explicitly representing TC.

## 2. Model description and experimental setup

To evaluate the performance of the GPI, a large ensemble simulation (64 members) was performed for the boreal summer (June-September) during 2009–2019. Nonhydrostatic ICosahedral Atmospheric Model (NICAM; Tomita and Satoh, 2004) is used for the ensemble simulation, of which horizontal grid interval is 14-km. The configuration of model is follows Kodama et al. (2021) with some modifications. The aerosol effect was not considered. Sea surface temperature was calculated by a slab ocean model with a 15-m depth and nudged toward delayed-mode National Oceanic and Atmospheric Administration daily optimum interpolation SST Version 2.1 (Huang et al., 2020) with a relaxation time of one week. The atmospheric initial conditions were interpolated from the Atmospheric General Circulation Model for the Earth Simulator–LETKF experimental ensemble reanalysis 2 (ALERA2; Enomoto et al., 2013).

The GPI defined by Emanuel and Nolan (2004) was used for evaluating

relationship between GPI and TC formation. In this study, we focused on the western North Pacific (WP), the eastern North Pacific (EP) and the North Atlantic (NA). Regional mean of GPI within 5–30° for each ocean basin were compared with TCs genesis frequency (TCGF) in the respective ocean basin. TCs formed in the simulation were detected by a TC tracking algorithm (Nakano et al., 2015).

### 3. Result and conclusion

For each ensemble member (64-member), correlation coefficient between interannual variabilities of seasonal GPI and TCGF (R) varied among ensemble members (0.2–0.9 for NA, 0.4–0.9 for EP and -0.3–0.8 for WP). On the other hand, in the 64-member ensemble mean, R is 0.89 for NA, 0.94 for EP and 0.69 for WP. GPI well correlated with TCGF for all the three ocean basins. This suggests that, in order appropriately evaluate the relationship between GPI and TCGF in interannual time scale, ensemble simulation is required.

#### References (in alphabetical order according to author)

1. Camargo, S. J., et al., (2007), Use of a genesis potential index to diagnose ENSO effects on tropical cyclone genesis, *J. Climate*, **20**, 4819–4834
2. Cavicchia, L., et al., (2023), Tropical cyclone genesis potential indices in a new high-resolution climate models ensemble: Limitations and way forward, *Geophys. Res. Lett.*, **50**, e2023GL103001
3. Emanuel, K. A., and D. S. Nolan, (2004), Tropical cyclone activity and global climate, Preprints, 26th Conf. on Hurricanes and Tropical Meteorology, Miami, FL, Amer. Meteor. Soc., 240–241
4. Enomoto, T., et al., (2013), Observing-system research and ensemble data assimilation at JAMSTEC. In: Park, S., Xu, L. (Eds.), *Data Assimilation for Atmospheric, Oceanic and Hydrologic Applications* (Vol. 2, pp. 509–526). Berlin, Heidelberg: Springer
5. Gray, W. M., (1998), The formation of tropical cyclone, *Meteorol. Atmos. Phys.* **67**, 37–69
6. Huang, B., et al., (2021), Improvements of the Daily Optimum Interpolation Sea Surface Temperature (DOISST) Version 2.1. *J. Climate*, **34**, 2923–2939
7. Kodama, C., (2021), The Nonhydrostatic ICosahedral Atmospheric Model for CMIP6 HighResMIP simulations (NICAM16-S): experimental design, model description, and impacts of model updates, *Geosci. Model Dev.*, **14**, 795–820
8. Nakano, M., Sawada, M., Nasuno, T., & Satoh, M. (2015), Intraseasonal variability and tropical cyclogenesis in the western North Pacific simulated by a global nonhydrostatic atmospheric model. *Geophys. Res. Lett.*, **42**, 565–571
9. Roberts, M. J., et al., (2020), Impact of model resolution on tropical cyclone simulation using the HighResMIP–PRIMAVERA multimodel ensemble, *J. Climate*, **33**, 2557–2583.
10. Tomita, H., and M. Satoh, (2004), A new dynamical framework of nonhydrostatic global model using the icosahedral grid, *Fluid Dynamics Res.*, **34**, 357–400
11. Seiki, T., and T. Nakajima, (2014), Aerosol effects of the condensation process on a convective cloud simulation, *J. Atmos. Sci.*, **71**, 833–853

# Reducing the Intensity of an Approaching Typhoon Forced by an Artificial Cold Pool Using the Stretched Version of a Non-hydrostatic Icosahedral Atmospheric Model (NICAM)

Marguerite Lee and Masaki Satoh

Atmosphere and Ocean Research Institute, University of Tokyo, Kashiwa, Chiba, Japan

(corresponding author: Marguerite Lee, leem@ori.u-tokyo.ac.jp)

This research was supported by JST Moonshot R & D Grant Number JPMJMS2282

This work is distributed under the Creative Commons Attribution 4.0 License (CC BY 4.0)

## 1 Introduction

The intensity of a tropical cyclone (TC) is highly sensitive to both internal and external conditions. Improvements in forecasting intensity has not kept pace with that of tracking [1]. Due to a TC's highly destructive nature, the Moonshot project of the Typhoon Control Research Aiming for a Safe and Prosperous Society is working towards finding artificial means to reduce an approaching typhoon. Therefore, making it less destructive. To achieve this, we initiate a cold pool, a region of cold air left behind due to evaporation under the clouds of thunderstorms, to suppress convection by cooling the air within 1km from the surface. The approaching typhoon will encounter this cooler air and the impact it has on its intensity is what we are trying to understand. The aim is only to reduce the intensity and not kill the storm. We will use typhoon Hagibis as our test case.

## 2 Model and Experiment Set-up

The stretched version of the non-hydrostatic icosahedral atmospheric model (NICAM) [3] was employed for the control and sensitivity tests. The model is designed so that NICAM solves the fully compressible non-hydrostatic governing equations on a stretched icosahedral grid with terrain following coordinates in the vertical. For more details on the model please refer to [2]. The icosahedral grid with a stretch factor of 100 is centred at 35 degrees north latitude and 135 degree east longitude. 78 vertical levels up to approximately 50km was used. The ERA5 reanalysis hourly data was used to initialise the model to produce the cyclone. To introduce the forcing in the sensitivity tests, a cooling effect of -1K/hr was introduced. This forcing is located at 27 degrees north latitude and 138 degrees East longitude. The forcing has a radius of 5km and a height of 1km. It is a fixed stationary point placed in the pathway of the approaching typhoon. Only the cyclone was allowed to move. The simulation lasted for 48 hours, 2 days prior to landfall.

## 3 Results and Conclusion

Several metrics are used to assess the intensity changes that occur due to the artificial forcing that is applied. However, for this extended abstract only the 10 m wind speed will be examined. Figure 1

shows the results of the 10m wind at  $t = 24$  hrs where there is no forcing applied which is the control run (figure 1a), when the cyclone meets the stationary forcing (figure 1b) and the difference between the two (figure 1c). In both figures 1a and 1b we can see the clearly developed eyewall with its intense winds where the highest winds are located in the top right quadrant of the cyclone. These wind speeds are in the range of 40-45m/s. The control run in this same quadrant has even more intense winds that range from 45-50m/s. This range is notably absent in the Forcing experiment. Although there has been some decrease in the wind speeds we see from figure 1c that there are areas that the winds speeds increased. In some areas the difference falls in the range of 8-12m/s. The upper portion of the cyclone appears to be more affected by the forcing as opposed to the lower portion. The small decrease in the wind speeds is a clear indicator that only reducing the temperature is not sufficient. Additionally, the small decrease in wind speeds may be attributed to the fact that the cooling effect is being advected due to the spiralling winds. As a consequence, the cooler air temperature is not concentrated enough so it is not able to effectively suppress convection. From these initial experiments we can see that applying a temperature forcing is not sufficient to adequately suppress convection. We will need to employ an evaporative rain cooling forcing in addition to the temperature forcing.

## References

- [1] Su H., L. Wu, J. H. Jiang, R. Pai, A. Liu A. J. Zhai, P. Tavallali, and M.DeMaria. Applying Satellite Observations of Tropical Cyclone Internal Structure to Rapid Intensification Forecast with Machine Learning. *Geophysical Research Letters*, 47:e2020GL089102, 2020.
- [2] Satoh M., T. Matsuno, H. Tomita, H. Miura, T. Nasuno, and S. Iga. Non-hydrostatic icosahedral atmosphere model (NICAM) for global cloud resolving. *J. Comput. Phys.*, 227:3486–3514, 2008.
- [3] Satoh Masaki, Hirofumi Tomita, Hisashi Yashiro, Hiroaki Miura, Chihiro Kodama, Tatsuya Seiki, Akira T. Noda, Yohei Yamada, Daisuke Goto, Masahiro Sawada, Takemasa Miyoshi, Yosuke Niwa, Masayuke Hara, Tomoki Ohno, Shin ichi Iga, Takashi Arakawa, Takahiro Inoue, and Hiroyasu Kubokawa. The Non-hydrostatic Icosahedral Atmosphere Model: description and development. *Progress in Earth and Planetary Science*, 1:18, 2014.

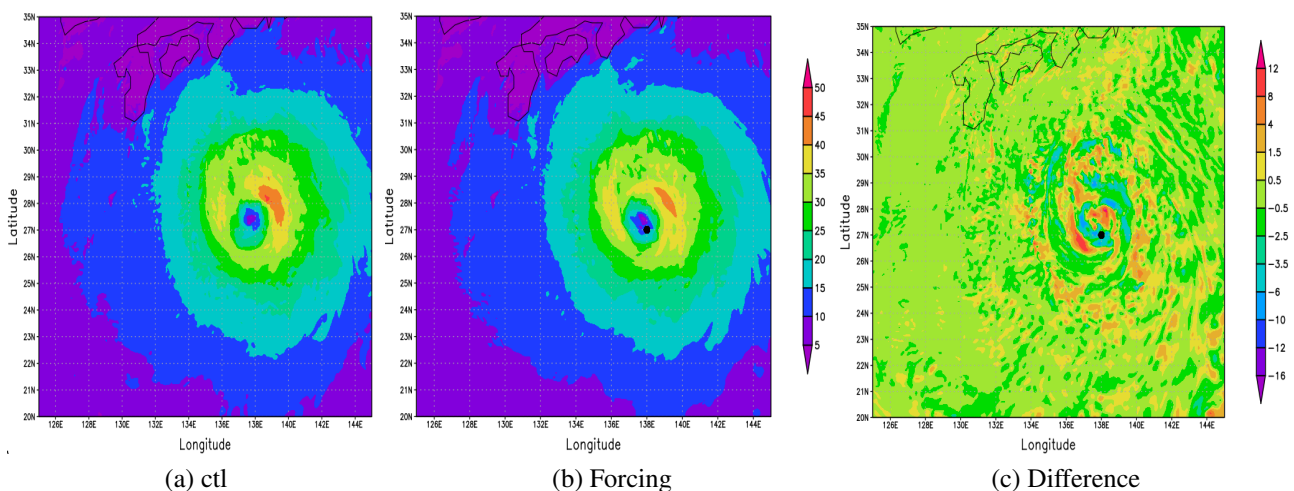


Figure 1: Top view of TC Hagibis at  $t=24$ hrs for the control 1a, forcing applied 1b and the difference between  $-1\text{K/hr}$  and control 1c. The black dot represents the position of the stationary forcing

# **The impact of air-sea interaction on the fluctuation of the monsoon trough in ensemble experiments with a coupled general circulation model**

Yutaro NIRASAWA<sup>1</sup>, Tomoki MIYAKAWA<sup>1</sup>, Takao KAWASAKI<sup>1</sup>, and Ryusuke MASUNAGA<sup>2</sup>

<sup>1</sup>Atmosphere and Ocean Research Institute; the University of Tokyo, Kashiwa, Japan

<sup>2</sup>Japan Agency for Marine-Earth Science and Technology, Yokohama, Japan

(Corresponding author: Yutaro NIRASAWA, e-mail: nirasawa@aori.u-tokyo.ac.jp)

This work is distributed under the Creative Commons Attribution 4.0 License (CC BY 4.0)

## **1. Introduction**

The monsoon trough (MT) over the Western North Pacific (WNP) varies due to various factors. Specifically, boreal summer intra-seasonal oscillation (BSISO) affects the MT in an intra-seasonal time scale (Kikuchi, 2021). Air-sea interaction may play an important role in the evolution of the MT through BSISO, in which case an atmosphere and ocean coupled model is required.

## **2. Model description and experimental setup**

In this study, we conducted 10-member ensemble numerical experiments with a non-hydrostatic global atmospheric model “NICAM (Tomita and Satoh, 2004)” and its ocean coupled version “NICOCO (Miyakawa et al., 2017)”. In NICOCO experiments, we interpolated an ocean reanalysis data “CMEMS (Drévilion et al., 2022)” onto the ocean model grid and used a flux adjustment method (Masunaga et al., 2023) to simulate the ocean more realistically. In NICAM experiments, daily-mean SST simulated in NICOCO was given as a boundary condition in two ways, fixed values and slab ocean.

## **3. Result and conclusion**

We calculated bimodal BSISO index (Kikuchi, 2020) in order to investigate the variation of convections associated with BSISO (Fig. 1). Figure 1 shows that BSISO amplitudes in many members of NICAM with slab ocean are larger than reanalysis data during phase 6 and 7, when major convections are located over the WNP. At that time, westerlies around 10°N are significantly different between models (Fig. 2). These suggest that the way to give an ocean condition influences BSISO and the fluctuation of the MT. We will analyze the factor of these differences between models with focusing on air-sea interaction.

## Acknowledgements

This work was supported by JSPS KAKENHI Grant Number JP19H05703 and JP22H01297. Computational resources of the supercomputer “Fugaku” were provided through the Fugaku General Project (Project number: hp230108).

## References (in alphabetical order according to author)

1. Drévillon, M. et al., (2022), Global Ocean Reanalysis Products, Copernicus Marine
2. Kikuchi, K., (2020), Extension of the bimodal intraseasonal oscillation index using JRA-55 reanalysis, *Climate Dynamics*, **54**, 919-933
3. Kikuchi, K., (2021), The Boreal Summer Intraseasonal Oscillation (BSISO): A Review, *J. Meteor. Soc. Japan*, **99(4)**, 933-972
4. Masunaga, R. et al., (2023), Flux Adjustment on Seasonal-Scale Sea Surface Temperature Drift in NICOCO, *J. Meteor. Soc. Japan*, **101(3)**, 175-189
5. Miyakawa, T. et al., (2017), A Madden-Julian Oscillation event remotely accelerates ocean upwelling to abruptly terminate the 1997/1998 super El Niño, *Geophys. Res. Lett.*, **44(18)**, 9489-9495
6. Tomita, H. and M. Satoh, (2004), A new dynamical framework of nonhydrostatic global model using the icosahedral grid, *Fluid Dynamics Res.*, **34(6)**, 357-400

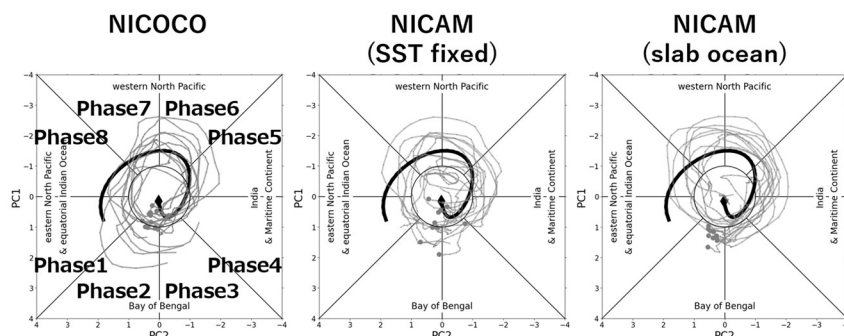


**Fig.1** The major convective regions calculated by bimodal BSISO index. Thick and thin lines indicate reanalysis data and model results, respectively.

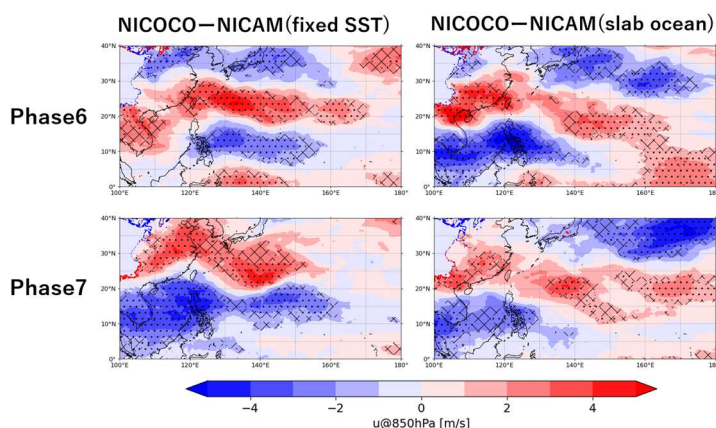


**Fig.2** Differences of zonal winds at 850hPa during phase6 (upper) and phase7 (bottom). Dots and hatching indicate that the significance of the difference is greater than 99 and 95 %, respectively.

## Session K: Framework

# Aerosol-Cloud Interactions in High Resolution, Idealized Two-Dimensional Hadley Circulation Simulations

Takanobu Yamaguchi<sup>1,2</sup>, Ryuji Yoshida<sup>3</sup>, and Graham Feingold<sup>2</sup>

<sup>1</sup>Cooperative Institute for Research in Environmental Sciences, University of Colorado  
Boulder, Boulder, USA

<sup>2</sup>National Oceanic and Atmospheric Administration Chemical Sciences Laboratory,  
Boulder, USA

<sup>3</sup>Yokohama National University, Yokohama, Japan

(Corresponding author: Takanobu Yamaguchi, e-mail: tak.yamaguchi@noaa.gov)

This work is distributed under the Creative Commons Attribution 4.0 License (CC BY 4.0)

## 1. Introduction

Large eddy simulation is a powerful tool to study aerosol-cloud interactions (ACIs). However, this approach has limitations related to both domain size and duration, which prevents one from studying the effect of ACIs on large spatiotemporal scale circulations, and how these feed back onto cloud properties. To circumvent these limitations, and conduct research into ACIs over the tropics and subtropics in a single model domain, we use a recently developed idealized two-dimensional Hadley circulation model. This model is proposed as a testbed in which one can perform high spatial resolution simulations approaching those used in large eddy simulations, as well as for month-long durations.

## 2. Model description and experimental setup

Following Satoh (1994), our two-dimensional Hadley circulation model has been developed (Yoshida et al. 2021) by introducing a prognostic equation of angular momentum and a meridional-vertical two-dimensional domain spanning from the South Pole to the North Pole in the System for Atmospheric Modeling (Khairoutdinov and Randall 2003). For the current study, we use an offline downscaling method that successively uses finer horizontal resolution to obtain a spun-up state with 240 m grid spacing. A 256-level stretched vertical grid with a 30-m constant grid spacing below 2 km altitude is used. For the spin-up simulation, we use a prescribed sea surface temperature based on ERA5 and a prescribed aerosol concentration based on CAMSRA. 3 types of aerosol loadings with either fixed SST or slab ocean model (total of 6 cases) are used for a sensitivity test. The duration of each simulation for the sensitivity test is 30 days.

## 3. Result and conclusion

This study is on an early stage of analyzing data set of 6 simulations and some results will be shown in the presentation. For 30-day duration, the Hadley circulation does not seem to be affected by both aerosol perturbation and SST configuration while the cloud radiative effect differs among the cases. This study is expected to shed light on the feedback between ACIs and large scale circulation.

## References

1. Khairoutdinov, M. F., and D. A. Randall (2003), Cloud resolving modeling of the ARM summer 1997 IOP: Model formulation, results, uncertainties, and sensitivities,

- J. Atmos. Sci.*, 60(4), 607-625, doi:10.1175/1520-0469(2003)060<0607:CRMOTA>2.0.CO;2.
2. Satoh, M. (1994), Hadley circulations in radiative–convective equilibrium in an axially symmetric atmosphere, *J. Atmos. Sci.*, 51(13), 1947-1968, doi:10.1175/1520-0469(1994)051<1947:HCIREI>2.0.CO;2.
  3. Yoshida, R., T. Yamaguchi, and G. Feingold, (2021), Two-dimensional idealized Hadley circulation simulation for global high resolution model development, *J. Adv. Model. Earth Syst.*, 14(1), e2021MS002714, doi:10.1029/2021MS002714.

# A multiscale modeling framework (MMF) for the E3SM climate model

Christopher Eldred<sup>1</sup>, Maciej Waruszewski<sup>1</sup>, Matthew Norman<sup>2</sup>, Mark Taylor<sup>1</sup>

<sup>1</sup>Sandia National Laboratories, Albuquerque, NM, USA

<sup>2</sup>Oak Ridge National Laboratories, Oak Ridge, TN, USA

(Corresponding author: Christopher Eldred, e-mail: celdred@sandia.gov)

This work is distributed under the Creative Commons Attribution 4.0 License (CC BY 4.0)

## 1. Introduction

As an alternative to high-resolution models such global convection permitting models (GCPMs), the US Department of Energy is additionally pursuing the development of a multiscale modeling framework (MMF, also known as superparameterization) to improve the representation of cloud and other small-scale processes in low resolution models. MMF embeds an independent cloud resolving model (CRM) at each grid cell of the host model. This offers the possibility of significantly enhanced throughput compared to GCPM, especially on the accelerator heavy architectures that characterize current and upcoming DOE supercomputers. As part of the E3SM-MMF project, a new CRM is being developed: the Portable Atmospheric Model (PAM).

## 2. Model description and experimental setup

PAM consists of a novel dynamical core: SPAM++ (the Structure Preserving Atmospheric Model in C++) coupled to SCREAM physics (P3 microphysics, SHOC macrophysics and RRTGMP radiation). SCREAM physics are designed for 1-5km resolution, matching those used in the MMF. To obtain high performance on a range of GPU machines, PAM is written in C++ using a performance portability framework (YAKL or Kokkos, depending on the component).

Unlike many dynamical cores, SPAM++ is based on writing the equation of motion using a *Hamiltonian formulation*, in terms of a symplectic operator and a Hamiltonian functional:

$$\frac{\partial \mathbf{x}}{\partial t} + \mathbf{J}(\mathbf{x}) \frac{\delta \mathcal{H}}{\delta \mathbf{x}} = 0$$

Using such a formulation leads to succinct expression of conservation laws through anti-symmetry of the symplectic operator (energy conservation) and it's null space (known as Casimirs, such as mass, entropy and potential vorticity). Additionally, this approach provides a framework for *structure-preserving discretization*, that is capable of emulating many of the key properties of the continuous equations, including conservation laws.

SPAM++ is based on a general advected densities model of the form

$$\frac{\partial \mathbf{v}}{\partial t} + \mathbf{Q} \times \mathbf{F} + \sum_k d_k \nabla B_k \quad \frac{\partial D_k}{\partial t} + \nabla \cdot (d_k \mathbf{F}) = 0$$

A specific choice of advected densities and Hamiltonian will determine the actual dynamics. We have implemented choices leading to the (thermal) shallow water equations, (multicomponent) anelastic equations and (multicomponent) compressible Euler equations. Additionally, for the anelastic and compressible Euler equations arbitrary thermodynamic potentials can be used.

The advected densities model is discretized using some novel structure-preserving (also known as mimetic) spatial and temporal numerics. These numerics preserve the key features of the continuous Hamiltonian formulation, and lead to a numerical model with discrete analogues of conservation laws, involution constraints and freedom from spurious computational modes.

For the spatial numerics, SPAM++ uses discrete exterior calculus (DEC), which is a double deRham complex mimetic discretization. Recent work has extended DEC to incorporate several key new features:

1. higher-order accurate Hodge stars (on structured grids)
  1. structure-preserving high-order oscillation-limiting, positive-definite (SPHOOOL-PD) transport operators
  2. consistent treatment of arbitrary boundaries with arbitrary boundary conditions
- These features (especially SPHOOOL-PD transport) are required for realistic simulations, and greatly extend the utility of DEC.

The time integrator in SPAM++ is an energy-conserving Poisson integrator based on discrete gradients, that preserves the features of the spatial discretization. Currently the average vector field is used, although other discrete gradients would be possible. The resulting nonlinear system is solved using a quasi-Newton method, with the approximate Jacobian given by the Jacobian of a linearized system. The resulting linear system can be simplified through pointwise elimination (static condensation) into a single positive-definite Helmholtz problem for a pressure-type variable. A direct solver based on FFT in the horizontal and banded diagonal solvers in the vertical is used for the Helmholtz problem. This last step is possible only on the simplified domains (no topography, horizontally uniform) used by the CRM within E3SM-MMF, on more general domains an iterative solver would be required.

The end result is a novel dynamical core with exact discrete conservation of mass, entropy and total energy to machine precision, with realistic SPHOOOL-PD transport operators and semi-implicit time stepping. This talk will discuss more details about the spatial and temporal numerics of PAM, as well as computational performance results from E3SM-MMF and recent simulation results.

## References

1. C. Eldred, W. Bauer. **An interpretation of TRiSK-type schemes from a discrete exterior calculus perspective**, *arxiv*
2. C. Eldred. **Structure-preserving numerical discretizations for domains with boundaries**, *Technical Report SAND2021-11517*, Sandia National Laboratories, 2021
3. C. Eldred, M. Norman, and M. Taylor. **PAM dynamical core- continuous formulation, discrete numerics and implementation**, *Technical Report WBS 2.2.3.05, Milestone ECP-AD-SE-15-1675*, Sandia National Laboratories, 2021

## **TaiwanVVM: Current Advancements and Future Development**

Chien-Ming WU

Department of Atmospheric Sciences, National Taiwan University, Taipei, Taiwan

(Corresponding author: Chien-Ming WU, e-mail: mog@as.ntu.edu.tw)

This work is distributed under the Creative Commons Attribution 4.0 License (CC BY 4.0)

In this study, we showcase the latest advancements and prospective development directions for TaiwanVVM, a high-resolution (500 m horizontally) vorticity equation-based cloud-resolving model encompassing the entire Taiwan region, an area characterized by intricate orography, including a complex network of valleys and ridges within a few hundred kilometers. TaiwanVVM employs the immersed boundary method (Wu and Arakawa, 2011; Chien and Wu, 2016) to represent surface topography, which allows for direct responsiveness to surface heating gradients without computational difficulties. The model incorporates the Noah land surface model (LSM, Chen et al. 1996) for land surface process representation, using surface properties at a 500 m horizontal resolution specific to Taiwan (Wu et al. 2019). This approach generates accurate diurnal cycle evolution of boundary layers and local circulation, crucial for the development of local afternoon thunderstorms and pollutant transport (Chang et al. 2021; Hsieh et al. 2022; Hsu et al. 2023). Numerical results obtained from TaiwanVVM can also provide guidance for in-situ field campaign in Taiwan (Chang et al. 2023). The Predicted Particle Properties scheme (P3, Morrison and Milbrandt, 2014) is utilized for microphysical process representation, enabling a broader precipitation spectrum due to reduced melting effects of hail particles (Huang and Wu 2020) which also contributes to bifurcate transition for convective aggregation caused by stronger moisture convection feedback (Huang and Wu 2022). Future developments include implementing a K-profile parameterization ocean model (KPP, Large et al. 1994) within VVM to further examine the interaction between diurnal convection and ocean processes; implementing of a chemistry module to investigate the chemical processes during pollutant transport (Fan and Wu 2023). Additionally, an explainable machine learning framework is being developed to extract essential features for specific storylines using TaiwanVVM simulations. This representation learning will facilitate evaluations of afternoon thunderstorm and pollution concentration changes under global warming scenarios.

References:

Chang, Y. H., Chen, W. T., Wu, C. M., Moseley, C., & Wu, C. C. (2021). Tracking the influence of cloud condensation nuclei on summer diurnal precipitating systems over complex topography in Taiwan. *Atmospheric Chemistry and Physics*, 21(22), 16709-16725.

- Chang, Y.-H., Chen, W.-T., Wu, C.-M., Kuo, Y.-H., & Neelin, J. D. (2023). Identifying the deep-inflow mixing features in orographically-locked diurnal convection. *Geophysical Research Letters*, 50, e2023GL103107. <https://doi.org/10.1029/2023GL103107>
- Chen, F., Mitchell, K., Schaake, J., Xue, Y., Pan, H., Koren, V., Duan, Y., Ek, M., Betts, A.: Modeling of land surface evaporation by four schemes and comparison with FIFE observations. *J. Geophys. Res.* 101(D3), 7251–7268 (1996). <https://doi.org/10.1029/95JD02165>
- Chien, M.-H., and C.-M. Wu (2016): Representation of topography by partial steps using the immersed boundary method in a vector vorticity equation model (VVM), *J. Adv. Model. Earth Syst.*, 8, 212–223, doi:[10.1002/2015MS000514](https://doi.org/10.1002/2015MS000514).
- Fan, Y.-H. and C.-M. Wu (2023): Implementation of chemistry module in a Vector Vorticity Equation Model (VVM) to study the effects of local circulation on pollutant transport. *Earth and Space Science*, under review.
- Hsieh, M. K., Y. W. Chen, Y. C. Chen, & C.-M. Wu (2022). The Roles of Local Circulation and Boundary Layer Development in Tracer Transport over Complex Topography in Central Taiwan. *Journal of the Meteorological Society of Japan. Ser. II*.
- Huang, J.-D., & Wu, C.-M. (2020). Effects of microphysical processes on the precipitation Spectrum in a strongly forced environment. *Earth and Space Science*, 7, e2020EA001190. <https://doi.org/10.1029/2020EA001190>
- Huang, J. D., & Wu, C. M. (2022). A Framework to Evaluate Convective Aggregation: Examples With Different Microphysics Schemes. *Journal of Geophysical Research: Atmospheres*, 127(5), e2021JD035886.
- Hsu, T. H., Chen, W. T., Wu, C. M., & Hsieh, M. K. (2023). The Observation-Based Index to Investigate the Role of the Lee Vortex in Enhancing Air Pollution over Northwestern Taiwan. *Journal of Applied Meteorology and Climatology*, 62(3), 427-439.
- Large, W. G., McWilliams, J. C., & Doney, S. C. (1994). Oceanic vertical mixing: A review and a model with a nonlocal boundary layer parameterization. *Reviews of geophysics*, 32(4), 363-403.
- Morrison, H., and J. A. Milbrandt, 2014: Parameterization of cloud microphysics based on the prediction of bulk ice particle properties. Part I: Scheme description and idealized tests. *J. Atmos. Sci.*, 72, 287–311.
- Wu, C. M., & Arakawa, A. (2011). Inclusion of surface topography into the vector vorticity equation model (VVM). *Journal of Advances in Modeling Earth Systems*, 3(2).
- Wu, C. M., Lin, H. C., Cheng, F. Y., & Chien, M. H. (2019). Implementation of the land surface processes into a vector vorticity equation model (VVM) to study its impact on afternoon thunderstorms over complex topography in Taiwan. *Asia-Pacific Journal of Atmospheric Sciences*, 55(4), 701-717.

# Development of Tropical Circulation Vector Vorticity Equation Cloud-resolving Model

Jin-De Huang and Chien-Ming Wu<sup>1</sup>

<sup>1</sup>Department of Atmospheric Sciences, Taiwan National University, Taipei, Taiwan  
(Corresponding author: Chien-Ming Wu, e-mail: mog@as.ntu.edu.tw)

This work is distributed under the Creative Commons Attribution 4.0 License (CC BY 4.0)

## 1. Introduction

The vector vorticity cloud-resolving model (VVM) was developed based on the three-dimensional vector vorticity equations (Jung and Arakawa 2008). The use of vorticities as the prognostic variables in VVM can better capture the circulation induced by the local buoyancy gradient, which plays a critical role in the development of aggregated convection (Chen and Wu 2019). In the tropics, convective aggregation is regarded as a process to understand the cyclogenesis, the initiation of the Madden-Julian Oscillation, and the impacts of the convection on the large-scale circulation. This study extends VVM to the tropical circulation VVM (TCVVM), which covers the tropical region with mesoscale permitting resolution. TCVVM aims to study the interactions between large-scale circulation and convective-scale systems. This study investigates the performance of TCVVM in representing the tropical mean state and wave responses.

## 2. Model description and experimental setup

The model used in this study is the vector vorticity equation cloud-resolving model (VVM). Horizontal components of anelastic vorticity equations are predicted in the VVM, and velocities are diagnosed by solving a three-dimensional elliptic equation. The use of the vorticity equations eliminates pressure gradient force and inherently couples the dynamics to the thermodynamics in the governing equation. The unique dynamical core of VVM can better capture the circulation associated with the thermal gradient. The radiation model (RRTMG), the land surface model (Noah LSM), the first-order turbulence closure, and the predicted particle properties microphysical scheme (Huang and Wu, 2020) have been implemented in the VVM for studying complicated interactions associated with convection.

We applied Held-Suarez's simulation of dry dynamical TCVVM, covering both tropical and midlatitude regions, to examine whether TCVVM can represent the Hedley circulation and the midlatitude jet. Then, we turn on the moist processes to investigate the responses of TCVVM. On the other hand, we also examine the

capability of representing the tropical wave responses through the Gill-type simulation. Both tests of dry dynamics and moist processes are performed to understand the performance of TCVVM.

### 3. Result

The preliminary results show TCVVM can capture the mean state of the Hadley circulation in both dry dynamics and the simulation with moist processes. Fig. 1 show that the convection in some region of the tropics aggregate at the equator, while there are double peaks in some regions. The regions with the double intratropical convergence zone (ITCZ) might have interactions with midlatitude cyclones. The results demonstrate that TCVVM can produce a reasonable mean state of tropical circulations. In the presentation, we will further show the performance of TCVVM in tropical wave responses and their interactions with moist convection.

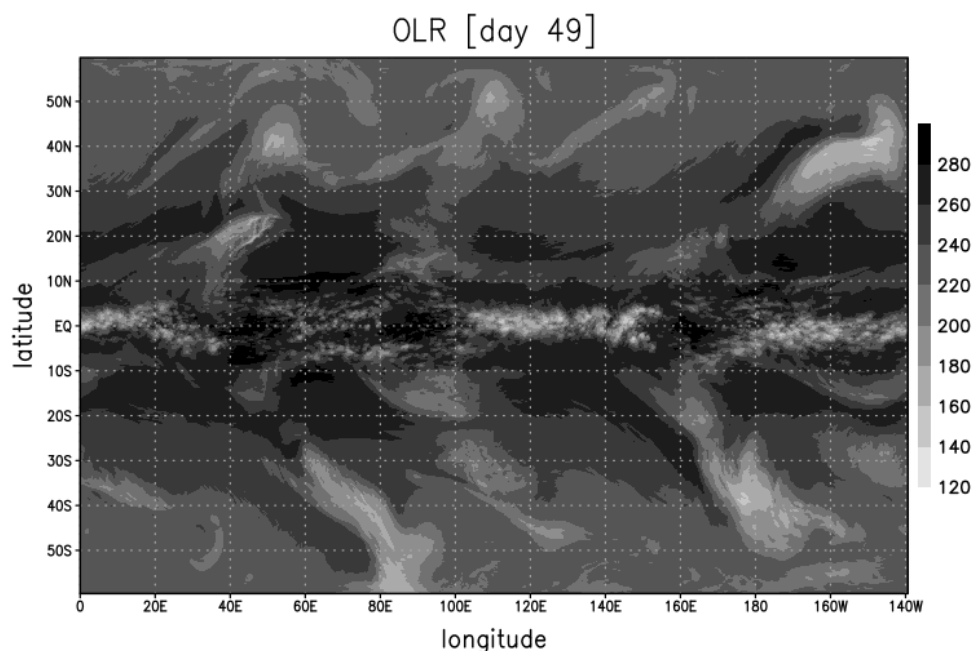


Fig 1. The daily averaged outgoing longwave radiation.

### References

1. Chen, Y.-T., & Wu, C.-M. (2019). The role of interactive SST in the cloud-resolving simulations of aggregated convection. *Journal of Advances in Modeling Earth Systems*, 11, 3321–3340.
2. Huang, J. - D., & Wu, C. - M. (2020). Effects of microphysical processes on the precipitation Spectrum in a strongly forced environment. *Earth and Space Science*, 7, e2020EA001190.
3. Jung, J.-H., & Arakawa, A. (2008). A three-dimensional anelastic model based on the vorticity equation. *Monthly Weather Review.*, 136(1), 276–294.

# A numerical model for the direct simulation of wind-wave interaction

Yasushi Fujiwara<sup>1</sup>

<sup>1</sup>Kobe University, Kobe, Japan

(Corresponding author: Yasushi Fujiwara, e-mail: fujiwara@port.kobe-u.ac.jp)

This work is distributed under the Creative Commons Attribution 4.0 License (CC BY 4.0)

## 1. Introduction

Ocean surface waves are known to modulate the momentum transfer between the atmosphere and the ocean because waves carry horizontal momentum, which is received from the wind via the surface form stress when they develop and is passed to the ocean current when they attenuate. It has been reported that, in the presence of remotely generated swells, the momentum flux deviates from pure wind-sea cases [e.g., Donelan et al., 1997]. However, the dependence of the momentum flux on the sea state is not well understood, resulting in the wide use of the simplified formulae that do not depend on wave conditions when estimating the momentum flux.

For a better understanding of the momentum transfer process and its model improvement, the direct numerical simulation (DNS) and large-eddy simulation (LES) of wind over waves is a promising approach as they provide us with the three-dimensional flow structure over swells. Out of possible numerical formulations, the use of a surface-fitting coordinate enables us to separate the interfacial momentum flux via normal (pressure) and tangential (viscous) stresses. This approach has been taken in many studies for the last two decades, mostly simulating the airflow over undulating walls. In contrast, some studies developed the dynamically coupled, air-water two-phase models, where the two-way interaction of wind field and waves can be simulated [e.g., Yang and Shen 2011]. These studies assumed that the inertia of water is so large that it can be considered as an undulating rigid wall over one integration time step. This assumption can cause errors in the momentum flux, particularly for those mediated by short waves. To avoid the influence of such an error, a full dynamical coupling between air and water is desired.

To accurately simulate the momentum exchange in the mixed seas, we developed a numerical formulation of air-water two-phase flows using a surface-following coordinate, with a pressure solver that achieves the full dynamical coupling between the air and water. There, special attention is paid to the conservation property of momentum and energy by adopting a full-flux form in the momentum equation.

## 2. Model description

The numerical scheme builds upon the free-surface water-side model introduced by Fujiwara et al. [2020]. The incompressible Navier-Stokes equation is solved for a two-phase fluid confined in a rectangular domain with periodic horizontal boundaries. The interface between air and water is assumed to be a one-valued function of horizontal position and time, so an overturn of the interface (wave breaking) is not allowed. Vertical coordinate transform is applied in each phase, which linearly maps the deformable physical space (between the top/bottom wall and interface) to a constant model space.

The momentum equation and mass-conservation equation are written in full-flux form so that the local conservation of momentum and mass is achieved. The equations are

discretized using the pseudo-spectral method in horizontal and the finite-volume method in vertical. To complete the time integration of the momentum equation, the pressure field must be computed so that the flow field would satisfy incompressibility. Pressure variables are located at cell centers, and the same number of equations arise due to the demand of incompressibility at each cell. In addition, pressure at the air-water interface is considered an unknown variable, and continuity at the interface is explicitly demanded using this additional degree of freedom. Under this treatment, an accurate pressure field that satisfies the incompressibility at both water and air and the continuity at the interface can be obtained with a single iteration loop. This dynamic and kinematic consistency would improve the accuracy of momentum flux between air and water.

This formulation can be seamlessly adopted to the air-only case where the water surface displacement is externally provided. This feature is useful for a spin-up computation for turbulent airflow over waves or the sensitivity study of dynamical coupling between wind and waves.

### 3. Performance tests and conclusion

The model performance was tested in various analytic cases, such as interfacial gravity waves, Kelvin-Helmholtz instability, and instability mechanism caused by laminar wind over waves [Miles, 1959]. The model well reproduced the analytic behavior even with a reasonable resolution. For example, in the interfacial gravity wave case, the numerical error in the energy of a poorly resolved wave ( $\Delta x = \Delta z = \lambda/16, \Delta t = T/120$ , where  $\lambda$  and  $T$  represent a wavelength and a wave period) was  $O(10^{-6})$  over one wave period. It was also confirmed that the total momentum was extremely well conserved, and the momentum exchange across the interface could be traced through the normal (pressure) and tangential (viscous) stresses evaluated at the interface.

To summarize, the newly developed wave-resolving two-phase model has promising capabilities for accurately simulating the air-sea momentum transfer mediated by waves. The author plans to examine processes where the conservation of energy and momentum would be important, such as the impact of swells on the surface drag under moderate wind.

### References

1. Donelan, M. A., Drennan, W. M., & Katsaros, K. B. (1997). The air-sea momentum flux in conditions of wind sea and swell. *Journal of Physical Oceanography*, **27**(10), 2087-2099.
2. Fujiwara, Y., Yoshikawa, Y., & Matsumura, Y. (2020). Wave-resolving simulations of viscous wave attenuation effects on Langmuir circulation. *Ocean Modelling*, **154**, 101679.
3. Miles, J. W. (1959). On the generation of surface waves by shear flows. Part 2. *Journal of Fluid Mechanics*, **6**(4), 568-582.
4. Yang, D., & Shen, L. (2011). Simulation of viscous flows with undulatory boundaries: Part II. Coupling with other solvers for two-fluid computations. *Journal of Computational Physics*, **230**(14), 5510-5531.

Session L:  
Urban modeling, Local scale phenomena

# Recent Development of City-Scale Large-Eddy Simulation model “City-LES”

Takuto SATO<sup>1</sup>, Hiroyuki KUSAKA<sup>1</sup>, Taisuke BOKU<sup>1</sup>, and Osamu TATEBE<sup>1</sup>

<sup>1</sup>Center for Computational Sciences, University of Tsukuba, Tsukuba, Japan  
(Corresponding author: Hiroyuki KUSAKA, e-mail: kusaka@ccs.tsukuba.ac.jp)

This work is distributed under the Creative Commons Attribution 4.0 License (CC BY 4.0)

## 1. Introduction

Large-eddy simulation (LES) models are powerful tools for simulating airflow and thermal environments in urban areas. The methods to generate inflow turbulence are important for the actual urban area simulation, but are still under discussion. The large output data and computational cost are also well-known problems for LES models. It is important to incorporate techniques in the field of high-performance computing, such as utilizing GPUs and optimization of the I/O part, to make the model applicable to the various settings.

In this presentation, we introduce recent developments in our LES model. To overcome the abovementioned difficulties, we implemented (1) a new inflow turbulence generation method (Sato and Kusaka, in revision) that can be used in the thermally driven convective boundary layer (CBL), (2) the GPU version of City-LES (Watanabe et al., 2021), and (3) a workflow to handle large output data of LES (Sato et al., 2019). (2) and (3) were done in collaboration with the high-performance computing division in CCS.

## 2. Model description

The LES model used is City-LES (Ikeda et al., 2015), which is developing at CCS. The basic equations are three-dimensional non-hydrostatic Boussinesq approximation equations. City-LES can explicitly resolve the buildings and street trees and consider the effect of wall/roof greening and mist spraying.

## 3. Result and conclusion

The new inflow turbulence generation method is an extension of the recycle-rescale method. We have improved the existing method to apply to the thermally driven CBL by using the parameters of the thermally driven CBLs (scale velocity and CBL height) and dealing with the perturbation of the potential temperature (Figure 1).

We introduced a workflow to handle the output data to optimize City-LES efficiently. In the proposed workflow, the output data is placed in a cache area instead of being persisted in the parallel file system (PFS) to avoid performance degradation.

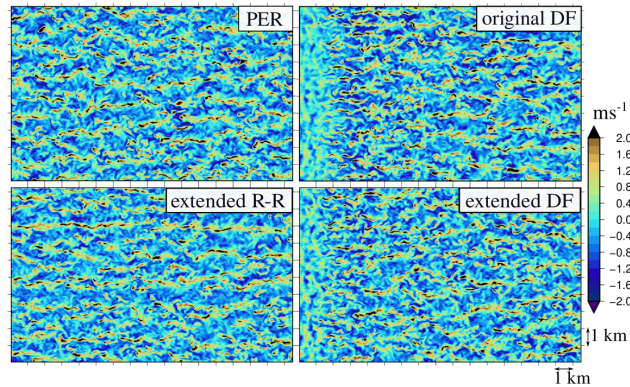


Fig. 1 Horizontal cross sections of vertical windspeed. Proposed method(extended R-R) can generate plausible turbulence near the inflow boundary (Sato et al., in revision).

Additionally, we implemented a two-stage read in which the analysis program reads data in a distribution pattern better in performance, and the data is re-distributed in a pattern for analysis after the read is done.

We implemented the GPU version of City-LES. In the GPU version, all simulation components are offloaded to the GPU. To avoid frequent CPU-GPU communications, this offloading includes the part where performance is not improved significantly by using GPU. This GPU version achieved 6- to 15-times speedup from the CPU version.

### Acknowledgement

This study was supported by JSPS KAKENHI (grant number JP21K03656). This study used the computational resources of Oakforest-PACS and Cygnus provided by the Multidisciplinary Cooperative Research Program at the Center for Computational Sciences, University of Tsukuba. We are grateful to Assoc. Prof. Tsubasa Okaze at the Tokyo Institute of Technology for his advice on implementation.

### References

1. Sato, T., and H. Kusaka, (2023), Applicability of methods for inflow turbulence generation developed in a CFD field to the thermally driven convective boundary layer simulations. *in revision*
2. Watanabe, K., K. Kikuchi, T. Boku, T. Sato, and H. Kusaka, (2021), High resolution of city-level climate simulation by GPU with multi-physical phenomena. *in proceedings of 18<sup>th</sup> Annual IFIP International Conference on Network and Parallel Computing (NPC2021)*, Online
3. Sato, T., O. Tatebe, and H. Kusaka, (2019), In-situ Data Analysis System for High Resolution Meteorological Large Eddy Simulation Model. *in proceedings of 6th IEEE/ACM International Conference on Big Data Computing, Applications and Technologies (BDCAT'19)*, pp.155-158, Auckland, New Zealand
4. Ikeda, R., H. Kusaka, Iizuka S. and T. Boku, (2015), Development of Urban Meteorological LES model for thermal environment at city scale. *9th International Conference for Urban Climate*, Toulouse, France

# **Sensitivity tests of WRF-UCM simulations of extreme heat events in Metro Manila**

Angela Monina Ticobay MAGNAYE<sup>1</sup> and Hiroyuki KUSAKA<sup>2</sup>

<sup>1</sup> Graduate School of Life and Environmental Sciences, University of Tsukuba, Japan

<sup>2</sup> Center for Computational Sciences, University of Tsukuba, Japan

(Corresponding author: Angela MAGNAYE, e-mail: s2230303@u.tsukuba.ac.jp)

This work is distributed under the Creative Commons Attribution 4.0 License (CC BY 4.0)

## **1. Introduction**

With the increasing trend in average global temperature, extreme heat events increased in the recent years, which affect human health and livelihood especially in highly populated areas. The increasing urbanization in growing megacities such as Metro Manila, Philippines raises a need to investigate the impact of urban land cover during extreme heat events. This study aims to assess how a numerical prediction model can capture observed extreme heat events with updated urban features.

## **2. Model description and experimental setup**

Cases of extreme heat events are first identified for at least 3-consecutive days of maximum daily temperature exceeding a daily threshold, based on a 90th percentile of 31-day window for a 6-year period of observation data from Weather Philippines Foundation (Fig. 1b). Sensitivity tests of physics schemes are conducted using Weather Research and Forecasting (WRF) model (Skamarock et al., 2019) coupled with Urban Canopy Model (UCM) (Kusaka et al., 2001; Chen et al., 2011) using two nests (Fig. 1a). The updated land use is based on a 2015 dataset from the National Mapping and Resource Information Authority (NAMRIA) Philippines, converted with MODIS 20-class categories (Fig. 1c). Aside from urban rate estimates, an estimated anthropogenic heat in 2010 (Varquez et al., 2021; Fig. 1d) is included for URBAN simulations (e.g. Doan et al., 2019), while urban grids are converted to cropland land cover for NOURBAN simulations. A set of simulations with different planetary boundary layer (PBL) schemes and initial and boundary conditions (ICBC) were compared with weather station data.

## **3. Results and conclusion**

A composite of 5 extreme heat events show that URBAN simulations captured observed diurnal variation of 2-m temperature compared to NOURBAN simulations especially during night conditions (Fig. 2a). Furthermore, composites of URBAN

simulations improved distribution (Fig. 2b), biases and pattern correlation compared to individual simulations (i.e. different PBL schemes and ICBC). This first step of model sensitivity experiments and assessment in present urban land cover will be used for further experiments especially comparing past and future urbanization of Metro Manila.

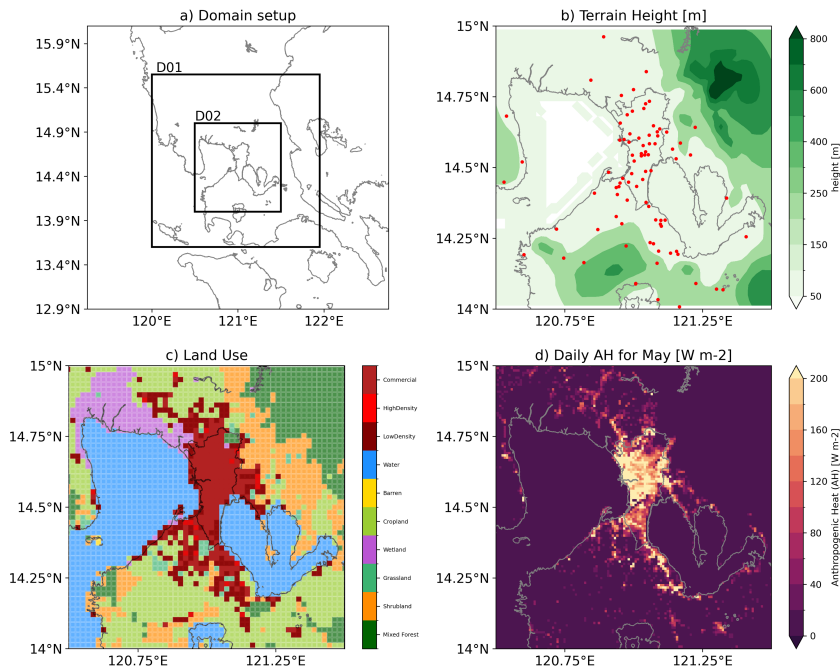


Fig. 1. a) WRF domain setup, b) terrain height (m), c) 2015 urban land use, and d) daily anthropogenic heat ( $\text{W m}^{-2}$ ) representing May 2010 for Metro Manila.

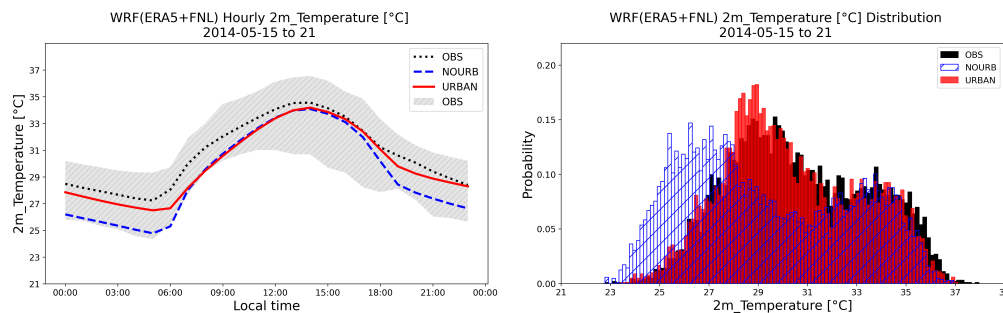


Fig. 2. a) Diurnal variation and b) distribution between URBAN (red), NOURBAN (blue) and observation (black and gray shaded area) for an extreme heat event in Metro Manila.

## References

- Chen, F., et al. (2011), *Int. J. Climatol.*, **31**, 273–288.
- Doan, V.Q., et al. (2019), *Sustainable Cities and Society*, **47**, 101479.
- Kusaka, H., et al. (2001), *Bound. Layer Meteorol.*, **101**, 329–358.
- Skamarock, C., et al. (2019), A Description of the A.R. WRF Model Version 4
- Varquez, A.C.G., et al. (2021), *Scientific Data*, **8(1)**, 64.

# The valuable local winds “Obonai-dashi” simulated by the WRF model

Tatsuki KUDO<sup>1</sup>, and Hiroyuki KUSAKA<sup>2</sup>

<sup>1</sup>Graduate School of Science and Technology, University of Tsukuba, Tsukuba, Japan

<sup>2</sup>Center for Computational Sciences, University of Tsukuba, Tsukuba, Japan

(Corresponding author: Hiroyuki KUSAKA, e-mail: kusaka.hiroyuki.ff@u.tsukuba.ac.jp)

This work is distributed under the Creative Commons Attribution 4.0 License (CC BY 4.0)

## 1. Introduction

The Obonai-dashi is easterly local winds blowing in the Tohoku region, northern Japan. This local winds blows in the Obonai district, which is located in a narrow basin-like area adjacent to the mountain range with a pass. The Obonai-dashi is believed to be valuable winds that bring good harvests because foehn winds blow from the pass even if cool easterly winds blow in the windward side in summer (Nagaho *et al.* 2021). The purpose of this study is to reveal the spatial structure of the Obonai-dashi by the three dimensional and high resolution numerical simulation.

## 2. Methodology

We used the WRF model. The finest grid spacing is 1 km. We reproduced wind and potential temperature of two cases of the Obonai-dashi, Case A and Case B. Case A of the Obonai-dashi blew after a migrative high pressure system passed the northern Japan and stopped blowing when an extratropical cyclone approached. Case B of the Obonai-dashi blew when the Okhotsk Sea high located on the north of Japan.

## 3. Results and conclusions

### Case A:

A southerly wind was blowing in most of the northern Tohoku region and a strong easterly wind was blowing only in the Obonai district. A part of the southerly wind blowing in the windward side changed to an easterly wind near the pass and was blowing toward the Obonai district (Fig. 1. top left). A south-southwest strong wind was blowing above the ridgeline of the mountain range. Potential temperature in the Obonai district was about 1 K higher than that of the windward side but was lower than that of the other lee side area and this lower potential temperature area extended along the blowing area (Fig. 1. top right).

### Case B:

An easterly wind was blowing in most of the northern Tohoku region, except for the southerly wind in the large basin of the windward side. Especially, a strong wind was blowing at the leeward foot of the mountain range. A part of the southeasterly wind blowing in the windward side changed to an easterly wind near the pass and was blowing toward the Obonai district (Fig. 1. bottom left). A weak southeasterly wind was blowing above the ridgeline of the mountain range. Potential

temperature in the Obonai district was almost the same as that of the windward side (Fig. 1. bottom right).

### Conclusions

It was common that a part of the wind blowing in the windward side changed to an easterly wind near the pass and blowing toward the Obonai district. There were differences in the direction of the inflow, the wind direction and wind speed above the ridgeline of the mountain range, and the difference in potential temperature between the windward side and the Obonai district.

### References

1. Nagaho, T., K. Niseki, and N. Sato, (2021), Climatological study on the local wind “Obonai-dashi” in Akita prefecture, Tohoku district of Japan, The Compiled Papers on the 70th Anniversary of Geographical Society of Hosei University, 147-158.

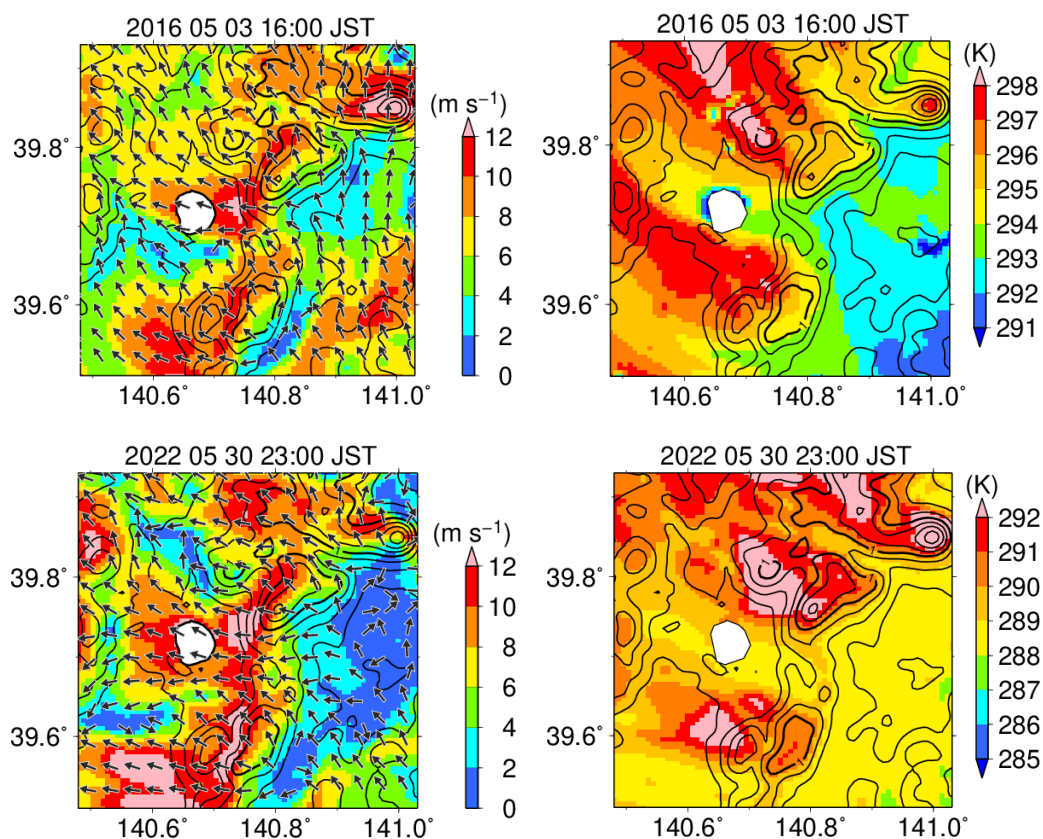


Fig. 1. Spatial structure of the Obonai-dashi.

(Top) Case A (Bottom) Case B

(Left) Wind speed and wind direction at 10m (Right) Potential temperature at 2m

# Effect of “Sado Island Block” on Snowfalls in Niigata City and the coastal plain

Nobuyasu Suzuki<sup>2</sup>, Hiroyuki Kusaka<sup>1</sup>, Masato Yabe, and Hiroki Kobayashi<sup>3</sup>

<sup>1</sup> Center for Computational Sciences, University of Tsukuba, Tsukuba, Japan

<sup>2</sup> Graduate School of Science and Technology, University of Tsukuba, Tsukuba, Japan

<sup>3</sup> Graduate School of Life and Environmental Sciences, University of Tsukuba, Tsukuba,  
Japan

(Corresponding author: Hiroyuki Kusaka, e-mail: kusaka.hiroyuki.ff@u.tsukuba.ac.jp)

This work is distributed under the Creative Commons Attribution 4.0 License (CC BY 4.0)

## 1. Introduction

Niigata City, located on Japan's Sea of Japan coast, experiences heavy snowfall regions, although experiences less snowfall than neighboring cities. Yagi and Uchiyama (1983) suggested that the Sado Island blocks and bypasses the winter monsoon, thereby reducing snowfall in the downwind Niigata Plain. However, Veals et al., (2019) statistical analysis of radar data shows that shadowing on Sado Island extends to the Niigata Plain during strong winds, suggesting a different mechanism.

Our study, statistical analysis using ground-based radar data and various numerical experiments to clarify 1) whether the "Sado Island Block" is occurring and 2) what the mechanism is.

## 2. Methods

First, using radar data from the Japan Meteorological Agency (JMA), we investigated cases in which precipitation in Niigata City was lower than in surrounding areas during winter-type pressure patterns. Among them, numerical experiments were conducted on 12 typical events. The WRF model version 4.2.2 was used for numerical simulations. The resolution of the simulation is 1 km. In this study, we conducted a numerical experiment with real terrain (CTRL), a simulation with Sado Island removed (No\_SD), a simulation with Sado Island moved 150 km northeast (NE\_SD), a simulation with Sado Island moved 200 km upwind (NW\_SD), and an experiment with different physical models and initial/boundary conditions. Finally, the mechanism of the "Sado Island Block" is discussed.

## 3. Result and conclusion

The results of numerical experiments for the CTRL case and the No\_SD, NE\_SD, and NW\_SD cases show that Sado Island reduces precipitation (creates a snow shadow) up to 150 km downwind. This snow shadow was found to be caused primarily by two effects:

(1) more precipitation occurs on the windward slope of Sado Island, reducing the advection of water vapor and liquid/ice particles downwind, and (2) Sado Island reduces heat fluxes from the sea surface by weakening leeward winds.

### Acknowledgments

A part of this study was supported by the Environment Research and Technology Development Fund JPMEERF20232003 of the Environmental Restoration and Conservation Agency provided by Ministry of the Environment of Japan.

### References

1. Kusaka, H., N. Suzuki, M. Yabe, and H. Kobayashi, (2023), The snow-shadow effect of Sado Island on Niigata City and the coastal plain, *Atmos. Sci. Lett.*, DOI:10.1002/asl.1182.
2. Veals, P.G., W.J. Steenburgh, S. Nakai, and S. Yamaguchi, (2019), Factors Affecting the Inland and Orographic Enhancement of Sea-Effect Snowfall in the Hokuriku Region of Japan, *Mon. Wea. Rev.*, **147**, 3121-3143.
3. Yagi, S., and Y. Uchiyama, (1983), Cloud movement and confluence around Noto peninsula and Sado Island in relation to heavy snowfall over Johetsu area. *Tenki*, **30**, 291-294 (in Japanese).

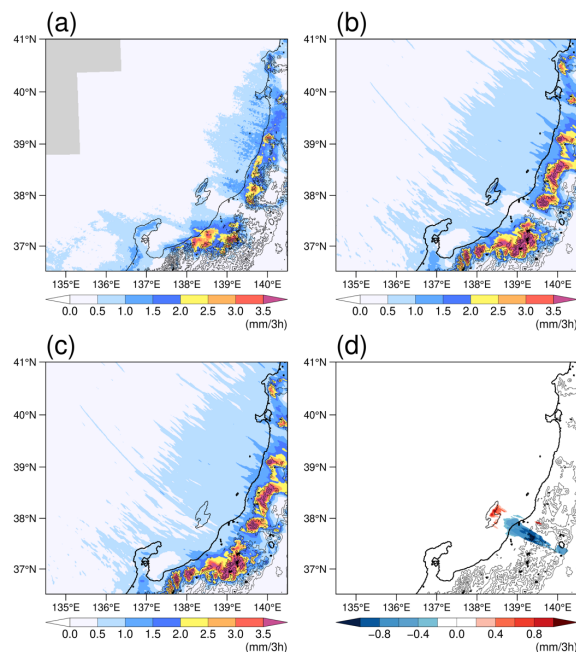


Fig. 1. Results of simulation. (a) Observed 3-h accumulated precipitation. (b) Simulated 3-h accumulated precipitation for Case CTRL. (c) Simulated 3-h accumulated precipitation for Case No\_SD. (d) Differences in 3-h accumulated precipitation between Cases CTRL and No\_SD. Only regions with a 95% confidence level in the Welch's t-test are shown in Figure (d). (Kusaka et al., 2023)

# Ensemble simulations of a heavy snowfall event in the Kanto area in Japan on Jan 22<sup>nd</sup>, 2018

Shigetoshi Saito<sup>1</sup>, Kentaro Araki<sup>2</sup>, and Tomoki Miyakawa<sup>1</sup>

<sup>1</sup> University of Tokyo, Tokyo, Japan

<sup>2</sup> Meteorological Research Institute, Japan

(Corresponding author: Shigetoshi Saito, e-mail: [saitou724@g.ecc.u-tokyo.ac.jp](mailto:saitou724@g.ecc.u-tokyo.ac.jp))

This work is distributed under the Creative Commons Attribution 4.0 License (CC BY 4.0)

## 1. Introduction

In Tokyo, located in the Kanto area in Japan, snowfall amount of 1cm or more per day have only been observed 124 times in the past 60 years, this is mainly due to “South-Coast Cyclones (SCCs)”. The SCC brings 10 cm or more of snowfall amount per day to Tokyo once every few years, leading to significant social impacts on the metropolitan area. However, snowfalls associated with SCCs are difficult to predict, and it is desired to elucidate its mechanism.

Heavy snowfall prediction due to SCC is very complex. Precipitation and temperature near the surface play a major role in determining whether a heavy snowfall occurs or not. To improve prediction of heavy snowfall due to SCC, we need to investigate past heavy snowfall cases. In this study, we focused on mesoscale phenomena such as cold-air damming (CAD), lower-level jet, and coastal front, which are associated with precipitation and temperature decreases near the surface. To analysis why heavy snowfall occurred, we tried ensemble simulations of past cases of heavy snowfall in Tokyo.

## 2. Model description and experimental setup

In this study, we conducted ensemble experiments of the heavy snowfall event on January 22<sup>nd</sup>, 2018, when snowfall amount of 23 cm was observed in Tokyo. The regional atmospheric model SCALE was used for the numerical simulations. The atmospheric initial conditions used in the ensemble experiments were derived from the forecast results of the operational global ensemble model of the Japan Meteorological Agency (JMA). The atmospheric boundary conditions used in the ensemble experiment were the JMA mesoscale analysis (MA). Land and sea surface temperature data used in the ensemble experiment were NCEP-FNL data. The horizontal resolution is 2 km and the number of vertical layers is 60, from 60 m to about 15000 m. The calculation domain covering Japan is  $1800 \times 1800$  grids centered at  $137.22^\circ\text{E}$ ,  $35.65^\circ\text{N}$ . The MA data was used to compare the reproducibility of the phenomena. Integral time of the simulation is since Jan 21<sup>st</sup> 12 (UTC) until Jan 23<sup>rd</sup> 00 (UTC). Cloud micro-physics scheme is Six-class two-moment bulk scheme. Cumulus parameterization is not used. Turbulence scheme is Smagorinsky-Lilly-type sub-grid model.

## 3. Result and conclusion

The ensemble simulation results showed that the SCC itself, as represented in the MA, was reproduced in both experiments. However, the location and intensity of the SCC in each experiment, as well as the temperature and precipitation near the ground, were different. Figure 1 shows 2 m air temperature ( $^\circ\text{C}$ ), sea level pressure (hPa), and 500 m horizontal wind ( $\text{m s}^{-1}$ ) at 12 UTC on January 22, 2018 for one member of ensemble experiments. U-shape isoline of sea-level pressure is the characteristics of CAD. The

CAD, which is the characteristics of mesoscale phenomena of heavy snowfall, is also indicated. Northeasterly winds at 500m in the Kanto region (showed by black circle), low temperature is represented due to CAD, and a coastal front with a large horizontal temperature gradient is represented in Chiba Prefecture (showed by green circle). The change in precipitation phase between rain and snow around the coastal front is showed in model experiment. The vertical cross section of the north-south direction shows lower potential temperature region north of 34.5°N in Fig. 2. It is indicated that this region represents the cold air layer due to CAD associated with the mountains in the northern Kanto region. In the presentation, we will also present the analysis results from other ensemble members and a discussion of the relationship between heavy snowfall and mesoscale phenomena.

### Acknowledgments

This research was supported by JSPS Grants-in-Aid for Scientific Research 20K14557 and JP22H01297. The numerical experiments in this study were conducted through the Fugaku General Proposal (Proposal No. hp230108) with computational resources provided by the supercomputer "Fugaku".

### References

1. Araki, K., 2019: Climatological features of heavy snowfalls in the Kanto and Koshin regions. *Meteor. Res. Notes*, **239**, 83-93.
2. Nishizawa, S., H. Yashiro, Y. Sato, Y. Miyamoto, and H. Tomita, 2015: Influence of grid aspect ratio on planetary boundary layer turbulence in large-eddy simulations. *GMD*, **8**, 3393-3419.
3. Sato, Y., S. Nishizawa, H. Yashiro, Y. Miyamoto, Y. Kajikawa, and H. Tomita, 2015: Impacts of cloud microphysics on trade wind cumulus: which cloud microphysics processes contribute to the diversity in a large eddy simulation?. *PEPS*, **2**, 23

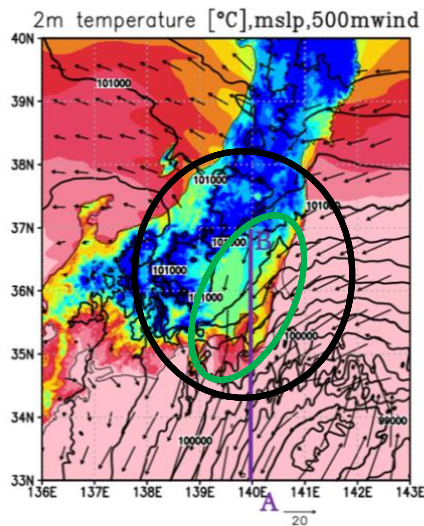


Fig. 1. 2 m air temperature ( $^{\circ}\text{C}$ ), sea level pressure (solid line, hPa), and 500 m horizontal wind (vector, m/s) at 12 UTC on January 22, 2018. Results from an experiment with a resolution of 2 km at one member.

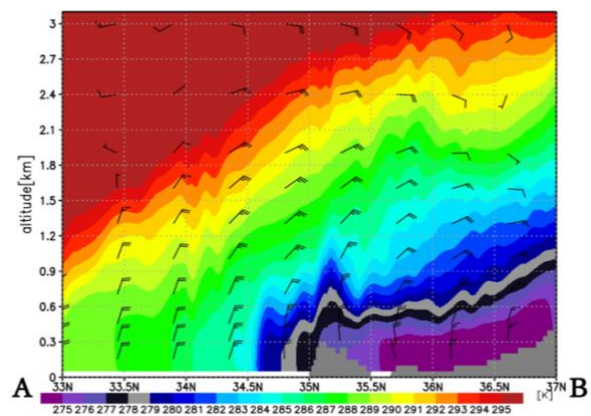


Fig. 2. Vertical cross section of potential temperature and horizontal wind (arrow feathers) at line AB in Figure 1. The short arrow feathers show 5 m/s and the long arrow feathers show 10 m/s.

## Session M: Dynamical core, LES

# Optimal Configurations for Storm-Resolving Atmospheric Simulations

William C. Skamarock

National Center for Atmospheric Research, Boulder, Colorado, USA

(Corresponding author: William C. Skamarock, e-mail: skamaroc@ucar.edu)

This work is distributed under the Creative Commons Attribution 4.0 License (CC BY 4.0)

## 1. Introduction

Skamarock et al (2019) showed that the horizontal global mesoscale kinetic energy (KE) spectra did not converge in simulations using the Model for Prediction Across Scales (MPAS; Skamarock 2012) using a 15 km mesh until the vertical mesh spacing approached 200 meters in the troposphere and lower stratosphere. We have since discovered that we can reduce the horizontal filtered in MPAS when employing the denser vertical mesh spacing, and as such increase our effective resolution. This result is depicted in the left-hand panel of figure 1, where the effective resolution is nearly doubled in the troposphere ( $z = 10$  km), from  $8\Delta x$  to  $4\Delta x$ , with the reduced dissipation configuration. The right panel in figure 1 shows the spectra for the coarse and fine vertical mesh spacing for the test case used to determine the default dissipation configuration in Skamarock (2012). The reduced-dissipation configuration produces an anomalous KE block at  $4\Delta x$  for the coarse vertical mesh, necessitating the increased damping in the default configuration. These results are for mesoscale resolutions. Here we report on testing at convection-permitting resolution.

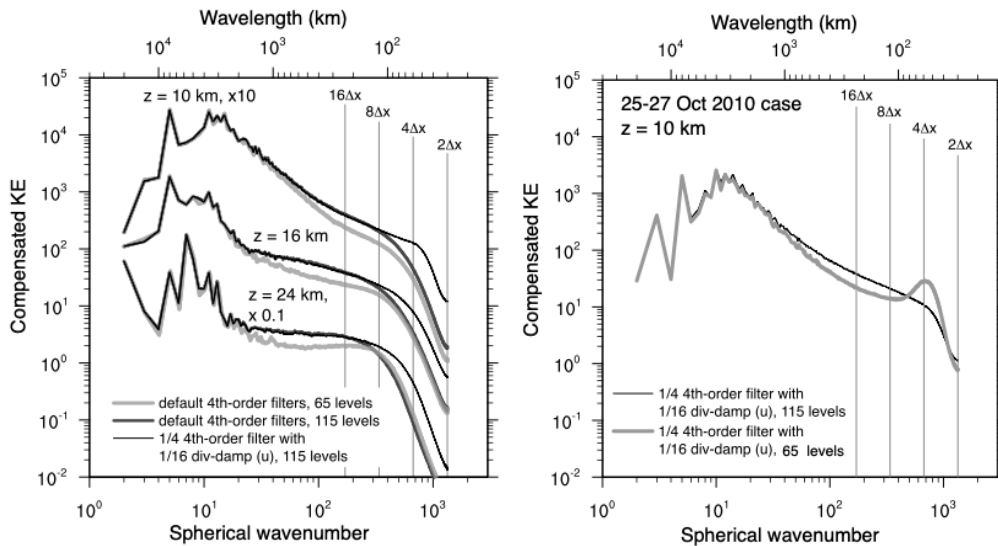


Figure 1: Horizontal KE spectra ( $\text{m}^2/\text{s}^2$ ) from MPAS using a 15 km horizontal mesh and 65 and 115 level configurations with different background horizontal filters. The maximum vertical level spacing in the troposphere is approximately 600 m and 250 m for the 65 and 115 level configurations, respectively.

## 2. Convective-scale tests

We utilize a variable-resolution 60-3 km horizontal cell-spacing mesh to simulate a case

of strong convection and tornado outbreak over the eastern US on 27-28 April 2011. We were able to utilize our standard timestep configuration in these tests, but modifications were made to stabilize the scalar transport in these simulations given the strong vertical velocities and high vertical Courant numbers in these tests. Concerning the effect of the filters, the left-hand panel in figure 2 depicts the area of updraft velocity greater than 5 m/s as a function of height in simulations using the two horizontal diffusion configurations discussed earlier, and a third configuration that increases the default horizontal divergence damping by a factor of 5. We find, paradoxically, that increasing (decreasing) the horizontal divergence damping increases (decreases) the updraft area and increases (decreases) the vertical velocities in the updraft (not shown). The right panel of figure 2 shows that the potential temperature in the updrafts increases with increased horizontal divergence damping, indicating less environmental entrainment/detrainment in the updrafts (the cores are less diluted). Convection-permitting model configurations typically produce too little detrainment at low- and mid-levels (Bryan and Morrison, 2012) and we highlight the effects of the divergence damping here to emphasize that relying upon it for stabilization may exacerbate the lack of lower-level detrainment at convection-permitting resolutions. Other aspects of the filter configurations will be presented at the workshop.

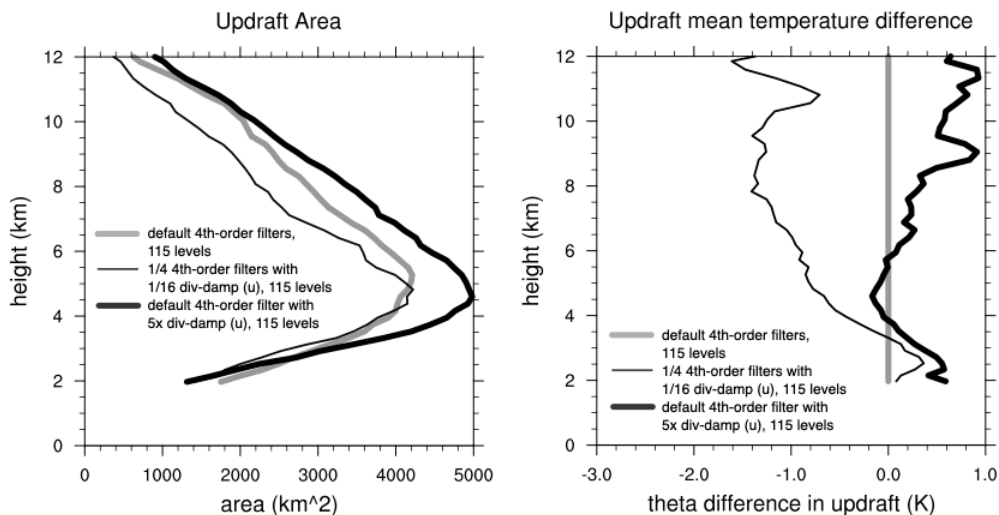


Figure 2: Updraft area ( $w > 5$  m/s) and updraft mean potential temperature difference (from the default 115 level configuration) on 0 UTC 28 April 2011.

## References

1. Bryan, G. H., and H. Morrison, 2012: Sensitivity of a Simulated Squall Line to Horizontal Resolution and Parameterization of Microphysics. *Mon. Wea. Rev.*, **140**, 202-225, doi:10.1175/MWR-D-11-00046.1
2. Skamarock, W. C, J. B. Klemp, M. G. Duda, L. Fowler, S.-H. Park, and T. D. Ringler, 2012: A Multi-scale Nonhydrostatic Atmospheric Model Using Centroidal Voronoi Tessellations and C-Grid Staggering. *Mon. Wea. Rev.*, **140**, 3090-3105. doi:10.1175/MWR-D-11-00215.1
3. Skamarock, W. C., C. Snyder, J. B. Klemp and S. Park, 2019: Vertical Resolution Requirements in Atmospheric Simulation. *Mon. Wea. Rev.*, **147**, 2641-2656, doi:10.1175/MWR-D-19-0043.1

# Large eddy simulation with a parameterization of fluctuating surface momentum fluxes

Junshi Ito<sup>1</sup> and Hideaki Mouri<sup>2</sup>

<sup>1</sup>Tohoku University, Sendai, Japan

<sup>2</sup>Meteorological Research Institute, Ibaraki, Japan

(Corresponding author: Junshi Ito, e-mail: junshi@tohoku.ac.jp)

This work is distributed under the Creative Commons Attribution 4.0 License (CC BY 4.0)

## 1. Introduction

The atmosphere and the ground exchange momentum and heat through the surface layer. Since numerical weather prediction models cannot resolve this process, they need parameterizations based on the law of the wall (or the Monin-Obukhov law).

When the resolution of those models is increased so that they can be considered as large eddy simulations (LES), the turbulent fluctuations of the wind speeds in the surface layer become too significant. The conventional diagnostic of the surface momentum flux becomes not valid. Recently, we proposed a new diagnostic that takes into account the fluctuations of the surface momentum flux and confirmed it with data from a wind tunnel experiment and a field observation<sup>1,2</sup>. The present study tests the LES with this new diagnosis.

## 2. LES and validations

We perform LES of a turbulent Ekman layer. Its configuration follows the previous study<sup>3</sup>. The vertical resolution is 1.25 m. The roughness length is set to be  $z_0 = 0.03$  or 0.01 m. The results of LES with the conventional law of the wall (LoW) are compared with those of the new diagnostic (MI23)<sup>1,2</sup>. For validation, we use the results of the wind tunnel experiment and the field observations at the Meteorological Research Institute.

## 3. Result and conclusion

Figure 1 shows the vertical profiles of mean horizontal wind speeds. The near-surface logarithmic layer is roughly reproduced by both diagnostics, LoW and MI23. Still, as compared with the data from the wind tunnel experiment, the results of MI23 are more natural.

Figure 2 shows the vertical profile of the variances of the horizontal streamwise velocity. At  $z/\delta = 0.05 \sim 0.1$ , where  $\delta$  is the thickness of the boundary layer, the results reproduce the logarithmic law of the variances found in the wind tunnel experiment and the field observation. Near the lowest level of the LES, the variances are much smaller than the estimates of the law, because subgrid-scale fluctuations are dominant in the LES. Nevertheless, the variances for MI23 are closer to the logarithmic law. The variations of the surface momentum flux are also 50% larger than those for LoW (not shown).

In conclusion, the use of the new diagnostic of MI23 increases the variances near the lowest level. As a result, the surface layer statistics become more reasonable with respect to the conventional diagnostic of LoW.

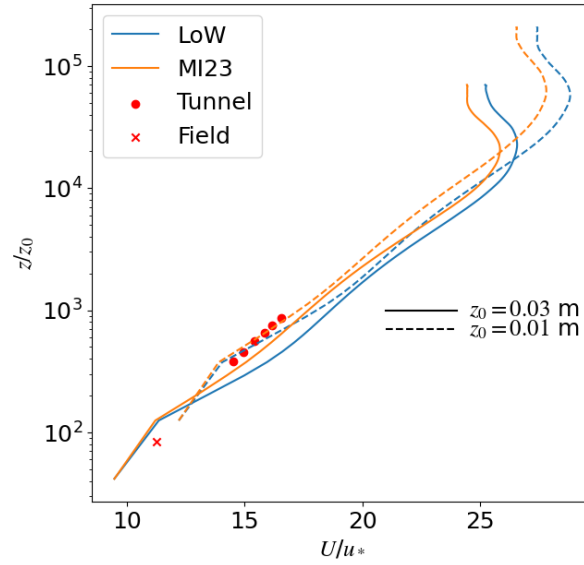


Fig. 1. Vertical profile of mean horizontal wind speed normalized by friction velocity.

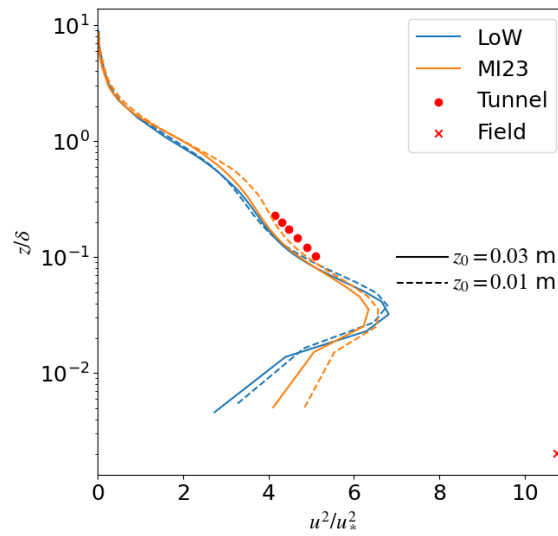


Fig. 2. Vertical profile of variances in horizontal streamwise wind speed normalized by the square of the friction velocity.

## References

1. Mouri, H. and J. Ito: Momentum flux fluctuations in wall turbulence formulated along the distance from the wall (2023), *Phys. Fluids*, **35**, 075104.
2. Mouri, H. and J. Ito: Momentum flux fluctuations in wall turbulence: a formula beyond the law of the wall (2022), *Phys. Fluids*, **34**, 035109.
3. Jiang, Q., S. Wang, and P. Sullivan (2018). Large-Eddy Simulation Study of Log Laws in a Neutral Ekman Boundary Layer. *J. Atmos. Sci.*, **75**, 1873–1889.

# Development of a global atmospheric nonhydrostatic dynamical core using discontinuous Galerkin method

Yuta KAWAI and Hirofumi TOMITA

RIKEN Center for Computational Science, Kobe, Japan

(Corresponding author: Yuta KAWAI, e-mail: yuta.kawai@riken.jp)

This work is distributed under the Creative Commons Attribution 4.0 License (CC BY 4.0)

## 1. Introduction

Considering high-resolution atmospheric simulations with  $O(10\text{ m})$  grid spacing near the future, we recently investigated on numerical accuracy of atmospheric dynamical core necessary for performing large eddy simulation precisely [3, 4]. Our study suggested the required order of accuracy for classical grid-point methods is much higher than the second order. However, such low-order methods are typically used as a spatial discretization in state-of-the art global nonhydrostatic atmospheric models (e.g., [5]). Thus, we newly develop a global dynamical core using the discontinuous Galerkin method (DGM), which is characterized by its simplicity and compactness for the high-order strategy. To validate it and evaluate the effect of high-order scheme on the atmospheric fields, we are performing a series of numerical experiments and investigating the behavior of numerical convergence. We will present the preliminary results in this presentation.

## 2. Model description and experimental setup

The governing equations are a fully compressible nonhydrostatic equations of dry atmosphere. To treat spherical geometry, a cubed-sphere coordinate is adopted. The spatial discretization is based on nodal DGM. The computational domain is divided using hexahedral elements with  $(p+1)^3$  nodes where  $p$  is the order of polynomial. The numerical fluxes are calculated by the Rusanov flux. As the temporal discretization, we use a horizontal explicit and vertical implicit (HEVI) scheme with the third-order accuracy.

To validate our dynamical core, we conduct a series of numerical experiments. This presentation focuses on two test cases of gravity wave and baroclinic instability. The experimental setup of gravity wave test is based on [1]. The horizontal and vertical effective grid spacing are changed as  $(\Delta_h, \Delta_z) \sim (313\text{ km}, 417\text{ m}), (156\text{ km}, 208\text{ m}), (78\text{ km}, 104\text{ m})$  using  $p=1, 3, 7$  and the self-convergence of numerical solutions is investigated. The experimental setup of baroclinic wave is based on [2]. The horizontal effective grid spacing is changed as  $\Delta_h \sim 250\text{ km}, 125\text{ km}, 63\text{ km}$  using  $p=7$ . Following [2], we fix the number of vertical degree of freedom, which is set to 24 in this study.

### 3. Results and conclusion

Figure (a) show a dependence of spatial resolution on L2 error norms of winds for the gravity wave test. This indicates the convergence rate for the zonal wind follows almost  $p+1$ -order accuracy. On the other hand, the convergence rate for the vertical wind related to fast modes is smaller than the  $p+1$ -order accuracy for  $p > 4$  due to temporal errors of HEVI scheme. Figure (b) shows a temporal evolution of L2 error norms of surface pressure and the spatial resolution dependence for the baroclinic wave test. The dashed lines represent the results obtained from Mcore [6]. The results of both models become comparable when the baroclinic wave starts to develop significantly. The decrease in the error slows down when  $\Delta_h < 250$  km. One of the reasons may be related to the experimental setup of fixed vertical resolution. However, the L2 errors for  $\Delta_h < 250$  km are within a range of uncertainty suggested by [2] (represented by shaded in the figure), and we consider that the numerical solutions from our model based on DGM are reasonable.

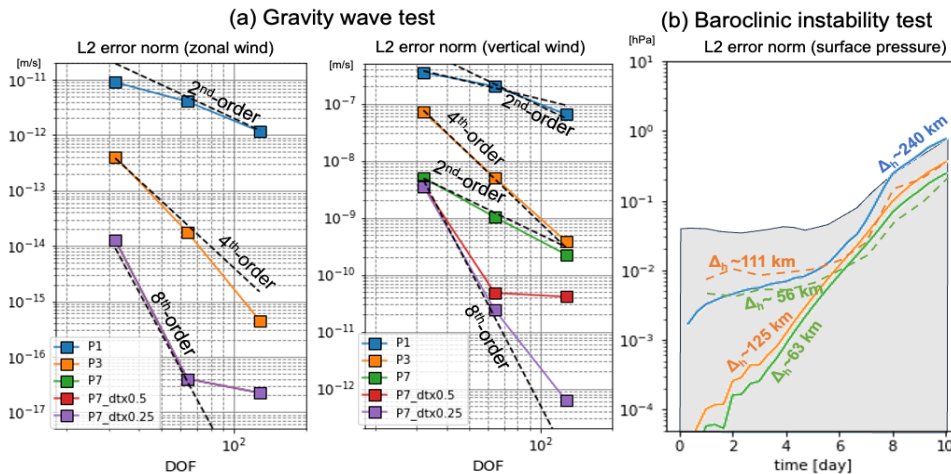


Figure: (a) L2 error norm of zonal and vertical winds obtained from a test case of gravity wave. For  $p=7$  case, we also show the results when the time step decreases by a factor of 1/2 and 1/4. (b) L2 error norm of surface pressure obtained from a baroclinic instability test. The solid lines represent the result of our study. For comparison, the results from Mcore [6] are shown by the dotted lines.

### References

- Baldauf, M. and Brdar, S. (2013), An analytic solution for linear gravity waves in a channel as a test for numerical models using the non-hydrostatic, compressible Euler equations. *Q.J.R. Meteorol. Soc.*, **139**, 1977-1989.
- Jablonowski, C. and Williamson, D.L. (2006), A baroclinic instability test case for atmospheric model dynamical cores. *Q.J.R. Meteorol. Soc.*, **132**, 2943-2975.
- Kawai, Y., and Tomita, H. (2021), Numerical Accuracy of Advection Scheme Necessary for Large-Eddy Simulation of Planetary Boundary Layer Turbulence, *Mon. Weather. Rev.*, **149**, 2993-3012.
- Kawai, Y., and Tomita, H. (2023), Numerical Accuracy Necessary for Large-Eddy Simulation of Planetary Boundary Layer Turbulence Using the Discontinuous Galerkin Method, *Mon. Weather. Rev.*, **151**, 1479-1508.
- Tomita, H. and Satoh, M. (2004), A new dynamical framework of nonhydrostatic global model using the icosahedral grid. *Fluid Dyn. Res.*, **34**, 357.
- Ullrich, P. A., and Jablonowski, C., (2012), Mcore: A non-hydrostatic atmospheric dynamical core utilizing high-order finite-volume methods. *J. Comput. Phys.*, **231**, 5078-5108

# OctaHEALPix grid: a new, equal-area quadrilateral grid on a sphere which admits spherical harmonics transform

Daisuke Hotta<sup>1</sup>, Milan Klöwer<sup>2</sup>, and Sam Hatfield<sup>3</sup>

<sup>1</sup>Meteorological Research Institute, Japan Meteorological Agency, Tsukuba, Japan

<sup>2</sup>Massachusetts Institute of Technology, Cambridge, MA, US

<sup>3</sup>European Centre for Medium-Range Weather Forecasts, Reading, UK

(Corresponding author: Daisuke Hotta, e-mail: dhotta@mri-jma.go.jp)

This work is distributed under the Creative Commons Attribution 4.0 License (CC BY 4.0)

## 1. Introduction

The choice of grids for global spectral models has been constrained by the requirement to ensure exact spherical harmonics transforms (SHTs). For this reason, most global spectral models adopt some variant of Gaussian grids. Recent developments that strenuously reduce the computational cost of SHTs, like the use of single-precision arithmetic (Hatfield et al. 2019; DOI: [10.1145/3324989.3325711](https://doi.org/10.1145/3324989.3325711)) and non-exact Fast Legendre Transform (Wedi et al. 2013; DOI: [10.1175/MWR-D-13-00016.1](https://doi.org/10.1175/MWR-D-13-00016.1)), have demonstrated that the numerical exactness of SHTs is not essential for NWP models, which opens up many possibilities as to the choice of the grids other than the classic Gaussian grid. The HEALPix grid (Fig 1e; Gorski et al. 2005; DOI: [10.1086/427976](https://doi.org/10.1086/427976)) is a particularly attractive alternative with many desirable features like tessellation by equal-area cells that are quadrilateral, alignment of cell centers along latitude circles, and natural nestability.

## 2. Aliasing issue with the HEALPix grid and its resolution with OctaHEALPix

SHTs on the HEALPix grid have an issue with respect to aliasing. On HEALPix grid, lat-lon aspect ratio is geometrically fixed at 1:1. Now, given triangular truncation at wavenumber  $N_{trunc}$ , for any grid, we need more than  $2N_{trunc}$  latitude nodes pole-to-pole to avoid cubic aliasing in the meridional direction of a purely meridional mode, and likewise, we need more than  $4N_{trunc}$  longitude points along the Equator to avoid cubic aliasing in the zonal direction of a purely zonal mode. Hence, HEALPix requires more than  $4N_{trunc}$  latitude nodes just to avoid zonal aliasing, requiring three times more gridpoints than the octahedral grid (Fig 1c,d; which needs only  $2N_{trunc}$  latitude nodes) for a same spectral resolution. Here we propose to resolve this issue with a new grid (Fig1f), the OctaHEALPix, which we so name motivated by its similarity with both the octahedral grid and the HEALPix grid. This grid is constructed by dividing the sphere into 4 rhomboids instead of 12 as in the original HEALPix, which simplifies the construction procedure compared to the classical HEALPix. Thus, OctaHEALPix preserves HEALPix's attractive features of equal-area and nestable

tessellation into quadrilateral cells, yet allowing for consistent aliasing in the zonal and meridional directions. Like octahedral grid, OctaHEALPix requires three times fewer gridpoints than HEALPix for a same spectral truncation and thus runs faster. At T31 cubic truncation, for example, we found that OctaHEALPix is more than twice faster than the original HEALPix.

### 3. Model description and experimental setup

We implemented HEALPix and OctaHEALPix grids on *SpeedyWeather.jl* model (<https://github.com/SpeedyWeather>). *SpeedyWeather.jl* is a flexible GCM, written entirely in Julia language, intended as a playground for trying out new ideas. It currently supports 2D barotropic and shallow-water models, and the 3D primitive equations with and without humidity. Here, we tested HEALPix and OctaHEALPix grids by running the shallow-water version of *SpeedyWeather.jl* model for the barotropic instability testcase of Galewsky et al. (2004; [DOI:10.3402/tellusa.v56i5.14436](https://doi.org/10.3402/tellusa.v56i5.14436)) and by comparing the results obtained on the tried-and-truth full Gaussian grid.

### 4. Results and conclusion

SHTs on HEALPix and OctaHEALPix are not exact, unlike Gaussian or Clenshaw-Curtis grids. Unit test of SHTs on these grids (not shown) showed that, while transforms on HEALPix and OctaHEALPix are not exact, their errors reduce monotonically as the resolution increases, so that, at wavenumber  $\sim 1,000$ , they become nearly as accurate as single-precision transforms on Gaussian grid. Results of Galewsky (2004) test (Fig 2) show that the model is equally accurate irrespective of the choice of the grids, even at resolution as low as T31, suggesting that error sources other than spectral transforms contribute more to the total errors.

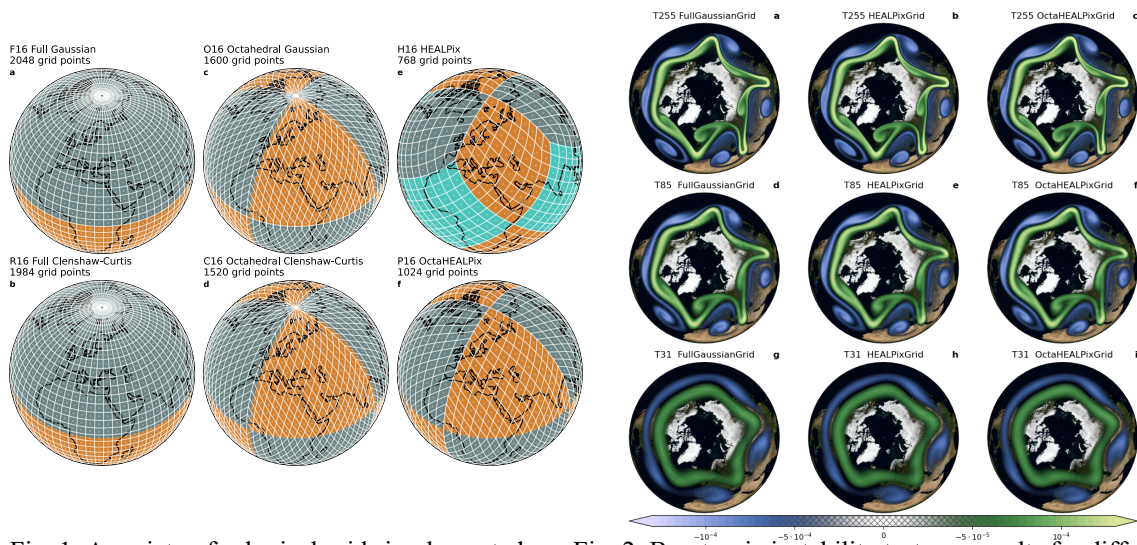


Fig. 1: A variety of spherical grids implemented on SpeedyWeather.jl model.

Fig. 2: Barotropic instability test case results for different grids (columns) with different resolutions (rows).

# Dependency of the entrainment rate on the grid spacing

Shun-ichi WATANABE, Kenta SUEKI<sup>1</sup>, and Junshi ITO<sup>1</sup>

<sup>1</sup>Meteorological Research Institute, Tsukuba, Japan

<sup>2</sup>Tohoku University, Sendai, Japan

(Corresponding author: Shun-ichi WATANABE, e-mail: swatanabe@mri-jma.go.jp)

This work is distributed under the Creative Commons Attribution 4.0 License (CC BY 4.0)

## 1. Introduction

The entrainment and detrainment processes are key processes for the development of cumulus convection. The representation of these processes has a crucial impact on cumulus parameterization (de Rooy et al. 2013). Recently, the entrainment rate has been estimated using simulations of cumulus convection by high-resolution models. In this study, the dependency of the entrainment rate on the grid spacing is evaluated.

## 2. Model description and experimental setup

An idealized simulation of a back-building convective system proposed by Ito et al. (2021) is performed by the JMA operational non-hydrostatic model, ASUCA. The size of the numerical domain is 240 km in the  $x$ -direction, 144 km in the  $y$ -direction, and 20 km in the vertical ( $z$ -) direction. Horizontal grid spacings are 2 km, 1 km, 500m, 250m, and 125 m and the vertical grid spacing is 125 m except near the surface. In this simulation, an advection of a passive tracer is also calculated to estimate the entrainment rate.

## 3. Result

A back-building convective system is simulated in all experiments with different grid spacings. A cumulus updraft is defined as a consecutive region in a horizontal plane where vertical velocity exceeds  $5 \text{ m s}^{-1}$ . The size of the cumulus updraft is defined by the area of this region ( $S$ ).

The tracer concentration in the steady cumulus updrafts satisfies the following:

$$\frac{d\hat{\Psi}}{dz} = \epsilon(\hat{\Psi} - \bar{\Psi}), \quad (1)$$

where  $\hat{\Psi}$  is the tracer concentration in the cumulus updraft,  $\epsilon$  is the entrainment rate, and  $\bar{\Psi}$  is the tracer concentration in the environment. We assume  $\bar{\Psi} = 1 - z/H$  ( $H = 20000 \text{ m}$ ) for the initial condition.  $\hat{\Psi}$  is analytically obtained if we assume constant  $\epsilon$ .

The tracer concentration in the cumulus updrafts monotonically decreases with height below 6 km (Fig. 1a), which is consistent with eq. (1). The estimated entrainment rate is

10-30% below 6km. The tracer concentration decreases more rapidly in the experiments with smaller grid spacing, indicating a larger entrainment rate. Figure 1b-f show the tracer concentration averaged over cumulus updrafts with different size. The entrainment rate increases as the horizontal scale of the cumulus updraft decreases. On the other hand, the dependency of the entrainment rate on the grid spacing is found to be small for the cumulus updraft with a similar horizontal scale. Since more small-scale convective updrafts are represented as the grid spacing decreases (not shown), the average entrainment rate is larger for smaller grid spacing.

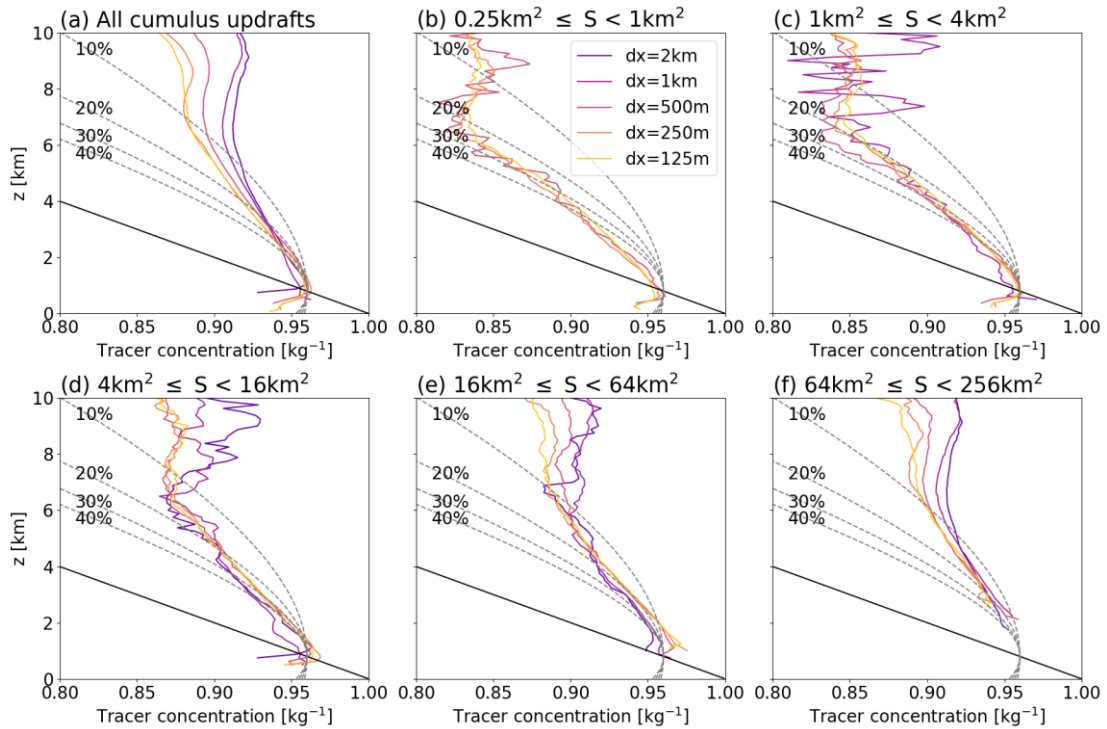


Fig. 1 Tracer concentration averaged over (a) all cumulus updrafts and (b)-(f) cumulus updrafts with different sizes. The solid line is the tracer concentration in the environment. Dashed lines are analytical solutions of eq. (1) with different entrainment rates.

## References

1. de Rooy, W. C, P. Bechtold, K. Fröhlich, H. Jonker, D. Mironov, A. P. Siebesma, J. Teixeira, J-I. Yano (2013) Entrainment and detrainment in cumulus convection: an overview. *Q. J. R. Meteorol. Soc.*, **139**, 1–19.
2. Ito, J., H. Tsuguchi, S. Hayashi, and H. Niino, (2021), Idealized high-resolution simulations of a back-building convective system that causes torrential rain, *J. Atmos. Sci.*, **78**, 117 – 132.

Session N:  
Radiative convective equilibrium, Convection

# Characteristic horizontal structure of large-scale self-aggregation of clouds in radiative–convective equilibrium

Tomoro YANASE<sup>1</sup>, Seiya NISHIZAWA<sup>1</sup>, Hiroaki MIURA<sup>2</sup>, Hirofumi TOMITA<sup>1</sup>

<sup>1</sup>RIKEN, Kobe, Japan

<sup>2</sup>The University of Tokyo, Tokyo, Japan

(Corresponding author: Tomoro YANASE, e-mail: tomoro.yanase@riken.jp)

This work is distributed under the Creative Commons Attribution 4.0 License (CC BY 4.0)

## 1. Introduction

Deep convective clouds often organize into large-scale systems such as mesoscale convective systems, tropical cyclones, and MJOs. While cloud organization in the real atmosphere is manifested under the influence of various external factors, clouds also self-organize on a large-scale in idealized numerical experiments of radiative-convective equilibrium (RCE) with horizontally uniform boundary conditions [1,3]. In this study, we performed cloud-resolving RCE experiments in which the horizontal domain size is increased up to about 25000 km to eliminate the influence of the computational domain as much as possible, with the aim of understanding the natural horizontal structure of large-scale self-aggregation of clouds.[5]

## 2. Model description and experimental setup

We used a fully-compressible, non-hydrostatic, regional atmospheric model SCALE-RM [2,4]. In the horizontally squared three-dimensional computational domain, the doubly periodic lateral boundary condition is imposed. The sea surface temperature at the lower boundary is set to 300 K constant. The physical parameterizations for cloud microphysics, radiation, sub-grid scale turbulence, and surface processes are used. We performed six experiments by doubling the horizontal domain size from 768 km to 24576 km. The horizontal grid spacing is 8 km. The integration time is 150 days for the two cases with the largest domain sized, and 200 days for the other experiments.

## 3. Result and conclusion

Figure 1 shows the horizontal distribution of precipitable water on a transient phase and a quasi-equilibrium phase for each experiment. In the 768- and 1536-km runs, a single circular structure is formed in the moist cloud areas, and a single band structure is formed in the 3072-km run. The more complicated structure in the 6144-km run is consistent with a previous study [3]. In the 12288- and 24576-km runs, a mesh-like pattern with a

characteristic distance of 3000-4000 km is formed. Although the mesh-like structure is often observed in convection phenomena [2], it is interesting that such structure also appear in the organization of deep moist convection. In the future, we hope to elucidate why such shapes and scales are selected from the energetics viewpoint.

### Acknowledgments

The RIKEN JRA and SPDR Program supported the first author. JSPS Scientific Research 19H01974 partly supported this study. The simulations were conducted on "Fugaku", RIKEN Center for Computational Science.

### References (in alphabetical order according to author)

1. Muller, C., Yang, D., Craig, G., Cronin, T., ... & Sherwood, S. C. (2022). Spontaneous aggregation of convective storms. *Annual Review of Fluid Mechanics*, 54, 133-157.
2. Nishizawa, S., Yashiro, H., Sato, Y., Miyamoto, Y., & Tomita, H. (2015). Influence of grid aspect ratio on planetary boundary layer turbulence in large-eddy simulations. *Geoscientific Model Development*, 8(10), 3393-3419.
3. Patrizio, C. R., & Randall, D. A. (2019). Sensitivity of convective self-aggregation to domain size. *Journal of Advances in Modeling Earth Systems*, 11(7), 1995-2019.
4. Sato, Y., Nishizawa, S., Yashiro, H., Miyamoto, Y., Kajikawa, Y., & Tomita, H. (2015). Impacts of cloud microphysics on trade wind cumulus: which cloud microphysics processes contribute to the diversity in a large eddy simulation?. *Progress in Earth and Planetary Science*, 2, 1-16.
5. Yanase, T., Nishizawa, S., Miura, H., & Tomita, H. (2022). Characteristic Form and Distance in High-Level Hierarchical Structure of Self-Aggregated Clouds in Radiative-Convective Equilibrium. *Geophysical Research Letters*, 49(18), e2022GL100000.

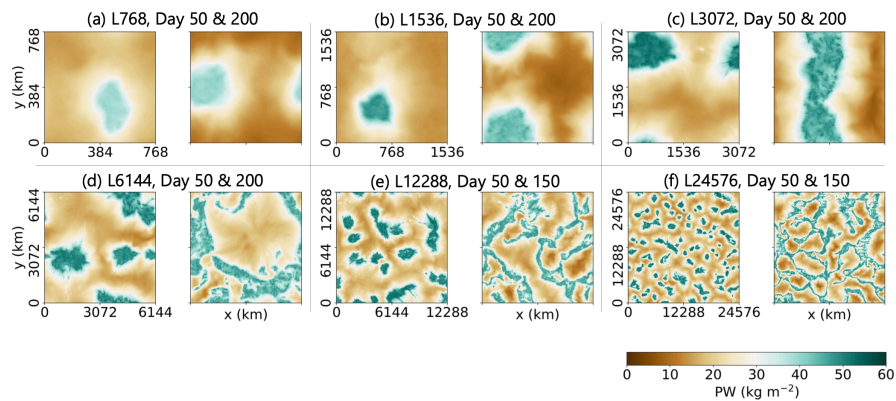


Fig. 1. Horizontal distribution of daily-averaged precipitable water on day 50 and final day of each run. From Yanase et al. (2022, GRL) Figure 1.

# A Study of Convective Clouds in Radiative Convective Equilibrium Using GFDL FV3-Based Non-hydrostatic Cloud Resolving Model

Ming Zhao

GFDL/NOAA, Princeton, New Jersey, USA

(Corresponding author: Ming Zhao, e-mail: [ming.zhao@noaa.gov](mailto:ming.zhao@noaa.gov))

## 1. Introduction

GFDL FV<sup>3</sup>-based non-hydrostatic (NH) global storm resolving model is now available. But running this model is still too expensive for climate simulations. We created a simple version of the FV<sup>3</sup>-based NH model for idealized RCE simulations using doubly periodic lateral boundary conditions with fixed SSTs, radiative gases, and solar forcings. We explore the model-simulated characteristics in convection, clouds, and climate to study convection parameterization in coarse resolution global climate models (GCM) as well as cloud feedback to a warmer climate. Moist convection in GCMs is typically produced from two distinct modules (parameterized convection and explicit clouds). Their partition affects many aspects of GCM characteristics including the mean climate, transient variability, and cloud feedback. It is however unclear how to determine this partition, especially at high resolutions. This is important to scale-aware parameterization. Meanwhile, we also study the impact of model resolution on clouds and cloud feedbacks.

## 2. Model description and experimental setup

The model follows Held et. al (2007) except using the NH FV<sup>3</sup> dynamical core with a modified LIN microphysics. The simulation setup follows the RCEMIP (Wing et. al 2018). We chose 3 different SSTs (295, 300, 305K) with a fixed domain (6144 x 384 km) at incrementally larger horizontal grid-spacing (3, 6, 12, 24, 48) km. The runs (R3, R6, R12, R24, R48) have identical settings except with different timesteps. We also run a 1.5km resolution model (R1.5) with halved domain size. No convection parameterization is used for all simulations except one additional 48km resolution run (R48C), in which we turn on the GFDL AM4 convection scheme. Each run is integrated for 1 year with the last 6 months used for analysis.

## 3. Result and conclusion:

Using the high-resolution model output we can compute the vertical transport of total water  $\overline{wq}$  averaged at increasingly larger subdomain  $d=(2, 4, 6, 8, 16, 32, 64, 128)\Delta x$ . Overbar is an average over a chosen subdomain  $d$ . We can partition the total transport it into grid-scale ( $\overline{wq}$ ) and sub-grid eddy transport  $\overline{w'q'} = \overline{(w - \overline{w})(q - \overline{q})}$ . The eddy transport can be written as:  $\sigma(\overline{w'q'})_c + (1 - \sigma)(\overline{w'q'})_e + \sigma(1 - \sigma)(w_c - w_e)(q_c - q_e)$ , where  $\sigma$  is fractional area of convective updraft. In the case of a single homogeneous plume model, the eddy transport may be approximated as:  $\sigma(1 - \sigma)(w_c - w_e)(q_c - q_e)$ . This has been referred to as a unified plume model (Arakawa and Wu 2013) and it can be compared with the conventional plume model:  $\sigma w_c(q_c - \overline{q})$ , which assumes  $\sigma \ll 1$ ,  $w_e \ll w_c$ ,  $q_e \approx \overline{q}$ . Fig. 1 shows the vertical transport of total water and its partitions into grid-scale and eddy components at various subdomain sizes. As the subdomain (grid) size  $d$  decreases, the grid-scale transport dominates the total transport while the eddy transport peaks at roughly 6-12km grid size and then decreases to zero. The two plume models produce nearly identical results when the convective updraft properties are provided exactly with the simulation. However, the properties of convective plumes are difficult to model precisely due to the uncertainty in the parameterization of cumulus mixing. If we arbitrarily introduce a 10% error to the updraft properties, we find the convective plume model produces a much larger error at a smaller grid size while the unified plume model produces a much smaller error and still decreases to zero as subdomain size approaches the model original resolution. This indicates a significant benefit by explicitly considering the effect of  $(1-\sigma)$  in the formulation of the plume model. Fig. 1c shows that even at a resolution of 100km, nearly 50% of total transport comes from a large scale, which is quite different from Arakawa and Wu (2013). Fig. 1d shows the  $\sigma$  values estimated using the 3 highest-resolution simulations. They are sensitive to the original resolution used to derive these quantities,

especially for subdomain sizes of 24 km and below. A higher resolution simulation would be needed to obtain  $\sigma$  values for  $d=20\text{km}$  and below.

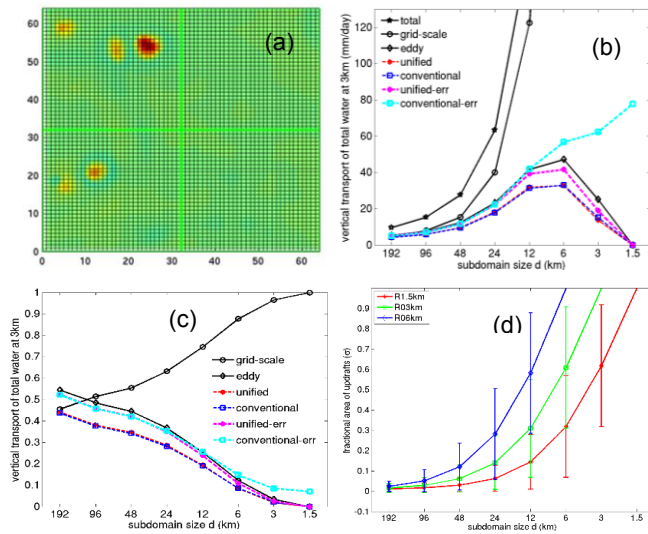


Fig. 1. (a) A snapshot of a portion of the model simulated vertical velocity  $w$  field at 3km height. Black mesh indicates the mode's original resolution at  $\Delta x=1.5\text{km}$ . Thick green mesh shows a coarse grid ( $d = 32\Delta x$ ). (b) shows the vertical transport of total water and its partitions into grid-scale and eddy components (black lines). Red and blue lines show results from the unified and convective plume models respectively. Magenta and cyan lines are the same as the red and blue lines except with 10% error introduced to the updraft properties (total water). (c) As in (b) except showing the fraction of total water transport from grid-scale, eddy, and the different plume models. (d) fractional area of updrafts  $\sigma$  estimated using the 3 highest resolution simulations.

(c) As in (b) except showing the fraction of total water transport from grid-scale, eddy, and the different plume models. (d) fractional area of updrafts  $\sigma$  estimated using the 3 highest resolution simulations.

Fig. 2a shows that TOA net incoming radiation decreases sharply with decreasing resolutions. This is due to a sharp decrease in total CRE. TOA net radiative feedback is not robust across resolutions. The two highest-resolution simulations show net positive feedback. This is due to large positive cloud feedback, especially as SST increases from 300K to 305K. Fig. 2b shows the CRE sensitivity to resolution is largely due to the SW component, which can be explained by the low cloud amount. The low cloud amount increases sharply with decreasing model resolution. Fig. 2c shows the response of LW CRE is complicated in this model. LW CRE exhibits less sensitivity to resolution. There is no indication of a reduction of high cloud amount in these simulations except for the one with parameterized convection (R48C).

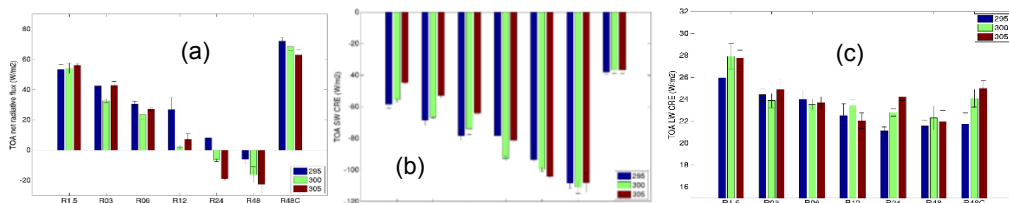


Fig. 2. Domain averaged top-of-atmosphere (a) net incoming radiative fluxes, (b) SW cloud radiative effect (CRE) and (c) LW CRE from the various resolution simulations.

To summarize, we have used large domain  $FV^3$ -based NH CRM simulations of RCE to quantify the amount of convection that needs to be parameterized as model resolution increases. Results suggest a large fraction of total transport is taken care of through resolved flow even at resolutions of 100km. An explicit representation of the  $(1-\sigma)$  effect in plume models is important to scale-aware parameterization. But the estimate of  $\sigma$  may be resolution-dependent. The  $FV^3$ -based RCE tends to produce strong positive cloud feedback. This is due to 1) a large decrease in low cloud amount and shallowing low cloud depth, especially over subsidence regions. 2) a lack of reduction in high cloud amount and LW CRE from the subsidence region and a shift of regions from large-scale descent to ascent. This model shows robust weakening of large-scale circulation and no indication of increased aggregation in warmer climates.

## References

Held, IM., M. Zhao, and B. Wyman, 2007: Dynamic radiative-convective equilibria using GCM column physics. *J. Atmos. Sci.*, 64(1), 228-238.

# Novel Perspectives on Diurnal Convection over Complex Topography through VVM Simulations

Wei-Ting Chen, Yu-Hsiu Wang, and Chien-Ming Wu<sup>1</sup>

<sup>1</sup>Department of Atmospheric Sciences, National Taiwan University, Taipei, Taiwan  
(Corresponding author: Wei-Ting Chen, e-mail: weitingc@ntu.edu.tw)

This work is distributed under the Creative Commons Attribution 4.0 License (CC BY 4.0)

## 1. Introduction

This study provides a conceptual framework to understand the diurnal convection dominated by local circulation over complex topography. The results are analyzed from the perspective of deep-inflow mixing of convection, focusing on the non-local dynamic in entraining high upstream moist static energy (MSE) and its related convective strength. Deep-inflow mixing (Schiro et al., 2018) proposes that the MSE required for convective development can be dynamically entrained from the environment through the small-scale turbulence or coherent flow from deep lateral inflow, emphasizing the dynamic effect of MSE transported from the environment that provides the convective buoyancy. Chang et al (2023) applied this framework to complex topography and proposed that the low-level coherent flow driven by local circulation is an important pathway to transport upstream MSE to convection, thereby enhancing precipitation intensity. The structure and strength of local circulation may be affected by complex topography, while the varying environmental conditions also affect diurnal convection.

Our work provides a new perspective based on energy considerations to understand diurnal convection under idealized terrain configuration and environmental conditions. Specifically, we attempt to understand the importance of MSE transport driven by local circulation in diurnal convection and its responses to varying environmental conditions.

## 2. Model description and experimental setup

We used the Vector Vorticity equation cloud resolving Model (VVM, Jung and Arakawa, 2008; Wu and Arakawa, 2011; Wu et al., 2019), which is sensitive to surface fluxes induced turbulence and horizontal buoyancy gradient, with high horizontal resolution (100-m) that can represent the detailed local circulation evolutions and convection structures. An idealized terrain configuration is applied, which includes ocean (50-km wide), plain (25-km wide), and mountain (1-km high), to simulate the 12-hr evolution of diurnal convection over the mountain island. The simulation is initialized with a simplified sounding composited from typical local circulation dominated environment. To highlight the role of local circulations in energy transport over complex topography, we devised a scenario with limited CAPE and the presence of CIN. Convection is more likely to occur through the lifting mechanisms of the mountainous area, and deep convection is hindered in the plain area, allowing the local circulation to persist and dominate the overall mechanism. We then explore the impact of environmental variability on diurnal convection by increasing and decreasing the free troposphere relative humidity by 20% in the initial condition, which characterizes how sounding is influenced by the variability of the strength of subtropical high.

## 3. Result and conclusion

In all simulations, the diurnal precipitation time series exhibits multiple peaks in time. The first two peaks, in which the developments are closely related to the evolution of sea-valley breeze circulations, show negative relationships between precipitation intensity

and convective available potential energy (CAPE). The deep-inflow mixing features are observed in both two peaks (Figure 1), particularly in the 2nd peak with stronger local circulations and upstream MSE transport, which enhances precipitation intensity. The linear increase of updraft below 6 km denotes a deep lateral inflow to convection. The local circulation driven upstream MSE transport below 1 km dominates the deep MSE inflow. The sensitivity experiment with changing the free troposphere relative humidity shows that the degree of contribution of low-level upstream MSE transport depends on the background MSE distribution.

We conclude that the non-local dynamic of entraining upstream MSE strengthens convection. The low-level upstream MSE transport via local circulation dominates the deep MSE inflow, and the degree of contribution depends on the background environment conditions. As the local circulation develops further, stronger inflow increases upstream MSE transport, enhancing the precipitation intensity.

### References (in alphabetical order according to author)

1. Chang, Y. H., Chen, W. T., Wu, C. M., Kuo, Y. H., & Neelin, J. D. (2023). Identifying the Deep-Inflow Mixing Features in Orographically-Locked Diurnal Convection. *GRL*, 50(10), e2023GL103107.
2. Jung, J.-H., & Arakawa, A. (2008). A three-dimensional anelastic model based on the vorticity equation. *MRW*, 136(1), 276-294.
3. Schiro, K. A., Ahmed, F., Giangrande, S. E., & Neelin, J. D. (2018). GoAmazon2014/5 campaign points to deep-inflow approach to deep convection across scales. *PNAS*, 115(18), 4577-4582.
4. Wu, C. M., & Arakawa, A. (2011). Inclusion of surface topography into the vector vorticity equation model (VVM). *JAMES*, 3(2).
5. Wu, C.-M., Lin, H.-C., Cheng, F.-Y., & Chien, M.-H. (2019). Implementation of the land surface processes into a vector vorticity equation model (VVM) to study its impact on afternoon thunderstorms over complex topography in Taiwan. *APJAS*, 55, 701-717.

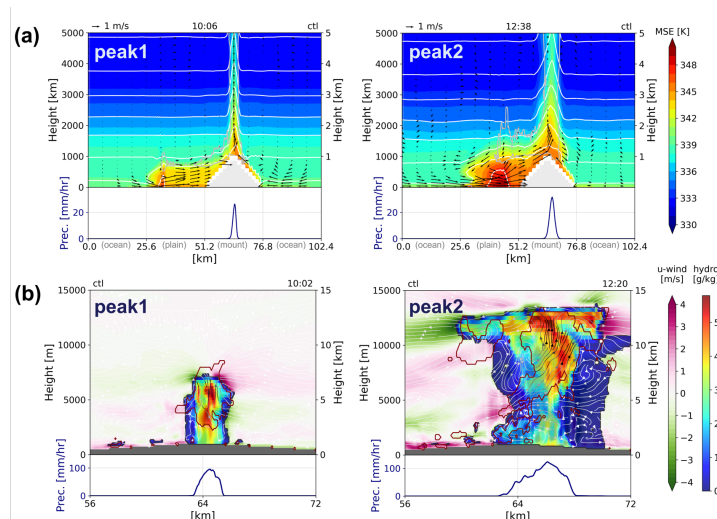


Fig. 1. Features of local circulation and convection in the first two rainfall peaks in the control simulation. (a) Averaged vertical structures of MSE (shading), moisture (white contours), cloud (grey contours), and low-level circulation (vectors) and along the y-direction. (b) Snapshots of hydrometeors distribution (rainbow shading) and circulation (pink-green shading and streamlines). Blue lines in the lower panels represent precipitation rate (y-averaged in (a) and snapshot in (b)).

# **EUREC<sup>4</sup>A-MIP: A model intercomparison project on mesoscale organisation of shallow cumulus clouds in a present and future climate**

A. Pier Siebesma<sup>1,2</sup>, Abraham Torres Alavez<sup>3</sup>, Christoph Schär<sup>3</sup>, Alessandro Savazzi<sup>1</sup>, Fredrik Jansson<sup>1,\*</sup>, Hauke Schulz<sup>4,5</sup>, Gheylla Liberia<sup>1</sup>

<sup>1</sup>Department of Geoscience & Remote Sensing, Delft University of Technology

<sup>2</sup>Royal Netherlands Meteorological Institute, de Bilt, Netherlands

<sup>3</sup>Institute for Atmospheric and Climate Science, ETH Zürich, Zürich, Switzerland

<sup>4</sup>Atmosphere in the Earth System, Max Planck Institute for Meteorology, Hamburg, Germany

<sup>5</sup>Cooperative Institute for Climate, Ocean, and Ecosystem Studies (CICOES), University of Washington, Seattle, WA, United States

(Corresponding author: Pier Siebesma, e-mail: a.p.siebesma@tudelft.nl,

\*presenting author: Fredrik Jansson, e-mail: f.r.jansson@tudelft.nl)

This work is distributed under the Creative Commons Attribution 4.0 License (CC BY 4.0)

## **1. Introduction**

Shallow Cumulus over the subtropical oceans is the most abundant cloud type in our climate system and its radiative response to global warming is highly uncertain. Previous MIPs on shallow cumulus convection have primarily explored the representation of spatially unorganised shallow cumulus convection and their response to climate warming. It has become clear however over the last decade that marine shallow cumulus convection has a natural strong tendency to develop into mesoscale organised cloud structures and that unorganised shallow cumulus convection is the exception rather than the rule. It is for this reason that we propose a MIP on shallow cumulus convection over the Northern Atlantic subtropical ocean such as observed during the EUREC<sup>4</sup>A field campaign in January- February 2020.

The main objectives of this MIP are:

1. Assessing the simulation capability of the observed shallow cloud mesoscale organisation over the subtropical ocean.
2. Understanding the underlying dynamical processes that lead to these mesoscale cloud patterns.
3. Assessing the radiative response of this abundant cloud regime to climate warming using the Pseudo-Global Warming (PGW) framework [1].

Two different model approaches are proposed in this MIP: one on storm-resolving resolutions of 0.5~2.5km resolution on domains of several thousands of kilometres and another one on turbulence resolving resolutions of 50~250 meter on domains of several hundreds of kilometres. The domains are shown in figure 1. The simulations are carried out under present day conditions such as observed during the EUREC<sup>4</sup>A field campaign and additionally for future weather conditions by using a Pseudo Global Warming perturbation [1] based on global +4K SST AMIP runs. The initial and boundary conditions for both the present day and +4K conditions are provided.

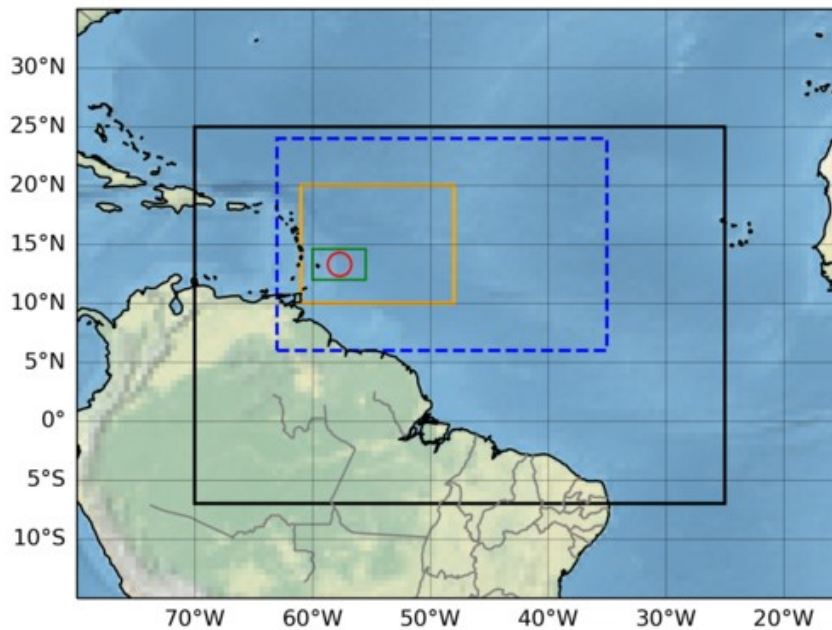


Figure 1: Domains for the EUREC<sup>4</sup>A-MIP experiment. Initial and boundary conditions from ERA5 are provided in the outermost rectangle. The dashed rectangle is a suggested domain for storm-resolving models. The innermost rectangle is the domain for LES models and includes the island Barbados. The circle shows the flight path of the HALO aircraft deploying dropsondes during the EUREC<sup>4</sup>A campaign.

In this presentation the intercomparison project will be presented and the first results will be discussed. We welcome contributions with additional models, please see the full description of the EUREC<sup>4</sup>A-MIP protocol at <https://eurec4a.eu/> for information on how to contribute and contact persons.

## References

1. C. Heim, D. Leutwyler, C. Schär (2023). Application of the pseudo-global warming approach in a kilometer-resolution climate simulation of the tropics. *Journal of Geophysical Research: Atmospheres*, 128, e2022JD037958. <https://doi.org/10.1029/2022JD037958>

# Cloud Botany - a shallow cumulus ensemble of large eddy simulations

Fredrik Jansson<sup>1</sup>, Martin Janssens<sup>1,2</sup>, Johanna H. Grönqvist<sup>3,4</sup>, A. Pier Siebesma<sup>1,5</sup>,  
Franziska Glassmeier<sup>1</sup>, Jisk Attema<sup>6</sup>, Victor Azizi<sup>6</sup>, Masaki Satoh<sup>7</sup>, Yousuke Sato<sup>8,9</sup>,  
Hauke Schulz<sup>10,11</sup>, Tobias Kölling<sup>10</sup>

<sup>1</sup>Department of Geoscience & Remote Sensing, Delft University of Technology

<sup>2</sup>Department of Meteorology & Air Quality, Wageningen University & Research

<sup>3</sup>Department of Physics, Åbo Akademi University, Turku, Finland

<sup>4</sup>Institute of Physics, University of Amsterdam, Amsterdam, Netherlands

<sup>5</sup>Royal Netherlands Meteorological Institute, de Bilt, Netherlands

<sup>6</sup>Netherlands eScience Center, Amsterdam, Netherlands

<sup>7</sup>Atmosphere and Ocean Research Institute, University of Tokyo, Kashiwa, Japan

<sup>8</sup>Department of Earth and Planetary Sciences, Faculty of Science, Hokkaido University,  
Sapporo, Japan

<sup>9</sup>RIKEN Center for Computational Science, Kobe, Japan

<sup>10</sup>Atmosphere in the Earth System, Max Planck Institute for Meteorology, Hamburg, Germany

<sup>11</sup>Cooperative Institute for Climate, Ocean, and Ecosystem Studies (CICOES), University of  
Washington, Seattle, WA, United States

(Corresponding author: Fredrik Jansson, e-mail: [f.r.jansson@tudelft.nl](mailto:f.r.jansson@tudelft.nl))

This work is distributed under the Creative Commons Attribution 4.0 License (CC BY 4.0)

## 1. Introduction

Shallow cumulus clouds in the trade-wind region show a wide variety of mesoscale organization patterns [1], which have recently been studied extensively with the EUREC<sup>4</sup>A field observation campaign. We present Cloud Botany, an ensemble of 103 large-eddy simulations on domains of 150 km over the tropical ocean [2]. Each simulation in the ensemble is run in an idealized, fixed, larger-scale environment, described with six parameters. The aim of the ensemble is to determine if these patterns can occur by self-organizing small-scale processes, and clarify how cloud formation and cloud organization depend on the large-scale meteorological conditions. We vary the parameters over characteristic ranges for the winter trade wind regions, including the parameter combinations observed during the EUREC<sup>4</sup>A field campaign. We find that any simulation that supports cumulus clouds eventually develops mesoscale patterns in their cloud fields. We also find a rich variety in these patterns as our control parameters change, a few examples are shown in Figure 1. The patterns include small unorganized cumulus, cold pools lined by cloudy arcs, bands of clouds or clouds aggregated in patches, and sometimes cold pools topped by thin anvils, reminiscent of the pattern called “flowers” [1].

The simulations were made with the Dutch Atmospheric Large Eddy Simulation (DALES) model running on supercomputer Fugaku. We will discuss the experience of porting DALES to Fugaku, and our attempts at tuning the model for this architecture.

## 2. Accessing the data

The cloud botany dataset is available online, and can be accessed through the EUREC<sup>4</sup>A intake catalog ([https://howto.eurec4a.eu/botany\\_daless.html](https://howto.eurec4a.eu/botany_daless.html)). The data is stored in the

Zarr format, making it possible to access and analyze it with Python and xarray, with the data being downloaded as required. In particular, this format makes it possible to access subsets or slices without first downloading the full dataset.

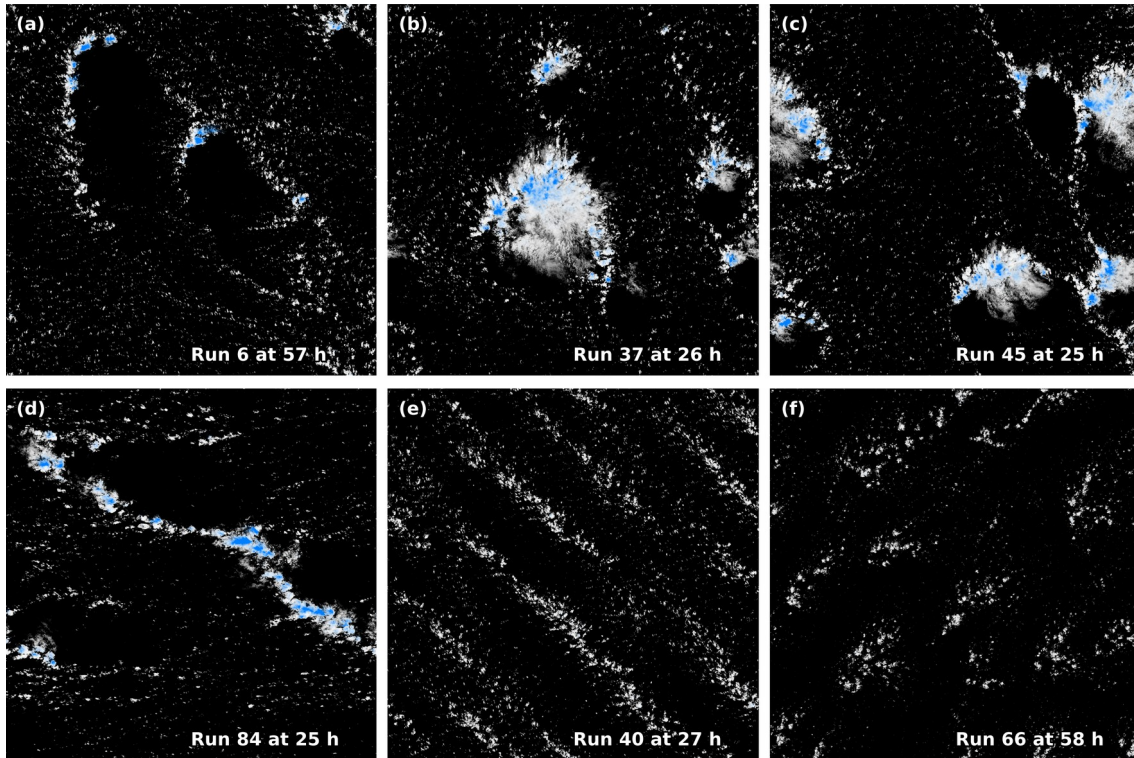


*Figure 1: Six members of the ensemble showing different organization patterns. The images show cloud albedo in white and liquid water path in blue.*

### **Acknowledgements**

We gratefully acknowledge access to Fugaku through RIKEN HPCI project hp200321, funding from the projects CONSTRAIN (European Union Horizon 2020 Project No. 820829), and ESiWACE (European Union Horizon 2020 Project No. 823988), DKRZ for hosting the data, and ECMWF and SurfSARA for additional computing and storage.

### **References**

1. S. Bony, H. Schulz, J. Vial, B. Stevens (2020), Sugar, gravel, fish, and flowers: Dependence of mesoscale patterns of trade-wind clouds on environmental conditions. *Geophysical research letters*, 47 (7), e2019GL085988.
2. F. Jansson, M. Janssens, J. H. Grönqvist, A. P. Siebesma, F. Glassmeier, J. J. Attema, V. Azizi, M. Satoh, Y. Sato, H. Schulz, T. Kölling (2023), Cloud Botany: Shallow cumulus clouds in an ensemble of idealized large-domain large-eddy simulations of the trades. Under revision for JAMES, DOI: [10.22541/essoar.168319841.11427814/v1](https://doi.org/10.22541/essoar.168319841.11427814/v1)